The role of the novel adipokines WISP1 and sFRP4 in obesity and type 2 diabetes and their impact on insulin action and energy metabolism in muscle and liver

Inaugural-Dissertation

zur Erlangung des Doktorgrades
der Mathematisch-Naturwissenschaftlichen Fakultät
der Heinrich-Heine-Universität Düsseldorf

vorgelegt von

Tina Hörbelt
aus Coesfeld

Düsseldorf, Juli 2018

aus dem Institut für Klinische Biochemie und Pathobiochemie
des Deutschen Diabetes-Zentrums
Leibniz-Zentrum für Diabetesforschung
an der Heinrich-Heine-Universität Düsseldorf

Gedruckt mit der Genehmigung der
Mathematisch-Naturwissenschaftlichen Fakultät der
Heinrich-Heine-Universität Düsseldorf

Berichterstatter:
1. Prof. Dr. Hadi Al-Hasani
2. Prof. Dr. Michael Feldbrügge

Tag der mündlichen Prüfung: 09.10.2018

All that is necessary for faith is the belief that by doing our best we shall succeed in our aims: the improvement of mankind.

Rosalind Franklin

Zusammenfassung

Die allgemeine Zunahme von Fettleibigkeit (Adipositas) ist ein aktuelles globales Gesundheitsproblem, insbesondere da sie mit einem erhöhten Risiko für die Entwicklung eines Typ 2 Diabetes (T2D) und auch einer nicht-alkoholischen Fettleber (NAFLD) assoziiert ist. Das weiße Fettgewebe ist in den letzten Jahren in den Fokus der Diabetes-Forschung gerückt, da es neben seiner zentralen Funktion als Speicherorgan für überschüssige Nahrungsenergie in Form von Lipiden, in Abhängigkeit der Schwere der Adipositas verschiedenste bioaktive Proteine, sogenannte Adipokine, exprimiert und sekretiert. Adipokine können auto-, para- sowie endokrin wirken und so direkt den Stoffwechsel metabolisch aktiver Organe wie z.B. Leber und Skelettmuskel beeinflussen. Einhergehend mit dem Schweregrad der Adipositas und der Störung der metabolischen Funktion des Fettgewebes, ändert sich das Sekretionsprofil der Adipokine. Kürzlich wurden die Wnt-Proteine Wnt1-Inducible Signaling Pathway Protein 1 (WISP1) und Secreted Frizzled-Related Potein 4 (sFRP4) als Adipokine bei Mensch und Maus identifiziert.

Obwohl WISP1 und sFRP4 bereits mit Adipositas und/oder T2D in Zusammenhang gebracht wurden, gab es bislang kaum Hinweise über ihre Rolle im Stoffwechsel. Das Ziel der vorliegenden Arbeit bestand in der Klärung der Rolle von WISP1 und sFRP4 bei Adipositas und T2D sowie ihre potentielle Interaktion mit dem Leber- und Skelettmuskel Metabolismus.

Untersuchungen von Seren normalgewichtiger Männer und adipöser Probanden ohne und mit T2D zeigten, dass WISP1 unabhängig vom Diabetesstatus in adipösen Männern gesteigert war. Dies konnte auch für die mRNA-Expression von *WISP1* in viszeralen Fettgewebsproben (VAT) bestätigt werden. Hingegen war die Expression von *sFRP4* in VAT von adipösen Typ 2 Diabetikern zusätzlich gesteigert. Physiologisch korrelierten die Serum- und mRNA-Level von WISP1 positiv mit Insulinresistenz (HOMA-IR), und zirkulierendes WISP1 in Serum korrelierte negativ zum Gutt´s Index der Insulinsensitivität in adipösen Individuen. Analog zu WISP1 konnten Korrelationen für die *sFRP4* VAT-Expression mit Insulinresistenz sowie den nüchtern Insulinwerten ermittelt werden, die jedoch BMI-abhängig waren. Zusätzlich assoziierte die *sFRP4* VAT-Expression unabhängig von Alter und BMI signifikant mit Triglyzeriden und Adiponektin im Serum. Die Stimulation von Skelettmuskel-Zellen und Hepatozyten mit rekombinantem WISP1 *in vitro*, führte zu einer verminderten Insulinwirkung auf Ebene des Insulinrezeptor-initiierten Akt-Signalweges. In primären humanen Skelettmuskel-Zellen resultierte dies in einer reduzierten Insulin-vermittelten Glykogensynthese und in primären murinen Hepatozyten in einer verminderten Insulin-induzierten Unterdrückung der Expression der Glukoneogenese-assoziierten Gene *Pck1* (*Phosphoenolpyruvate Carboxykinase 1*) und *G6Pc* (*Glucose-6-Phosphatase*). In *in vitro* Experimenten mit Myotuben, die mit

rekombinantem sFRP4 behandelt wurden, konnte gezeigt werden, dass die mitochondriale Atmung, die Proteasomaktivität sowie die Degradation von IRS-1 durch sFRP4 induziert wurden und eine gesteigerte Abundanz der E3 Ubiquitin Ligasen MuRF1 and MAFbx/atrogin-1 über einen AMPK-FoxO3a-vermittelten Signalweg nachweisbar war. Rekombinantes sFRP4 bewirkte *in vitro* in Hepatozyten, die aus Lebern von C57Bl6-Kontrollmäusen isoliert wurden, eine reduzierte Insulinwirkung auf die Phosphorylierung von Akt, GSK3β und FoxO1, sowie eine gesteigerte Degradation von IRS-1. sFRP4 reduzierte auch die Insulinwirkung auf die Phosphorylierung von Akt, GSK3β und FoxO1 in metabolisch-beeinträchtigten Hepatozyten, isoliert aus dem lipodystrophen NAFLD-Mausmodell aP2-SREBP-1c. FoxO konnte als ein gemeinsamer Endpunkt der sFRP4-Wirkung in Skelettmuskel-Zellen und in Hepatozyten nachgewiesen werden. Untersuchungen des Glukose- und des Lipidstoffwechsels an isolierten C57Bl6 Hepatozyten zeigten, dass sFRP4 die Insulinwirkung auf die mRNA-Expression von *G6pc* und *Pck1* sowie der Glykogensynthese beeinträchtigte und die Lipidsynthese steigerte. In aP2-SREBP-1c Hepatozyten konnte jedoch kein Effekt auf die Insulin-vermittelte Lipidsynthese nachgewiesen werden. Diese durch sFRP4 induzierten differentiellen Effekte fanden sich auch in den Resultaten der Sekretomanalysen von Hepatozyten aus C57Bl6 und aP2-SREBP-1c Mäusen wieder. So wurde in bioinformatischen Analysen z.B. der Glukokortikoid-Rezeptor Signalweg als maßgebend für das Sekretionsmuster beider Modelle identifiziert.

Zusammenfassend konnte im Rahmen dieser Arbeit dargelegt werden, dass WISP1 und sFRP4 als Indikatoren für Adipositas und/oder T2D herangezogen werden können. WISP1 konnte als ein maßgeblicher Faktor für Adipositas unabhängig von T2D nachgewiesen werden, der mit einer systemischen und fettgewebespezifischen Inflammation sowie einer zellspezifisch verminderten Insulinwirkung in Skelettmuskel-Zellen und Hepatozyten einhergeht. sFRP4 bewirkte eine gesteigerte Proteasomaktivität in Skelettmuskel-Zellen, die mit dem Abbau von IRS-1 assoziierte. Im Gegensatz dazu induzierte sFRP4 in metabolisch-intakten und dysfunktionalen Hepatozyten einen selektiv insulin-resistenten Status, der sich in einer Inhibition des Insulin-Signalweges aber in einer Zunahme oder Aufrechterhaltung der Insulin-vermittelten Lipidsynthese widerspiegelte. Basierend auf den Resultaten der vorliegenden Arbeit, stellen WISP1 und sFRP4 vielversprechende Kandidaten für weitere Forschungsansätze dar, die der therapeutischen Prävention und Behandlung von Adipositas, Insulinresistenz und metabolischen Erkrankungen wie Diabetes und NAFLD dienen können.

Summary

The general increase in obesity is a current global health problem, especially as it is associated with an increased risk of developing type 2 diabetes (T2D) and non-alcoholic fatty liver disease (NAFLD). White adipose tissue (WAT) has moved into the focus of diabetes research in recent years, since in addition to its central function as a storage organ for excess food energy in form of lipids, WAT expresses and secretes various bioactive proteins, called adipokines, depending on the severity of obesity. Adipokines act in auto-, para- and endocrine manner and thus directly affect the metabolism of organs such as liver and skeletal muscle. Along with the severity of obesity and metabolic dysfunction of WAT, the secretion profile of adipokines changes. Recently the Wnt proteins Wnt1-inducible signaling pathway protein 1 (WISP1) and secreted frizzled-related protein 4 (sFRP4) were identified as adipokines in humans and mice. Although WISP1 and sFRP4 have already been linked to obesity and/or T2D, their role in metabolism is still incompletely understood. The objective of the present work was to clarify the influence of WISP1 and sFRP4 in obesity and T2D and their potential interaction with liver and skeletal muscle metabolism.

Examinations of serum samples of normal-weight men and obese probands without and with T2D revealed an increase of WISP1 in obese men independent of their diabetes status. This also has been found for the mRNA expression of *WISP1* in visceral adipose tissue (VAT) biopsies. In contrast, *sFRP4* VAT expression was further increased in obese type 2 diabetics.

Physiologically, serum and mRNA levels of WISP1 positively correlated with insulin resistance (HOMA-IR), while circulating WISP1 negatively correlated to the Gutt´s Index of insulin sensitivity in obese individuals. Similar to WISP1, *sFRP4* VAT expression correlated with insulin resistance and fasting insulin values but in dependence of BMI. In addition, *sFRP4* VAT expression significantly associated with serum triglycerides and adiponectin levels independently of age and BMI.

Stimulation of skeletal muscle cells and hepatocytes with recombinant WISP1 *in vitro* reduced the insulin effect on level of the insulin receptor-activated Akt signaling pathway. In primary human skeletal muscle cells this resulted in reduced insulin-induced glycogen synthesis and in primary murine hepatocytes in an impaired insulin-mediated suppression of the expression of the gluconeogenic genes *phosphoenolpyruvate carboxykinase 1* (*Pck1*) and *glucose-6-phosphatase c* (*G6pc*).

In *in vitro* experiments with myotubes treated with recombinant sFRP4 it has been shown that mitochondrial respiration, proteasome activity and degradation of IRS-1 were induced while the abundance of the E3 ubiquitin ligases MuRF1 and MAFbx/atrogin-1 was increased via an AMPK-FoxO3a-mediated signaling pathway. Recombinant sFRP4 reduced the insulin action on

the phosphorylation of Akt, GSK3β and FoxO1, but promoted degradation of IRS-1 in hepatocytes isolated from livers of C57Bl6 control mice. sFRP4 also remarkably diminished the effect of insulin on phosphorylation of Akt, GSK3β and FoxO1 in metabolically impaired hepatocytes isolated from the lipodystrophic NAFLD mouse model aP2-SREBP-1c. Thus, FoxO was identified as a common endpoint affected by sFRP4 *in vitro* in skeletal muscle cells and hepatocytes. Studies of glucose and lipid metabolism in isolated C57Bl6 hepatocytes showed that sFRP4 impaired the insulin action on *G6pc* and *Pck1* expression and glycogen synthesis while enhanced insulin action on lipid synthesis. However, in aP2-SREBP-1c hepatocytes no effect on the insulin-mediated lipid synthesis could be detected. These differential effects of sFRP4 were also found in the evaluation of hepatocytes secretomes from C57Bl6 and aP2-SREBP-1c mice. Thus, bioinformatic analyses identified that the secretion profile of both mouse models was for instance predominantly determined by the glucocorticoid receptor signaling pathway.

In conclusion, this work demonstrated that WISP1 and sFRP4 can be used as indicators for obesity and/or T2D. WISP1 has been detected as a significant factor for obesity independent of T2D, which associated with systemic and adipose tissue inflammation and with a cell-specific reduced insulin effect on skeletal muscle cells and hepatocytes.

sFRP4 increased proteasome activity in skeletal muscle cells that associated with the degradation of IRS-1. Whereas in metabolically intact and dysfunctional hepatocytes, sFRP4 induced a selective insulin-resistant state reflected in an impaired insulin signaling pathway but an increase or maintenance of insulin-mediated lipid synthesis. Based on the results of the present work, WISP1 and sFRP4 are promising candidates for further research approaches in the therapeutic prevention and treatment of obesity, insulin resistance and metabolic diseases such as diabetes and NAFLD.

Table of contents

List of Figures

List of Tables

List of Abbreviations

2-DOG	2-deoxy-D-glucose
ACC	Acetyl-CoA carboxylase
ADA	American Diabetes Association
AML12	Alpha Mouse Liver 12
AMPK	AMP-activated protein kinase
APC	Adenomatous polyposis coli
aPKC	Atypical protein kinase C
APS	Ammonium persulfate
BMI	Body mass index
BMP	Bone morphogenetic protein
BSA	Bovine serum albumin
BZ	Bortezomib
cDNA	Complementary DNA
CEBPA	CCAAT/enhancer-binding protein alpha
ChREBP	Carbohydrate-responsive element-binding protein
CK-1α	Casein kinase-1-alpha
CompC	Compound C
CPM	Counts per minute
CPT1	Carnitine palmitoyltransferase 1
CRD	Cysteine-rich domain
CREB	Cyclic AMP response element-binding protein
CRP	C-reactive protein
CTCK	Cysteine knot-like domain
DAG	Diacylglycerol
DGAT	Diacylglycerolacyltransferase
DMSO	Dimethyl sulfoxide
DNL	*De novo* lipogenesis
EASL	European association for study of liver
ECAR	Extracellular acidification rate
ECM	Extracellular matrix
FAO	Fatty acid oxidation
FAS	Fatty acid synthase
FBS	Fetal bovine serum
FCCP	Carbonyl cyanide p-trifluoromethoxyphenylhydrazone
FFA	Free fatty acid
FGF21	Fibroblast growth factor 21

FoxO1/3a	Forkhead box protein O1/3a
FZD	Frizzled receptors
G6P	Glucose-6-phosphate
G6Pc	Glucose-6-phosphatase c
GLDH	Glutamate dehydrogenase
GLUT2/4	Glucose transporter type 2/4
GOT	Glutamat-oxalacetat-transaminase
GPAT	Glycerol-3-phosphate-acyltransferase
GPT	Glutamat-pyruvat-transaminase
GS	Glycogen synthase
GSK3β	Glycogen synthase kinase 3β
h	Hours
$HbA1_c$	Hemoglobin $A1_c$
HDL	High-density lipoprotein
HOMA-IR/B	Homeostasis model assessment of insulin resistance/β-cell function
hSkMC	Human skeletal muscle cells
IDF	International Diabetes Federation
IGF-1	Insulin-like growth factor-1
IGFBP	Insulin-like growth factor binding protein
IHTG	Intrahepatic triglyceride
IL-1β/6	Interleukine-1β/6
IRS-1/2	Insulin receptor substrate-1/2
IRβ	Insulin receptor β
JNK	c-Jun N-terminal *kinases*
kDa	Kilodalton
KRH	Krebs-Ringer-HEPES
MAFbx	Muscle atrophy F-box
MCP-1	Monocyte chemoattractant protein-1
min	Minutes
mTORC1/2	Mammalian target of rapamycin complex 1/2
MuRF1	Muscle RING-finger protein 1
NAFLD	Non-alcoholic fatty liver disease
NAS	NAFLD activity score
NASH	Non-alcoholic hepatosteohepatitis
NEFA	Non-esterified fatty acid
NFκB	Nuclear factor kappa-light-chain-enhancer of activated B-cells
NTR	Netrin-related motif

OCR	Oxygen consumption rate
OGTT	Oral glucose tolerance test
OD	Optical Density
PBS	Phosphate-buffered saline
PC	Pyruvate carboxylase
PCK1	Phosphoenolpyruvate carboxykinase 1
PCR	Polymerase chain reaction
PDK4	Pyruvate dehydrogenase kinase 4
PDPK1	3-phosphoinositide-dependent kinase1
PI3K	Phosphatidylinositol-3-OH kinase
PKC_{ε}	Protein kinase c epsilon
PPARα/γ	Peroxisome proliferator-activated receptor alpha/gamma
qRT-PCR	Quantitative real-time PCR
ROS	Reactive oxygen species
RT	Room temperature
SAT	Subcutaneous adipose tissue
sFRP4/5	Secreted frizzled-related protein 4/5
SIRT	Sirtuin
SREBP-1c	Sterol regulatory element-binding transcription factor-1c
SVF	Stromal vascular fraction
T1D	Type 1 diabetes
T2D	Type 2 diabetes
TAG	Triacylglycerol
TBS	Tris-buffered saline
TCF/LEF	T-cell factor/lymphoid enhancer factor
TCF7L2	Transcription factor 7-like 2
TG	Triglycerides
TGF-β	Transforming growth factor-beta
TGFβR	Transforming growth factor β receptor
TNF-α	Tumor necrosis factor-alpha
TSR	Thrombospondin type I repeat
VAT	Visceral adipose tissue
VWFC	Von Willebrand factor type C repeat
WAT	White adipose tissue
WHO	World health organization
WISP1	Wnt1-inducible signaling pathway protein1
Wnt	Wingless-type

1 Introduction

1.1 Obesity

Obesity is still one of the largest public chronic health problems, no longer just concerning industrialized, developed countries but also societies that encounter inferior socio-economic conditions in developing countries. According to the world health organization (WHO), in 2016 worldwide more than 650 million individuals (≥ 18 years) were obese while already 1.9 billion of the adult´s population were overweight resulting in proportions of 13% and 39% of the world´s population, respectively (World Health Organization (WHO), 2018). Thereby, the global prevalence of obesity has been approximately 3-fold higher compared to 1975 (WHO, 2018) and is suggested to still rise in future (Kelly et al., 2008).

Obesity is defined by a profuse accumulation of fat caused by an imbalance in intake and consumption of energy accompanied by insufficient physical activity (WHO, 2018).

Obesity is assessed by body mass index (BMI) that is defined by the quotient of the weight of an individual (kilograms) and squared height (meters) (kg/m^2) (WHO, 2018) (Table 1). Calculation of BMI does not consider the distribution of fat within the body which is decisive for obesity-related health problems. Thus, further methods are used for classification of obesity including determination of body fat composition and waist circumferences (Leitner et al., 2017).

Table 1. International BMI-based classification of normal-weight and obese adults.

Classification	BMI (kg/m^2)	
	Principal cut-off points	Additional cut-off points
Normal range	18.50-24.99	18.50-22.99 23.00-24.99
Overweight	≥ 25	25.00-27.49 27.50-29.99
Obese class I	30.00-34.99	30.00-32.49 32.50-34.49
Obese class II	35.00-39.99	35.00-37.49 37.50-39.99
Obese class III	≥40.00	≥40.00

Adapted and modified according to WHO.

1.2 Obesity-associated metabolic diseases

Besides favoring social, psychological and physiological problems, the onset of obesity is a crucial risk factor for the development of insulin resistance and severe metabolic disorders including type 2 diabetes (T2D) and non-alcoholic fatty liver disease (NAFLD).

The WHO demonstrated that obesity accounts for 44% in the onset of type 2 diabetes (WHO, 2018; Frühbeck et al., 2013). Furthermore, 80% of individuals with NAFLD were obese (Williams et al., 2011; Bellentani, 2017). Thus, changes in lifestyle such as physical activities, eating behavior but also pharmacological intervention or bariatric surgery aimed to reduce body weight, improve fat mass distribution and energy control are in focus of therapeutic interventions to prevent obesity-related diseases (Leitner et al., 2017).

1.2.1 Type 2 diabetes (T2D)

Diabetes mellitus, short diabetes, is as a chronic disorder characterized by either an impaired insulin production or the inefficient utilization of insulin resulting in pathological high plasma glucose levels described as a state of hyperglycemia (American Diabetes Association (ADA), 2017; IDF, 2017; WHO, 2018). Estimated by the International Diabetes Federation (IDF), in 2017 approximately 425 million individuals had diabetes around the world with an assumed rising prevalence of 629 million people diagnosed with diabetes in 2045 probably provoke by demographic and economic changes and unhealthy lifestyles (IDF, 2017). The onset of diabetes is frequently associated with the pathogenesis of further disorders including kidney failure and cardiovascular diseases (WHO, 2018). In 2015, 1.6 million people died due to direct causes of diabetes. According to estimations, in 2030 diabetes will be on position seven among the causes that lead to human death (WHO, 2018). The WHO and ADA stated cut-off values for plasma glucose levels to discriminate between the healthy and hyperglycemic state. Thus, the diagnosis of diabetes is based on increased circulating blood glucose either assessed under fasting conditions, randomly, two hours after an oral glucose tolerance test (OGTT) with ingestion of 75 g glucose or by hemoglobin $A1_c$ amount ($HbA1_c$) (Table 2) (ADA, 2017; IDF, 2017; WHO, 2018).

Table 2. Diagnostic criteria for diabetes according to the WHO and ADA.

Plasma glucose parameter	Cutt-off concentration mg/dl (mmol/l)
Fasting plasma glucose	≥ 126 mg/dl (7.0 mmol/l)
2-h plasma glucose after OGTT	≥ 200 mg/dl (11.1 mmol/l)
Random glucose	≥ 200 mg/dl (11.1 mmol/l)
$HbA1_c$	≥ 6.5% (48 mmol/mol)

Adapted and modified according to WHO and ADA.

Type 2 diabetes (T2D) is the most common form of diabetes with 90% of overall diabetes cases (IDF, 2017; Shah et al., 2015). The onset of T2D is linked to conditions of the modern society as a result of increased aging population, insufficient physical activity, high caloric food intake and enhanced urbanization (IDF, 2017), with obesity as well as increased ectopic abdominal fat accumulation as the major risk factors (IDF, 2017).

T2D is characterized by an inappropriate insulin secretion and impaired action of metabolic peripheral tissues including liver, skeletal muscle and/or adipose tissue or the whole organism in response to insulin, a state described as insulin resistance (Das and Elbein, 2006; IDF, 2017; Reaven et al., 2005; WHO, 2018).

Beside T2D there are other forms of diabetes, noteworthy type 1 diabetes (T1D). This disease develops in response to an autoimmune reaction against pancreatic β-cells resulting in insufficient or even absolute destructed insulin production (IDF, 2017; WHO, 2018). Based on current knowledge T1D emerges from genetic susceptibility and environmental factors and is not preventable (IDF, 2017; WHO, 2018).

Hence, insulin is a key molecule in the development of diabetes. Primary physiological actions of insulin which is secreted by pancreatic β-cells in response to elevated systemic glucose levels, comprise the suppression of glucose production and fatty acid oxidation and promoting *de novo* lipogenesis (DNL), glycolysis and glycogen synthesis in liver while induces glucose uptake and glycogen synthesis in skeletal muscle (Figure 1). In the postprandial state, the liver is exposed to portal vein-derived insulin, with levels approximately 3-fold higher than in the systemic circulation (Samuel and Shulman, 2012). In liver and skeletal muscle, insulin directly

induces the tyrosine activity of the insulin receptor β (IRβ) that in turn phosphorylates tyrosine residues on insulin receptor substrate-1 (IRS-1) and -2 (IRS-2) which subsequently interacts with the SH2-domain of phosphatidylinositol-3-OH kinase (PI3K) (Eckstein et al., 2017; Franke et al., 1997; Hanke and Mann, 2009). As a consequence, Akt is recruited to the membrane where it is phosphorylated at residues Thr-308 and activated by 3-phosphoinositide-dependent kinase-1 (PDPK1) whereas mTORC2 (mammalian target of rapamycin complex) mediated phosphorylation of Akt at Ser-473 (Eckstein et al., 2017; Samuel and Shulman, 2018). Hence, insulin-activated Akt induces glycogen synthesis in skeletal muscle and liver via stimulation of glycogen synthase (GS) through the allosteric activator glucose-6-phosphate (G6P) and inhibitory phosphorylation of glycogen synthase kinase 3 (GSK3) (Cross et al., 1995). In liver this also entails an inhibition of glucose production by induction of the phosphorylation and the nuclear exclusion of forkhead box protein O1 (FoxO1) that results in the suppression of the expression of key rate gluconeogenic genes including phosphoenolpyruvate carboxykinase 1 (*PCK1*) and glucose-6-phosphatase C (*G6PC*) (Cohen et al., 1999; Nakae et al., 2001; Peterson et al., 1998). Insulin stimulates hepatic DNL via the PI3K/Akt pathway and through atypical protein kinase C (aPKC) by increasing the expression of the *sterol regulatory element-binding transcription factor-1c* (*SREBP-1*c) and the proteolytic cleavage of the immature, nascent protein to mature, active SREBP-1c (Brown and Goldstein, 2008; Sanders and Griffin 2016). In turn, the mature, transcriptionally active SREBP-1c translocates to the nucleus and amongst others induces the expression of lipogenic genes including *acetyl-CoA carboxylase* (*ACC*) and *fatty acid synthase* (*FAS*) (Brown and Goldstein, 2008; Kawano and Cohen, 2013; Magana and Osborne, 1996; Magana et al., 1997; Shao and Espenshade, 2012). Beyond the direct stimulatory action of insulin on hepatic DNL, acetyl-CoA that is derived from hepatic glycolysis serves as a further fuel for DNL (Smith and Tsai, 2007). Systemic diet-derived glucose is disposed by the membrane glucose transporter type 2 (GLUT2) of hepatocytes in an insulin-independent fashion (Bechmann et al., 2012) and converted to G6P which is further metabolized via glycolysis to acetyl-CoA in the mitochondria or synthesized to glycogen depending on the cellular energy level (Pilkis and Claus, 1991).

During hepatic lipid synthesis, cytoplasmic acetyl-CoA is carboxylated to malonyl-CoA by ACC. Following, malonyl-CoA is elongated via the key-rate limiting FAS to saturated palmitic acid (Ameer et al., 2014; Bechman et al., 2012). The produced fatty acids are esterified to a glycerol backbone generating diacylglycerol (DAG) catalyzed by mitochondrial glycerol-3-phosphate-

acyltransferase (GPAT). DAG is converted via diacylglycerolacyltransferase (DGAT) to synthesize triacylglycerol (TAG) either for hepatic storage in lipid droplets or very low-density lipoprotein (VLDL)-dependent secretion in the circulation for delivery to adipose tissue for TAG storage and as energetic fuel to muscle (Bechmann et al., 2012; Coleman and Lee, 2004). While TAG esterification and DNL are induced by insulin, the assembly and release of VLDL particles from hepatocytes are suppressed by insulin resulting in triglyceride accumulation in liver (Sparks et al., 2012.).

While in liver IRS-1 and IRS-2 are important in insulin signaling, in skeletal muscle IRS-1 plays a key role in the activation of PI3K/Akt signaling (Eckstein et al., 2017). Activated Akt induces Akt substrate of 160 kDa (AS160) that stimulates glucose uptake in skeletal muscle by mediating the translocation of glucose transporter 4 (GLUT4) to the plasma membrane while prevents fatty acid uptake and oxidation and proteolysis through inhibition of FoxO1/3a at Ser256/253 and Thr24/32 (Bastie et al, 2005; Brunet et al., 1999; Eckstein et al., 2017). In skeletal muscle, active FoxO1 shifts oxidation of glucose as a fuel to fatty acids via upregulation of pyruvate dehydrogenase kinase 4 (PDK4) and lipoprotein lipase while FoxO3a induced the expression of E3 ubiquitin ligases (Furuyama et al., 2003; Kamei et al., 2003; Koh et al., 2013). Insulin mediates suppression of white adipose tissue (WAT) lipolysis that results in reduced glycerol generation and delivery to liver for conversion to glucose as well as decreased non-esterified fatty acid (NEFAs) limiting the acetyl-CoA pool that entails an inhibition of hepatic pyruvate carboxylase activity (PC) and thus hepatic lipid synthesis (Perry et al., 2014, 2015) (Figure 1).

However, in T2D insulin is unable to promote blood glucose disposal via uptake by skeletal muscle while fails to suppress glucose production in liver. Consequently, plasma glucose levels further rise entailing hyperglycemia, a hallmark of T2D (DeFronzo et al., 1992; Stummvoll et al., 2005). To compensate for insulin resistance and thus to reduce elevated plasma glucose levels, β-cells, the primary site for insulin synthesis in pancreas, increase insulin production and secretion leading to hyperinsulinemic conditions that, over time, provoke defective β-cells insulin secretion and β-cells dysfunction (ADA, 2017; IDF, 2010; Lin et al., 2010). The hyperinsulinemic insulin resistant state in turn induces hepatic *de novo* lipogenesis and anti-lipolytic responses in adipose tissue and thus promotes secretion of VLDL and NEFAs evoking hypertriglyceridemia along with enhanced adipose tissue associated inflammation (Czech et al., 2017; De Luca et al., 2006; Wellen and Hotamisligil, 2005). T2D evokes a state of

hyperglycemia, hyperinsulinemia and hypertriglyceridemia along with whole-body insulin resistance, hence it is strongly associated with dysfunctions in multiple tissues. To alleviate or cure T2D and its associated complications, therapeutic interventions of T2D focused on the consolidation of a healthy lifestyle based on the reduction of excess body weight along with lowering of plasma glucose levels obtained by a balanced diet and increased physical activity (IDF, 2017; WHO, 2018). If this is not sufficient to reduce plasma glucose levels, insulin treatment or oral blood glucose lowering medication including metformin, sulfonylureas, thiazolidinediones, dipeptidylpeptidase-4 (DPP-4) and/or sodium/glucose cotransporter2 (SGLT2) inhibitors alone or in combination were used to further control and maintain blood glucose to healthy, normal levels (IDF, 2010).

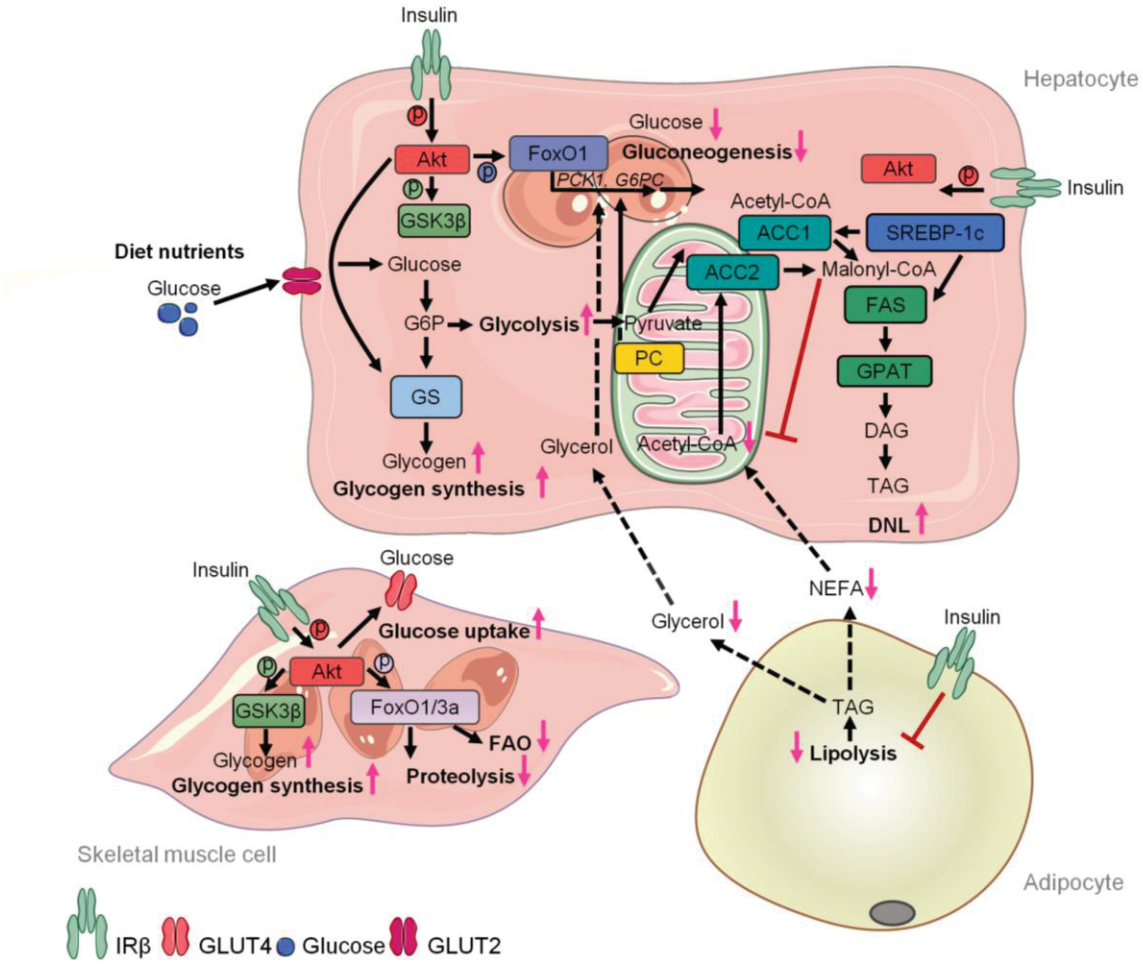

Figure 1. Insulin action on energy metabolism in liver, skeletal muscle and adipose tissue. Insulin binds and activates IRβ leading to phosphorylation and activation of Akt. In turn, Akt suppresses expression of hepatic gluconeogenic genes and thus glucose production via phosphorylation and inactivation of FoxO1 while stimulates GS induced glycogen synthesis in liver and skeletal muscle and GLUT4-dependent glucose uptake in muscle. In liver, insulin signaling directly activates SREBP-1c that induces the expression of *FAS* and *GPAT* resulting in

increased lipogenic activity (DNL). Diet-derived glucose uptake via insulin-independent GLUT2 transporter stimulates hepatic glycolysis and provided substrates for hepatic DNL. Here, initially, acetyl-CoA is carboxylated to malonyl-CoA by ACC. Malonyl-CoA is converted by FAS, esterified to DAG by GPAT and further converted to TAG for storage. Insulin prevents proteolysis and fatty acid oxidation via phosphorylation of FoxO1 and FoxO3a in skeletal muscle while suppresses lipolysis in adipocytes leading to reduced glycerol and NEFA level. Limited glycerol from adipocytes provokes decreased hepatic glucose production while reduced adipocytes-derived NEFAs result in decreased hepatic PC activity and thus control hepatic glucose production and DNL. ACC, acetyl-CoA-carboxylase; DAG, diacylglycerol; FAS, fatty acid synthase; FoxO1/3a, forkhead box protein O1/3a; *G6PC*, glucose 6-phosphatase; GPAT, glycerol-3-phosphate-acyltransferase; GS, glycogen synthase; IRβ, insulin receptor β; NEFA, non-esterified fatty acid; PC, pyruvate carboxylase; *PCK1*, phosphoenolpyruvate carboxykinase 1; SREBP-1c, sterol regulatory element-binding transcription factor-1c; TAG, triacylglycerol. Modified according to Samuel and Shulman, 2018.

1.2.2 Non-alcoholic fatty liver disease (NAFLD)

Obesity is also a crucial risk factor for the development of NAFLD, the most common liver disease in western society (Fabbrini et al., 2010; Younossi et al., 2016). According to estimations, 20-30% of western adult population while 24.4% individuals worldwide are diagnosed for NAFLD (Satapathy and Sanyal, 2015; Zhu et al., 2015). Thereby, the global prevalence of NAFLD without the onset of obesity comprises just around 10-30% (Kim and Kim, 2017).

Hence, an obesity-related unhealthy lifestyle associated with modern society along with an excessive high caloric and fat containing food intake may contribute to the development of NAFLD (Bray and Popkin, 2014). The prevalence of NAFLD frequently emerges in concert with metabolic co-morbidities including hypertension, dyslipidemia, a state characterized by increased plasma triglycerides, and type 2 diabetes that further link NAFLD to a rising public health problem (Adams et al., 2005; Marchesini et al., 2003). 18-33% of NAFLD diagnoses walk along with the onset of type 2 diabetes while more than 90% of obese individuals with type 2 diabetes have been diagnosed for NAFLD (Lopez-Velazquez et al., 2014; Tolman et al., 2007).

NAFLD is characterized by an increased intrahepatic triglycerides (IHTG) content, described as hepatic steatosis. The pathological progress of NAFLD may cause hepatic inflammation and fibrosis, known as non-alcoholic steatohepatitis (NASH) and liver cirrhosis, a severe pathological tissue remodeling of the liver leading to liver dysfunction (Fabbrini et al., 2010; Kleiner et al., 2005; Ludwig et al, 1980; Masuka and Chalasani, 2013). Among the individuals with NAFLD, 5-20% are diagnosed for NASH of which less than 5% develop severe hepatic

cirrhosis and liver failure, the third leading cause for liver transplantation (Bataller et al., 2011; Charlton et al., 2011). The diagnosis of NAFLD is based on histological sections and/or imaging approaches including magnetic resonance spectroscopy (MRS) or computed tomography (CT) used to assess the IHTG content and thus steatosis. NAFLD is present when accumulated hepatic triglyceride amount exceeds 5% of liver weight or volume or ≥ 5% of hepatocytes exhibit accumulated TG independent of secondary steatosis caused by chronic liver disease or excessive alcohol intake (Hoyumpa et al., 1975; Kleiner et al., 2005). Diagnosis of progressed NAFLD evoking NASH or cirrhosis along with lobular inflammation, fibrosis and hepatocyte degeneration (hepatocellular ballooning) requires sampling and analysis of liver biopsies (European association for study of liver (EASL), 2016).

The molecular mechanisms underlying the pathogenesis of NAFLD are multifactorial. Besides genetic determinants, NAFLD-mediated alterations in energy metabolism play a major role (Romeo et al., 2008). The latter encompass an imbalance of higher uptake of fatty acids into liver originated from diet and adipose tissue and enhanced activity of hepatic *de novo* lipogenesis while reduced hepatic fatty acid oxidation and increased release of VLDL containing triglycerides from liver. Donnely et al. described that the major content of hepatic triglycerides found in individuals with NAFLD probably primary derived from adipose tissue lipolysis with 59% while 26% were synthesized by DNL and 15% originated from diet (Donelly et al., 2005; Sanders and Griffin 2016).

The enhanced accumulation of hepatic triglycerides, a key characteristic of NAFLD, rather than increasing BMI or visceral adiposity highly associated and is a crucial estimator for the onset of hepatic insulin resistance (Kumashiro et al., 2011). NAFLD along with hepatic insulin resistance associated with an increased risk for T2D and hepatocellular carcinoma (Fabbrini et al., 2010; Michellotii et al., 2013; Peterson et al., 2006). Therefore, the treatment of individuals with NAFLD is crucial and initially focused on the reduction of hepatic triglyceride content along with improving hepatic insulin responsiveness. Thus, primary goals of therapeutic interventions include weight loss either obtained by a strict low-caloric diet or bariatric surgery (Baldry et al., 2017; Billeter et al., 2016; Froylich et al., 2016; Lewiset al., 2006; Schauer et al., 2017).

1.3 Obesity and its role in adipose tissue dysfunction

1.3.1 Adipose tissue as metabolic organ

In humans and rodents, WAT plays a crucial role in whole-body energy homeostasis by regulating energy storage, peripheral lipid availability and insulin sensitivity (Wronska and Kmiec, 2012). In the postprandial state, circulating glucose and free fatty acid (FFA) enter the adipocytes and are processed via re-esterification for storage as triglycerides (TG) (Freedland et al., 2004). Under fasting conditions or a high energy demand, adipocytes-derived TG are hydrolyzed via lipolysis to fatty acids that are released in the bloodstream to provide sufficient energy utilized by peripheral tissues including skeletal muscle and liver (Wronska and Kmiec, 2012). WAT is predominantly composed of adipocytes but also comprises cells of the stromal vascular fraction (SVF) including pre-adipocytes, fibroblasts, lymphocytes, endothelial cells and macrophages (Ouchi et al., 2011).

The two major fat depots in WAT, the visceral adipose tissue (VAT) and the subcutaneous adipose tissue (SAT), are characterized by their anatomical location and fulfill distinct functional and structural roles (Komolka et al., 2014; Ouchi et al., 2011). The VAT of the abdominal cavity predominantly comprises the retroperitoneal, omental and mesenteric fat depots (Wronska and Kmiec, 2012). Blood derived from the latter two fat depots directly accesses the liver via the portal vein (Komolka et al., 2014; Wronska and Kmiec, 2012). Further, VAT is more vascularized and innervated than SAT (Ibrahim et al., 2010). SAT is localized as a layer under the skin and is drainaged by systemic veins (Ibrahim et al., 2010; Wronska and Kmiec, 2012). The specific activities of the distinct adipose tissue depots VAT and SAT vary in insulin responsiveness, fat cell types and lipolysis ability (Ibrahim et al., 2010). VAT has been identified to be the depot with higher metabolic activity showing larger production and infiltration of pro-inflammatory cells (Ibrahim et al., 2010; Komolka et al., 2014; Weisberg et al., 2003). Adipogenic precursor cells (APC) from VAT expand by hypertrophy, have more mesenchymal-stem cell-like characteristics and pro-inflammatory potential. In contrast, SAT-derived APCs showed no alterations in their metabolic activity and expansion occurred via hyperplasia (Del Pozo et al, 2011; Fawcett et al., 2010; Ibrahim et al., 2010; Misra et al., 2003). In states of overnutrition, when energy supply overwhelms SAT capacity to store free fatty acids and glycerol as triglycerides, excessive energy is transported to distinct peripheral tissues instead, resulting in ectopic fat accumulation in non-adipose tissues and increased VAT mass featuring visceral abdominal obesity (Freedland et al., 2004; Ibrahim et al., 2010). Visceral

abdominal adiposity rather than peripheral adiposity has been described to account for impairments in glucose and lipid metabolism and is frequently associated with the onset of insulin resistance, T2D and/or NAFLD (Figure 2) (Freedland et al., 2004; Ibrahim et al., 2010; Kumashiro et al., 2011).

Furthermore, in the development of obesity and related diseases, the adipose tissue undergoes remodeling events characterized by mass expansion, increased adipocyte size (hypertrophy), enhanced adipocyte number (hyperplasia), remodeling of the extracellular matrix (ECM), attraction and infiltration of immune cells that might result in adipose tissue dysfunction including inflammation or fibrosis (Figure 2) (Gustafson et al., 2013; Ouchi et al., 2011). Therefore, obesity is associated with chronic-low grade inflammatory conditions (Ibrahim et al., 2010). Previous studies in human showed that with obesity, changes in transcriptional expression of lipolytic and lipogenic genes were more pronounced in VAT.

1.3.2 The role of white adipose tissue as endocrine organ

Besides its role in energy storage and supply, adipose tissue acts as a crucial active endocrine organ that releases and secretes several bioactive factors including amongst others chemokines, cytokines and proteins (Mohamed-Ali et al., 1998; Trayhurn and Wood, 2004). The secretome of WAT, the so called adipokinome, describes the WAT-derived, secreted proteins (Lehr et al., 2012a). Adipocyte-secreted factors are termed adipokines and so far, proteomic profiling approaches identified more than 600 potential secreted adipokines (Lehr, 2012b; Trayhurn and Wood, 2004).

Adipokines act in an auto-, para- or endocrine manner and thus execute both local and systemic physiological and pathophysiological effects including adipose tissue remodeling, systemic lipid and glucose metabolism, insulin sensitivity, inflammation and stress responses (Fasshauer and Bluher, 2015; Ouchi et al., 2011; Trayhurn and Wood, 2004).

Adipokines are often categorized by their function in inflammatory responses (Ouchi et al., 2011). The adipokines leptin, interleukine-6 (IL-6), chemerin and monocyte chemoattractant protein-1 (MCP-1) have been characterized by their pro-inflammatory activities (Figure 2, 3) (Ouchi et al., 2011). Leptin, discovered in 1994 and thus belongs to one of the first identified adipokines predominantly produced and secreted by SAT-derived adipocytes promoting WAT lipolysis and fatty acid oxidation while on a systemic level controls energy expenditure, thermogenesis, lipid metabolism and food intake (Ahima et al., 2000; Ceddia et al., 2000; Lehr

et al., 2012b; Zhang et al., 1994). Stimulation of adipose tissue organ cultures with IL-6 resulted in enhanced adipose tissue lipolysis while in 3T3-adipocytes, IL-6 has been described to induce insulin resistance (Rotter et al., 2003; Trujillo et al., 2004).

MCP-1 and chemerin act as inducers of fibrosis and adipocytes differentiation, respectively (Goralski et al., 2007; Sell et al., 2006). Further, adipocyte-derived MCP-1 has been associated with increased infiltration and activation of macrophages in WAT (Ibrahim et al., 2010; Trayhum et al., 2011). Well-described adipokines which exhibit anti-inflammatory properties are adiponectin, omentin-1, secreted frizzled-related protein 5 (sFRP5) and heme oxygenase-1 (HO-1) (Figure 1, 2) (Yamawaki et al., 2011). Omentin-1 and the more VAT adipocyte-specific adiponectin has been described to have insulin sensitizing abilities (Freedland et al., 2004; Ohashi et al., 2014; Tan et al., 2010). Thus, omentin-1 has been shown to promote glucose uptake in adipocytes (Yang et al., 2006). Adiponectin has been associated with a reduction in adipose-tissue inflammation while promoting fat storage in SAT (Kim et al., 2007). sFRP5 is suggested to mediate anti-inflammatory activities and adipogenesis while adipocyte-specific loss of sFRP5 has been associated with increased mitochondrial content and function (Mori et al., 2012; Ouchi et al., 2010). HO-1 is expressed and secreted by primary human adipocytes and its induction in adipocytes has been described to increase adiponectin levels and pre-adipocyte number but reduce adipocytes hypertrophy and pro-inflammatory cytokines (Kim et al., 2008; Lehr et al., 2012; Vanella et al., 2011, 2013). In rodents, the presence of HO-1 has been associated with attenuating diabetes and obesity whereas reduced HO-1 promoted insulin resistance and adiposity (Burgess et al., 2010; Li et al., 2007;).

In the state of obesity, the chronic and metabolic disturbances and alterations of the WAT phenotype further are associated with an altered adipokine secretion profile favoring the production and secretion of pro-inflammatory adipokines (e.g. leptin, chemerin, IL-6, MCP-1) that impair in an auto-/para- and endocrine manner the biological function of peripheral tissues including skeletal muscle and liver (Figure 2) (Lehr et al., 2012; Romacho et al., 2014). An increase in pro-inflammatory adipokine secretion along with enhanced ectopic accumulation of VAT during obesity is crucial in the development of systemic inflammation, insulin resistance, hyperinsulinemia, hyperglycemia, hypertriglyceridemia and thus the pathogenesis of T2D and NAFLD (Czech et al., 2017; Kloting et al., 2010; Romacho et al., 2014; Zhang et al., 2018).

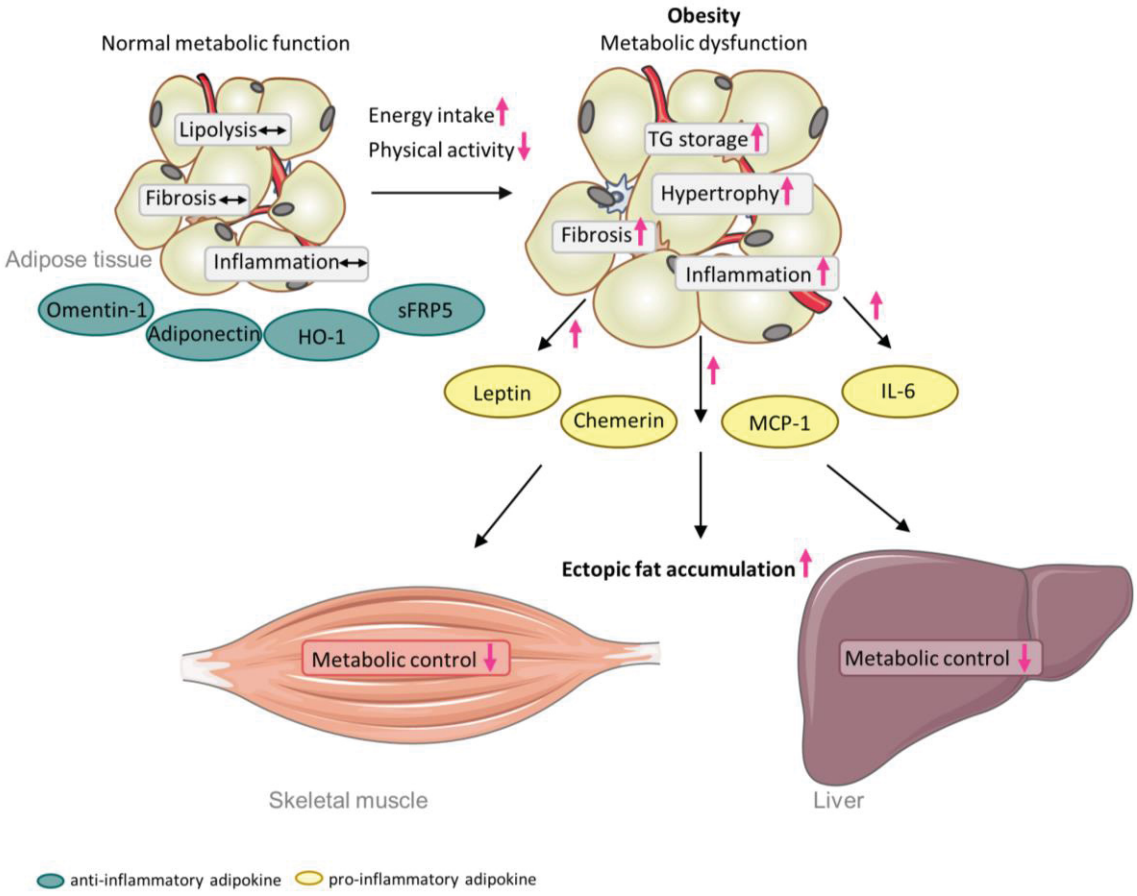

Figure 2. Adipose tissue phenotype in obesity. Under conditions with balanced energy intake adipose tissue exhibits a normal metabolic function linked with the release of ant-inflammatory adipokines. The obesity-related pathophysiological state promotes adipose tissue hypertrophy, inflammation, accumulation of TG and may lead to adipose tissue dysfunction and fibrosis. Impaired adipose tissue function is associated with the secretion of pro-inflammatory adipokines and induces ectopic fat accumulation in peripheral tissues which likely entails impaired metabolic function of skeletal muscle and liver. MCP-1, monocyte chemoattractant protein-1; sFRP5, secreted frizzled-related protein 5; TG, triglyceride.

1.4 The role of adipokines in inter-organ communication with skeletal muscle and liver

Due to secretion in the circulation, adipokines are important regulators of inter-organ crosstalk. Hence, adipokines affect on a systemic level metabolic functions and physiology of distinct peripheral tissues including skeletal muscle and liver. Skeletal muscle and liver express and secrete active substances that in turn serve as mediators for a bi-directional inter-tissue communication (Figure 3).

1.4.1 Cross-talk of adipose tissue and skeletal muscle

The skeletal muscle is the major regulatory tissue of glucose uptake and storage and thus modulating whole-body glucose disposal and insulin sensitivity (Meyer et al., 2002). *In vitro*, co-culture approaches of adipocytes and skeletal muscle cells and subjection of adipocyte-derived conditioned media to skeletal muscle cells resulted in lipotoxicity, decreased mitochondrial function, increased stress response and insulin resistance in skeletal muscle indicating a direct signaling between these organs (Dietze et al., 2002; Sell et al., 2006). Adipocyte-derived adiponectin has been shown to induce muscle fatty acid oxidation via AMPK stimulation as well as expression of peroxisome proliferator-activated receptor gamma coactivator 1-alpha (PGC1-α) resulting in enhanced mitochondrial content (Figure 3 A) (Iwabu et al., 2010; Turer et al., 2012; Yamauchi et al., 2002).

Leptin promotes insulin sensitivity by stimulation of skeletal muscle glucose uptake and fatty acid oxidation whereas reduces oxidative stress, inflammation and storage of triglycerides (Ceddia et al., 1998; Muoio et al., 1997; Sainz et al., 2010). Further, leptin has been described to have positive effects on skeletal muscle mass amongst others by decreasing the expression of the E3 ubiquitin ligases Muscle RING-finger protein 1 (MuRF1) and muscle atrophy F-box (MAFbx)/atrogin-1 (Hamrick et al., 2010; Sainz et al., 2009). Chemerin was demonstrated to induce insulin resistance in skeletal muscle cells resulting in reduced insulin-mediated glucose uptake (Sell et al., 2009).

Besides the identification of novel adipokines, several proteomic profiling studies have been focused on the secretome of skeletal muscle, termed the myokinome, representing skeletal muscle as a further active endocrine organ (Febbraio et al., 2005; Trayhum et al., 2011). The skeletal muscle secretes numerous distinct factors, called myokines, including amongst others hormones, cytokines and growth factors that exert multiple effects on processes including inflammation, systemic lipid and glucose metabolism and skeletal muscle growth (Pedersen et al., 2012). IL-6 has been described as the prototype for myokines since its discovery as a myokine in the year 2000. IL-6 exerts its effects either in an auto- and paracrine fashion or systemically (Steensberg et al., 2000). IL-6 increases fatty acid oxidation in skeletal muscle via AMPK activation while stimulated lipolysis in adipose tissue and thus is an essential modulator of energy metabolism (Van Hall et al., 2003; Pedersen et al., 2012).

The pro-inflammatory MCP-1 has been identified either as an adipokine as well as a myokine and is associated with promoting insulin resistance in both adipose tissues and skeletal muscle

(Figure 3 B) (Trayhum et al., 2011; Sell et al., 2006). The myokines profile has been shown to be altered in response to skeletal muscle contraction with increasing myokine levels upon physical activity (Lambernd et al., 2012; Nikolic et al., 2012; Raschke et al., 2013). Beyond the secretion of myokines, the skeletal muscle is a primary site for releasing essential metabolic fuels. Dependent on systemic energy demand, the skeletal muscle supplies glucose stored as glycogen and provides amino acids by protein breakdown amongst others serving as substrates for glucose production via gluconeogenesis in liver (Wolfe et al., 2006). Thus, the skeletal muscle is an important mediator in the inter-organ communication with distant peripheral tissues including adipose tissue and liver to maintain of whole-body homeostasis.

1.4.2 Cross-talk of adipose tissue and liver

Besides its role in detoxification processes and immune responses, the liver is a key metabolic organ that tightly controls systemic glucose and lipid homeostasis by storage, consumption, synthesis and delivery of lipids, carbohydrates and proteins (Nordlie et al., 1999). Thereby, the liver continuously interacts with distinct extrahepatic tissues including adipose tissue and skeletal muscle to coordinate systemic metabolisms.

Adipose tissue derived metabolites (e.g. NEFAs and glycerol) and adipokines directly enter the liver via the portal vein system (Komolka et al., 2014; Wronska and Kmiec, 2012;). Glycerol and NEFAs from adipose tissue are used for hepatic mitochondrial fatty acid β-oxidation and glucose production via gluconeogenesis (Rui et al., 2014; Perry et al., 2015). Adipocyte-secreted adiponectin has been described to have beneficial effects on liver mediated via hepatic adiponectin receptor 2 (Figure 3 A) (Yamauchi and Kadowaki, 2008). Adiponectin improves hepatic insulin resistance and mediates anti-inflammatory activities by promoting deacetylation of ceramide sphingolipids, inhibition of nuclear factor kappa-light-chain-enhancer of activated B-cells (NFκB) and suppression of pro-inflammatory cytokines and hepatic gluconeogenesis and thus glucose production (Combs et al., 2001; Holland et al., 2011; Kadowaki et al., 2006; Zhou et al., 2005). Further, adiponectin has been associated with anti-fibrotic properties and suppression of hepatic glucose production and lipid accumulation all found to be mediated by activation of AMPK (Adachi and Brenner, 2008; Kamada et al., 2003; Ouchi et al., 2011; Yamauchi et al., 2001, 2002).

Several studies demonstrated that leptin improves insulin sensitivity in liver resulting in improved insulin-mediated suppression of hepatic glucose production, however the

underlying mechanism are yet largely unknown (Figure 3 B) (Barzilai et al., 1997; Burcelin et al., 1999; Shimomura et al., 1999). WAT-derived IL-6 has been shown to induce anti-insulin-sensitizing effects in liver via a mechanism involving the induction of a suppressor of cytokine signaling 3 (SOCS-3) (Carey et al., 2006; Senn et al., 2003; Sabio et al., 2008). However, acute administration of IL-6 to healthy individuals showed no effects on systemic glucose homeostasis and thus insulin sensitivity suggesting that IL-6 effects highly depend on its site of action and time of exposure (Steensberg et al., 2003).

Although expressed in adipose tissue and muscle, the liver is the major site for fibroblast growth factor 21 (FGF21), one of the best described hepatokines (Figure 3) (Itoh, 2014). Hepatokines are factors released by the liver that act either in local but also endocrine manner, thus affecting metabolism of distant extrahepatic organs such as adipose tissue and skeletal muscle. FGF21 has been described to be induced during fasting by peroxisome proliferator-activated receptor alpha (PPARα) and involved in stimulation of lipid oxidation and thus improvement of insulin resistance and steatosis in liver (Badman et al., 2007; Gimeno et al., 2014; Fisher et al., 2014). In WAT, FGF21 has been associated with increased GLUT1 expression, lipid oxidation and reduced lipolysis resulting in overall improved glucose disposal and insulin sensitivity (Ge et al., 2011; Gimeno and Moller, 2014; Inagaki et al., 2007). An imbalance in the hepatokine production and secretion towards pro-inflammatory factors has been linked to pathophysiological changes including insulin resistance and the development of T2D and NAFLD (Xu et al., 2003; Zhang et al., 2018).

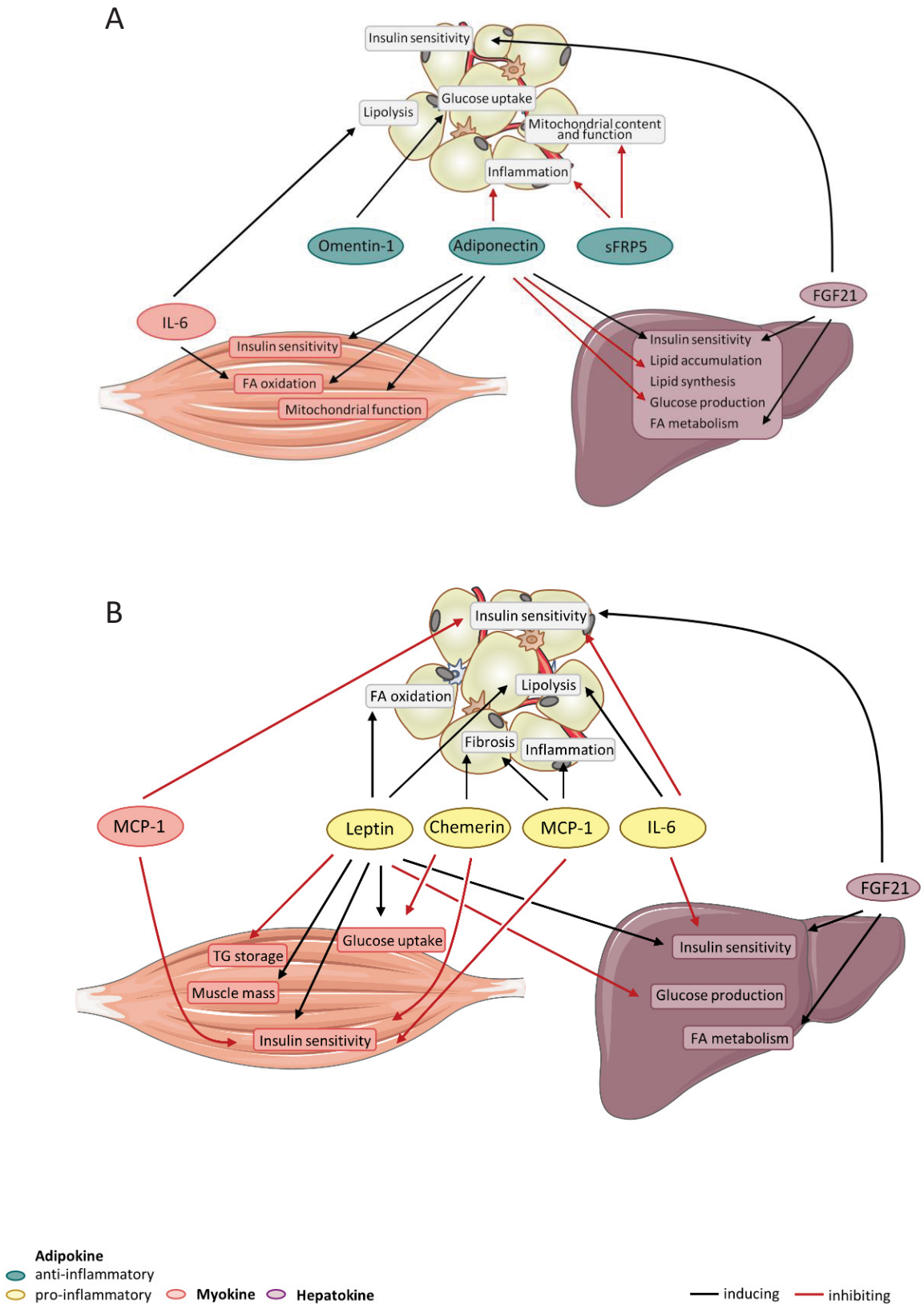

Figure 3. Metabolic cross-talk of adipose tissue, skeletal muscle and liver. Adipose tissue expressed and released bioactive factors, the adipokines. Adipokines exert their effects locally in an auto-/paracrine fashion and systemically by secretion in the circulation. On endocrine level and normal metabolic conditions, adipokines

affect metabolic function and physiology of distinct peripheral tissues including skeletal muscle and liver, by release of mainly ant-inflammatory adipokines (**A**). While skeletal muscle and liver express and secrete substances termed myokines and hepatokines, respectively that in turn serve as mediators for a bi-directional inter-tissue communication. Under adverse metabolic conditions, the adipokine secretion profile may shift towards more pro-inflammatory factors entailing dysregulation of skeletal muscle and liver (**B**). IL-6, interleukine-6; MCP-1, monocyte chemoattractant protein; sFRP5, secreted frizzled-related protein.

1.5 The Wnt signaling pathway in health and disease

The mammalian wingless-type MMTV integration site (Wnt) signaling pathway is crucial for the regulation of cell-fate decision, cell survival, proliferation and differentiation processes and contributes to the pathophysiology of tumorigenesis (Logan and Nusse, 2004). However, accumulating evidence also linked the Wnt signaling pathway to inflammation, the development of insulin resistance and type 2 diabetes (Abiola et al., 2009; Gustafson et al., 2013; Paalsgaard et al., 2012; Zhou et al., 2012). The regulation of the activity of the Wnt pathway is tightly controlled by its multiple components. In human and rodents, 19 different Wnt ligands have been identified that bind to a family of 10 distinct transmembrane frizzled receptors (FZD), and co-receptors, the most well-known being the low-density lipoprotein receptor-related proteins 5 and 6 (LRP5/6) (Niehrs, 2012). The interaction between Wnt ligand and FZD receptor regulates the activity of either the well-characterized canonical or the non-canonical Wnt pathway (Nusse and Clevers, 2017). The canonical Wnt pathway is activated amongst others by direct binding of Wnt ligands to FZD (Figure 4). Wnt signaling activation results in inhibition of glycogen synthase kinase 3β (GSK3β) and casein kinase-1-alpha (CK-1α), both components of the destruction complex together with adenomatous polyposis coli (APC) and axin, and thus prevent the phosphorylation and proteasomal degradation of β-catenin (Figure 4). Subsequently, β-catenin accumulates in the cytosol and translocates in the nucleus where it binds to T-cell factor/lymphoid enhancer factor (TCF/LEF) resulting in the transcriptional activation of numerous target genes such as *Axin2*, one of the first described targets (MacDonald et al., 2009; Jho et al., 2002). Inactivation of Wnt signaling in absence of Wnt ligands mediates the phosphorylation and ubiquitination of β-catenin followed by its proteasomal degradation and suppression of target gene expression. In contrast, the non-canonical, β-catenin-independent Wnt pathway is rather involved in the regulation of cell-polarity, calcium release and protein kinase c (PKC) activity via FZD signaling (Semenov et al., 2007).

Several secreted glycoproteins, including members of the secreted frizzled-related protein (sFRP) and Dickkopf (DKK) family have been described to be important modulators of the canonical Wnt signaling pathway by mechanisms including the direct binding of FZDs or the neutralization of Wnt ligands and thus exert inhibitory or activating effects on Wnt signaling (Bovolenta et al., 2008).

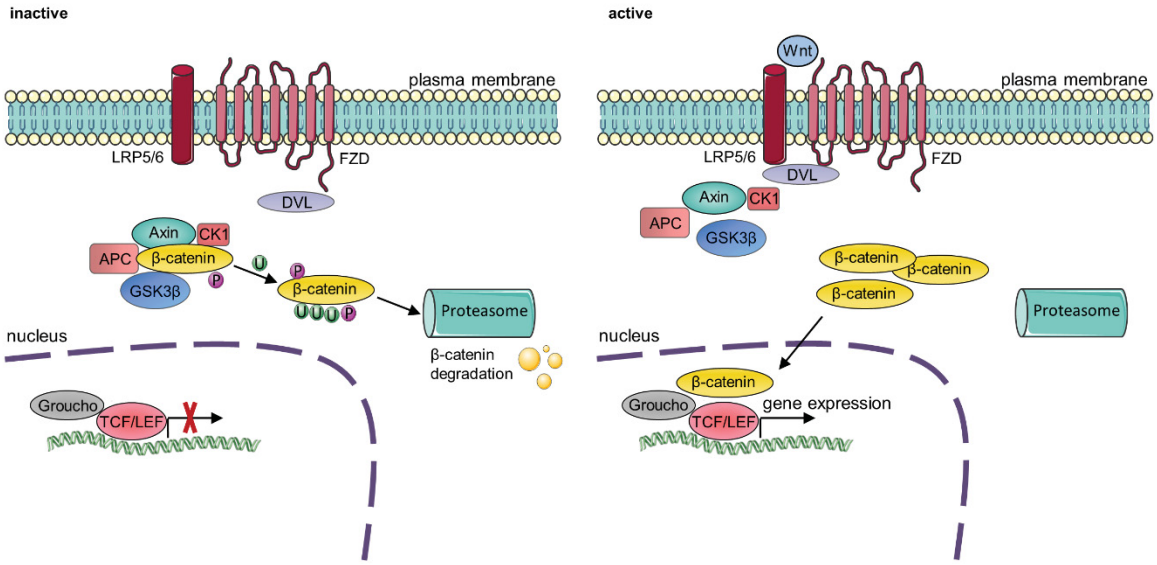

Figure 4. Canonical Wnt signaling pathway. The abscence of Wnt ligands results in inactivation of Wnt signaling by phosphorylation of β-catenin via CK1 and GSK3β, both components of the destruction complex together with APC and Axin (left panel). Phosphorylation of β-catenin results in its ubiquitination and degradation by the proteasome. Along with the absence of β-catenin and its nuclear exclusion, TCF/LEF form a nuclear, inhibitory complex with Groucho that suppresses gene expression. Binding of Wnt ligands to FZD or the LRP 5/6 co-receptor induces Wnt signaling and results in the recruitment of DVL to the plasma membrane (right panel). DVL mediates the inhibition of the destruction complex. Hence, β-catenin accumulates in the cytosol and translocates into the nucleus where it displaces Groucho by binding to TCF/LEF and induces gene expression. APC, adenomatous polyposis coli; CK1, casein kinase 1; DVL, disheveled; FZD, frizzled receptor; GSK3β, glycogen synthase kinase 3β; LRP, lipoprotein receptor-related protein; TCF/LEF, t-cell factor/lymphoid enhancer factor (modified according to Zhan et al., 2017).

Impaired Wnt signaling is implicated in the development of multiple metabolic dysfunctions like insulin resistance and diseases including T2D (Abiola et al., 2009; Paalsgaard et al., 2012; Zhou et al., 2012). An extensive investigation study revealed that single nucleotide polymorphism in the genes of the Wnt co-receptor *LRP5*, *Wnt5a* and *transcription factor 7-like 2* (*TCF7L2*) (also known as *TCF4*) are highly linked to obesity and the susceptibility of type 2 diabetes (Ferrari et al., 2004; Grant et al., 2006; Kanazawa et al., 2004).

Multiple studies demonstrated that the canonical Wnt signaling pathway strongly associated with inhibition of adipogenesis via mechanisms underlying suppression of peroxisome proliferator-activated receptor gamma (PPARG) and CCAAT/enhancer-binding protein alpha (CEBPA) (Bennett et al., 2002; Ross et al., 2000).

Moreover, interactions between the Wnt and insulin signaling pathway has been observed in several studies which take place on different molecular levels via distinct substrates and show highly cell-type specific effects. By performing LRP5 or insulin/ insulin-like growth factor-1 (IGF-1) receptor ablations in pre-adipocytes, Palsgaard et al. showed that the stimulatory effect of insulin on the phosphorylation of Akt and its substrate GSK3β not only depends on the presence of intact insulin/IGF-1 receptor but also on the Wnt co-receptor LRP5 suggesting that alterations in the Wnt signaling activity might contribute to pathophysiologies related to insulin resistance and T2D (Palsgaard et al., 2012). Further studies using liver-specific gain- and loss-of-function mice models for β-catenin, found that the insulin signaling on the phosphorylation levels of IRS, Akt and GSK3β were enhanced along with improved insulin tolerance in livers of mice deleted for β-catenin, whereas overexpression of β-catenin exerted reciprocal effects (Liu et al., 2011). Additionally, under fasting conditions β-catenin enhanced hepatic glucose production by rather binding to FoxO than TCF4 resulting in enhanced activity of FoxO and thus expression of key-rate limiting gluconeogenic genes (Liu et al., 2011). In contrast, in the skeletal muscle cell line C2C12, IRS-1, one of the key regulators of insulin signaling, was found to be a direct transcription target of the β-catenin-TCF4 axis, upregulated on gene and protein level in cells incubated with Wnt3a (Yoon et al., 2010). Further, these findings were accompanied by enhanced mitochondrial biogenesis and insulin-mediated phosphorylation of Akt as well as glycogen synthesis (Yoon et al., 2010) indicating that the activity of the β-catenin-TCF4 axis might be crucial for the prevention of insulin resistance in skeletal muscle. In line with these, the activation of the Wnt/β-catenin pathway in primary myotubes has been found to enhance the insulin effects on GLUT4-dependent glucose transport by inducing the Akt and AMPK pathways while inhibited the accumulation of intramyocellular lipids (Abiola et al., 2009).

1.5.1 Role of the Wnt proteins WISP1 and sFRP4 in health and disease

Recent proteomic and bioinformatic profiling studies identified proteins belonging to the Wnt signaling family as novel adipokines in humans and rodents including Wnt1-inducible signaling

pathway protein 1 (WISP1) and secreted frizzled-related protein 4 (sFRP4) (Ehrlund et al., 2013; Lehr et al., 2012; Murahovschi et al., 2015).

1.5.1.1 Structure, regulation and physiological action of WISP1

The extracellular matrix-associated WISP1, also known as CCN4, belongs to the family of secreted, homologous cysteine-rich CCN proteins and is a target of the canonical Wnt signaling pathway (Pennica et al., 1998; Xu et al., 2000). CCN family comprises six highly conserved members whereby the three first identified CCN proteins were decisive for the family name: cysteine-rich 61 (CYR61/CCN1), connective tissue growth factor (CTGF/CCN2), and nephoblastoma overexpressed (NOV/CCN3) (Jun and Lau, 2011). Pennica et al. identified three further CCN proteins the Wnt-inducible signaling pathway proteins among them WISP1/CCN4, WISP2/CCN5 and WISP2/CCN6 (Birgstock et al., 2003; Pennica et al., 1998). The human *WISP1* gene consists of four introns and five exons coding for 367 amino acids long WISP1 protein with a predicted molecular weight of 40 kDa (kilodalton) (2.2.8) (Figure 5). The full length WISP1 protein is characterized by four potential N-linked glycosylation sites and 38 conserved cysteine residues and prone to post-translational modifications (Inkson et al., 2008; Pennica et al., 1998). The modular structure of CCN proteins comprises an NH2-terminus exhibiting a secretory signal peptide followed by four conserved structural domains that are coded by distinct exons (Figure 5). These modules resemble the sequences of insulin-like growth factor binding protein (IGFBP), Von Willebrand factor type C repeat (VWFC), thrombospondin type I repeat (TSR) and a carboxyl-terminus (COOH) including a cysteine knot-like domain (CTCK) except for CCN5 lacking this COOH module (Chen et al., 2009; Pennica et al., 1998). Thereby, the IGFBP module has been shown to potentially interfere with IGF1/2 signaling, the VWC domain consists a binding site for bone morphogenetic protein (BMP) and transforming growth factor β (TGF-β) and exhibits oligomerization properties, the TSR interferes with several cell-surface proteins such as heparin, fibronectin and collagen and the COOH part has heparin-binding and oligomerization properties (Berschneider and Konigshoff, 2011; Chen and Lau, 2009; Holbourn et al., 2008; Leask and Abraham, 2006).

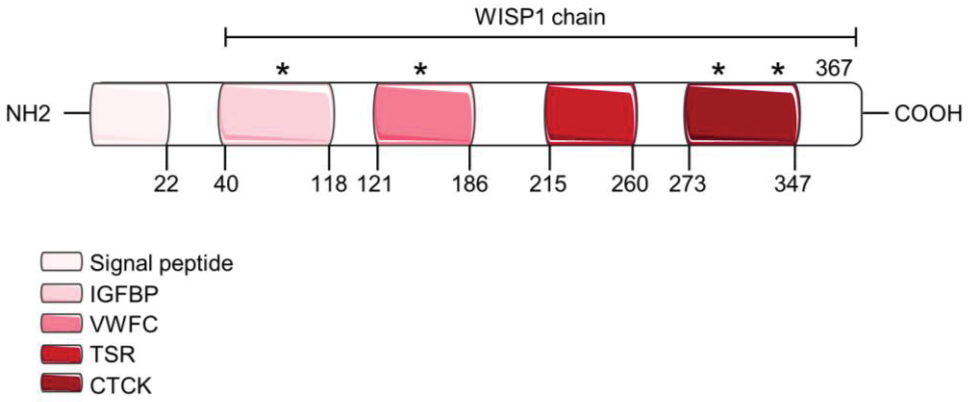

Figure 5. Human WISP1 protein structure. The WISP1 protein comprises a NH2-terminal signal peptide followed by the main chain including an IGFBP domain, a VWFC and TSR motif and is terminated by a COOH-terminus containing a CTCK domain. IGFBP, insulin-like growth factor binding protein; VWFC, Von Willebrand factor type C repeat; TSR, thrombospondin type I repeat; CTCK, cysteine knot-like domain. * indicated potential N-linked glycosylation sites.

Human *WISP1* mRNA is downregulated in adult tissue but still expressed in pancreas, heart, kidney, ovary, spleen and small intestine whereas no or rare levels were found in skeletal muscle, liver, brain, breast, testis, prostate, thymus, colon and peripheral blood leukocytes (Pennica et al., 1998). The expression and abundance of WISP1 is tightly regulated during development by distinct stimuli on transcriptional and translational level including growth factors, oxygen deprivation, steroid hormones and inflammatory cytokines suggesting that WISP1 is crucial for the regulation of development processes and tissue remodeling (Figure 6A) (Jun and Lau, 2011).

First studies identified WISP1 as a classical target gene of the canonical Wnt/β-catenin pathway induced by the Wnt ligands Wnt1 and Wnt3a (Berschneider et al., 2011; Calvisi et al., 2005; Pennica et al., 1998; Xu et al., 2000). Xu et al. found that Wnt1 induced *WISP1* expression *in vitro* by activation of cyclic AMP response element-binding protein (CREB) (Xu et al., 2000). *In vitro* studies in cardiac fibroblast showed that the tumor necrosis factor-α (TNF-α) induced *WISP1* expression via activation of ERK1/2 and CREB signaling (Venkatachalam et al., 2009). In human lung fibroblast, TGF-β and TNF-α enhanced WISP1 expression and protein and linked WISP1 to pulmonary fibrosis (Klee et al., 2016). Further, WISP1 was enhanced by interleukin-1β (IL-1β) and TNF-α in ventricular myocytes while in cardiomyocytes WISP1 increased its own expression (Colston et al., 2007; Venkatesan et al., 2010). In primary murine osteoblasts, TGF-β and BMP2 enhanced whereas cortisol inhibited

WISP1 expression (Parisi et al., 2006). BMP3 which has been identified to be upregulated with adiposity in rodents, increased *WISP1* expression and induced proliferation of mesenchymal-derived adipocytes (Cernea et al., 2016). WISP1 levels were found to be aberrantly increased in numerous cancers including breast cancers and lung cancer (Berscheinder et al., 2011; Margalit et al., 2003; Xie et al., 2001). However, *WISP1* expression was also increased in lung fibrosis, in cardiac fibroblast and in the myocardium upon myocardial infarction (Berscheinder et al., 2011; Colston 2007; Venkatachalam et al., 2009). WISP1 expression and abundance have been found to be upregulated during human adipogenesis, whereas levels were decreased during adipocyte differentiation in mice (Ferrand et al., 2017; Murahovschi et al., 2015). WISP1 induction by Wnt signaling and overexpression of WISP1 has been described to result in inhibition of the adipogenic marker PPARγ and lipid accumulation in murine pre-adipocytes (Ferrand et al., 2017). Moreover, recent studies reported that insulin induced *WISP1* expression *in vitro* in human cultures adipocytes (Murahovshi et al., 2015).

The structure of the modular domains of WISP1 controls cell-type specificity and multiple cellular interactions involved in development processes including differentiation, cell growth and survival, apoptosis, and gene expression (Jun and Lau, 2011). WISP1 has been found to be crucial for wound healing, and tissue repair. Impaired WISP1 expression and signaling have been shown to play a pivotal role in inflammation and the pathogenesis of fibrosis, atherosclerosis and cancer (Figure 6B) (Berschneider et al., 2011; Gurbuz and Chiquet-Ehrismann, 2015; Jun and Lau, 2011; Zhong et al., 2017). Several studies demonstrated that WISP1 exerts its effects by modulating the activity of the PI3K/Akt signaling pathway that is involved in many cellular processes including, growth, survival, apoptosis and insulin signaling (Colston et al., 2007, Murahovschi et al., 2015; Su et al., 2002, Venekatesan et al., 2010).

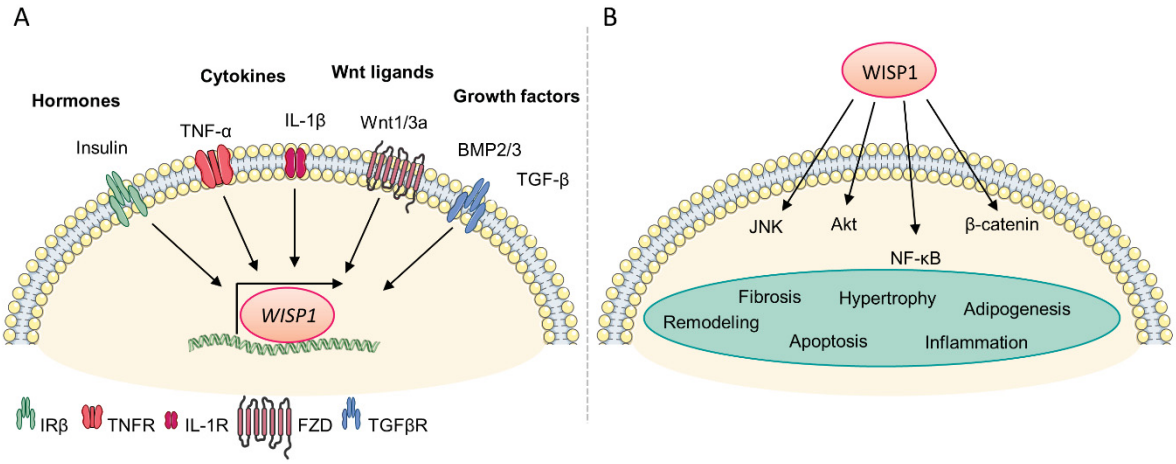

Figure 6. Transcriptional regulation and physiological action of WISP1. Numerous extracellular factors including hormones, cytokines and growth factors induce *WISP1* gene expression (**A**). WISP1 mediates multiple molecular and cellular effects on JNK, Akt, NF-κB and β-catenin signaling amongst others involved in fibrosis, tissue remodeling, inflammation, hypertrophy and adipogenesis (**B**). JNK, c-Jun N-terminal kinase; IRβ, insulin receptor β; TNFR, tumor necrosis factor receptor; IL-1R, interleukin-1 receptor; TGFβR, transforming growth factor β receptor (modified according to Jun and Lau, 2011).

1.5.1.2 WISP1 as an adipokine

Emerging proteomic profiling approaches and *in vitro* studies focus on the identification of potential novel adipokines among them several factors belonging to the Wnt signaling family (Dahlman et al., 2012; Lehr et al., 2012; Ouchi et al., 2010). Recently, WISP1 has been identified as an adipokine in mice and human expressed and secreted from adipocytes (Ferrand et al., 2017; Murahovschi et al., 2015;). Furthermore, emerging evidence suggest an association of WISP1 with obesity (Barchetta et al., 2017; Murahovschi et al., 2015). WISP1 expression and secretion from SAT were decreased by diet-induced weight loss in humans whereas increased in adipose tissue of high-fat diet-induced obese mice (Murahovschi et al., 2015). Ferrand et al. illustrated increased expression levels of WISP1 in adipose tissue of diet-induced obese mice and leptin-deficient *ob/ob* mice (Ferrand et al., 2017).

1.5.1.3 Structure and physiological function of sFRP4

sFRP4 is one of the five family members of sFRPs (sFRP1-5) in humans. Thereby, sFRP4 and sFRP3 have a high similar genomic organization encoded by six exons whereas sFRP1, sFRP2 and sFRP5 are closely related and encoded by three exons (Bovolenta et al., 2008; Garcia-Hoyes et al., 2004). The coding sequence of the human *sFRP4* mRNA transcript comprises 1041

base pairs (bp) (2.2.8). Human sFRP4 protein is predicted to have a molecular weight of 39.9 kDa containing 346 amino acids (Carmon and Loose, 2010). sFRP4 exhibits a modular protein structure consisting of two independent domains: i) an amino-terminus (NH2-terminus) exhibiting a secretion signal peptide, followed by ii) the sFRP4 main chain including a cysteine-rich domain (CRD) (FZ-domain) and terminated by a carboxy-terminus (COOH-terminus) (Figure 7) (Bovolenta et al., 2008; Carmon and Loose, 2010; Rattner et al., 1997). The CRD region comprised ten conserved cysteine residues forming disulfide bridges and has a high sequence homology to the extracellular CRD region and Wnt ligand binding site in FZDs (, Bovolenta et al., 2008; Roszmus et al., 2001). The COOH-terminus has six cysteine residues forming three disulfide bridges and consists of a positively charged residues segment with potential heparin-binding properties and further exhibits nine serine/threonine phosphorylation sites as targets for specific kinases in humans (Chong et al., 2002; Hoang et al., 1996; Uren et al., 2000). These segments of the COOH-terminal part characterized the netrin-related motif (NTR). sFRP4 has been found to be expressed in multiple tissues amongst others heart, adipose tissue, ovary, mammary gland, pancreas and brain (Carmon and Loose, 2010).

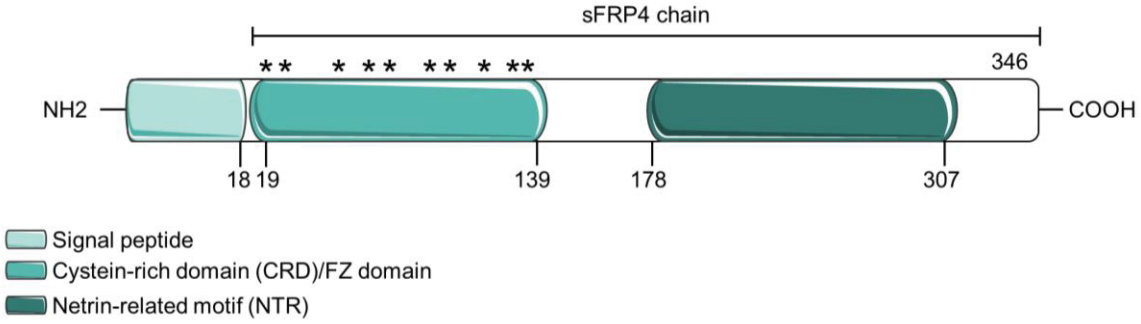

Figure 7. Human sFRP4 protein structure. The sFRP4 protein comprises a NH2-terminal signal peptide followed by the main chain including a CRD domain, a netrin-related motif and terminated by a COOH-terminus. * indicated conserved cysteines within the CRD region (modified according to Carmon and Loose, 2010).

The modular structure of sFRPs entails distinct functions and cell-specificities indicating a number of mechanisms by which sFRPs exert their effects.

Several biochemical and *in vitro* studies focused on the underlying mechanisms of sFRPs as soluble modulator proteins in the interaction with distinct CRD regions in FZDs, multiple Wnt

ligands and other Wnt-independent molecules including cell surface receptors and integrins (Bafico et al., 1999).

Distinct models have been proposed for the physical interaction of sFRPs with other Wnt signaling proteins including i) binding of sFRPs with the CRD of FZDs to form homo- and heterodimeric complexes resulting in inhibition of Wnt signaling, ii) sFRPs enhanced Wnt signaling by binding of both, Wnt ligand and FZD, and thus promote the interaction of the components, iii) sFRPs function as a classical antagonist of Wnt signaling by binding specific Wnt ligands via the CRD or NTR domain. The latter described mechanism has been verified in several *in vitro* studies (Bovolenta et al., 2008; Leyns et al., 1997; Lin et al., 1997). Carmon et al. found that sFRP4 inhibited Wnt7a-induced β-catenin and non-canonical JNK signaling pathway by sequestering Wnt7a and thus prevented endometrial cell proliferation indicating sFRP4 as a potential tumor suppressor (Carmon et al., 2008). In contrast, Constantinou et al. showed that sFRP4 promoted differentiation of mammary epithelial cells by inhibiting Wnt3a-induced activation of β-catenin and Akt signaling (Constantinou et al., 2008). Although, in studies using plasmon-resonance approaches have been found that sFRP4 bound Wnt3a in a nanomolar range, sFRP4 was not able to inhibit Wnt3a-mediated β-catenin signaling in fibroblast cells (Wawrzak et al., 2007).

sFRP4 has been implicated in distinct cellular interactions including differentiation, adipogenesis, stress response and apoptosis (Lacher et al., 2003; Maganga et al., 2008; Muley et al., 2010; Visweswaran et al., 2015). Further, sFRP4 has been shown to reduce insulin secretion and exocytosis in pancreatic β-cells via decreased expression of islets calcium channels via activation of canonical β-catenin-TCF-signaling but independent of Wnt ligands. Moreover, pancreatic sFRP4 expression and release were stimulated by IL-1β indicating an association of sFRP4 with inflammation (Mahdi et al., 2012). In cardiomyocyte-like cells, sFRP4 inhibited cardiac differentiation by binding to integrin α1β1 resulting in focal adhesion kinase (FAK) activation followed by inhibition of cardiac gene expression (Tian et al., 2016).

1.5.1.4 sFRP4 as an adipokine

Previously, Lehr and colleagues identified sFRP4 as a novel adipokine, expressed and secreted from primary human adipocytes (Lehr et al., 2012). Studies by Ehrlund et al. confirmed sFRP4 as an adipokine, expressed and released from human white adipose tissue, from adipocytes as well as the stromal vascular fraction and further linked sFRP4 to visceral adiposity (Ehrlund

et al., 2013). The role of sFRP4 as an adipokine has aroused its interest in the settings of obesity and T2D. Recent studies revealed that sFRP4 serum levels were elevated in individuals with type 2 diabetes, even several years before the diagnosis of diabetes (Mahdi et al., 2012). While other investigations found increased circulating sFRP4 levels in individuals with obesity but independent of type 2 diabetes (Garufi et al., 2015). Circulating sFRP4 has been demonstrated to associate with insulin sensitivity and BMI (Anand et al., 2016; Garufi et al., 2015). In line, BMI has been described as a strong predictor for sFRP4 (Brix et al., 2016).

1.6 Objectives

Several proteomic approaches and molecular studies focused on the characterization of the secretome of WAT that aimed to identify potential novel, bioactive proteins, known as adipokines. In the circulation released adipokines are crucial mediators in the communication with distinct peripheral tissue including skeletal muscle and liver. Here, adipokines exert multiple direct or indirect effects that amongst others may result in the regulation of energy homeostasis and metabolism dependent on the adipokine´s nature. During obesity, adipose tissue undergoes remodeling processes associated with adipose tissue dysfunction and an altered adipokine secretion profile. Hence, adipokines frequently have been linked to obesity-related metabolic impairments that might be involved in the development of insulin resistance and severe metabolic disorders including T2D and NAFLD.

Recent proteomic and *in vitro* studies identified WISP1 and sFRP4 as novel adipokines in humans and mice (Ehrlund et al., 2013; Lehr et al., 2012; Murahovschi et al., 2015).

Although clinical studies suggest an association of WISP1 and sFRP4 with obesity, insulin sensitivity and/or T2D, available data on their potential relevance and involvement in the pathophysiology of obesity and T2D are limited. Especially, so far very little is known about the functional role of these adipokines and their interference with insulin action in two major insulin-responsive tissues, skeletal muscle and liver.

Hence, the first purpose of this thesis aimed to elucidate the role of WISP1 *in vivo* in obesity and T2D combined with its impact on insulin action *in vitro* in primary human skeletal muscle cells and murine hepatocytes. For this purpose, serum samples and adipose tissue biopsies of normal-weight and obese men with and without T2D were screened for WISP1 and associated with important variables for insulin sensitivity and resistance, glycemic control and

inflammation. *In vitro*, the effects of WISP1 on insulin action in skeletal muscle cells and hepatocytes have been explored on molecular signaling level and functional on skeletal muscle glycogen synthesis and hepatic gluconeogenic gene expression.

The second aim of this thesis purposed to explore the association of sFRP4 with obesity and T2D in humans and the contribution of adipose tissue to the circulating sfrp4 pool *in vivo* in mice as well as the direct impact of sFRP4 on energy, glucose and lipid metabolism in skeletal muscle cells and hepatocytes *in vitro*. Therefore, *sFRP4* expression has been analyzed in adipose tissue biopsies of obese men with and without T2D and correlated with indices of insulin resistance and metabolic variables including glucose and triglyceride levels. The functional role of sFRP4 on energy metabolism, protein catabolism and insulin action in skeletal muscle cells has been elucidated on molecular signaling level and by functional studies revealing its impact on mitochondrial function, glycolysis, fatty acid uptake and protein breakdown *in vitro*.

The proposed role of adipose tissue to be an important origin for sFRP4 has been explored by the examination of *sfrp4* expression in important insulin-responsive target tissues and its abundance in blood of C57Bl6 mice and lipodystrophic aP2-SREBP-1c mice that lack adipose tissue. The impact of sFRP4 on insulin signaling and the regulation of mitochondrial function, glucose and lipid metabolism in liver has been analyzed in isolated murine hepatocytes of healthy C57Bl6 mice. Thereby, the direct effect of sFRP4 on the expression and protein abundance of crucial regulatory molecular factors as well as on insulin-mediated gluconeogenesis, glycogen-synthesis, fatty acid metabolism and lipid synthesis was studied. To unravel the role of sFRP4 on insulin action in healthy and diseased livers, hepatocytes isolated from aP2-SREBP-1c mice that already displayed a metabolic impaired phenotype were used *in vitro*. In addition, the impact of sFRP4 on the secretory protein profile from hepatocytes of both mice genotypes was investigated by comprehensive analyses of the hepatocyte´s secretomes.

2 Material and Methods

2.1 Material

2.1.1 Instruments and disposables

Conventional instruments belonging to the standard laboratory equipment are not listed in the Table below.

Table 3. Instruments used in the study.

Instruments	Manufacturer (name, location)
AE31 Trinocular inverted microscope	Motic, Wetzler, Germany
Analytical Balance	Sartorius, Göttingen, Germany
BECKMAN COULTER LS 6000LL/LS 6000IC	BECKMAN COULTER, Krefeld, Germany
Electronic Precision Balance U4100	Sartorius, Göttingen, Germany
Heracell™ 240i CO_2 incubator	Thermo Fisher Scientific, Darmstadt, Germany
Heraeus LaminAir HB 2448 S GS	Thermo Fisher Scientific, Darmstadt, Germany
Heraeus™ Multifuge™ X3 Zentrifuge	Thermo Fisher Scientific, Darmstadt, Germany
iMark Microplate Reader	Biorad Laboratories, Munich, Germany
Maxwell® 16 Instrument	Promega, Mannheim, Germany
Mini PROTEAN Tetra System	Biorad Laboratories, Munich, Germany
Mini Trans-Blot®	Biorad Laboratories, Munich, Germany
Molecular Imager® VersaDoc™ MP 4000 system	Biorad Laboratories, Munich, Germany
Moticam Pro 282B	Motic, Wetzler, Germany
Multiplex Immunoassay Bioplex, Bio-Plex™ Protein Array System	BioRad, Munich, Germany
NanoDrop™ 2000/2000c spectropmeter	Thermo Fisher Scientific, Darmstadt, Germany
Neubauer counting chamber	BRAND®, Wertheim, Germany
Orbital shaker	Assistent GmbH, Altnau, Switzerland
Peristaltic pump	Gilson's MINIPULS® 3, Middleton, USA
Power Pac Basic power supply	Biorad Laboratories, Munich, Germany
PURA water bath	Julabo, Seelbach, Germany
QIAcube (110) robotic workstation	QIAGEN, Hilden, Germany
Reaxtop shaker	Heidolph, Schwabach, Germany
Spacer plates for SDS gels	Biorad Laboratories, Munich, Germany

Instruments	Manufacturer (name, location)
Sprout® Mini Centrifuge, HS120301	Heathrow Scientific, Vernon Hills, IL, USA
StepOnePlus Real-time PCR system	Applied Biosystems, Darmstadt, Germany
T100™ thermal cycler	Biorad Laboratories, Munich, Germany
Table centrifuge 5417 R	Eppendorf, Wesseling-Berzdorf, Germany
Tecan Infinite 200 reader	Tecan, Maennersdorf, Germany
Thermomixer comfort	Eppendorf, Wesseling-Berzdorf, Germany
Tissue Lyser II	QIAGEN, Hilden, Germany
XF^{e}96 extracellular flux analyzer	Agilent Technologies, Santa Clara, CA, USA

Table 4. Disposables used in the study.

Disposables	Manufacturer (name, location)
96-well high-binding assay plates	Sarstedt, Nümbrecht, Germany
Cell culture plates, sterile (6-, 48-, 96-well)	Greiner Bio-One, Frickenhausen, Germany
Cell culture plates, sterile (12-well)	VWR, Darmstadt, Germany
Cell scraper	Sarstedt, Nümbrecht, Germany
ClearLine® cell strainers, 70 µm	Kisker Biotech, Steinfurt, Germany
Electrode paper NovaBlot™	GE Healthcare, Freiburg, Germany
Falcon® cell culture dishes, sterile	VWR, Darmstadt, Germany
Immobilon-P Membran, PVDF, IPVH00010	Merck Chemicals GmbH, Darmstadt, Germany
Injekt®-F syringe, 1 ml	B. Braun, Hessen, Germany
MicroAmp® Fast Optical 96-Well Reaction Plate	Thermo Fisher Scientific, Darmstadt, Germany
MicroAmp® Optical Adhesive Film	Thermo Fisher Scientific, Darmstadt, Germany
Rotlabo®-syringe filter, sterile, P666.1	Carl Roth, Karlsruhe, Germany
Stainless Steel Beads, 5 mm	QIAGEN, Hilden, Germany
Standard laboratory, normal-caloric chow	Ssniff, Soest, Germany
Sterican® cannula G 26 / ø 0,45 x 25 mm	B. Braun, Hessen, Germany
Steritop™ filter unit	Merck Chemicals GmbH, Darmstadt, Germany
Surgical blades	VWR, Darmstadt, Germany

2.1.2 Chemicals

All standard chemicals and self-mixed components that were used for buffers and solutions were purchased from AppliChem or Sigma-Aldrich and are not listed in the Table below.

Table 5. Used chemicals.

Chemicals	Manufacturer (name, location)
[^{14}C]-acetate	PerkinElmer Cellular Technologies GmbH, Hamburg, Germany
[^{14}C]-palmitic acid	PerkinElmer Cellular Technologies GmbH, Hamburg, Germany
[9,10-^{3}H(N)]-Palmitic Acid	PerkinElmer Cellular Technologies GmbH, Hamburg, Germany
10% formalin, neutral buffered	Sigma-Aldrich, Darmstadt, Germany
2-Deoxy-D-glucose (2-DG)	Sigma-Aldrich, Darmstadt, Germany
Ammonium persulfate (APS)	Roth, Karlsruhe Germany
Antibiotic-Antimycotic Solution (100x)	Gibco®, Thermo Fisher Scientific, Darmstadt, Germany
Bovine serum albumin (BSA) Fraction V, fatty acid free	Carl Roth, Karlsruhe, Germany
Bromphenol Blue	AppliChem GmbH, Darmstadt, Germany
BSA Fraction V, very low endotoxin	Carl Roth, Karlsruhe, Germany
Collagenase type IV	Worthington Biochemical Corp., Lakewood, NJ
Complete Protease Inhibitor Cocktail	Roche, Mannheim, Germany
D-[^{14}C(U)]-glucose (2 µCi/mL)	PerkinElmer Cellular Technologies GmbH, Hamburg, Germany
D-glucose	AppliChem GmbH, Darmstadt, Germany
Dimethyl sulfoxide (DMSO)	Sigma-Aldrich, Darmstadt, Germany
Disodium hydrogen phosphate dihydrate ($Na_2HPO_4 \bullet 2H_2O$)	Sigma-Aldrich, Darmstadt, Germany
Dithiothreitol (DTT)	VWR, Darmstadt, Germany
Fetal bovine serum (FBS)	Biochrom GmbH, Berlin, Germany
GlutaMAX™ (100x)	Gibco®, Thermo Fisher Scientific, Darmstadt, Germany
Glycogen from rabbit liver Type III	Sigma-Aldrich, Darmstadt, Germany
Hepes PUFFERAN®	Carl Roth, Karlsruhe, Germany

Chemicals	Manufacturer (name, location)
Horse serum	Gibco®, Thermo Fisher Scientific, Darmstadt, Germany
Human serum albumin, A1887	Sigma-Aldrich, Darmstadt, Germany
Insulin from porcine pancreas	Sigma-Aldrich, Darmstadt, Germany
L-carnitin	Sigma-Aldrich, Darmstadt, Germany
L-glutamine	Sigma-Aldrich, Darmstadt, Germany
MEM NEAA (100x)	Gibco®, Thermo Fisher Scientific, Darmstadt, Germany
MEM Vitamin Solution (100x)	Gibco®, Thermo Fisher Scientific, Darmstadt, Germany
Nonfat dried milk powder	AppliChem GmbH, Darmstadt, Germany
Nonidet P-40 (NP-40)	Sigma-Aldrich, Darmstadt, Germany
Oil red O, O-0625	Sigma-Aldrich, Darmstadt, Germany
Penicillin- Streptomycin (100x)	Thermo Fisher Scientific, Darmstadt, Germany
Percoll gradient (Easycoll)	Biochrom GmbH, Berlin, Germany
PhosSTOP Phosphatase Inhibitor	Roche, Mannheim, Germany
Precision Plus Protein™ Standard	Biorad Laboratories, München, Germany
Rat tail type-I collagen stock (4 mg/ml)	CellSystems®, Troisdorf, Germany
Rotiszint® eco plus	Carl Roth, Karlsruhe, Germany
SDS (sodium dodecyl sulfate)	AppliChem GmbH, Darmstadt, Germany
Sodium acetate	AppliChem GmbH, Darmstadt, Germany
Sodium bicarbonate ($NaHCO_3$)	Merck Chemicals GmbH, Darmstadt, Germany
Sodium bicarbonate ($NaHCO_3$) solution (7.5%)	Thermo Fisher Scientific, Darmstadt, Germany
Sodium deoxycholate	AppliChem GmbH, Darmstadt, Germany
Sodium dihydrogen phosphate monohydrate ($NaH_2PO_4 \bullet H_2O$)	Sigma-Aldrich, Darmstadt, Germany
Sodium lactate	AppliChem GmbH, Darmstadt, Germany
Sodium pyruvate (100 mM)	Gibco®, Thermo Fisher Scientific, Darmstadt, Germany
Tetraethylethylenediamin (TEMED)	Roth, Karlsruhe Germany
Tetrasodium Pyrophosphate Decahydrate ($Na_4P_2O_7 \bullet 10H_2O$)	Sigma-Aldrich, Darmstadt, Germany
TriPure isolation reagent	Roche Diagnostics, Mannheim, Germany

Chemicals	Manufacturer (name, location)
Tris(hydroxymethyl)aminomethane (TRIS)	Roth, Karlsruhe Germany
Trypan blue solution (0.4%) Tween® 20	Sigma Aldrich, St Louis, MO, USA AppliChem GmbH, Darmstadt, Germany
β-Mercaptothanol	Thermo Fisher Scientific, Darmstadt, Germany

2.1.3 Buffers and solutions

Table 6. Used buffers and solutions.

Buffers and solutions	Formulation
0.2% trypan blue working solution	1:2 (v/v) dilution of 0.4% trypan blue solution in 1x phosphate-buffered saline (PBS)
1x HANK´S Buffered Salt Solution (HBSS) buffer	1:5 (v/v) dilution of 5x HBSS in sterile 1x PBS
5x HBSS buffer	26.65 mM KCl, 2.2 mM KH_2PO_4, 1.7 mM Na_2HPO_4, 0.69 M NaCl, 20.85 mM $NaHCO_3$, 27.8 mM glucose, 2.5 mM EGTA, 125 mM Hepes, add 1000 ml H_2O (pH 7.4)
5x Laemmli sample buffer	312.5 mM Tris-HCl (pH 6.8), 10% SDS, 50% glycerol, 500 mM DDT, 0.01% bromphenol blue
90% Percoll working solution	Percoll gradient diluted in 10x PBS
Collagen-coating solution (50 µg/ml)	1.25% of collagen stock (4 mg/ml) diluted in 1x PBS, for Seahorse experiments diluted in 0.02 M acetic acid
Complete Protease working solution	1 tablet dissolved in 1ml H_2O
Liver perfusion buffer	1x HBSS including 0.5 mM EGTA and 25 mM HEPES
Membrane Stripping buffer	20 ml 10% SDS, 12.5 ml 0.5M Tris-HCl (pH 6.8), 67.5 ml H_2O, 0.8 ml β-mercaptoethanol
Oil red O stock	0.7 g Oil red O dissolved in 200 ml isopropanol
Oil red O working solution	60% (v/v) of Oil red O stock diluted in H_2O
PhosSTOP working solution	1 tablet dissolved in 1ml H_2O
Rat tail type-I collagen	CellSystems®, Troisdorf, Germany

Buffers and solutions	Formulation
Resolving gel (8%)	4 ml 30% acrylamide, 3.78 ml 0.5 M Tris-HCl (pH 8.8), 150 µl 10% SDS, 7.3 ml H_2O, 15 µl TEMED, 75 µl 10% APS
RIPA lysis buffer	30 mM Tris-HCl (pH 7.5), 1 mM EDTA, 150 mM NaCl, 0.5% Triton X-100, 0.5% Na-deoxycholate (Na-DOC) supplemented with 1:10 (v/v) of Complete Protease Inhibitor working solution and 1:10 (v/v) PhosStop Phosphatase Inhibitor cocktail working solution
SDS-PAGE running buffer (1x)	25 mM Tris, 190 mM glycine, 0.1% SDS
Seahorse cell lysis buffer	10 mM Tris-HCl, 10 mM $Na_2HPO_4 \bullet 2H_2O$, 10 mM $NaH_2PO_4 \bullet H_2O$ (pH 7.5), 130 mM NaCl, 10 mM $Na_4P_2O_7 \bullet 10H_2O$, 1% Triton X-100
Stacking gel (4%)	1.98 ml 30% acrylamide, 3.78 ml 0.5 M Tris-HCl (pH 6.8), 150 µl 10% SDS, 9 ml H_2O, 15 µl TEMED, 75 µl 10% APS
TBS-T (Tris-buffered saline with Tween® 20) wash buffer	20 mM Tris (pH 7.5), 150 mM NaCl, 0.1% Tween® 20
Western Blot transfer buffer (1x)	25 mM Tris, 190 mM glycine, 20% methanol

2.1.4 Cell culture and assay medium and commercial cells

All media used for culture and maintenance of cells and assay media are listed in the Table below and were purchased from Gibco®, Thermo Fisher Scientific (Darmstadt, Germany), if not stated otherwise.

Table 7. Cell culture media used in this study.

Media	Supplements
α-modified Eagle's (αMEM)/Ham's F-12 (hSkMC growth medium) + supplement pack for primary human skeletal muscle cells (hSkMC)	5% fetal bovine serum (FBS), 50 µg/ml bovine fetuin, 10 ng/ml epidermal growth factor, 1 ng/ml basic fibroblast growth factor, 10 µg/ml insulin, 0.4 µg/ml dexamethasone, 2.2 g/l $NaHCO_3$ and 0.2% antibiotic-antimycotic mixture
αMEM (hSkMC differentiation medium)	2% horse serum, 2.2 g/l $NaHCO_3$ and 0.2% antibiotic-antimycotic solution

Media	Supplements
Dulbecco's modified Eagle'smedium (DMEM), 41966 (C2C12 growth medium)	10% FBS and 0.2% penicillin-streptomycin mixtures
DMEM (C2C12 differentiation medium)	2% horse serum and 0.2% penicillin-streptomycin mixtures
DMEM, 22320-022 (liver digestion buffer)	100 units/ml or 130 units/ml collagenase IV, 1 mM sodium pyruvate and 2% antibiotic-antimycotic mixtures
DMEM, 22320-022 (washing medium)	10% FBS 1 mM sodium pyruvate, 1 µM dexamethasone, 0.1 µM insulin and 2% antibiotic-antimycotic mixtures
DMEM/F-12 + GlutaMAXTM, 31331-028 (hepatocyte plating medium)	10% FBS, 1.5 mM sodium pyruvate, 1 µM dexamethasone, 0.1 µM insulin and 2% antibiotic-antimycotic mixtures
DMEM/F-12 + GlutaMAX™ (hepatocyte serum-starvation medium)	1.5 mM sodium pyruvate, 0.2% BSA with or without fatty acids and 2% antibiotic-antimycotic mixtures

Table 8. Assay media used in this study.

Assay media/buffer	Supplements
Gluconeogenesis assay medium	1:1 (v/v) mixture of DMEM/F-12 + GlutaMAX™ (31331-028, Thermo Fisher Scientific, Darmstadt, Germany) and DMEM without glucose (D5030; Sigma-Aldrich, Darmstadt, Germany) supplemented with 2.5 mM GlutaMAX™, 2.4 g/l $NaHCO_3$, 1.5 mM sodium pyruvate and 2% antibiotic-antimycotic mixture
Glucose starvation medium	DMEM (D5030, Sigma Aldrich, St Louis, MO, USA) without glucose, supplemented with 1.5 mM sodium pyruvate, 2.5 mM GlutaMAX™, 1x MEM Vitamin Solution, 1x MEM Non-Essential Amino Acids Solution and 2.4 g/l $NaHCO_3$
Glucose production medium	DMEM (D5030; Sigma Aldrich, Darmstadt, Germany) without glucose and phenol red, supplemented with 15 mM HEPES, 2.5 mM GlutaMAX™, 0.24% $NaHCO_3$ and 2% antibiotic-antimycotic mixtures

Assay media/buffer	Supplements
Krebs-Ringer-HEPES (KRH) buffer	136 mM NaCl, 4.7 mM KCl, 1.25 mM $MgS0_4$, 1.25 mM $CaCl_2$, 10 mM HEPES and 0.1% fatty acid free BSA (pH 7.4).
KRH transport buffer	KRH buffer supplemented with 2.5 µM BSA, 5 µM palmitate and 8.5 nM [^{3}H]-palmitate
Seahorse mitochondrial respiration assay medium	DMEM (D5030; Sigma Aldrich, Darmstadt, Germany) supplemented with 10 mM glucose, 2 mM L-glutamine and 1 mM sodium-pyruvate (hepatocytes) and 25 mM glucose, 2 mM L-glutamine and 1 mM sodium-pyruvate (myotubes)
Seahorse glycolysis assay medium	DMEM (D5030; Sigma Aldrich, Darmstadt, Germany) supplemented 2 mM L-glutamine

Table 9. Commercial cells used in this study.

Cells	Organism	Tissue	Cell type	Manufacturer (name, location)
Primary skeletal muscle cells (hSkMC), CC-2580	human	quadriceps or psoas muscle	satellite cells	Lonza, Basel, Switzerland
C2C12, C3H, CRL1772™	mouse	muscle	myoblasts	ATCC®, Wesel, Germany
AML12 (alpha mouse liver 12)	mouse	liver	Hepatocyte cell line	ATCC®, Wesel, Germany

ATCC, America Type Culture Collection.

2.1.5 Commercial kits

All commercial kits used in this study are listed in the Table below.

Table 10. Used kits.

Kits	Manufacturer (name, location)
CellTiter-Glo® Luminescent Cell Viability	Promega, Heidelberg, Germany
CellTox™ Green Cytotoxicity Assays	Promega, Heidelberg, Germany
Duoset human WISP-1/CCN4 Elisa assay	R&D Systems, Wiesbaden, Germany
Glucose (GO) Assay Kit	Sigma-Aldrich, Darmstadt, Germany
GoScript™ Reverse Transcription System	Promega, Heidelberg, Germany
GoTaq® qPCR Master Mix	Promega, Heidelberg, Germany

Kits	Manufacturer (name, location)
Immobilon Western HRP Substrat	Merck Chemicals GmbH, Darmstadt, Germany
Maxwell® 16 LEV simplyRNA Kit	Promega, Heidelberg, Germany
Mouse Secreted Frizzled Related Protein 4 (SFRP4) ELISA kit	BIOZOL, Eching, Germany
Pierce™ BCA Protein Assay Kit	Thermo Fisher Scientific, Darmstadt, Germany
Proteasome-Glo™ Cell-Based Assay	Promega, Heidelberg, Germany
RNeasy Mini Kit	QIAGEN, Hilden, Germany
RNeasy® Lipid Tissue Mini Kit	QIAGEN, Hilden, Germany
Seahorse XFe96 FluxPaks (inc. mini)	Santa Clara, CA, USA
SIRT-Glo™ Assay System	Promega, Heidelberg, Germany
TaqMan™ Gene Expression Master Mix	Thermo Fisher Scientific, Darmstadt, Germany

2.1.6 Oligonucleotides and probes

All designed oligonucleotides were purchased from Eurogentec (Cologne, Germany). Oligonucleotides were reconstituted to 10 nmol in H_2O. Commercial primer assays were purchased as Quantitect assays (Qiagen, Hilden, Germany). All TaqMan probes are obtained from Thermo Fisher Scientific (Darmstadt, Germany).

Table 11. Used oligonucleotides.

Species	Target	Accession	Forward 5'->3'	Reverse 5'->3'
Human	*ADIPOQ*	*NM_004797*	QT00014091 Quantitect assay	
Human	*CCL2*	NM_002982	QT00212730, Quantitect assay	
Human	*EIF4A2*	NM_001967	TGTGCAACAAGTGTC TTTGGTT	CACCTTTCCTCCCAAAT CGAC
Human	*HMOX1*	NM_002133	TCCGATGGGTCCTTA CACTCA	TCACATGGCATAAAGC CCTACA
Human	*ITLN1*	NM_017625	TCAGCTTCCTGCTGT TTCTCATA	GGAGACGAAGAACAG GTCCATT
Human	*RARRES2*	NM_002889	QT00091945, Quantitect assay	

Species	Target	Accession	Forward 5'->3'	Reverse 5'->3'
Human	*RPLP0*	NM_001002	GCTTCCTGGAGGGTGTCC	GGACTCGTTTGTACCCGTTG
Human	*RPS18*	NM_022551	QT02323251, Quantitect assay	
Human	*sFRP4*	NM_003014	CACCCATCCCTCGAACTCAA	TGTGTGGACACTGGCAAGAAG
Human	*SLC2A4/GLUT4*	NM_001042	GCATCCACAGGCTTTTGACC	GTGTTTCCAGGCAGCCTTTC
Human	*UBE2D2*	NM_003339	CACAAGGAATTGAATGATCTGGCA	ATAGGGACTGTCATTTGGCCC
Human	*WISP1*	NM_003882	GGCCAGGCTCTTCCTTGAAT	TAGAGGAGTGTTCCAGGGCA
Human	*YWHAZ*	NM_003406	TCTGGCTCCACTCAGTGTCT	CTGTGGGATGCAAGCAAAGG
Mouse	*Hprt1*	NM_013556	AGCAGTACAGCCCCAAAATG	ATCCAACAAAGTCTGGCCTGT
Mouse	*Rps18*	NM_011296	AAATTCGAGCCCATAGAGGG	AGAGACTCATTTCTTCTTGGAT

Adipoq, adiponectin; CCl2, C-C motif chemokine ligand 2; *EIF4A2*, *eukaryotic translation initiation factor 4A2*; *HMOX1*, *heme oxygenase 1; ITLN1*, *intelectin1/omentin1; RARRES2*, *retinoic acid receptor responder 2*; *RPLP0*, *ribosomal protein lateral stalk subunit P0*; *RPS18*, *ribosomal protein S18 hypoxanthine phosphoribosyltransferase 1;sFRP4, secreted frizzled related protein 4*; *UBE2D2*, *ubiquitin-conjugating enzyme E2 D2*; *WISP1*, *WNT1 inducible signaling pathway protein 1*; *YWHAZ, tyrosine 3-monooxygenase/tryptophan 5-monooxygenase activation protein zeta*.

Table 12.Used TaqMan probes.

Species	Target	Accession	Product number
Mouse	*G6pc*	NM_008061	Mm00839363, TaqMan™ Assays
Mouse	*Pck1*	NM_011044	Mm01247058, TaqMan™ Assays
Mouse	*18S*	X03205	4310893E, TaqMan™ Assays
Mouse	*Sfrp4*	NM_016687	Mm00840104, TaqMan™ Assays

G6pc, *glucose-6-phosphatase catalytic subunit*; *Pck1*, *phosphoenolpyruvate carboxykinase 1*; *18S ribosomal RNA*, *18S.*

2.1.7 Antibodies

Table 13. Antibodies.

Antibodies	Origin	Dilution[1]	Product number	Manufacturer (name, location)
Primary				
ACC, monoclonal	rabbit	1:1,000 (v/v) 5% BSA	3676	Cell Signaling Technology, Danvers, MA, USA
Akt, polyclonal	rabbit	1:1,000 (v/v) 5% BSA	9272	Cell Signaling Technology, Danvers, MA, USA
AMPKα, monoclonal	rabbit	1:1,000 (v/v) 5% BSA	5831	Cell Signaling Technology, Danvers, MA, USA
FoxO1, monoclonal	rabbit	1:1,000 (v/v) 5% BSA	2880	Cell Signaling Technology, Danvers, MA, USA
FoxO3a, monoclonal	rabbit	1:1,000 (v/v) 5% BSA	2497	Cell Signaling Technology, Danvers, MA, USA
GAPDH, monoclonal	rabbit	1:5,000 (v/v) 5% MP	2118	Cell Signaling Technology, Danvers, MA, USA
GSK3β, monoclonal	rabbit	1:1,000 (v/v) 5% BSA	9323	Cell Signaling Technology, Danvers, MA, USA
Phospho-GSK3β-Ser9, monoclonal	rabbit	1:1,000 (v/v) 5% BSA	9315	Cell Signaling Technology, Danvers, MA, USA
IRS-1, polyclonal	rabbit	1:500 (v/v) 5% MP	06-248	Millipore, Charlottesville, USA
IRβ, polyclonal	rabbit	1:500 (v/v) 5% MP	sc-711	Santa Cruz Biotechnology, Santa Cruz, CA, USA
IRS-2, polyclonal	rabbit	1:500 (v/v) 1:1 5% MP/BSA		provided for this work from Prof. Dr. Ouwens, used as described (Telting et al., 2001)

Antibodies	Origin	Dilution[1]	Product number	Manufacturer (name, location)
MAFbx/atrogin-1 (F-9), monoclonal	mouse	1:250 (v/v) 5% MP	sc-166806	Santa Cruz Biotechnology, Santa Cruz, CA, USA
MuRF1 (C-11), monoclonal	mouse	1:250 (v/v) 5% MP	sc-398608	Santa Cruz Biotechnology, Santa Cruz, CA, USA
p70S6kinase, monoclonal	rabbit	1:1,000 (v/v) 5% BSA	2708	Cell Signaling Technology, Danvers, MA, USA
phospho-ACC-Ser79, monoclonal	rabbit	1:1,000 (v/v) 5% BSA	1181	Cell Signaling Technology, Danvers, MA, USA
phospho-Akt-Ser473, polyclonal	rabbit	1:1,000 (v/v) 5% BSA	9271	Cell Signaling Technology, Danvers, MA, USA
phospho-Akt-Thr308, monoclonal	rabbit	1:1,000 (v/v) 5% BSA	4056	Cell Signaling Technology, Danvers, MA, USA
phospho-AMPKα-Thr172, monoclonal	rabbit	1:1,000 (v/v) 5% BSA	2535	Cell Signaling Technology, Danvers, MA, USA
phospho-FoxO1 (Thr24)/FoxO3a (Thr32), polyclonal	rabbit	1:1,000 (v/v) 5% BSA	9464	Cell Signaling Technology, Danvers, MA, USA
phospho-FoxO1-Ser256, polyclonal	rabbit	1:1,000 (v/v) 5% BSA	9461	Cell Signaling Technology, Danvers, MA, USA
phospho-FoxO3a-Ser253, polyclonal	rabbit	1:1,000 (v/v) 5% BSA	9466	Cell Signaling Technology, Danvers, MA, USA
phospho-IRβ-Tyr1150/1151, monoclonal	mouse	1:250 (v/v) 5% MP	sc-81500	Santa Cruz Biotechnology, Santa Cruz, CA, USA
phospho- p70S6K Thr389, monoclonal	rabbit	1:1,000 (v/v) 5% BSA	9234	Cell Signaling Technology, Danvers, MA, USA

Antibodies	Origin	Dilution[1]	Product number	Manufacturer (name, location)
α-Tubulin, monoclonal	mouse	1:1,000 (v/v) 5% MP	3873	Cell Signaling Technology, Danvers, MA, USA
β-Actin, monoclonal	mouse	1:1,000 (v/v) 5% MP	3700	Cell Signaling Technology, Danvers, MA, USA
Secondary				
Anti-rabbit IgG, HRP-linked	goat	1:1,000 (v/v) 5% MP or 5% BSA	7074	Cell Signaling Technology, Danvers, MA, USA
Anti-mouse IgG, HRP-linked	horse	1:1000 (v/v) 5% MP or 5% BSA	7076	Cell Signaling Technology, Danvers, MA, USA

[1]5% non-fat dry milk powder (MP) or 5% bovine serum albumin (BSA) were dissolved in 1x TBS-T; HRP, horseradish peroxidase; IgG, immunoglobulin G

2.1.8 Recombinant proteins, inhibitors and reagents

Table 14. Recombinant proteins.

Recombinant protein	Manufacturer (name, location)
Recombinant Human sFRP4 Protein, 1827-SF	R&D Systems, Wiesbaden, Germany
Recombinant Human WISP1 Protein, 120-18	Peprotech, Hamburg, Germany

Table 15. Used inhibitors and reagents.

Inhibitor/Reagent	Solvent	Manufacturer (name, location)
Bortezomib (BZ)	DMSO	Merck Chemicals GmbH, Darmstadt, Germany
Compound C (CompC)	DMSO	Merck Chemicals GmbH, Darmstadt, Germany
Oligomycin	DMSO	Sigma-Aldrich, Darmstadt, Germany
Carbonyl cyanide p-trifluoromethoxyphenylhydrazone (FCCP)	DMSO	Sigma-Aldrich, Darmstadt, Germany

Inhibitor/Reagent	Solvent	Manufacturer (name, location)
Etomoxir	DMSO	Sigma-Aldrich, Darmstadt, Germany
Antimycin	DMSO	Sigma-Aldrich, Darmstadt, Germany
Rotenone	DMSO	Sigma-Aldrich, Darmstadt, Germany

2.2 Methods

2.2.1 Study participants

All human serum samples, adipose tissue biopsies and patient related data used in this work were obtained from participants from the Obster (Ruige et al., 2012) and HebObster (Bekaert et al., 2016) study which were conducted at the Department of Internal medicine at Ghent University (Belgium) (Clinical Trials Registration nos. NCT00740194 and B67020084018). Written informed consent was obtained from all study participants and study protocol was approved by the Ethics Board of the Ghent University Hospital and conducted according to the principles of the Declaration of Helsinki. Data for body mass index (BMI), fat (% body weight), visceral and subcutaneous adipocyte cell size were measured and analyzed at Ghent University as described previously (Bekaert et al., 2016) and kindly provided for this work by Prof. Dr. Bruno Lapauw and his group from Department of Internal medicine.

Individuals of the study cohort were assigned into three groups consisting of 33 normal-weight men (controls), 56 obese men and 46 obese men who had type 2 diabetes according to the American Diabetes Association criteria (ADA, 2017). The sFRP4 analyses were performed with 28 normal-weight men and 88 obese men of whom 42 had type 2 diabetes. Type 2 diabetic and/or obese patients underwent bariatric surgery either for gastric banding or gastric bypass surgery, whereas the normal-weight men were scheduled for abdominal elective surgery such as adhaesiolysis, hernia diaphragmatica, intestinal resection or Nissen fundoplication as previously described (Bekaert et al., 2016; Ruige et al., 2012). At day of surgery, blood samples were obtained after an overnight fast. VAT and SAT biopsies were collected during surgeries and frozen in liquid nitrogen for storage at -80°C for further applications. Exclusion criteria for study participation and the detailed study design have been described previously (Bekaert et al., 2016; Ruige et al., 2012).

2.2.1.1 Experimental animals

For this work, plasma samples, tissue biopsies and hepatocytes were obtained from male C57Bl6 mice and transgenic mice that overexpress the truncated transcriptional active form of human sterol regulatory element-binding protein (SREBP)-1c (aa 1-436) in adipose tissue under the control of the adipocyte-specific aP2 enhancer/promoter (Shimomura et al., 1998). In the DDZ the aP2-SREBP-1c mice were backcrossed on C57Bl6 genetic background for >20 generations. Mice were housed with up to four animals per cage in a controlled environment

on 12-hour light-dark cycle (22 ± 1°C, 50 ± 5% humidity), received water *ad libitum* and standard laboratory, normal-caloric chow. Mice were sacrificed by CO_2 asphyxiation followed by collection of blood samples via left ventricle cardiac puncture and isolation of tissues or underwent the protocol for primary hepatocyte isolation. All animal experiments were approved by the Animal Care Committee of the University Düsseldorf (approval number Az.84-02.04.2015.A424, 2015).

Phenotypical characterization data of the utilized mice were provided by Dr. J. Kotzka and Dr. B. Knebel of the German Diabetes Center. In brief, serum diagnostics of clinical measures, and surrogate parameters of insulin resistance were performed as previously described (Knebel et al., 2012, 2015, 2018; Kotzka et al., 2012). Serum FFA and hepatic total fatty acid contents were determined by gas chromatography. Hormone concentrations (insulin and leptin) in serum were determined with the Multiplex Immunoassay Bioplex System according to the supplier's instructions.

2.2.2 Cell culture techniques

2.2.2.1 Isolation and culture of primary murine hepatocytes

Primary hepatocytes were isolated from perfused livers from 18 to 24-week-old male C57Bl6 and aP2-SREBP-1c mice by two-step collagenase perfusion of the liver as described previously (Akie and Cooper, 2015). Mice were sacrificed by CO_2 asphyxiation followed by liver perfusion via the abdominal inferior *vena cava*. Briefly, thoracic *vena cava* got disconnected by a clamp to avoid pressure loss and perfusion through this part followed by insertion of the needle into the inferior *vena cava* and perfusion with liver perfusion buffer (Table 5) at 3 ml/min for approximately 2-3 min (C57Bl6) and 5 ml/min for ~4 min (aP2-SREBP-1c). The perfusate left the liver via the severed portal vein (Figure 8). Then, the liver was digested by perfusion with liver digestion buffer (Table 7) containing 100 Units/ml (U/ml) (C57Bl6) for 3.5 ml/min for ~6 min or 120 U/ml (aP2-SREBP-1c) collagenase for 5 ml/min for approximately 10 min until the liver appeared enlarged. After digestion, the liver was excised from the mouse followed by removal of gall bladder. The digested liver was scraped using blades in washing medium (Table 5) and cell suspension was filtered using a 70 µm cell strainer. To separate parenchymal hepatocytes from the non-parenchymal-cell fraction, the hepatic cell suspension was pelleted (5 min, 50x g, 4°C) and washed two times in washing medium (Table 5) by centrifugation (5 min, 50x g, 4°C) (Figure 8). Subsequently, hepatocytes were purified and separated from non-

viable cells by using a 90% Percoll gradient (Table 5, 6) at 50x g, 10 min, 4°C (acceleration: 3, dissceleration:2) and an additional wash step (Figure 8). Cell number and viability of hepatocytes were assessed by trypan blue staining (2.2.2.4). Hepatocytes with a viability count ≥70% were used for experiments. Hepatocytes were cultured at a density of 6.25x 10^4 cells/cm^2 on rat tail type-I collagen coated plates, with final concentration of 50 µg/ml collagen diluted in 1x PBS, in hepatocytes plating medium (Table 7) for 4h, 37°C, 5% CO_2. Following, hepatocytes were incubated in serum-starvation medium (Table 7) overnight at 37°C, 5% CO_2 and subjected to experiments. For *in vitro* experiments, hepatocytes were used for up to 24h in culture.

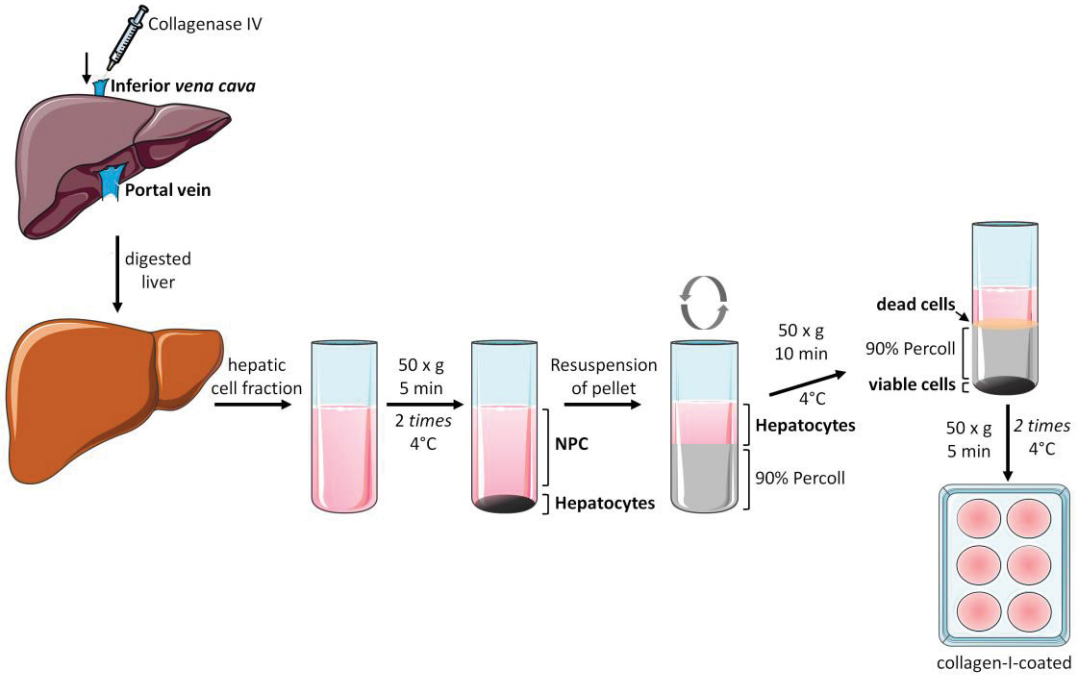

Figure 8. Isolation procedure of primary murine hepatocytes. Detailed procedure is described in text 2.2.2.1. NPC, non-parenchymal-cell fraction.

2.2.2.2 Cultivation of primary human skeletal muscle cells (hSkMC)

Primary human skeletal muscle cells were purchased as isolated proliferating satellite cells from the quadriceps or psoas muscle (Table 9). In this work, hSkMC of 6 healthy Caucasian donors (3 males and 3 females aged between 16-32) were cultured with a density of 1x 10^4 cells/cm^2 in growth medium (Table 7) in a humidified atmosphere containing 5% CO_2 at 37°C as described previously (Wiza et al., 2013). When cells reached approximately 50-60%

confluence, cells were cultured in differentiation medium (Table 7) to facilitate differentiation of myoblast to multinucleated myotubes. On day 6 of differentiation, cells were starved in serum-free differentiation medium and used for experiments up to day 7 in culture.

2.2.2.3 Cultivation of C2C12 myotubes

C2C12 myoblasts were seeded at a density of 5x 10^3 cells/cm^2 and cultured in growth medium (Table 7) in a humidified atmosphere containing 5% CO_2 at 37 ˚C. When cells were almost confluent, differentiation was initiated by incubating C2C12 in differentiation medium (Table 7) for 6 days. Following, myotubes were serum-starved in serum-free differentiation medium and used for experiments up to day 7 in culture.

2.2.2.4 Cultivation of AML12 hepatocytes

The mouse AML12 (alpha mouse liver 12) hepatocyte cell line was purchased from America Type Culture Collection (Wesel, Germany), and cultured in Dulbecco's Modified Eagle's Medium/Nutrient F-12 Ham 1:1 (v/v) medium (Thermo Fisher Scientific, Waltham, MA) supplemented with 15 mM L-Glutamine, 1.2 g/l HEPES, 5 µg/ml insulin, 0.005 mg/ml transferrin, 5 ng/ml selenium, 40 ng/ml dexamethasone and 10% foetal bovine serum (FBS). For experiments, the cells were seeded in a density of 3x 10^4 cells/cm^2 and cultured for 48h. Following, AML12 hepatocytes were starved for serum for 4h prior staring the experiments.

2.2.2.5 Determination of cell count

Trypan blue staining was used for the determination of viable cells in a cell suspension. The staining is based on the principle that the membrane integrity of viable cells prevents the intrusion of the dye, whereas non-viable cells are stained blue because of their perforated membranes. Briefly, the cell suspension is diluted with 0.2% trypan blue solution (Table 5, 6) and pipetted in a *Neubauer* cell counting chamber (Table 3). Cell number is assessed by counting of viable cells in the large square.

2.2.2.6 Cell culture treatment

For analysis of the effect of sFRP4 or WISP1 on insulin signaling and the regulation of energy metabolism in hSkMC, C2C12, AML12 and primary hepatocytes, cells were treated with

100 ng/ml sFRP4, 0.1 ng/ml or 1 ng/ml WISP1 (Table 14) dissolved in PBS with 0.1% BSA (Table 5, 6) in respective serum-starvation medium for 4h and/or 24h as indicated.

For 24h treatments, recombinant protein was already added to the serum-starvation medium overnight. 4h treatment with recombinant protein was started after 20h incubation of the cells in serum-starvation medium followed by stimulation with 100 nM insulin for 10 min in insulin signaling studies. For experiments with inhibitors, cells were preincubated with Bortezomib (BZ, 10 nM) or Compound C (CompC, 20 µM) (Table 15) in serum-starvation medium for 30 min (37°C, 5% CO_2) followed by addition of sFRP4 for the indicated time.

For stimulation of AMP-activated protein kinase (AMPK) phosphorylation, cells were incubated for 4h with oligomycin (0.5 µM and 1 µM).

For analysis of gluconeogenic gene expression, cells were glucose-starved in gluconeogenesis assay medium in presence or absence of recombinant protein sFRP4 or WISP1 for 4h before end of experiment. Further, insulin (100 nM) was added to the cells 60 min before end of experiment.

In metabolic assays, the ionophor FCCP (hepatocytes and hSkMC were exposed to 0.5 µM or 1 µM) or inhibitors of the fatty acid β-oxidation including oligomyocin, antimycin A/rotenone or etomoxir (each 0.5 µM) were added 15 min before adding the fatty acids. In all controls, the final concentration of the respective solvent of recombinant protein, inhibitor or reagent (DMSO or 0.1% (w/v) BSA/PBS) was used as vehicle.

2.2.3 Molecular biological methods

2.2.3.1 RNA isolation and cDNA synthesis

Total RNA was isolated from ≤100 mg frozen human adipose tissue biopsies or from 10-50 mg murine adipose tissue, liver, gastrocnemius muscle (GAS) and pancreas. Therefore, tissues were lysed using stainless steel beads and 1 ml TriPure isolation reagent (Table 10) on a TissueLyser instrument (Table 3) for 2 min at 20 Hz in two cycles. Homogenate was transferred to a fresh tube and 200 µl chloroform was added, tube was inverted a few times and incubated for 2-3 min at RT prior centrifugation 12,000x g, 15 min, 4°C for phase separation. 400 µl of the aqueous phase was used for RNA purification with the RNeasy® Lipid Tissue Mini Kit (Table 10) on the QIAcube workstation (Table 3) according to manufacturer's protocol. RNA was eluted in 30 µl RNAse free H_2O.

Total RNA from cells was extracted using RNeasy Mini Kit (Table 10) for hepatocytes and Maxwell® 16 instrument with the Maxwell® 16 LEV simplyRNA Purification Kit for hSkMC and C2C12 according to manufacturer's instructions. RNA content and quality were examined using NanoDrop™ spectrophotometer via measurement of optical density (OD) at a wavelength of 260 nM. Further, the ratio of OD_{260}/OD_{280} indicated a contamination with either proteins, genomic DNA (deoxyribonucleic acid) or aromatic substances. The synthesis of complementary DNA (cDNA) from the isolated RNA was performed by polymerase chain reaction (PCR) using GoScript™ reverse transcription system kit and Oligo (dT) primers (Table 10) according to manufacturer´s instructions. 100 ng RNA of tissues and 500-1000 ng RNA of cells were transcribed. cDNA was diluted in H_2O as required for qRT-PCR analysis.

Table 16. Components of PCR reaction mixture for cDNA synthesis.

Components (stock)	Volume (µl)
5x Reaction buffer	4
dNTPs Mix (10 mM)	1
$MgCl_2$(25 mM)	1.2
Nuclease-free H_20[1]	variable
Oligo$(dT)_{15}$ primer (500 µg/ml)	1
Reverse transcriptase	1
Ribonuclease inhibitor (400 u/µl)	0.5

[1]volume depends on mRNA concentration

Table 17. cDNA synthesis PCR program using GoScript™ reverse transcription system kit.

Steps	Temperature	Duration	Cycles
Heating[1]	70°C	5 min	-
Annealing[2]	25°C	5 min	40 x
Extension	42°C	1 h	

[1]mixture includes RNA, Oligo$(dT)_{15}$ primer and nuclease-free H_2O, [2]before annealing step reaction buffer, dNTPs Mix, $MgCl_2$, reverse transcriptase and ribonuclease inhibitor mixture was added

2.2.3.2 Quantitative real-time PCR (qRT-PCR)

Quantitative real-time PCR is a fluorescence-based measurement for the amplification of cDNA generated during each PCR cycle in real time. The PCR-amplification products were monitored by an increase in fluorescence emission either detected by intercalation of non-specific fluorescent dyes in the double stranded DNA or by the use of sequence-specific DNA

probes consisting of a fluorophore and quencher probe that hybridize to the target DNA (Raso and Biassoni, 2014). In this study, relative gene expression levels were determined via real time PCR on a StepOne Plus real-time PCR system with a standard PCR protocol (Table 20, 21) using either the fluorescence dye system GoTaq® qPCR Master Mix (Table 18) or TaqMan™ probe assays (Table 19) according to manufacturer´s instructions. The relative expression of a target gene was calculated from triplicate measurements of the obtained threshold cycle (Ct) values in a sample normalized to the geometric mean of corresponding Cts assessed for stable reference genes by ΔCt method. For analysis of relative changes in the expression of a target transcript in a sample to that of another sample the $2^{-\Delta\Delta Ct}$ method was used (Schmittgen and Zakrajsek, 2000; Winer et al., 1999). The oligonucleotides and probes used in this study were listed in Table 11 and 12.

Table 18. Components of qRT-PCR mixture using GoTaq® qPCR Master Mix.

Components	Volume (µl)
GoTaq® Master Mix	5
Primer oligonucleotides	4
cDNA	1
per 96-well	10

Table 19. Components of qRT-PCR mixture using TaqMan™probe assays.

Components	Volume (µl)
TaqMan™probe	0.27
H_2O	6.35
TaqMan™ Gene Expression Master Mix	5.34
cDNA	0.54
per 96-well	12.5

Table 20. qRT-PCR program using GoTaq® qPCR Master Mix.

Steps	Temperature	Duration	cycles
Holding stage	95°C	2 min	-
Denaturation	95°C	15 sec	40 x
Annealing/Elongation	60°C	60 sec	
Dissociation/Melt curve	60-95°C	1 min 30 sec	-

Table 21. qRT-PCR program using TaqMan™probe assays.

Steps	Temperature	Duration	cycles
Holding stage	50°C	2 min	-
	95°C	10 min	-
Denaturation	95°C	15 sec	40 x
Annealing/Elongation	60°C	60 sec	

2.2.4 Biochemical methods

2.2.4.1 Serum analysis

Human serum samples for assessment of WISP1 were kindly provided by the Department of Internal medicine at Ghent University. Human WISP1 levels were measured in fasting serum samples by a Duoset human WISP-1/CCN4 Elisa assay (Table 10) combined with human serum albumin (Table 5) on 96-well high-binding assay plates (Table 4) according to manufacturer's instructions. This ELISA assay detected serum levels in the range of 7.5-1000 pg/ml.

Further, data for oral glucose tolerance test, fasting glucose and insulin levels, $HbA1_c$ (hemoglobin A1C), triglyceride levels, adiponectin levels, serum leptin, MCP-1, chemerin, omentin, CRP, HO-1 and leptin levels were collected and analyzed as described (Bekaert et al., 2016; Hörbelt et al., 2018; Ruige et al., 2012) and kindly provided for this work from Department of Internal medicine at Ghent University, where the study was conducted. Homeostasis model for assessment of insulin resistance (HOMA-IR) calculation was performed as followed: (fasting glucose [mmol/l] x fasting insulin [µU/ml])/22.5 (Matthews et al., 1985). For the calculation of HOMA2-%B, a computer model of homeostasis model assessment (HOMA) for β-cell function (%B), the formula (20 x fasting insulin [µU/ml]) / (glucose [mmol/l]-3.5) was used (Levy et al., 1998).

2.2.4.2 Collection and analysis of plasma samples from mice

Blood samples from mice were collected from male 18 to 24-week-old C57Bl6 mice and aP2-SREBP-1c mice sacrificed as described in 2.2.2.1 by cardiac puncture. First, the abdominal cavity followed by the lung cavity were dissect open. Then, the needle that before was rinsed with 0.1 M EDTA, was inserted in the ventricle and blood was withdrawn slowly to avoid collapsing of the heart and transferred to EDTA-coated tubes and cooled on ice. To remove cells and cellular debris, samples were centrifuged 10 min, 2,000x g, 4°C. The supernatant was the resulting plasma. Plasma samples were stored at -80°C for further analysis. Circulating

mouse sfrp4 levels were determined using a mouse sfrp4 ELISA kit (Table 10) according to manufacturer´s handbook. The detection range is 0.156-10 ng/ml.

2.2.4.3 Cell lysis and protein isolation for SDS-PAGE and Western blot analysis

Whole protein lysates were extracted from cells for sodium dodecylsulfate polyacrylamide gel electrophoresis (SDS-PAGE) and Western blot analysis. At the end of experiments, cells were rinsed twice with ice-cold PBS on ice and stored at -20°C for a minimum of 2h. Following, 100 µl of ice-cold RIPA buffer supplemented with Complete Protease Inhibitor and PhosStop Phosphatase Inhibitor cocktail (Table 5) was added to the cells and incubated for 5 min on ice by swirling the plate for uniform spreading of buffer. Cells were lysed in RIPA buffer using a cell scraper. Cell lysates were collected and transferred to a tube and centrifuged at 14,000x g for 10 min to pellet and remove cell debris. Supernatant including cytosolic and nuclear proteins were collected and used for further analysis. For determination of protein concentration, samples were diluted 1:10 (v/v) in H_2O. Protein concentration in lysates was assessed by using Pierce BCA Protein Assay Kit (Table 10) according to supplier´s instructions on a micro plate reader (Table 3).

2.2.4.4 Cell lysis and protein isolation from 96-well plates form Seahorse measurements

At the end of experiments, cultured wells of 96-well plates form Seahorse measurements were rinsed once with PBS and incubated with 30 µl Seahorse cell lysis buffer (Table 6) for 1h at - 20°C followed by a thawing period of 30 min on an orbital shaker. This freeze-thaw cycle was repeated two times. Cell lysates were diluted 1:2 (v/v) in H_2O and subjected to determination of protein concentration using Pierce BCA Protein Assay Kit (Table 10) according to supplier´s instructions.

2.2.4.5 Cell lysis and protein isolation for metabolic cell-based assays

For *de novo* lipogenesis (2.2.5.5), fatty acid oxidation (2.2.5.7) and fatty acid uptake (2.2.5.8), 10 µl of undiluted 0.1 M HCl cell lysates were used for protein determination via Pierce BCA Protein Assay Kit. While 10 µl of cells lysed in RIPA buffer derived from glucose production (2.2.5.6) and 10 µl of cells lysed in 1 M NaOH from glycogen synthesis experiments (2.2.5.4) were subjected to determination of protein concentration using Pierce BCA Protein Assay Kit (Table 10) according to supplier´s instructions.

2.2.4.6 Western blot analysis

Proteins were electrophoretically separated by size via denaturing SDS-PAGE. 8-15 µg of proteins were diluted with 1x Laemmli sample buffer (Table 6), denatured for 5 min at 95°C and separated via SDS-PAGE on 8-10% tris-glycine-acrylamide-gels at 120 V for approximately 60 min. Following, proteins were transferred to polyvinylidene difluoride (PVDF) membranes in a semidry or wet-tank blotting (3h, 4°C at 0.2 A) apparatus. Membranes were blocked using Tris-buffered saline (TBS) containing 0.1% Tween-20 (TBS-T) supplemented with either 5% non-fat dry milk or 5% BSA and incubated overnight at 4°C with specific primary antibodies (Table 13). Following membranes were washed with TBS-T and incubated with secondary horseradish peroxidase-coupled antibody according to manufacturer´s instructions at RT. Proteins were visualized by chemiluminescent using Immobilon Western HRP Substrat detection reagents on VersaDoc™ MP 4000 Imager. Protein signals were quantified by Image Lab™ Software and normalized for protein abundance of corresponding loading control including GAPDH, α-tubulin or β-actin (Table 13).

2.2.4.7 Secretome analyses of primary murine hepatocytes

Isolated hepatocytes of C57Bl6 and aP2-SREBP-1c mice were incubated in serum-starvation medium without phenol red (Table 7) overnight at 37°C, 5% CO_2 and were maintained in culture for up to 24h. Cells were either incubated with sFRP4 (100 ng/ml; 24h) or left untreated. Cell medium was collected at time of experiment. The secretome analyses of the supernatants including sample preparation, mass spectrometry and analyses of raw data were performed by Dr. S. Hartwig and U. Kettel at the Proteomics Core Facility (Head: Dr. S. Lehr) of the German Diabetes Center.

2.2.5 Cell-based assays

2.2.5.1 Analysis of cell viability and cytotoxicity

To determine suitable concentrations of the used inhibitor BZ for *in vitro* studies, CellTiter-Glo® Luminescent Cell Viability or CellTox™ Green Cytotoxicity Assays were performed in primary hSkMC and primary hepatocytes according to manufacturer's instructions. The latter is based on the principle that a fluorescence dye is only able to bind the DNA in non-viable cells due to their perforated membrane integrity but not in viable cells. The dye-DNA interaction enhances the fluorescence which is directly proportional to the cytotoxicity.

Cells were seeded and cultured with a density of 2x 10^4 cells per 96-well (primary hepatocytes) and at a density of 4x 10^3 cells per 96-well (primary myotubes). Following, cells were exposed to increasing concentrations of BZ (1-100 nM) for 24h. 0.01% DMSO was used as a vehicle. Then, cells were incubated with luminogenic substrate or fluorescence dye according to supplier´s protocol. The fluorescence and luminescence were measured using Tecan Infinite 200 reader (Table 3).

2.2.5.2 Proteasome activity assay

To assess the effect of sFRP4 on proteasome activity, cells were seeded as described above at a density of 2 x 10^4 cells per 96-well for primary hepatocytes and at a density of 4x 10^3 cells per 96-well for primary myotubes. Following, cells were pre-incubated for 30 min with or without the cell-permeable proteasome inhibitor BZ (10 nM) followed by addition of 100 ng/ml sFRP4 for further 24h in serum-starvation medium. 0.01% DMSO was used as a vehicle. Then, cells were incubated with luminogenic substrate using Proteasome-Glo™ Cell-Based Assay according to supplier´s protocol. The luminescence was measured using Tecan Infinite 200 reader and is directly proportional to the chymotrypsin-like activity of the proteasome.

2.2.5.3 Analysis of sirtuin activity

Sirtuins (SIRTs) are NAD^+-dependent histone deacetylase class III enzymes. To study the effect of sFRP4 on sirtuin activity in hepatocytes and hSkMC, cells were exposed 4h or 24h to 100 ng/ml sFRP4 followed by cell lysis in 1x PBS supplemented with 1% nonidet P-40 (NP-40). 5 µg of cell lysate were analyzed using luminescence-based SIRT-Glo™ Assay System according to manufacturer's instructions. Luminescence was measured 15 min after adding the protease and luciferase mixture to the lysates and was directly proportional to deacetylase activity.

2.2.5.4 Glycogen synthesis

Primary hSkMC and primary hepatocytes were treated with either recombinant sFRP4 or WISP1 as described above (2.2.2.5). To study the effect of the recombinant protein on basal and insulin-stimulated glycogen synthesis, myotubes and hepatocytes were starved for glucose in glucose starvation medium (Table 8) for 90 min at 37°C, 5% CO_2. Following, myotubes were incubated in serum-free differentiation medium (Table 7) and hepatocytes in serum-starvation-medium (Table 5) both supplemented with D-[^{14}C(U)]-glucose (2 µCi/mL) in

the presence or absence of 100 nM insulin for 3h at 37°C, 5% CO_2 as previously described (Hessvik et al., 2010). After washing cells twice with ice-cold 1x PBS, cells were solubilized in 1 M potassium hydroxide (KOH). Then, samples were incubated with a final concentration of 3 M KOH and 20 mg/ml glycogen (Table 6) and heated at 80°C for 20 min. Glycogen precipitation occurred by adding ice-cold absolute ethanol to the samples. After centrifugation of the samples (2,000 × g, 20 min, 4 C), the supernatant was discarded. The glycogen precipitates were washed once with ethanol 70% and resuspended in 500 µl H_2O_{bidest}. Incorporated D-[^{14}C(U)]-glucose was assessed by liquid scintillation counting of 300 µl lysate in 3 ml Rotiszint® eco plus. Protein content was determined in 10 µl cell lysates in duplicates by BCA Protein Assay Kit as described in 2.2.4.5 und used for normalization of corresponding CPM (counts per minute) measurements.

2.2.5.5 *De novo* lipogenesis (DNL) in primary hepatocytes

The impact of sFRP4 on DNL in primary hepatocytes was performed by assessing ^{14}C-acetate incorporation as previously described (Akie et al., 2015; Jelenik et al., 2017). Therefore, cells were exposed 24h to sFRP4 (100 ng/ml) in absence and presence of insulin (100 nM) in serum-starvation medium (Table 7) followed by addition of 10 µM acetate and 0.5 µCi [^{14}C]-acetate (Table 5) to the medium for additional 2h or 4h. Then, cells were washed two times with 1x PBS and lysed in 120 µl 0.1 M HCl by scraping. 10 µl of HCl lysate were used for determination of protein concentration by BCA Protein Assay Kit (2.2.4.5). Lipids were extracted by chloroform-methanol mixture (2:1, v/v) followed by vortexing, incubation for 5 min at RT and addition of 250 µl H_2O_{bidest}. After centrifugation at 3,000x g at RT, the lower lipid containing phase was measured for lipogenic activity by liquid scintillation counting in 4 ml Rotiszint® eco plus. ^{14}C incorporation was normalized to protein content.

2.2.5.6 Glucose production assay in primary hepatoytes

To determine the effect of sFRP4 on glucose production via glycogenolysis and gluconeogenesis in primary hepatocytes, 4h before termination of 24h sFRP4 exposure, serum-starvation medium was replaced to glucose production medium (Table 8) with or without 2 mM sodium lactate and 2 mM sodium pyruvate, 100 nM insulin and fresh recombinant sFRP4 at 37°C, 5% CO_2. Following, cell culture supernatant was collected and applied for enzymatic, colorimetric determination of glucose concentration using Glucose

(GO) Assay Kit (Table 10) on an iMark™ Microplate Absorbance Reader (Table 1) according to supplier´s instructions. Cells were lysed in RIPA buffer without PhosSTOP Phosphatase Inhibitor and Complete Protease Inhibitor Cocktail and protein concentration was assessed by Pierce BCA Protein Assay Kit (2.2.4.5). Glucose production in primary hepatocytes was calculated from glucose concentration normalized to protein concentration.

2.2.5.7 Fatty acid oxidation (FAO)

Fatty acid oxidation assays were performed using an oxidation chamber. Cells were seeded with a density of 3x 10^4 cells for hepatocytes and 5x 10^4 cells for hSkMC in a 48-well plate as described above. Cells were exposed to sFRP4 (100 ng/ml) for 4h or 24h in fatty acid free serum-starvation medium for hepatocytes and serum-free differentiation medium for hSkMC (Table 7). FCCP or inhibitors of the fatty acid β-oxidation including oligomyocin, antimycin A/rotenone or etomoxir were added to cells 15 min before fatty acids. An absorbent filter paper with a surface area of 4 m^2 was fitted to each well adjacent to a cell well and incubated with 50 µl 1 M NaOH. Then, cells were exposed to [^{14}C]-fatty acid working solution containing 0.3 µCi [^{14}C]-palmitic acid, 57 µM fatty acid free BSA and 9 µM L-carnitin in corresponding serum-starvation medium. Cell culture plates were fixed in the oxidation chamber and put for 4h at 37°C, 5% CO_2. Afterwards, cells were exposed to final 0.5 M HCl, cell culture supernatant and corresponding absorbent filter paper were transferred to new 48-well plate which was fixed in the oxidation chamber and incubated overnight 37°C, 5% CO_2. The release of $^{14}CO_2$ was absorbed on NaOH filter paper which was assessed by liquid scintillation counting in 3 ml Rotiszint® eco plus. 10 µl of lysate were used for determination of protein concentration by Pierce BCA Protein Assay (2.2.4.5). CPM measurements of $^{14}CO_2$ release were normalized to protein content presenting fatty acid oxidation.

2.2.5.8 Fatty acid uptake in primary hepatocytes

Primary hepatocytes were washed once with KRH buffer (Table 8). Cells were incubated in serum-starvation medium supplemented with 1% fatty acid free BSA for 2h at 37°C. Following, cells were washed three times with 37°C warm KRH/0.1% BSA and once with KRH without BSA. Cells were incubated with 1 ml KRH including 40 µmol/l BSA before palmitate uptake was performed by addition of 1 ml KRH transport buffer containing [^{3}H]-palmitate (Table 8) for 15 min at 37°C. The uptake was stopped by aspiration of medium followed by three times

washing steps with ice-cold KRH/0.1% BSA. Cell were lysed in 300 µl 0.1 M HCl and 100 µl of lysate were used for liquid scintillation counting in 3 ml Rotiszint® eco plus. For assessment of protein content, 10 µl of lysate were taken (2.2.4.5). CPM values of [^{3}H] palmitate uptake were normalized to protein.

2.2.5.9 Analysis of cellular mitochondrial respiration and glycolysis

The analysis of cellular mitochondrial respiration and glycolysis was accomplished by recording of oxygen consumption (OCR) and extracellular acidification (ECAR) rate in living cells using the Seahorse XF^{e}96 extracellular flux analyzer (Table 3) as previously described (Blumensatt et al., 2017). For this, primary hepatocytes were seeded with a density of 1x 10^4 cells per well and C2C12 myoblast with a density of 5,000 cells per well on XF^{e}96 cell culture microplates (Table 10). Primary hepatocytes were seeded on type-I collagen coated XF^{e}96 cell culture microplates, with final concentration of 50 µg/ml collagen diluted in 0.02 M acetic acid. Myoblast were differentiated on XF^{e}96 cell culture microplates into myotubes for experiments. Hepatocytes and myotubes were treated with sFRP4 for the indicated time points and as described above (2.2.2.6). For analysis of mitochondrial respiration from OCR, cell medium was switched to unbuffered Seahorse mitochondrial respiration assay medium (Table 8) (pH 7.4 at 37^{o}C) and cells were incubated in a non-CO_2 incubator at 37°C, 1h before starting the experiment. OCR was measured under basal conditions and upon consecutive injections of the following compounds: 1 µM oligomycin, 0.5 µM FCCP for hepatocytes and 1 µM FCCP for myotubes followed by 0.5 µM or 1 µM antimycin A and rotenone for hepatocytes and myotubes, respectively. For analysis of glycolysis from ECAR, myotubes were exposed to sFRP4 for 24h either in serum-free differentiation medium containing 5 mM (low Glc) or 25 mM (high Glc) glucose followed by incubation in unbuffered Seahorse glycolysis assay medium (Table 8). The ECAR measurement was performed under basal conditions followed by sequential injection of 10 mM glucose, 1 µM oligomycin and 100 mM 2-Deoxyglucose (2-DG). OCR and ECAR were recorded in 3 cycles during basal respiration or glycolysis and after each injection step. Each cycle consisted of 3 min mixing and 3 min measurement. Monitored data were analyzed with WAVE software (2.2.7). Cellular protein content in each XF^{e}96 cell culture microplate well was determined by lysis in Seahorse cell lysis buffer (Table 6) and Pierce BCA Protein Assay Kit as described in 2.2.4.4 and used for assay normalization.

2.2.6 Histological techniques

2.2.6.1 Oil red O staining of lipids

Oil red O is a dye suitable for staining of neutral lipids within cultured cells or histological tissues and therefore enables the quantification and imaging of lipid accumulation. The staining is based on the lipophilic property of the dye to be more soluble in lipoid material than in its solvent resulting in a red staining of lipids.

0.7 g oil red O powder (Table 6) was dissolved in 200 ml isopropanol. To prepare a 60% oil red O working solution, the stock solution was diluted with H_2O (v/v) and filtered (0.2 µm) immediately before use. Cell culture supernatant was removed, cells were washed once with 1x PBS and fixed with 500 µl of 10% formalin per 12-well for 1h at 37°C. After removing the formalin, cells were washed with 60% isopropanol and 400 µl of oil red O working solution per 12-well was added for 10 min at room temperature under gentle agitation. Following, cells were washed four times with H_2O. For imaging of lipid accumulation, cultured wells were filled with H_2O and observed under the microscope.

2.2.7 Statistical analysis and software

If not stated otherwise in Figures, data were presented as mean ± standard deviation (SD) or 95% confidence interval of the mean of independent experiments. To identify significant differences between datasets with at least three n´s, different statistical tests were applied. For comparison of differences between two groups, unpaired or paired two-tailed *t*-test was used. Multiple comparisons between groups were assessed with ANOVA (one-way or two-way) following Bonferroni, Dunnett´s, Holm-Sidak´s, Tukey´s or Sidak´s correction analysis. Correlations between datasets were calculated with (partial) Spearman correlation coefficients or analyzed with linear regression using four different models: (1) unadjusted, (2) adjusted for age, (3) adjusted for BMI and (4) adjusted for age and BMI. Statistical analyses for *in vitro* experiments were performed using GraphPad Prism version 7.0 (GraphPad Software, La Jolla, CA, USA). Statistical analysis on the clinical data was conducted using SPSS Statistics (IBM, version 24.0, Ehningen, Germany). In all analyses, *p*-values <0.05 were considered as statistically significant. Quantification of chemiluminescence signals was performed using Image Lab™ Software 6.0 (Biorad Laboratories, München, Germany). Assesment and analysis of OCR and ECAR were conducted using WAVE software version 2.6 (Santa Clara, CA, USA).

Data of the secretome proteomics were statistically analyzed with Spectronaut™ v11, (Biognosys, Zürich, Swizerland). Protein secretion classification was performed with http://www.cbs.dtu.dk/services/SecretomeP/, http://www.cbs.dtu.dk/services/SignalP/ (Bendtsen et al., 2004; Petersen et al., 2011). Knowledge based analyses of the differential abundant proteins was performed with Inguenity Pathway Analyses (IPA®), winter release 2017 (Qiagen, Hilden, Germany).

2.2.8 Databases

Information on protein structures and length were obtained from https://www.ncbi.nlm.nih.gov/protein and http://www.uniprot.org and details on genes were taken from https://www.ncbi.nlm.nih.gov/gene/6424.

3 Results

3.1 Association of WISP1 with obesity and T2D and its role in the regulation of insulin action and glucose metabolism in liver and muscle

Unless otherwise noted, the described results of this work on page 58 to 74 have been adopted and were parts from the result section of the under *References* and *Appendix* cited manuscript Hörbelt et al. (2018) which has been published in the journal *Diabetologia* (Epub ahead of print).

Patient raw data and material that were kindly provided by Prof. Dr. Lapauw of Ghent University are stated in material section 2.2.1. All analyses and calculations of the data sets shown in the result section were performed as part of this thesis and the manuscript unless otherwise noted.

3.1.1 Anthropometric and metabolic characteristics of the study participants

The characteristics of the 33 normal-weight men and 102 morbidly obese men, of whom 46 had type 2 diabetes were listed in Table 22. The obese men without type 2 diabetes had a higher BMI, fat mass, and larger adipocytes than normal-weight men (all $p<0.001$), increased fasting insulin levels ($p<0.01$), a reduced insulin sensitivity ($p<0.05$) and increased beta cell function ($p<0.001$), both estimated by HOMA modelling ($p<0.05$). The obese participants with type 2 diabetes were older than the obese men without type 2 diabetes ($p<0.001$). In addition, fat mass ($p<0.05$) and fasting glucose levels ($p<0.001$) were higher, and beta cell function ($p<0.05$) was reduced in the obese men with type 2 diabetes vs those without type 2 diabetes.

Table 22. Patient characteristics

Variable	Normal-weight	Obese		Obese + T2D		*p*
N (men)	33	56		46		
Age (years)	46.9 (42.3-51.5)	42.1 (39.2-45.1)		52.0 (49.2-54.8)	§§§	<0.001
BMI (kg^2/m)	24.2 (23.2-25.2)	41.2 (39.7-42.6)	***	43.1 (41.1-45.1)	***	<0.001
Fat, % body weight	24.2 (22.1-26.4)	37.6 (33.5-41.7)	***	44.1 (41.3-46.9)	***, §	<0.001
SAT cell size, μm^2	3508 (2724-4292)	6425 (5726-7123)	***	5765 (5237-6294)	***	<0.001
VAT cell size, μm^2	3494 (2679-4309)	6004 (5027-6982)	***	5576 (4899-6253)	***	<0.001
Metabolic variables						
Fasting glucose, mmol/l	5.06 (4.67-5.45)	5.67 (5.21-6.13)		8.09 (7.18-9.01)	***, §§§	<0.001
Fasting insulin, pmol/l	37.4 (30.0-44.7)	136 (90.3-181)	**	170 (135-204)	***	<0.001
HOMA-IR	1.20 (0.94-1.47)	5.79 (2.94-8.63)	*	8.85 (6.86-10.84)	**	<0.001
HOMA2-%B	81.8 (64.1-100)	139 (118-160)	***	106 (87.3-124)	§	<0.001
HbA_{1c} (%)[a] (mmol/mol)	NA	5.78 (5.47-6.09) (39.67 (36.28-43.06))		7.48 (6.51-8.45) (58.25 (47.65-68.85))	§§	
CRP, mg/l (nmol/l)	2.31 (1.08-3.54) (22 (10.29-33.71))	4.78 (3.57-5.99) (45.52 (34-57.05))	*	3.74 (2.62-4.87) (35.62 (24.95-46.38))		<0.01
Circulating adipokine levels						
Adiponectin, mg/l	8.86 (7.35-10.38)	5.04 (4.26-5.82)	***	4.37 (3.69-5.04)	***	<0.001
Chemerin, µg/l	188 (162.9-214.8)	206.70 (188-225.4)		235 (213.1-256.9)	*	<0.05
Leptin, µg/l	3.74 (2.41-5.06)	32.04 (24.71 -39.37)	***	34.94 (29.66 -40.23)	***	<0.001
MCP1, ng/l	220 (338-499.1)	334.9 (300.2-369.6)		408.1 (358.3-457.9)		<0.05
Omentin, µg/l	383.5 (349.5-417.6)	387.6 (348.8-426.5)		442.8 (400.6-485)		>0.05
HO-1, ng/l	555.0 (294.2–815.8)	867.1 (563.5-1170.7)		578.4 (344.4-812.3)		0.072
VAT expression (AU)						
ADIPO	171.7 (61.8-281.6)	43.6 (32.9-54.2)	**	54.6 (32.9-76.3)	**, §§	<0.01
RARRES	1.16 (0.87-1.45)	0.92 (0.82-1.02)		0.81 (0.70-0.93) *	*	<0.05
CCL2	3.09 (0.90-5.28)	1.463 (0.83-2.10)		1.39 (0.66-2.12)		>0.05
ITLN1	9.04 (-0.60-18.68)	13.86 (7.7-20.03)		16.56 (9.07-24.04)		>0.05
HMOX1[b]	1.75 (0.95-2.55)	1.96 (-0.29-4.22)		2.17 (1.18-3.16)		0.791

The data are presented as mean (95% CI). Differences between the participant groups were calculated using ANOVA and Bonferroni correction for multiple comparisons. *p<0.05, **p<0.01 and ***p<0.001 obese men vs normal-weight men; $^{§}p$<0.05, $^{§§}p$<0.01 and $^{§§§}p$<0.001, obese men with vs without type 2 diabetes. The p-values in the right-hand column show the corresponding significance across all three groups by ANOVA. [a]For HbA_{1c}, only data for ten obese participants and 15 participants with type 2 diabetes available. [b]For *HMOX1* expression, data for 15 normal-weight individuals, five obese individuals and 16 individuals with type 2 diabetes available. BMI, body mass index; SAT, subcutaneous adipose tissue; VAT, visceral adipose tissue; CRP, C-reactive protein; MCP1, monocyte chemotactic protein; T2D, type 2 diabetes; HOMA2-%B, computer model of homeostasis model assessment (HOMA) for β-cell function (%B) (according to Hörbelt et al., 2018). Contribution: Data except for *ADIPOQ, RARRES2, CCL2, ITLN1* and *HMOX1* were measured at Ghent University and kindly provided for analyses of this work. Additional measurements for *ADIPOQ, RARRES2, CCL2, ITLN1* and *HMOX1* were performed as part of this thesis.

A subgroup of 42 obese men, of whom eight had type 2 diabetes, underwent an OGTT. As expected, the post-load glucose levels were higher in individuals with type 2 diabetes (Figure 9A, B), while post-load insulin levels were lower (Figure 9C, D), when compared with participants without type 2 diabetes.

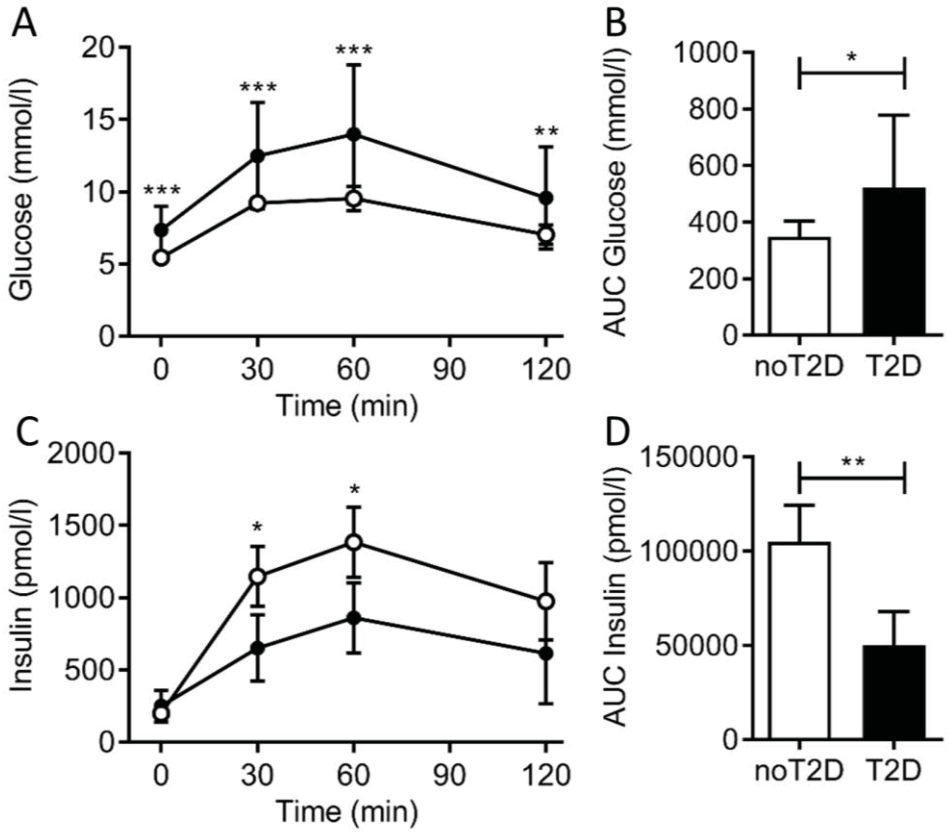

Figure 9. Glucose and insulin levels after an oral glucose tolerance test (OGTT). Glucose (**A**), AUC glucose (**B**), insulin (**C**), and AUC insulin (**D**) levels after an oral glucose tolerance test in morbidly obese men without (*n*=34, open circles) and with (*n*=8, filled circles) type 2 diabetes. AUC, area under the curve. The ***, **, and * indicate p<0.001, p<0.01, and p<0.05 for the differences between participants with or without type 2 diabetes as calculated by *t*-test, respectively**.**

3.1.2 WISP1 serum levels and gene expression in visceral adipose tissue in obesity and type 2 diabetes

WISP1 circulating levels were obtained in 123 out of 135 participants. In samples from two participants (one normal-weight and one obese), WISP1 levels were below the limit of detection; in the other participants without data, no serum sample was available for analysis. The circulating WISP1 level was 42.6 (28.5, 56.6) ng/l in normal-weight men (*n*=30) and 70.8 (55.2, 86.4) ng/l in obese men (*n*=93) (*p*<0.05, Figure 10A). There was no statistically significant difference in circulating WISP1 level between obese men with (69.4 [48.5, 90.3] ng/l; *n*=44) and without type 2 diabetes (72.2 [48.4, 95.6] ng/l; *n*=49) (Figure 10A).

VAT biopsies to analyze *WISP1* gene expression levels were available for 92 participants from the 'HepObster' cohort. The expression of *WISP1* was 1.9-fold higher in VAT from obese men (*n*=76) than in VAT from normal-weight men (*n*=16) (*p*<0.05). As with circulating WISP1 levels, no statistically significant differences in *WISP1* expression levels between obese men with (*n*=31) and without type 2 diabetes (*n*=45) were observed (Figure 10B). In paired SAT samples, *WISP1* mRNA levels were very low; reliable detection of *WISP1* (Ct<35 and single-peak melting curve) was achieved in only nine of the 33 samples analysed (data not shown). In addition, *WISP1* mRNA expression levels in the explants of paired SAT and VAT samples collected from study participants with obesity were compared (four men, two women, BMI 47.94 ± 3.96 kg/m^2, age 43.73 ± 4.59 years). In accordance with a previous report (Murahovschi et al., 2015), *WISP1* expression was ninefold higher in VAT than in SAT (*p*<0.05) (Figure 10C). Therefore, only values of the *WISP1* expression in VAT were used for further analysis.

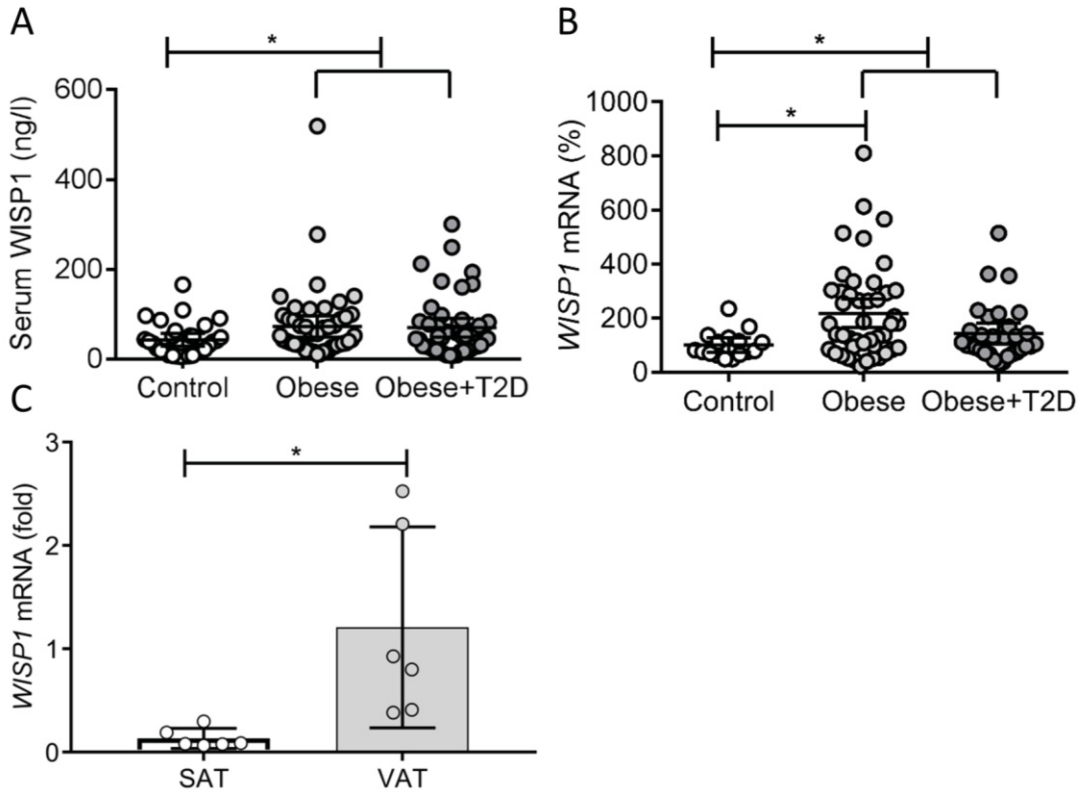

Figure 10. WISP1 serum levels and gene expression in visceral adipose tissue. WISP1 serum levels and gene expression in VAT. Quantification of circulating WISP1 levels (**A**) and gene expression in VAT normalized to *YWHAZ*, *RPS18*, *UBE2D2* **(B**) from normal-weight (control, *n*=30 (**A**), *n*=16 (**B**)) and obese men with (*n*=44 (**A**), *n*=31 (**B**)) and without (*n*=49 (**A**), *n*=45 (**B**)) type 2 diabetes. (**C**) Expression of *WISP1* in paired samples of VAT and SAT (**C**, *n*=6). Data (**A**-**C**) are presented as dot plot in which the mean and 95% CI for each group are shown. Differences among normal-weight men and obese men with and without T2D (brackets) were analysed by Mann-Whitney test (**A**, **B**). Brackets link data for obese men without and with T2D for analysis. Differences among all groups were analysed by ANOVA and Bonferroni correction for multiple comparisons (**B**). Data were analysed by paired *t*-test (**C**). **p*<0.05, obese vs normal-weight men (**A**, **B**); **p*<0.05, VAT vs SAT (**C**) (according to Hörbelt et al., 2018). Contribution: Measurements were performed as part of this thesis. Validating data of *WISP1* expression in explants of paired SAT and VAT biopsies of exemplified individuals were performed by Dr. Olga Pivovarova at the DIfE in Potsdam, Figure 10C.

3.1.3 Correlation of WISP1 serum levels and *WISP1* VAT gene expression with determinants of body composition and glucose metabolism

WISP1 VAT expression was positively associated with HOMA-IR (*r*=0.272, *p*=0.034) and with fasting glucose levels (r=0.262, *p*=0.042) (Table 23). Furthermore, a positive association with fasting insulin levels was observed (*r*=0.231), although this did not reach statistical significance (*p*=0.073).

Circulating WISP1 levels displayed a negative association with age (*r*=−0.193, *p*=0.034) and positive associations with determinants of body composition (e.g. BMI [*r*=0.207, *p*=0.022]) as well as with subcutaneous adipocyte cell size (*r*=0.368, *p*=0.015) (Table 23). There was also an association between circulating WISP1 level and visceral adipocyte cell size (*r*=0.292, *p*=0.058), although this did not reach statistical significance. Several determinants of glucose metabolism were positively associated with serum WISP1 levels: fasting insulin (*r*=0.255, *p*=0.022) and glucose (*r*=0.188, *p*=0.094); HOMA-IR (*r*=0.275, *p*=0.014); post-load glucose levels at multiple time points (30 min [*r*=0.312, *p*=0.072], 60 min [*r*=0.443, *p*=0.009], 120 min [*r*=0.335, *p*=0.052]) and AUC for glucose between 0 and 120 min (*r*=0.413, *p*=0.015) (Table 23). To note is, that calculations for HOMA-indices only were performed for normal-weight individuals and morbidly obese participants without type 2 diabetes and not taking glucose-lowering medication or insulin (Wallace et al., 2004).

Table 23. Correlation analysis for WISP1 expression and serum levels with anthropometric and metabolic markers.

Variable	*WISP1* VAT	WISP1 serum
N (men)	78	123
Age, years	0.183 (0.084)	-0.193 (0.034)*
BMI, kg/m^2	0.019 (0.859)	0.207 (0.022)*
Fat, % body weight	-0.477 (0.339)	0.279 (0.067)
SAT cell size, μm^2	0.040 (0.932)	0.368 (0.015)*
VAT cell size, μm^2	-0.064 (0.891)	0.292 (0.058)
Fasting glucose, mmol/l[a]	0.262 (0.042)*	0.188 (0.094)
Fasting insulin, pmol/l[a]	0.231 (0.073)	0.255 (0.022)*
HOMA-IR[a,b]	0.272 (0.034)*	0.275 (0.014)*
HOMA2-%B[a,b]	0.019 (0.886)	0.130 (0.252)
ISI Gutt$_{0–120\ min}$[b]	0.001 (0.995)	-0.401 (0.035)*
Insulin, OGTT, at 0 min[a,b]	0.142 (0.408)	0.110 (0.541)
Insulin, OGTT at 30 min[a,b]	0.114 (0.507)	-0.008 (0.963)
Insulin, OGTT, at 60 min[a,b]	0.073 (0.672)	0.205 (0.252)
Insulin, OGTT, at 120 min[a,b]	0.007 (0.969)	0.176 (0.326)
Insulin, OGTT, AUC$_a$	0.051 (0.769)	0.100 (0.579)
Glucose, OGTT, at 0 min[a,b]	-0.048 (0.778)	0.172 (0.330)
Glucose, OGTT at 30 min[a,b]	0.019 (0.910)	0.312 (0.072)

Variable	*WISP1* VAT	WISP1 serum
Glucose, OGTT, at 60 min[a,b]	0.014 (0.934)	0.443 (0.009)**
Glucose, OGTT, at 120 min[a,b]	-0.044 (0.795)	0.335 (0.052)
AUC glucose$_{0–120\ min}$, mmol/l[a,b]	0.025 (0.884)	0.413 (0.015)*

The data are presented as Pearson's *r* (*p*). [a]Variables with a skewed distribution were log-transformed prior to the regression analysis. [b]In the analysis of OGTT data, participants with insulin treatment were excluded from the analysis. ISI, insulin sensitivity index; OGTT, oral glucose tolerance test. **p*<0.05 and ***p*<0.01 (according to Hörbelt et al., 2018). Contribution: Data were measured at Ghent University and kindly provided for analyses of this work.

As shown in Table 24, adjusting for age had no major impact on the relationship between *WISP1* gene expression and HOMA-IR (β=0.261, *p*=0.041) but the associations with fasting glucose (β=0.232, *p*=0.085) and fasting insulin (β=0.233, *p*=0.069) lost their statistical significance (Table 24). The association between HOMA-IR and *WISP1* gene expression lost statistical significance upon adjustment for age and BMI (β=0.240, *p*=0.101).

Table 24. Regression analysis of *WISP1* expression in visceral adipose tissue.

Variable	Unadjusted	Age adjusted	Age and BMI adjusted
BMI, kg/m^2	0.024 (0.824)	0.020 (0.854)	NA
Fat, % body weight	-0.477 (0.339)	-0.497 (0.401)	-4.584 (0.320)
SAT cell size, μm^2	0.040 (0.932)	0.037 (0.944)	1.052 (0.733)
VAT cell size, μm^2	-0.064 (0.891)	-0.188 (0.775)	-2.729 (0.320)
Fasting glucose, mmol/l[a]	0.262 (0.042)*	0.232 (0.085)	0.212 (0.120)
Fasting insulin, pmol/l[a]	0.231 (0.073)	0.233 (0.069)	0.205 (0.168)
HOMA-IR[a,b]	0.272 (0.034)*	0.261 (0.041)*	0.240 (0.101)
HOMA2-%B[a,b]	0.019 (0.886)	0.065 (0.630)	0.002 (0.988)
ISI Gutt$_{0–120\ min}$[b]	0.001 (0.995)	-0.007 (0.974)	-0.068 (0.753)

The data indicate standardized regression coefficient β, with *p*-value shown in parentheses using measured *WISP1* expression data of study participants of all groups (normal-weight, obese, obese+T2D) combined. [a]Variables with a skewed distribution were log-transformed prior to the regression analysis. [b]Participants treated with insulin were excluded from the analysis. **p*<0.05 and ***p*<0.01 (according to Hörbelt et al., 2018). Contribution: Data were measured at Ghent University and kindly provided for analyses of this work.

The associations of WISP1 serum levels with BMI (β=0.192, *p*=0.033), subcutaneous adipocyte size (β=0.322, *p*=0.039), post-load glucose at 60 min (β=0.442, *p*=0.013) and AUC glucose$_{0–}$

$_{120min}$ (β=0.428, *p*=0.021) remained significant after adjusting for age (Table 25). After adjusting for age and BMI, the associations between circulating WISP1 and post-load glucose at 60 min (β=0.434, *p*=0.018), and AUC glucose $_{0\text{-}120min}$ (β=0.420, *p*=0.028) were still statistically significant (Table 25). Moreover, circulating WISP1 levels were negatively associated with Gutt's index of insulin sensitivity (*r*=−0.401, *p*=0.035; *n*=28; Table 25) and this association remained significant after adjusting for age and BMI (β=−0.438, *p*=0.037; Table 25).

Table 25. Regression analysis of circulating WISP1 levels.

Variable	Unadjusted	Age adjusted	Age and BMI adjusted
BMI, kg/m^2	0.207 (0.022)*	0.192 (0.033)*	NA
Fat, % body weight	0.279 (0.067)	0.288 0.056)	-0.115 (0.794)
SAT cell size, μm^2	0.368 (0.015)*	0.322 (0.039)*	0.191 (0.399)
VAT cell size, μm^2	0.292 (0.058)	0.265 (0.081)	0.146 (0.397)
Fasting glucose, mmol/l[a]	0.202 (0.091)	0.201 (0.079)	0.183 (0.114)
Fasting insulin, pmol/l[a]	0.241 (0.044)*	0.182 (0.123)	0.128 (0.385)
HOMA-IR[a,b]	0.262 (0.028)*	0.210 (0.073)	0.171 (0.231)
HOMA2-%B[a,b]	0.099 (0.415)	0.035 (0.771)	-0.056 (0.676)
ISI Gutt$_{0–120\ min}$[b]	-0.401 (0.035)*	-0.397 (0.042)*	-0.438 (0.037)*
Glucose, OGTT at 30 min[a,b]	0.312 (0.072)	0.312 (0.107)	0.313 (0.108)
Glucose, OGTT, at 60 min[a,b]	0.443 (0.009)**	0.442 (0.013)*	0.434 (0.018)*
Glucose, OGTT, at 120 min[a,b]	0.335 (0.052)	0.331 (0.077)	0.320 (0.100)
AUC glucose$_{0–120\ min}$, mmol/l[a,b]	0.416 (0.015)*	0.428 (0.021)*	0.420 (0.028)*

The data indicate standardized regression coefficient β, with *p*-value shown in parentheses using measured WISP1 serum data of study participants of all groups (normal-weight, obese, obese+T2D) combined. [a]Variables with a skewed distribution were log-transformed prior to the regression analysis. [b]Participants treated with insulin were excluded from the analysis. **p*<0.05 and ***p*<0.01 (according to Hörbelt et al., 2018). Contribution: Data were measured at Ghent University and kindly provided for analyses of this work.

3.1.4 Correlates of WISP1 serum and gene expression levels with markers of adipose tissue and systemic inflammation

Because WISP1 has been shown to induce an inflammatory response in human macrophages (Murahovschi et al., 2015), next the association of *WISP1* expression and serum levels with markers of adipose tissue inflammation (mRNA levels of *ADIPOQ*, *RARRES2*, *CCL2*, *ITLN1*) and systemic inflammation (adiponectin, CRP, chemerin, leptin, MCP-1, omentin) were in focus of

investigation. Moreover, the association of WISP1 with serum HO-1 which is associated with insulin resistance and adipose tissue inflammation and activates Wnt signaling was studied (Li et al., 2008; Vanella et al., 2013). Compared with normal-weight participants, circulating levels of adiponectin, leptin and CRP were increased and VAT *ADIPOQ* mRNA levels were decreased in obese individuals ($p<0.001$, $p<0.001$, $p=0.014$ and $p=0.002$, respectively) (Table 22). Serum levels of chemerin and VAT levels of *RARRES2* mRNA were higher in obese individuals with vs without diabetes ($p=0.014$ and $p=0.010$, respectively) (Table 22).

Circulating WISP1 levels showed a negative association with serum adiponectin ($r=-0.190$, $p=0.031$) and a highly significant positive association with serum HO-1 levels ($r=0.437$, $p=1.3 \times 10^{-5}$) (Table 26). An association with serum adiponectin remained significant after adjusting for age (β=-0.176, $p=0.041$). The association with serum adiponectin remained significant after adjusting for age ($\beta=-0.176$, $p=0.041$); the association with HO-1 remained significant after adjusting for age ($\beta=0.319$, $p=0.002$) and for age and BMI ($\beta=0.303$, $p=0.004$). *WISP1* mRNA expression in VAT showed a positive correlation with *CCL2* expression ($r=0.253$, $p=0.021$) (Table 26) and this association remained statistically significant after adjusting for age and BMI (β=0266, $p=0.015$).

Table 26. Correlation analysis of WISP1 expression and serum levels with inflammatory markers.

Variable	*WISP1* VAT	WISP1 serum
N (men)	78	123
CRP, nmol/l[a]	0.045 (0.691)	-0.110 (0.246)
Adiponectin, mg/l[a]	-0.092 (0.410)	-0.190 (0.031)*
Chemerin, µg/l	0.074 (0.511)	-0.068 (0.449)
Leptin, µg/l	0.114 (0.476)	0.103 (0.358)
Omentin, µg/l	0.135 (0.228)	-0.095 (0.283)
MCP1, ng/l[a]	0.080 (0.482)	-0.181 (0.055)
HO-1, ng/l	-0.261 (0.073)	0.437 ($1.3x10^{-5}$)***
ADIPOQ VAT (AU)	0.030 (0.797)	-0.004 (0.963)
RARRES2 VAT (AU)	-0.132 (0.235)	0.005 (0.961)
CCL2 VAT (AU)	0.253 (0.021)*	0.008 (0.931)
ITLN1 VAT (AU)	0.118 (0.295)	-0.174 (0.070)
HMOX1 (AU)[b]	0.122 (0.795)	0.124 (0.470)

[a]Variables with a skewed distribution were log-transformed prior to the analysis. Correlation analysis was performed using Pearson or Spearman test dependently on the data distribution and presented as *r* (*p*) or rho

(*p*). [b] n=36. ***, ** and * indicate p<0.001, *p*<0.01, and *p*<0.05 (according to Hörbelt et al., 2018). Contribution: Data except for *ADIPOQ, RARRES2, CCL2, ITLN1* and *HMOX1*, were measured at Ghent University and kindly provided for analyses of this work. Additional measurements for *ADIPOQ, RARRES2, CCL2, ITLN1* and *HMOX1* were performed as part of this thesis.

3.1.5 Effects of WISP1 on insulin signaling and glucose metabolism in myotubes and hepatocytes

The observed relationship between circulating WISP1 and HOMA-IR as well as post-load glucose levels, together with the previous observation of the negative association between *WISP1* VAT expression and hyperinsulinaemic–euglycaemic clamp-derived insulin sensitivity (Murahovschi et al., 2015) suggest that WISP1 may interfere with insulin signaling. To examine this in more detail, primary hSkMC were exposed to recombinant WISP1 before analysis of insulin action. As shown in Figure 11A, B the insulin-mediated induction of Akt on Thr308 and Ser473 phosphorylation in primary hSkMC was reduced by 40% in cells that were exposed to 1 µg/l WISP1 before the addition of insulin. The reductions in insulin-mediated Akt phosphorylation induced by WISP1 were accompanied by decreases in insulin-mediated GSK3β-Ser9, p70S6K-Thr389 and IRβ-Tyr-1150/1151 phosphorylation (Figure 11C-E). This inhibition of the insulin-mediated phosphorylation was achieved already in the presence of 0.1 µ/l WISP1.

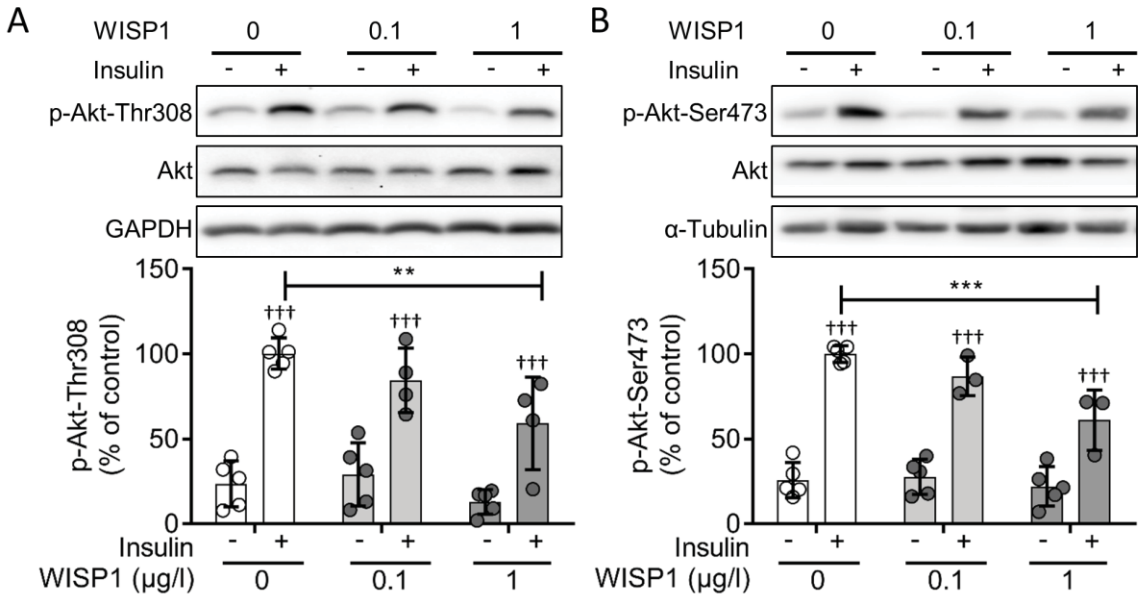

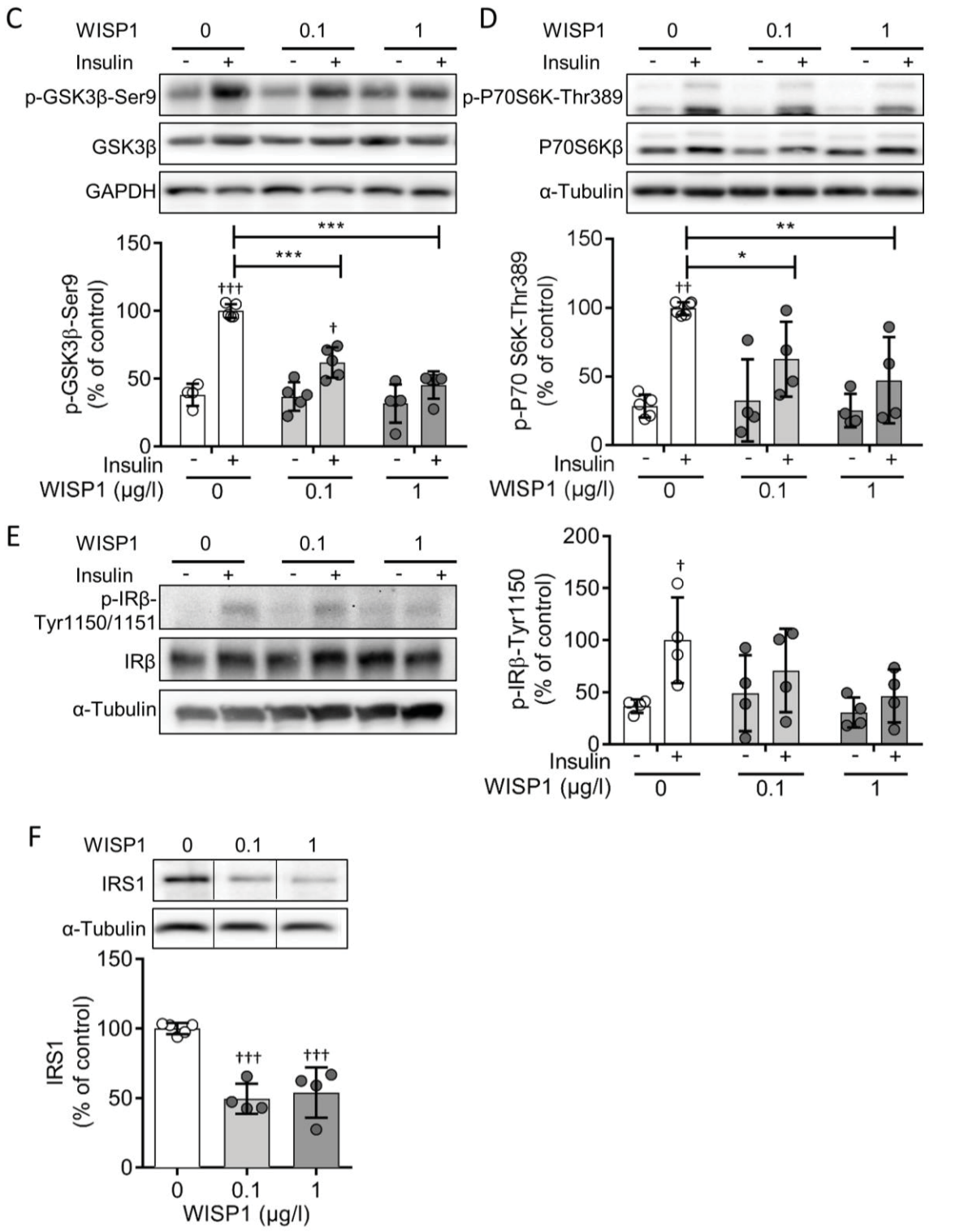

Figure 11. Effect of WISP1 on insulin signaling in primary hSkMCs. Representative western blots and bar graphs show the effects of WISP1 on insulin-stimulated phosphorylation of Akt-Thr308 (**A**), Akt-Ser473 (**B**), GSK3β-Ser9 (**C**), and p70 S6 kinase-Thr389 (**D**), IRβ-Tyr1150/1151 (**E**) and on protein abundance of IRS-1 (**F**). The dividing lines in the blots in (**F**) indicate places where the blot has been cut. The scattered bar graphs indicate the mean ± SD for the phosphorylation levels obtained in four to five (**A, C, D**), three to five (**B**), four (**E**, **F**) independent experiments in primary hSkMCs obtained from different donors. The phosphorylation levels were normalized for the protein abundances of the non-phosphorylated proteins, GAPDH or α-tubulin, as indicated. The values

obtained in cells incubated with 100 nM insulin only were considered as the control and set at 100%. The effects of WISP1 and insulin were analysed by two-way ANOVA with Bonferroni correction for multiple comparisons. *p<0.05 **p<0.01 and ***p<0.001, with vs without WISP1 incubation; $^{\dagger}p$<0.05 $^{\dagger\dagger}p$<0.01 and $^{\dagger\dagger\dagger}p$<0.001, with vs without insulin stimulation. Differences among groups were calculated by one-way ANOVA with Tukey´s multiple comparisons test (**F**). $^{\dagger\dagger\dagger}p$<0.001, with vs without WISP1 incubation (according to Hörbelt et al., 2018).

Of further note, the reductions in phosphorylation levels could not be ascribed to changes in the protein abundances of Akt, IRβ, GSK3β or p70S6K (Figure 12). In contrast, the abundance of IRS-1 protein was reduced by ~50% in cells that were exposed to WISP1 (Figure 11F).

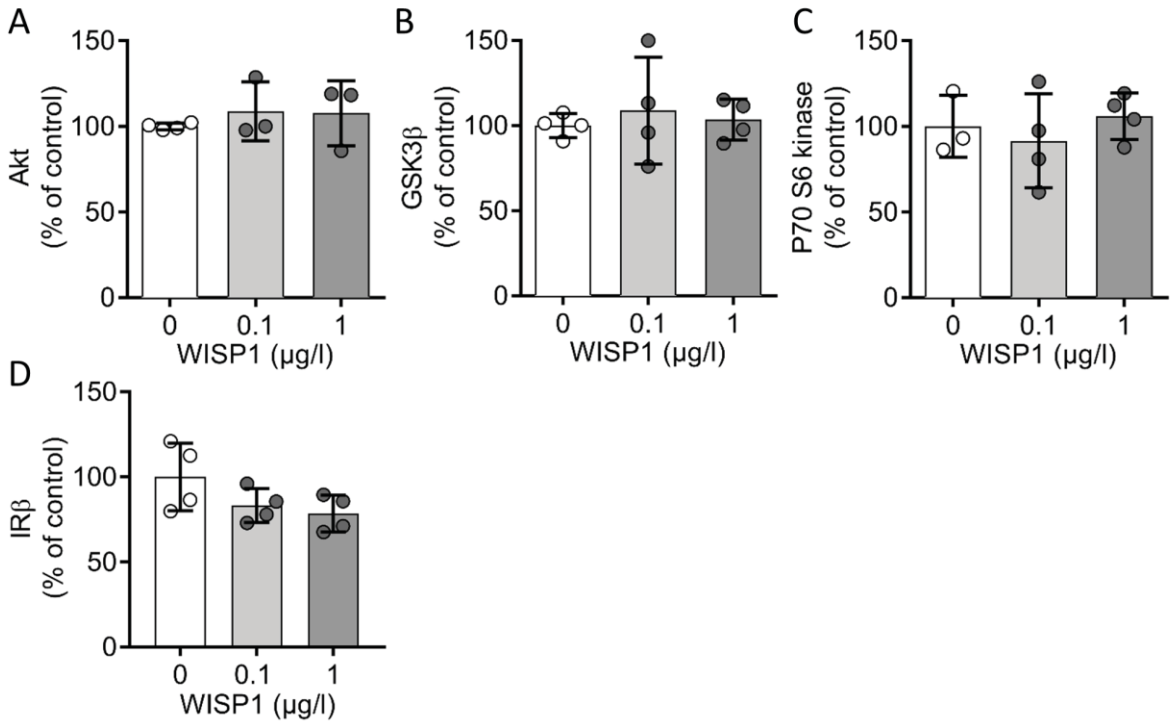

Figure 12. Effect of WISP1 on protein abundance of components of insulin action in primary hSkMC. The graphs show the mean ± SD for the protein abundance of Akt (**A**), GSK3β (**B**), p70 S6 kinase (**C**) and IRβ (**D**) in cells kept untreated (0 µg/l) or exposed to WISP1. The expression levels were normalized for the protein abundances of GAPDH and α-tubulin, respectively. The values obtained in cells that were kept untreated only were considered as control and set at 100% (according to Hörbelt et al., 2018).

To demonstrate the functional relevance of the reduced insulin signaling, further effects of the WISP1 treatment on insulin-stimulated glycogen synthesis were investigated. Insulin treatment (100 nM) for 3h significantly increased glycogen synthesis in primary human myotubes compared with basal conditions, whereas in cells pre-incubated with 0.1 or 1 µg/l WISP1 for 24h, this effect was completely abrogated (Figure 13).

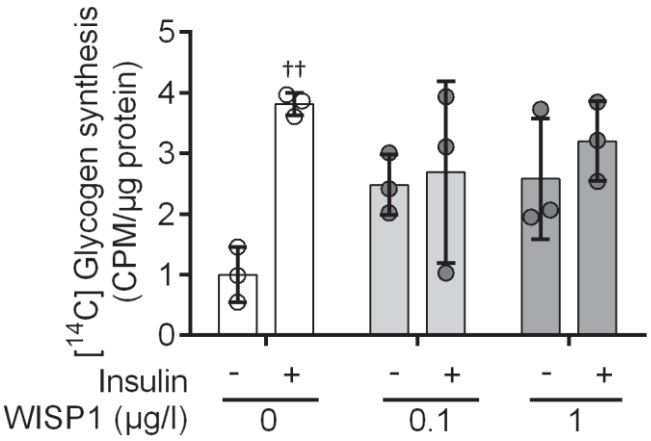

Figure 13. Effect of WISP1 on insulin-stimulated glycogen synthesis in primary hSkMC. Myotubes were exposed to WISP1 for 24h before glycogen synthesis was determined as incorporation of D-[U-^{14}C]-glucose into glycogen in the absence or presence of insulin (100 nM) for 3h. Data are normalised to amount of protein for three independent experiments (*n*=3) and are shown as mean ± SD. The effects of WISP1 and insulin were analyzed by two-way ANOVA and Bonferroni correction for multiple comparisons. $^{††}p<0.01$, with vs without insulin (according to Hörbelt et al., 2018).

Largely comparable data were obtained for the murine hepatocyte cell line AML12. Exposing AML12 cells to WISP1 caused a dose-dependent reduction in insulin-induced Akt-Thr308 and Akt-Ser473 phosphorylation (Figure 14A, B). The induction of GSK3β-Ser9 phosphorylation by insulin in hepatocytes was not affected by WISP1 (Figure 14C) whereas the inhibition of insulin-induced Akt phosphorylation was accompanied by a reduction in p70S6K-Thr389 and IRβ-Tyr-1150/1151 phosphorylation (Figure 14D, E). Therefore, to corroborate the effects of WISP1 on distal Akt signaling, another Akt substrate, namely phosphorylation of FoxO1 at Ser256, was analyzed. Figure 14F shows that incubating AML12 cells with 0.1 and 1 µg/l WISP1 impaired the induction of FoxO1-Ser256 phosphorylation by insulin.

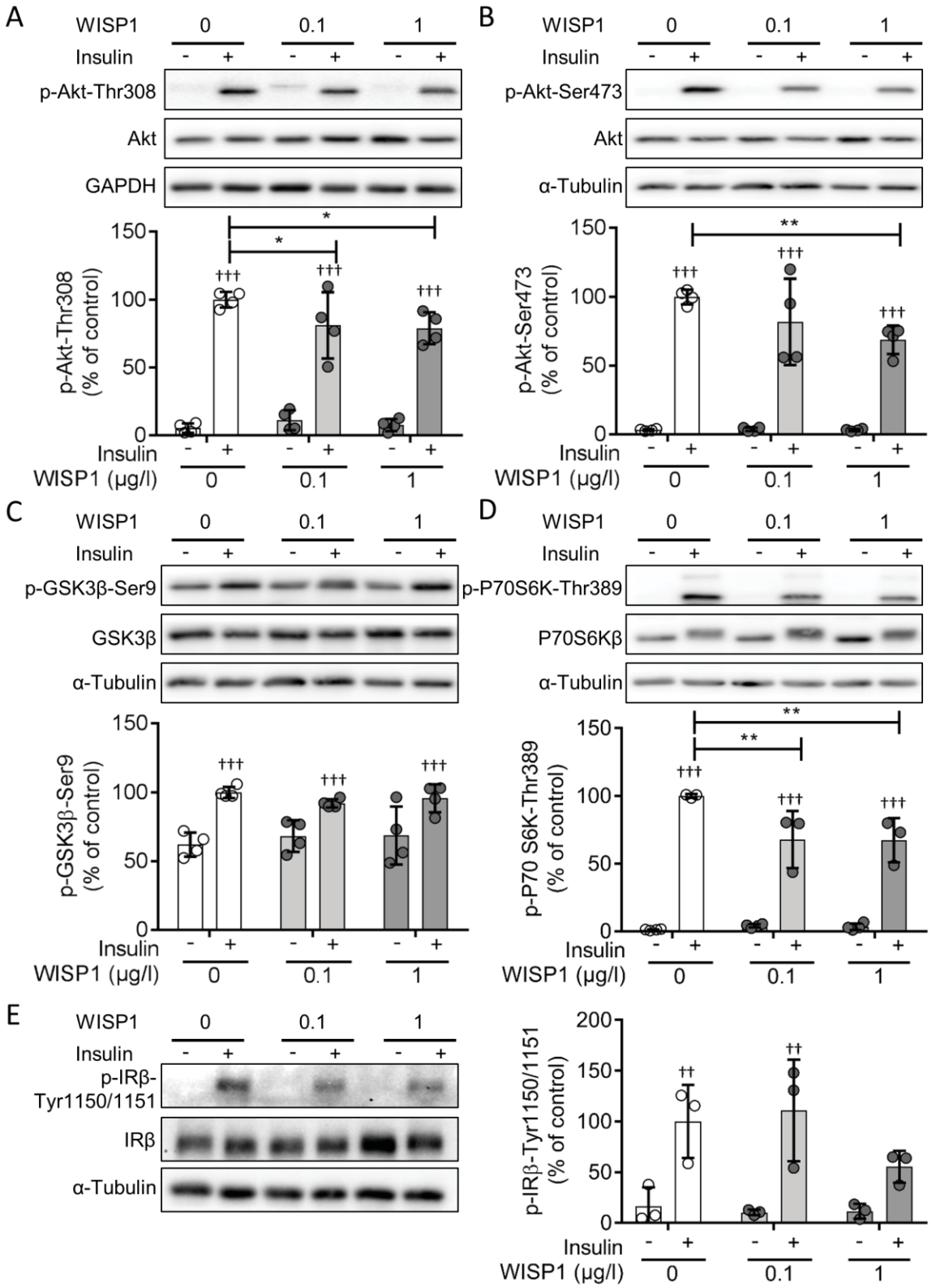
A
WISP1
0
0.1
1
Insulin
- + - + - +
p-Akt-Thr308
Akt
GAPDH
p-Akt-Thr308 (% of control)
150
100
50
0
*
*
†††
Insulin
WISP1 (µg/l)
B
p-Akt-Ser473
α-Tubulin
p-Akt-Ser473 (% of control)
**
C
p-GSK3β-Ser9
GSK3β
α-Tubulin
p-GSK3β-Ser9 (% of control)
D
p-P70S6K-Thr389
P70S6Kβ
p-P70 S6K-Thr389 (% of control)
E
p-IRβ-Tyr1150/1151
IRβ
p-IRβ-Tyr1150/1151 (% of control)
200
150
††

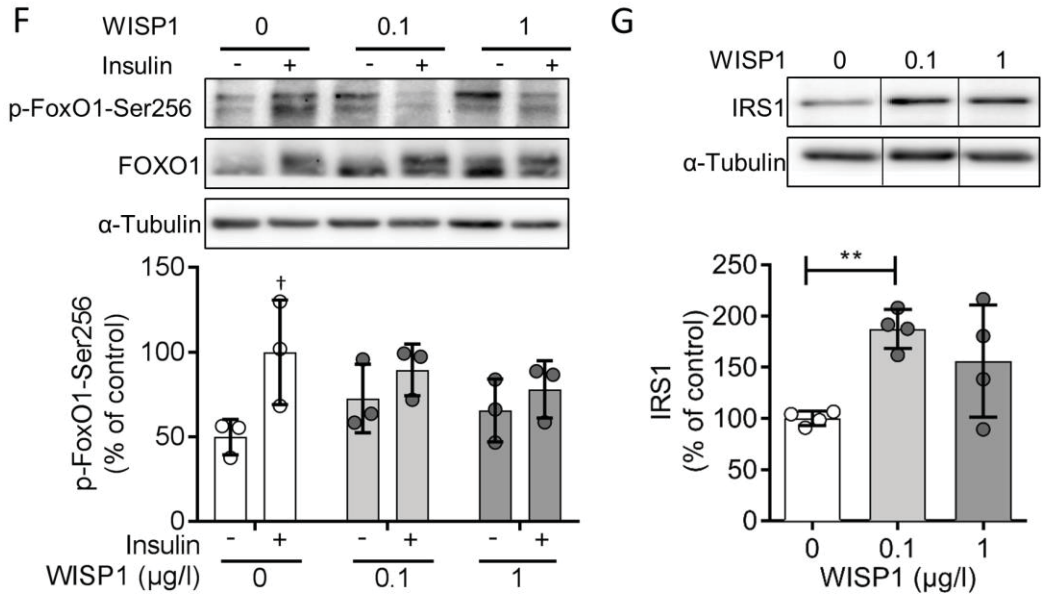

Figure 14. Effect of WISP1 on insulin signaling in AML12 hepatocytes. Representative Western blots and bar graphs show the effects of WISP1 on insulin-stimulated phosphorylation of Akt-Thr308 (**A**), Akt-Ser473 (**B**), GSK3β-Ser9 (**C**), p70 S6 kinase-Thr389 (**D**), IRβ-Tyr1150/1151 (**E**) and FoxO1-Ser256 (**F**) and on protein abundance of IRS-1 (**G**). The dividing lines in the blots in **G** indicate places where the blot has been cut. The scattered bar graphs indicate the mean ± SD for the phosphorylation levels obtained in three to four independent experiments. The phosphorylation levels were normalized for the protein abundances of the non-phosphorylated protein, GAPDH or α-tubulin, as indicated. The values obtained in cells incubated with 100 nM insulin only were considered as the control and set at 100%. The effects of WISP1 and insulin were analyzed by two-way ANOVA with Bonferroni (**A**-**F**) and one-way ANOVA (**G**) with Dunnett´s correction for multiple comparisons. *p<0.05 and **p<0.01, with vs without WISP1 incubation; $^{\dagger}p$<0.05 $^{\dagger\dagger}p$<0.01 and $^{\dagger\dagger\dagger}p$<0.001, with vs without insulin stimulation (according to Hörbelt et al., 2018).

In contrast to the findings in myotubes, the abundance of IRS-1 protein was doubled in AML12 cells exposed to WISP1 (Figure 15G), whereas the abundances of Akt, GSK3β, p70S6K, IRβ and FoxO1 were not affected (Figure 15). In addition, WISP1 incubation had no effect on the abundance of IRS-2 (Figure 15F).

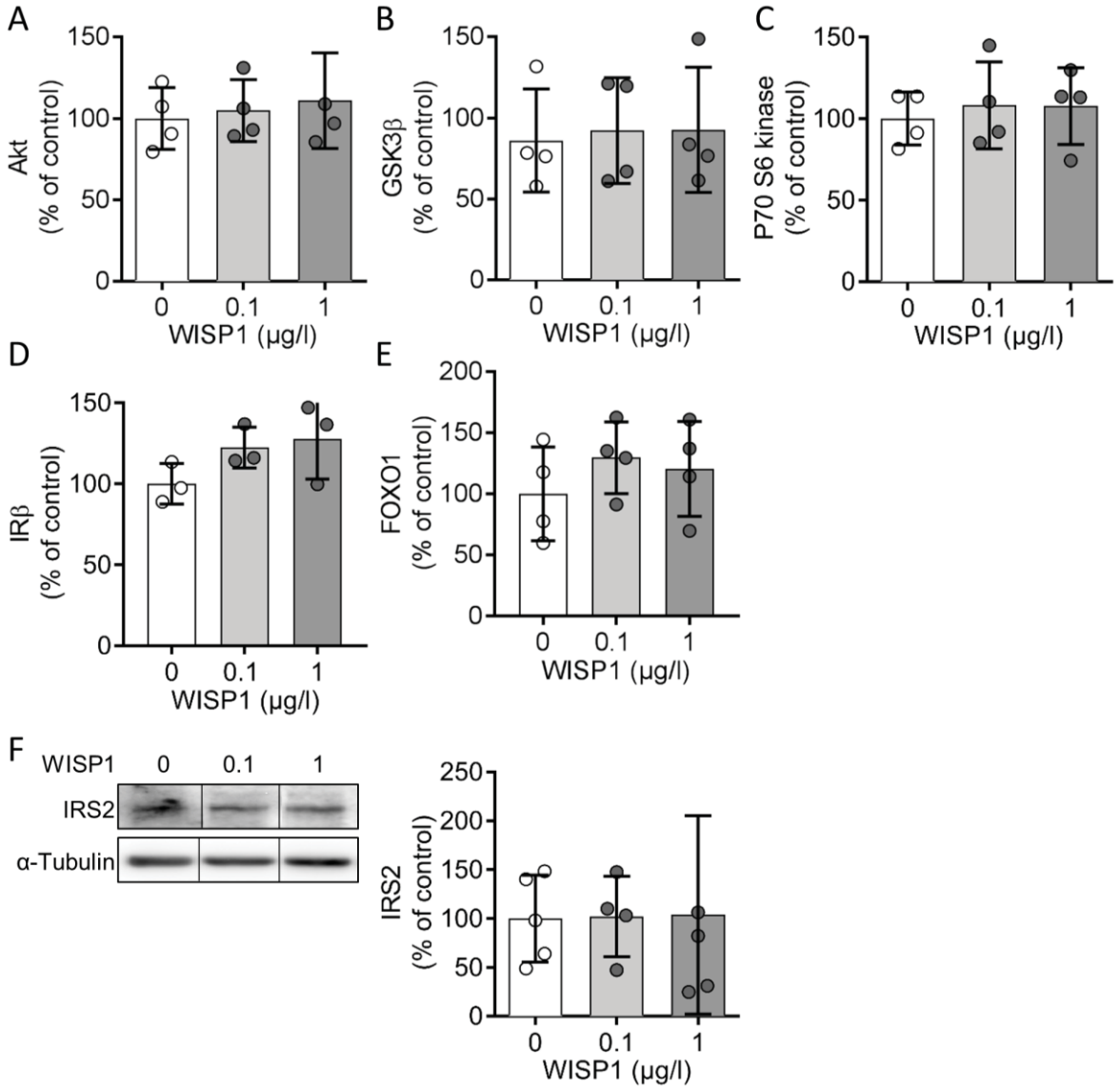

Figure 15. Effect of WISP1 on protein abundance of components of insulin action in mouse AML12 hepatocytes. The graphs show the mean ± SD for the protein abundance of Akt (**A**), GSK3β (**B**), p70 S6 kinase (**C**), IRβ (**D**), FoxO1 (**E**) and IRS-2 (**F**) in cells kept untreated (0 µg/l) or exposed to WISP1. The expression levels were normalized for the protein abundances of GAPDH and α-tubulin, as indicated. The values obtained in cells that were kept untreated only were considered as control and set at 100% (according to Hörbelt et al., 2018).

Further, WISP1 treatment abrogated the insulin-mediated suppression of the gluconeogenic genes *Pck1* and *G6pc* in primary mouse hepatocytes (Figure 16).

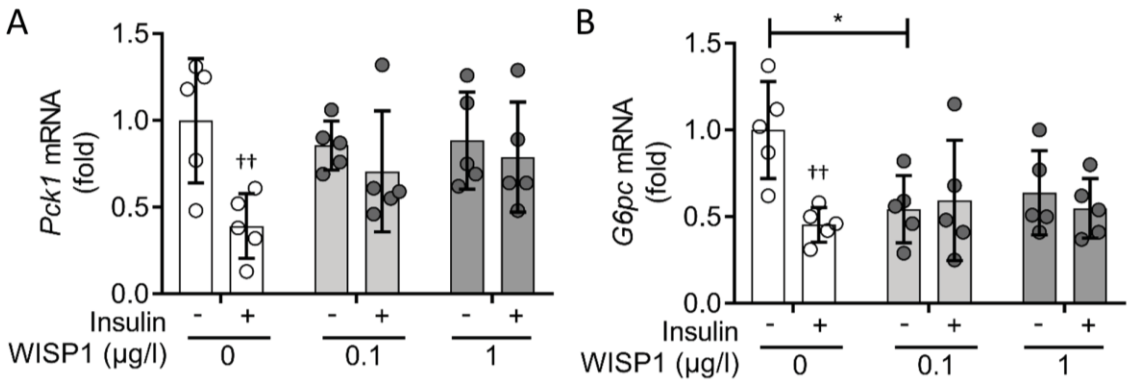

Figure 16. WISP1 impaired the insulin-mediated suppression of gluconeogenic gene expression in primary hepatocytes. Hepatocytes were exposed to WISP1 for 24h. The last 60 min of the WISP1 incubation was carried out in the absence or presence of insulin (100 nM). *Pck1* (**A**) and *G6pc* (**B**) expression levels were assessed by quantitative RT-PCR and normalized to *18S*. Data represent mean ± SD of the expression levels of five independent experiments using cells from different mice. The values obtained for untreated cells were considered as controls and set as 1. Differences among conditions were calculated by two-way ANOVA with Bonferroni correction for multiple comparisons. *p<0.05, with vs without WISP1 incubation; $^{††}p$<0.01, with vs without insulin stimulation (according to Hörbelt et al., 2018).

3.2 Association of the adipokine sFRP4 with obesity and type 2 diabetes and its functional role in skeletal muscle and liver physiology

The second part of this thesis focuses on the investigation whether the expression of the adipokine *sFRP4* was altered with obesity and/or type 2 diabetes and associated with insulin resistance. Further, this part examines the impact of sFRP4 on the regulation of insulin action and energy metabolism in two major insulin-sensitive cell-types including skeletal muscle cells and hepatocytes (unpublished data).

3.2.1 Anthropometric and metabolic characteristics of the study participants

The basic characteristics of the 28 normal-weight men, 46 obese men and 42 obese men with type 2 diabetes are presented in Table 27. For the analyses, the data were kindly provided by colleagues from the Department of Internal medicine at Ghent University as stated in 2.2.1. Obese men with type 2 diabetes differed in their ages in comparison to obese participants without type 2 diabetes (p<0.01). In addition to higher BMI, obese study participants without type 2 diabetes had significant elevated fasting insulin levels (p<0.01), triglycerides (p<0.05) and C-reactive protein (CRP) (p<0.01) levels compared to normal-weight men. Study participants with type 2 diabetes had enhanced fasting glucose levels in comparison to obese subjects without type 2 diabetes and normal-weight individuals (both p<0.001) and higher fasting insulin levels (p<0.001) and an increased HOMA-IR compared to normal-weight men (p<0.01). In contrast, all obese men showed significant lower adiponectin levels (p<0.001) but higher serum leptin levels (all p<0.001) than normal-weight men. Additionally, obese individuals with and without type 2 diabetes had lower *SLC2A4/GLUT4* expression levels in VAT than normal-weight men (all p<0.01).

Table 27. Clinical cohort characteristics of normal-weight (controls) and obese study participants with and without type 2 diabetes.

Variable	Normal-weight	Obese	Obese + T2D	*p*
N (men)	28	46	42	
Age (years)	48.61	42.54##	51.33	0.003
BMI (kg²/m)	24.12 (23.05 - 25.18)	40.96 39.4 - 42.52)***	42.91 (40.80 - 45.02)***	<0.001
Metabolic variables				
Fasting glucose (mmol/l)	5.71 (4.44 - 6.99)	5.72 (5.21 - 6.22) ##	7.63 (6.72 - 8.54)**	0.001
Fasting insulin (pmol/l)	35.21 (27.87 - 42.55)	133.3 (76.93 – 189.6)**	164.7 (125.1 – 204.3)***	0.001
HOMA-IR	1.32 (0.91 - 1.72)	5.85 (2.34 - 9.35)	8.05 (5.91 - 10.18)**	0.006
Triglycerides (mg/dl)	132.9 (105.9 - 159.8)	217.7 (158 – 277.4)*	214.4 (174.4 – 254.4)	0.04
CRP (mg/l)	2.06 (0.77 - 3.35)	4.72 (3.39 - 6.06) **	3.46 (2.3 - 4.63)	0.02
Circulating adipokine levels				
Adiponectin (mg/l)	9.35 (7.44 - 11.25)	4.96 (4.09 - 5.84)***	4.28 (3.51 – 5.05)***	<0.001
Leptin (µg/l)	4.03 (2.41 – 5.66)	30.56 (22.2 – 38.91)***	34.81 (28.71 – 40.91)***	<0.001
VAT expression (AU)				
SLC2A4/GLUT4	2.35 (1.53 - 3.17)	1.26 (0.95 - 1.57) **	1.34 (1.0 - 1.68)**	0.003

Data are presented as mean (95% CI). Differences between the participant groups were calculated using one-way ANOVA and Bonferroni correction for multiple comparisons. *vs normal-weight controls; #vs obese + T2DM. */#*p*<0.05, **/##*p*<0.01, ***/###*p*<0.001. *SLC2A4/GLUT4*, solute carrier family 2 (glucose transporter) member 4.

3.2.2 *sFRP4* mRNA expression in VAT of obese men with and without T2D and its association with markers of insulin resistance, glucose and lipid metabolism

sFRP4 mRNA expression was determined in VAT and SAT of study participants of the described cohort (Table 27). Interestingly, the expression of *sFRP4* in VAT was 1.9-fold higher than in SAT (Figure 17A, *p*<0.001). *sFRP4* mRNA expression in VAT was increased by 2.8-fold in obese individuals (*p*<0.01) and 3.7-fold in obese men with type 2 diabetes (*p*<0.001) compared to normal-weight men (Figure 17B). Furthermore, *sFRP4* mRNA was 1.3-fold higher expressed in VAT of obese, type 2 diabetic individuals than in men with obesity but without type 2 diabetes (Figure 17B). However, *sFRP4* mRNA expression in SAT neither was altered with obesity nor

with type 2 diabetes (Figure 17C). Therefore, only values for *sFRP4* expression in VAT were used for further analysis.

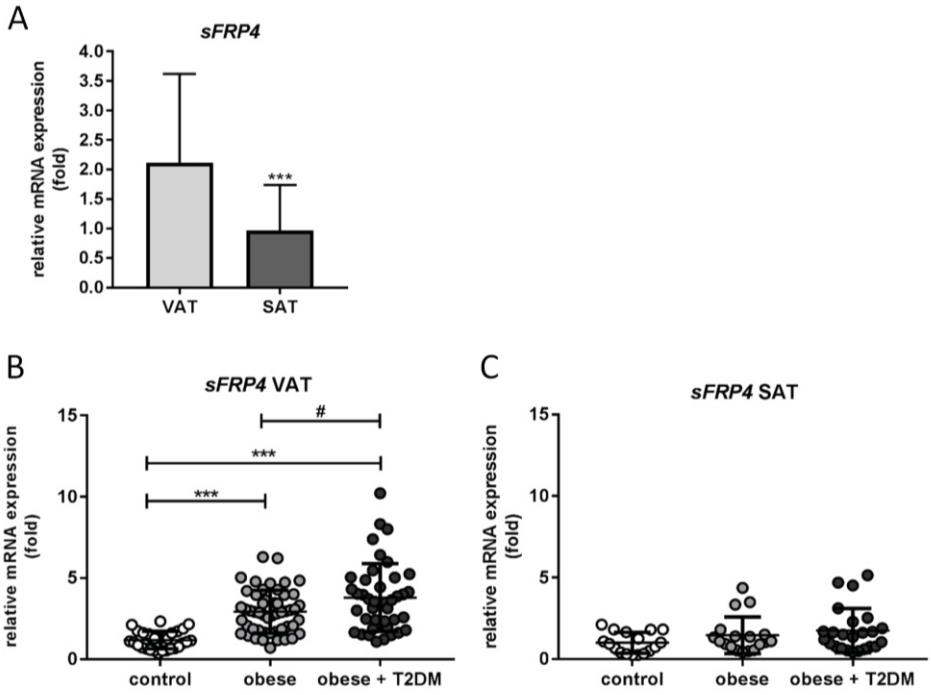

Figure 17. *sFRP4* mRNA expression in VAT and SAT of normal-weight (controls) and obese men with and without T2D. Relative mRNA expression levels of *sFRP4* in VAT and SAT of combined study participant groups (**A**, paired samples *n*=54) and grouped in normal-weight (controls) and obese men with and without T2D (**B** *n*=116, **C** *n*=59) were shown. Relative mRNA expression was obtained by qRT-PCR, normalized to geomean of *YWHAZ*, *RPS18*, *UBE2D2* and analyzed by $2^{-\Delta\Delta Ct}$-method. Data are given as mean and 95% CI. Differences among groups were analyzed using paired *t*-test or one-way ANOVA following Tukey´s multiple comparisons test. * versus normal-weight controls; # versus obese + T2DM. */# $p < 0.05$; **/## $p < 0.01$; ***/### $p < 0.001$.

It was examined whether *sFRP4* mRNA expression in VAT associates with established markers of insulin resistance, obesity and metabolic regulation in the study samples (all three groups combined) using four different models: (1) unadjusted, (2) adjusted for age, (3) adjusted for BMI and (4) adjusted for age and BMI. *sFRP4* mRNA expression in VAT was positively correlated with BMI (r_S=0.424, p<0.001), HOMA-IR (r_S=0.475, p<0.001), fasting glucose (r_S=0.233, p=0.014) and insulin (r_S=0.484, p<0.001), triglyceride (r_S=0.349, p<0.001), leptin (r_S=0.359, p=0.003) and serum CRP levels (r_S=0.231, p=0.022) whereas inversely associated with circulating adiponectin levels (r_S=-0.500, p<0.001) and *SLC2A4/GLUT4* mRNA expression in VAT (r_S=-0.451, p<0.001) (Table 28). All correlations remained significant after adjustment for age, except the associations of *sFRP4* VAT expression with fasting glucose (p=0.638), serum

leptin (p=0.098) and CRP levels (p=0.874) were cofounded by age. *sFRP4* VAT expression was no further correlated with *SLC2A4/GLUT4* VAT expression, glucose and insulin levels and HOMA-IR after adjustment for BMI. However, the associations of *sFRP4* with triglyceride levels (r_S=0.306, p=0.001) and circulating adiponectin levels (r_S=-0.279, p=0.004) were independent of BMI and still remained significant after adjustment for age and BMI.

Table 28. Association of *sFRP4* expression in VAT with metabolic variables and adipokines.

Variable	Unadjusted	Age adjusted	BMI adjusted	Age and BMI adjusted
Age*	0.057 (0.55)	NA	0.088 (0.360)	NA
BMI (kg/m$^{2)§}$	0.424 (<0.001)	0.387 (<0.001)	NA	NA
Metabolic variables				
Fasting glucose (mmol/l)	0.233 (0.014)	0.046 (0.638)	- 0.022 (0.821)	- 0.049 (0.618)
Fasting insulin (pmol/l)	0.484 (<0.001)	0.270 (0.005)	0.147 (0.129)	0.144 (0.138)
HOMA-IR	0.475 (<0.001)	0.217 (0.025)	0.100 (0.304)	0.096 (0.325)
Triglycerides (mg/dl)	0.349 (<0.001)	0.329 (<0.001)	0.300 (0.001)	0.306 (0.001)
CRP (mg/l)	0.231 (0.022)	0.016 (0.874)	- 0.108 (0.289)	- 0.100 (0.331)
Circulating adipokine levels				
Adiponectin (mg/l)	-0.5 (<0.001)	- 0.400 (<0.001)	- 0.272 (0.004)	- 0.279 (0.004)
Leptin (µg/l)	0.359 (0.003)	0.204 (0.098)	- 0.167 (0.177)	- 0.167 (0.179)
VAT expression (AU)				
SLC2A4/GLUT4	-0.451 (<0.001)	- 0.301 (0.018)	- 0.158 (0.225)	- 0.157 (0.232)

Data are given as partial Spearmen correlation coefficient r_s and corresponding p-values in parentheses. *****adjusted for BMI only. **§**adjusted for age only. *p<0.05 and **p<0.01.

3.3 The role of sFRP4 in the regulation of insulin action and energy metabolism in skeletal muscle cells

The results of the correlation analyses showed that sFRP4 associated with BMI, fasting glucose and insulin levels, overall peripheral insulin resistance and further strongly correlated triglycerides. These findings suggest that the adipokine sFRP4 might play role in the regulation of glucose and lipid metabolism in peripheral and insulin-responsive tissues. To address this,

first the effect of sFRP4 on glucose homeostasis and insulin action was investigated in skeletal muscle using differentiated C2C12 myotubes and primary human skeletal muscle cells (hSkMC).

3.3.1 The impact of sFRP4 on glycolysis, mitochondrial respiration and fatty acid oxidation in myotubes

The impact of sFRP4 on glycolysis was assessed by recording the extracellular acidification rate (ECAR) in C2C12 myotubes (Figure 18A-F). Cells exposed 24h to sFRP4 showed similar rates of glycolysis compared to controls under high as well as low glucose culture conditions (Figure 18A, B). Further, neither glycolytic capacity nor glycolytic reserve were altered by sFRP4 (C-F).

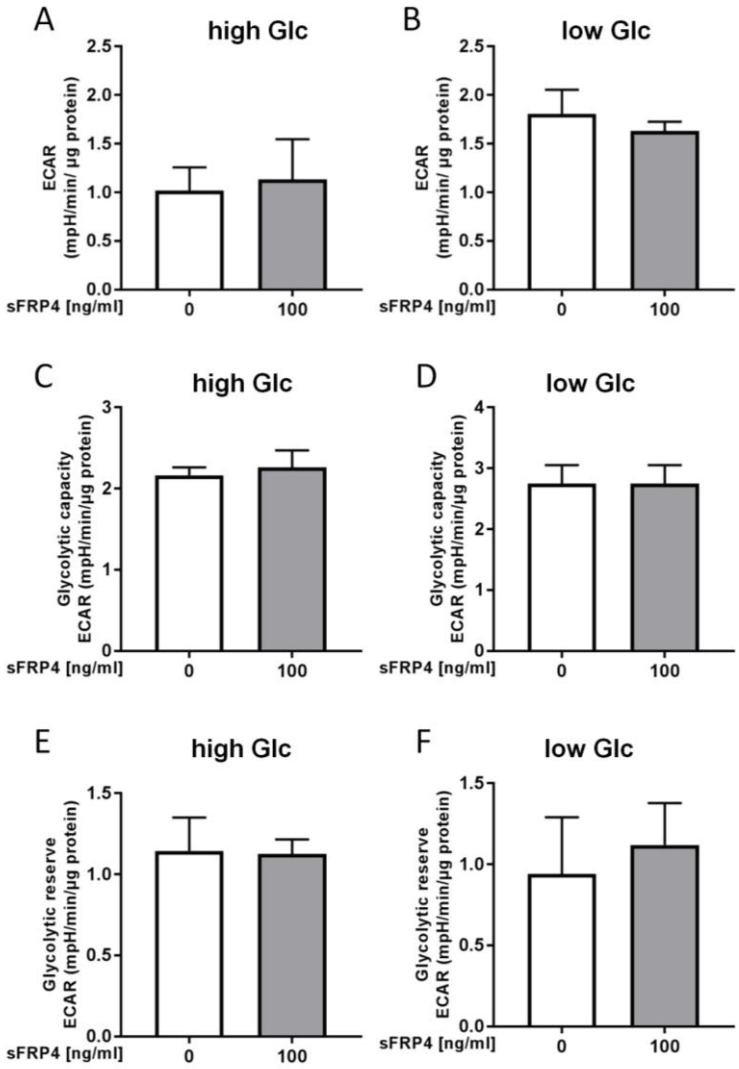

Figure 18. Effect of sFRP4 on glycolysis in myotubes. C2C12 myotubes were treated 24h with 100 ng/ml sFRP4 in medium containing high (**A**, **C**, **E**) or low (**B**, **D**, **F**) glucose (Glc). Following, ECARs were measured in controls (0 ng/ml sFRP4) and sFRP4-treated cells (100 ng/ml) after sequential injection of glucose (10 mM) oligomycin (1 µM) and 2-deoxy-D-glucose (2-DOG, 100 mM). The calculated ECARs were used for assessing glycolysis (**A**, **B**), glycolytic capacity (**C**, **D**), glycolytic reserve (**E**, **F**). The figures show the data presented as mean ± SD of three independent experiments (n=3).

To determine the effect of sFRP4 on mitochondrial respiration, spare respiratory capacity, ATP production and coupling efficiency, C2C12 myotubes were exposed to sFRP4 (100 ng/ml) for 24h followed by oxygen consumption rate (OCR) measurements in presence of specific inhibitors and inducers of the mitochondrial respiratory chain using an extracellular flux analyzer. 24h treatment of the cells with sFRP4 (100 ng/ml) did not affect spare respiratory capacity, but significantly increased basal and maximal mitochondrial respiration and ATP production by 1.22-, 1.2- and 1.19-fold (all $p<0.01$), respectively (Figure 19B, C, D).

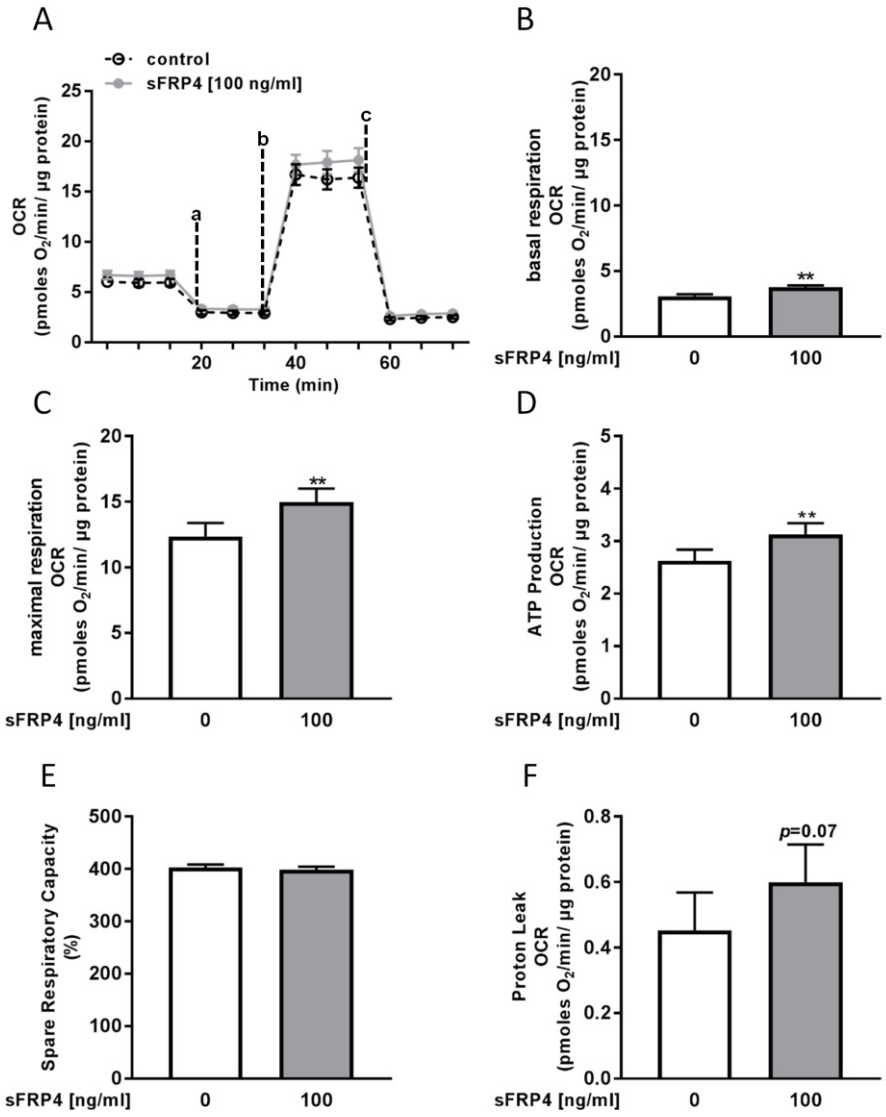

Figure 19. sFRP4 increased mitochondrial respiration in myotubes. C2C12 myotubes were treated with 24h sFRP4. In C2C12, OCRs were measured in controls (0 ng/ml sFRP4) and sFRP4-treated cells (100 ng/ml) after sequential injection of oligomycin (1 µM), FCCP (1 µM) and antimycin A/rotenone (each 1 µM). Figure shows a representative graph (**A**) of measured OCRs which were used for assessing basal respiration (**B**), maximal respiration (**C**), ATP production (**D**), spare respiratory capacity (**E**) and proton leak (**F**). The presented data are the mean ± SD of five independent experiments. Differences among groups were calculated by unpaired *t*-test. **p*<0.05, ***p*<0.01*, ***p*<0.001 for sFRP4 versus basal.

Furthermore, the proton leak was elevated in response to sFRP4 compared to untreated control cells but without reaching statistical significance (*p*=0.07) (Figure 19F).

Mitochondrial oxidation of fatty acids was examined by incubation of primary hSkMC with [^{14}C]-palmitic acid after 24h treatment with sFRP4 (100 ng/ml) followed by assessing the release of [^{14}C]-CO_2 which was produced in an oxidation chamber. The application of an inducer and inhibitors of the mitochondrial respiratory chain verified that the produced [^{14}C]-CO_2 can be ascribed to mitochondrial oxidation. Whereas FCCP significantly induced palmitic acid oxidation by 36% (*p*<0.05), oligomyocin, antimycin A/rotenone and etomoxir significantly inhibited oxidation in myotubes by 79%, 87% and 73% (all *p*<0.001, Figure 20A), respectively. However, 24h sFRP4 exposure to hSkMC did not affect palmitic acid oxidation (Figure 20B).

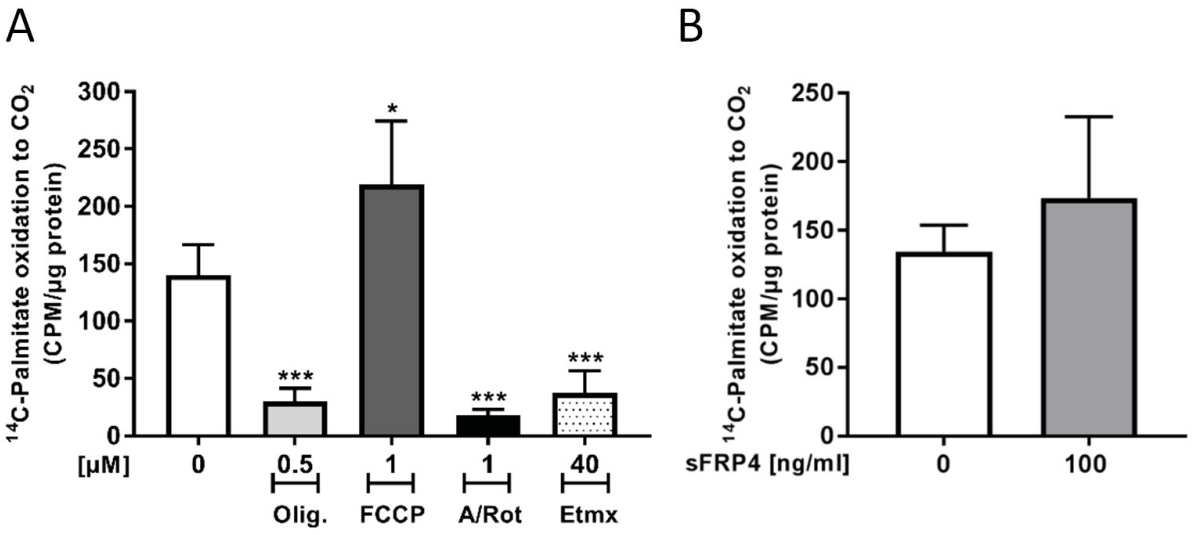

Figure 20. Effect of sFRP4 on fatty acid oxidation in primary hSkMC. Myotubes were exposed to sFRP4 (100 ng/m) for 24h (**B**) or to inducers (FCCP) and inhibitors (Oligomycin, Antimycin, Rotenone, Etomoxir) of fatty acid β-oxidation (**A**). Following, cells were incubated with ^{14}C-palmitate for 4h. Data show oxidation of isotopic labeled palmitate of four to five independent experiments (n=4-5) presented as mean ± SD in cultured hSkMC. The values obtained for sFRP4-untreated cells were considered as controls (0 ng/ml). Differences among conditions were calculated by *t*-test. **p*<0.05*, ***p*<0.001 versus control cells.

3.3.2 sFRP4 increased phosphorylation of AMPK in primary hSkMC

The effect of sFRP4 on AMP-activated protein kinase (AMPK) and acetyl-CoA carboxylase (ACC), essential regulators of mitochondrial biogenesis, glucose and lipid metabolism, was determined in hSkMC. Acute incubation with sFRP4 for 4h increased phosphorylation of AMPKα-Thr172 by 52% (p<0.05) and slightly increase phosphorylation of ACC-Ser79 by 44% without reaching statistical significance (p<0.16) compared to control cells (Figure 21A, B), indicating an increased activity of AMPK.

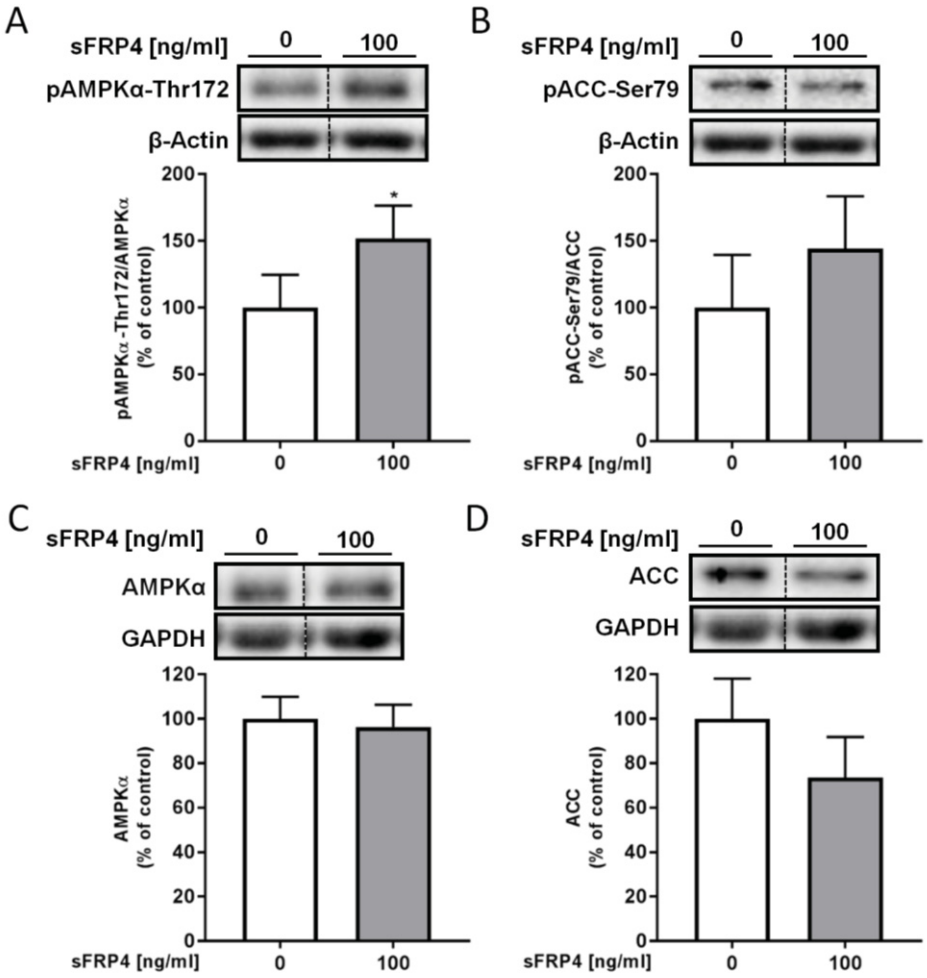

Figure 21. Effect of short-time exposure of sFRP4 on AMPK signaling in primary hSkMC. hSkMC were treated with 100 ng/ml sFRP4 for 4h. Following cell lysis, protein lysates were analyzed for phosphorylation levels of AMPKα-Thr172 and its substrate ACC-Ser79 (**A**, **B**) and abundance for AMPKα and ACC protein (**C, D**). The protein signals were normalized for the abundance of total protein (**A**, **B**) and/or loading control β-actin or GAPDH (**A-D**). Data show representative Western blots and mean ± SD of four independent experiments using cells from different donors (n=4). The values obtained for sFRP4-untreated cells were considered as controls (0 ng/ml). Differences among conditions were calculated by *t*-test. *p<0.05 for sFRP4-treated versus control cells.

Long time exposure of primary hSkMC with sFRP4 for 24h did not affect phosphorylation levels of AMPKα-Thr172 and its substrate ACC-Ser79 (Figure 22A, B). The abundances of AMPK and ACC were not affected by sFRP4 neither after 4h nor 24h incubation period (Figure 21C, D; 22C, D).

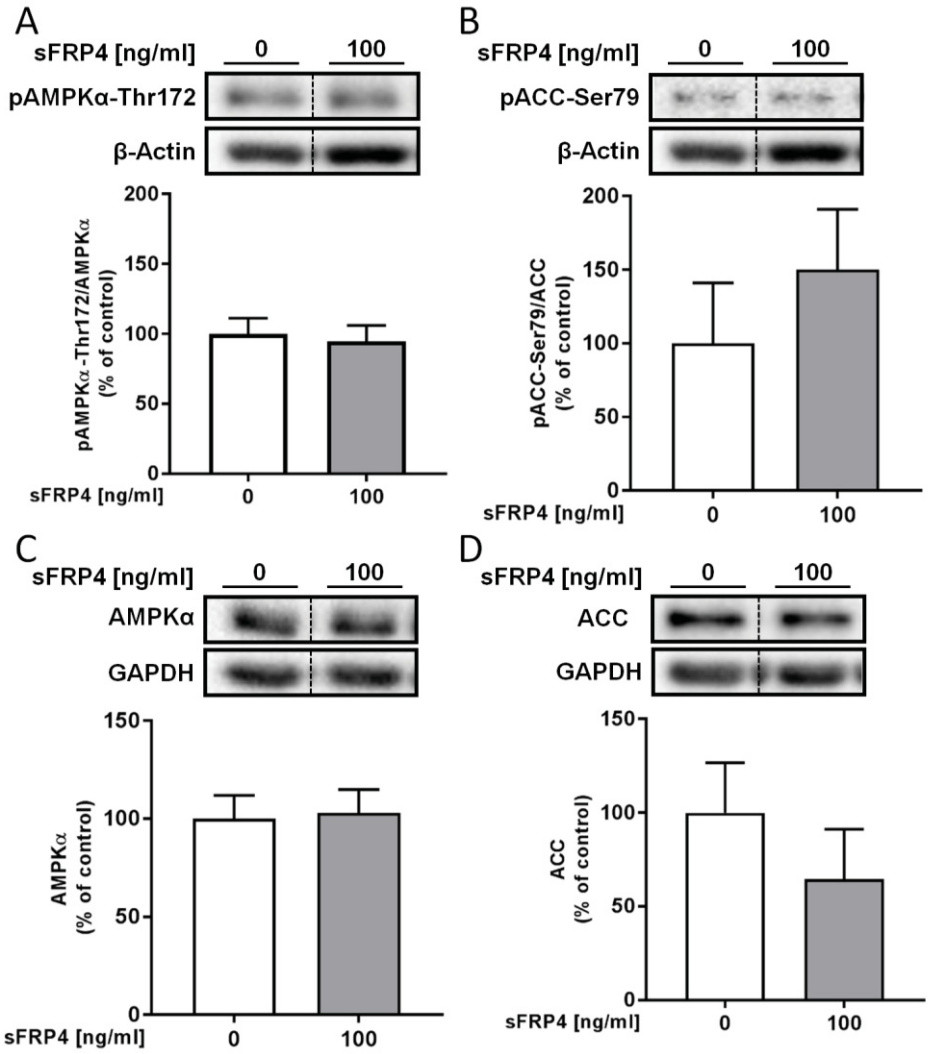

Figure 22. Effect of long-time sFRP4 exposure on AMPK-signaling in primary hSkMC. hSkMC were treated with 100 ng/ml sFRP4 for 24h. Following cell lysis, protein lysates were analyzed for phosphorylation levels of AMPKα-Thr172 and its substrate ACC-Ser79 (**A**, **B**) and abundance for AMPKα and ACC protein (**C, D**). The protein signals were normalized for the abundance of total protein (**A**, **B**) and loading control β-actin or GAPDH (**A-D**). Data show representative Western blots and mean ± SD of four independent experiments using cells from different donors (**n=4**). The values obtained for sFRP4-untreated cells were considered as controls (0 ng/ml). Differences among conditions were calculated by *t*-test. **p*<0.05, ***p*<0.01, ****p*<0.001 for sFRP4-treated versus control cells.

3.3.3 Effect of sFRP4 on AMPK-FoxO signaling in primary hSkMC

To determine whether the observed increase in the phosphorylation of AMPK was directly induced by sFRP4, hSkMC were exposed to sFRP4 (100 ng/ml) in the absence and presence of the selective and reversible AMP-kinase inhibitor Compound C (20 µM, CompC) for 4h. The sFRP4 induced increase on AMPK-Thr172 phosphorylation was abrogated by 40 % in cells pre-incubated with CompC (Figure 23A). CompC alone did not interfere with AMPK-Thr172 phosphorylation compared to untreated control cells (Figure 23A). Furthermore, the sFRP4-induced increase in AMPK phosphorylation was accompanied by decreased phosphorylation levels of FoxO3a-Ser253 by 45% (*p*=0.04) whereas pre-incubation with CompC abrogated the reduction of FoxO3a-Ser253 phosphorylation mediated by sFRP4 (Figure 23B).

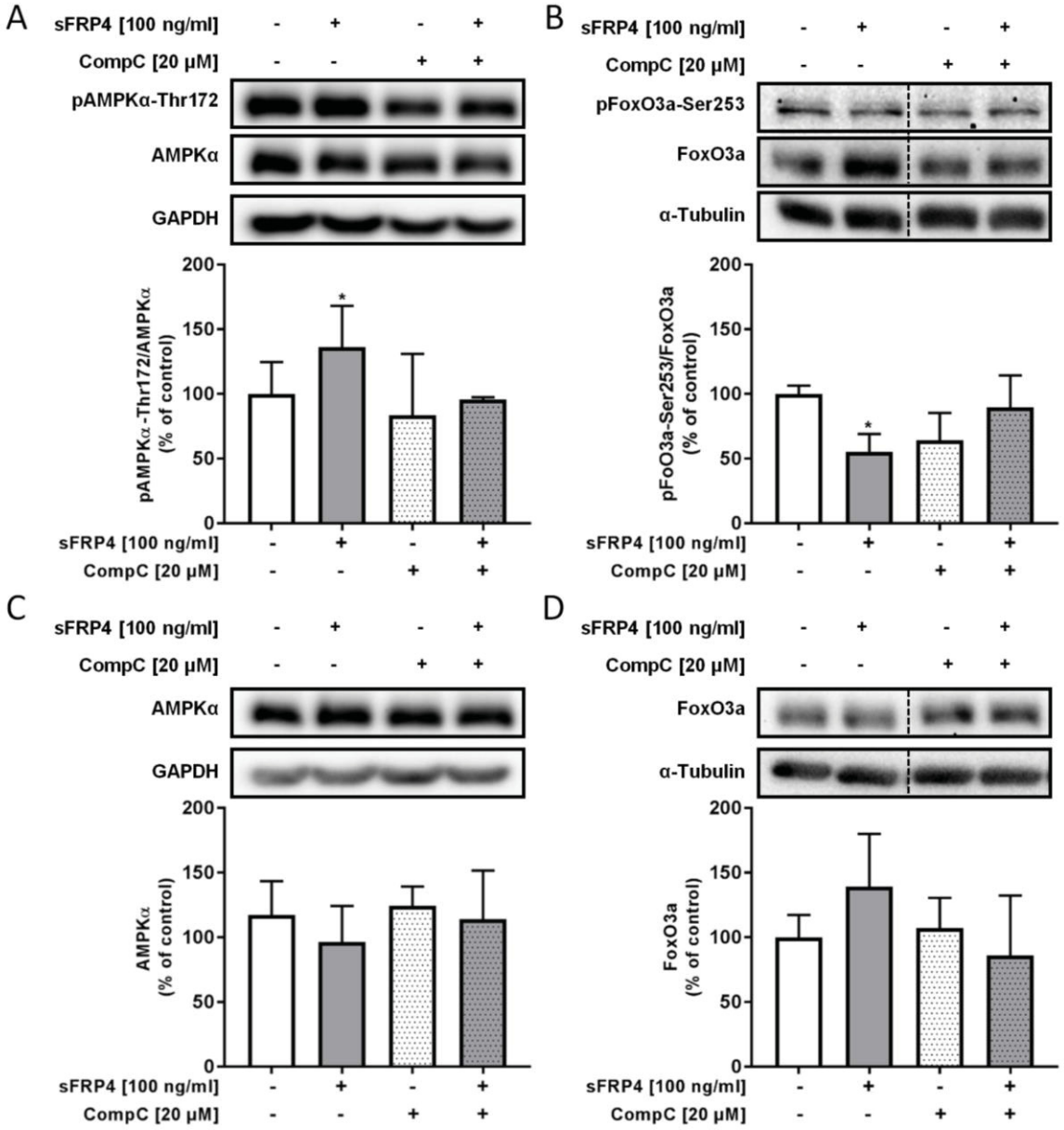

Figure 23. sFRP4 decreased inhibiting phosphorylation of FoxO3a via AMPK signaling in primary hSkMC. hSkMC were treated either with 100 ng/ml sFRP4 and/or 20 µM CompC for 4h. Following cell lysis, protein lysates were analyzed for phosphorylation levels of AMPKα-Thr172 and its substrates pFoxO3a-Ser256 (**A**, **B**) and abundance for AMPK, FoxO3a protein (**D**, **E**). The protein signals were normalized for the abundance of total protein and loading control GAPDH or α-tubulin. Data show representative Western blots and mean ± SD of independent experiments (n=3-7). The values obtained for sFRP4-untreated cells were considered as controls (0 ng/ml) and set as 100%. Differences among conditions were calculated by *t*-test. **p*<0.05 for sFRP4-treated versus control cells.

As illustrated in Figure 23C, D, neither AMPKα nor FoxO3a protein levels were affected by sFRP4 or CompC (Figure 23B).

3.3.4 The impact of sFRP4 on AMPK-FoxO-mediated induction of E3 ubiquitin ligases in primary hSkMC

Primary human myotubes were treated with sFRP4 for 4h in absence and presence of CompC to test whether sFRP4 regulated the abundance of MuRF1 and MAFbx/atrogin-1 E3 ubiquitin ligases via AMPK-FoxO signaling (Figure 24A, B). MuRF1 protein was significantly increased by 33% (*p*<0.05) in cells incubated with sFRP4 compared to untreated cells. In contrast, this effect was abolished when cells were exposed to CompC 30 min prior to sFRP4 administration for 4h (Figure 24A).

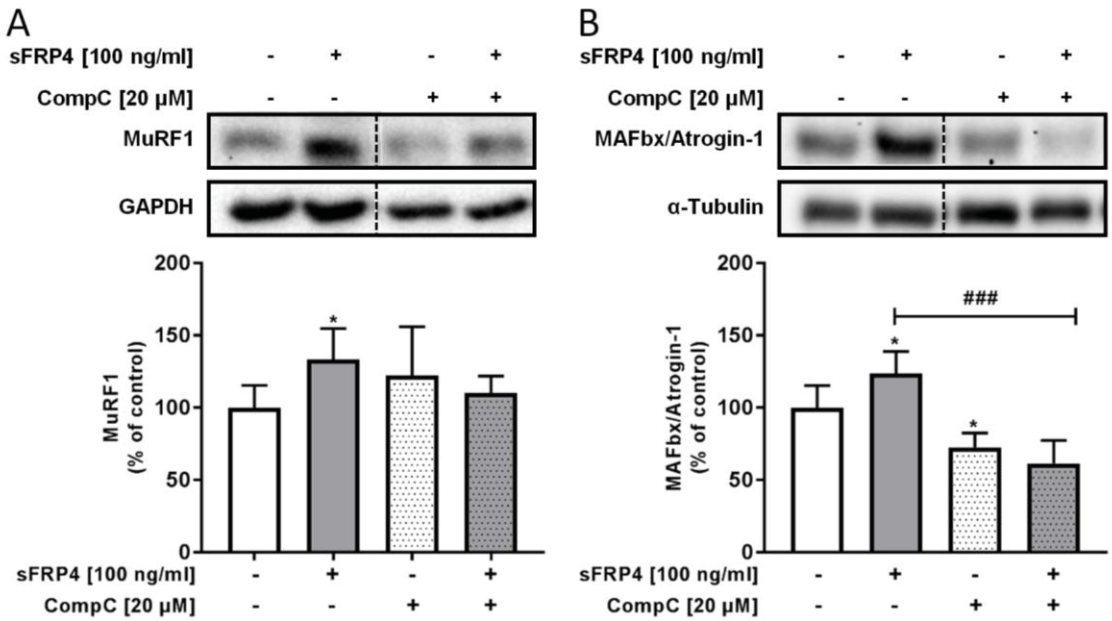

Figure 24. Impact of sFRP4 on E3 ubiquitin ligases MuRF1 and MAFbx/atrogin-1 in primary hSkMC. hSkMC were treated either with 100 ng/ml sFRP4 and/or 20 µM CompC for 4h. Following cell lysis, protein lysates were analyzed for MuRF1 and MAFbx/atrogin-1 (**A**, **B**). The protein signals were normalized for the abundance of the loading control GAPDH or α-tubulin. Data show representative Western blots and mean ± SD of five independent experiments (n=5). The values obtained for sFRP4-untreated cells were considered as controls (0 ng/ml) and set as 100%. Differences among conditions were calculated by one-way ANOVA followed by Dunnett´s or Holm-Sidak´s multiple comparisons test. **p*<0.05, ***p*<0.01, ****p*<0.001 for sFRP4-treated versus control cells; $^{\#}$*p*<0.001 versus sFRP4.

Similar results but with a larger extent were found for the impact of sFRP4 on MAFbx/atrogin-1. sFRP4 significantly induced MAFbx/atrogin-1 protein by 23% (123.9 ± 15.05%, *p*<0.05) whereas CompC alone even decreased MAFbx/Atrogin-1 abundance by 28% (72.61 ± 10.0%, *p*<0.05) compared to control cells (100 ± 15.49%) (Figure 24B). However, pre-incubation with CompC abrogated the sFRP4-induced increase of MAFbx/atrogin-1 protein (61.54 ± 15.94%, *p*<0.001).

3.3.5 Effect of sFRP4 on sirtuin activity in primary hSkMC

To determine the effect of sFRP4 in absence and presence of CompC on the activity of sirtuins (SIRT), NAD^+-dependent regulators of energy metabolism, primary hSkMC were pre-incubated with CompC (20 µM) for 30 min prior to administration of sFRP4 (100 ng/ml) for further 4h or 24h. Cellular SIRT activity was calculated from luminescence measurements. Figure 25A, B shows that neither 4h nor 24h sFRP4 exposure affected SIRT in hSkMC (*p*=0.2; *p*=0.85, respectively). In contrast, CompC incubation for 4h significantly inhibited SIRT activity by 3-fold (*p*<0.01) compared to untreated control cells. CompC still suppressed SIRT activity in cells simultaneously treated with sFRP4 for 4h (*p*<0.05) by 2.5-fold in comparison to control cells (Figure 25A). SIRT activity was reduced by 1.7-fold (*p*<0.001) in cells incubated with CompC for 24h. CompC administration followed by sFRP4 incubation for 24h reduced SIRT activity (*p*=0.06) compared to untreated hSkMC although did not reach statistical significance (Figure 25B).

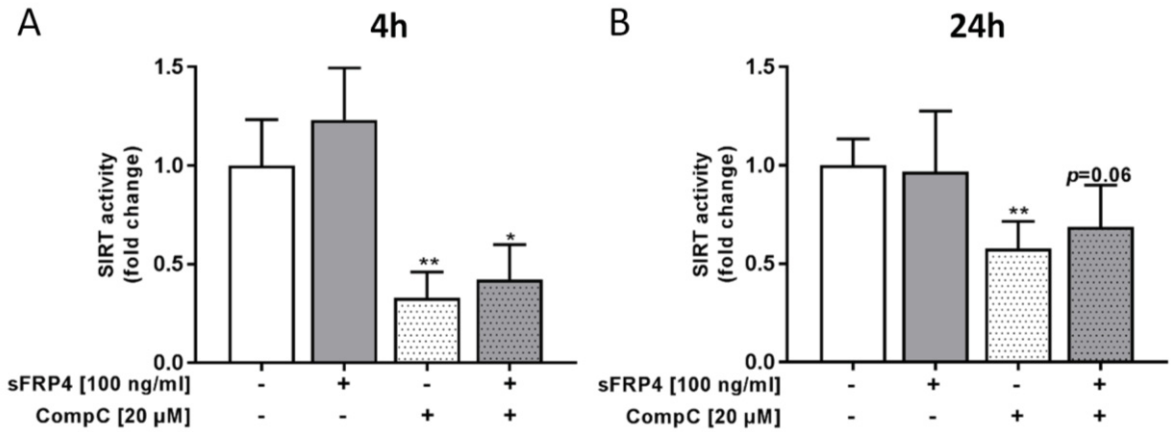

Figure 25. Effect of sFRP4 on sirtuin activity in primary human skeletal muscle cells. Primary hSkMC were exposed 4h (**A**) and 24h (**B**) to 100 ng/ml sFRP4 to assess its effect on cellular sirtuin activity using SIRT-Glo™. Data show the mean ± SD of independent experiments (n=3-4). Data of untreated cells were regarded as controls and set as 1. Differences between treatments were calculated by *t*-test. **p*<0.05, ***p*<0.01 versus untreated cells.

3.3.6 The impact of sFRP4 on proteasome activity in primary human skeletal muscle cells

To assess the effect of sFRP4 on proteasome activity in more detail, hSkMC were incubated with sFRP4 for 24h in absence and presence of Bortezomib (BZ), a cell-permeable and reversible inhibitor of the chymotrypsin-like 26S proteasome activity (Figure 26A, B). To exclude cytotoxic effects mediated by BZ exposure on hSkMC, first different concentrations of BZ (1-100 nM) were used for 24h treatment of cells followed by fluorescence measurements. As Figure 26A illustrated, none of the used BZ concentrations induced cytotoxicity in primary myotubes compared to the cytotoxicity control (100 ± 2.1%), cells treated with a lysis solution, and untreated control cells (28.54 ± 1.35%). 10 nM BZ have been used for further analysis. 24h sFRP4 exposure of hSkMC increased proteasome activity by 27% (p<0.01) compared to untreated control cells (Figure 26B). Pre-incubation of hSkMC with 10 nM BZ inhibited proteasome activity by 56% (p<0.001). In combination, sFRP4 did not affect proteasome activity in cells that were pre-treated with BZ (31.81 ± 5.11%) compared to cells incubated with the inhibitor alone (44.28 ± 2.72%).

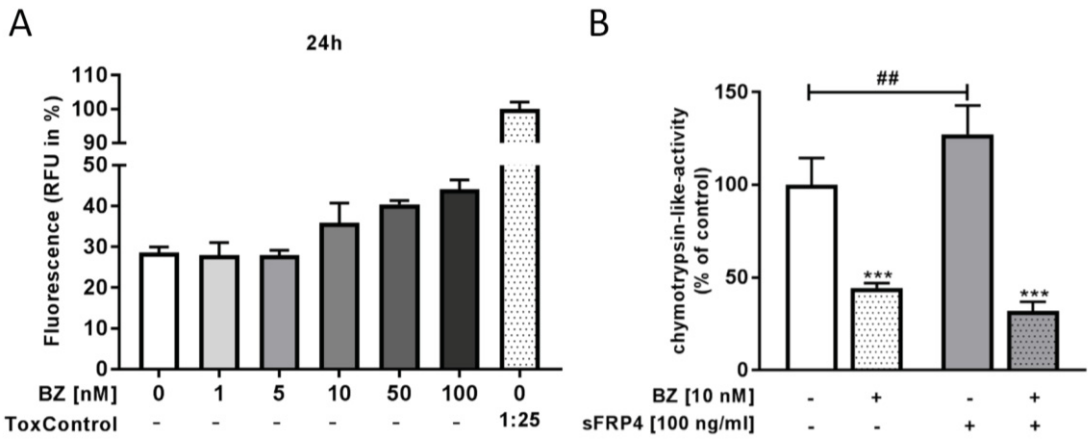

Figure 26. Analysis of sFRP4 on proteasome activity in primary hSkMC. hSkMC were exposed 24h to different concentrations of Bortezomib (BZ) to assess the effect of the used concentrations on cellular cytotoxicity and integrity using CellTox™ Green Cytotoxicity Assay (**A**, n=2). 100 ng/ml sFRP4 for 24h with or without 10 nM BZ have been used to examine their impact on proteasome activity (**B**). Data show the mean ± SD of two (**A**) and five (**B**) independent experiments using cells from different donors. Data of untreated cells were regarded as controls and set as 100%. Two-way ANOVA analyses followed by Sidak's multiple comparisons test were performed. ****p*<0.001 for BZ versus untreated or sFRP4 treated cells. $^{\#\#}p$<0.01 for sFRP4-treated versus untreated cells.

3.3.7 Effect of sFRP4 on IRS-1 levels in primary human skeletal muscle cells

The observed associations of sFRP4 with glucose levels and peripheral insulin resistance indicated that sFRP4 might interfere with insulin signaling. Therefore, the impact of sFRP4 on IRS-1, a key mediator of insulin action, was examined in primary hSkMC. IRS-1 protein levels were significantly reduced by 35% (p<0.001) upon 24h but not 4h sFRP4 exposure (100 ng/ml) in *in vitro* cultured hSkMC compared to untreated cells (Figure 27A, B). The effect of 24h sFRP4 treatment on IRS-1 protein was not due to decreased *IRS1* mRNA expression in primary hSkMC (Figure 27C).

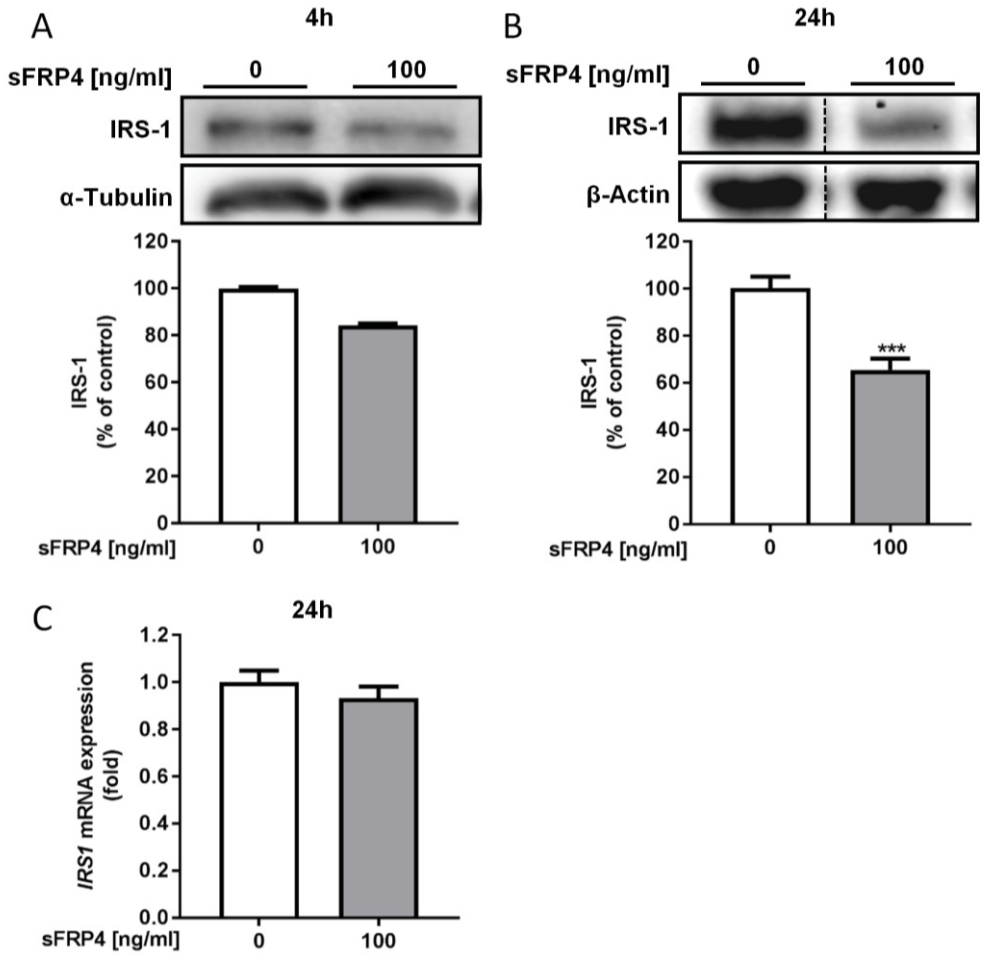

Figure 27. IRS-1 protein was decreased by sFRP4 in primary human skeletal muscle cells. IRS-1 abundance (**A**) in hSkMC were determined upon 4h (**A**) and 24h (**B**) sFRP4 treatment (100 ng/ml) and IRS-1 expression after 24h sFRP4 exposure (**C**). IRS-1 protein levels were assessed by Western blotting and normalized to β-actin or α-tubulin. Representative blots are shown. *IRS1* mRNA expression levels were measured by quantitative RT-PCR and normalized to *YWHAZ* and *EIF4A2*. Bar graphs represent data as mean ± SD of the IRS-1 levels of independent experiments using cells from different donors (n=3-5). The values obtained for sFRP4-untreated cells were considered as controls (0 ng/ml) and set as 1 or 100%. Differences among conditions were calculated by *t*-test. **p*<0.05, ***p*<0.01, ****p*<0.001 for sFRP4-treated versus control cells (**A**-**B**).

Given that sFRP4 induced proteasome activity and decreased IRS-1 abundance but not mRNA expression in hSkMC suggested that IRS-1 might be a target of proteasome-dependent degradation mediated by sFRP4. To further analyze this, hSkMC were exposed to sFRP4 with and without pre-incubation of BZ for 24h (Figure 28). BZ alone did not affect IRS-1 levels in hSkMC (86.94 ± 12.74%, p=0.39). Incubation of the cells with the proteasome inhibitor BZ, 30 min prior to sFRP4 exposure for further 24h, fully restored IRS-1 protein amount (p<0.05) to comparable levels of untreated control cells.

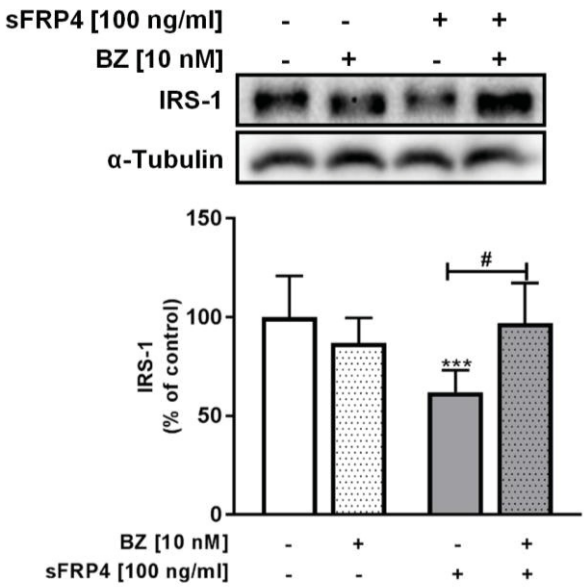

Figure 28. sFRP4 induced proteasome-dependent degradation of IRS-1 in primary hSkMC. 100 ng/ml sFRP4 for 24h with or without 10 nM BZ have been used to examine their impact on IRS-1 abundance. Data show the mean ± SD of independent experiments (n=5-6). Data of untreated cells were regarded as controls and set as 100 %. Two-way ANOVA analyses followed by the Sidak's multiple comparisons test were performed. ****p*<0.001 for BZ vs untreated or sFRP4 treated cells; $^{\#}p$<0.05 for sFRP4-treated vs untreated cells.

3.3.8 Effect of sFRP4 on cellular insulin signaling in primary hSkMC

To investigate *in vitro* whether reduced IRS-1 abundance in hSkMC was accompanied with impaired insulin signaling in response to sFRP4, phosphorylation levels of Akt and its substrates GSK3β and FoxO were determined in cells exposed 24h to sFRP4 prior to an acute insulin stimulus. Although sFRP4 did not affect basal and insulin-induced phosphorylation of Akt-Ser473, Akt-Thr308 and GSK3β-Ser9 in hSkMC, the insulin-mediated phosphorylation of FoxO1/3a-Thr24/32 was reduced by ~30% in response to sFRP4 (70.57 ± 18.24, p<0.01) compared to control cells (Figure 29A-D).

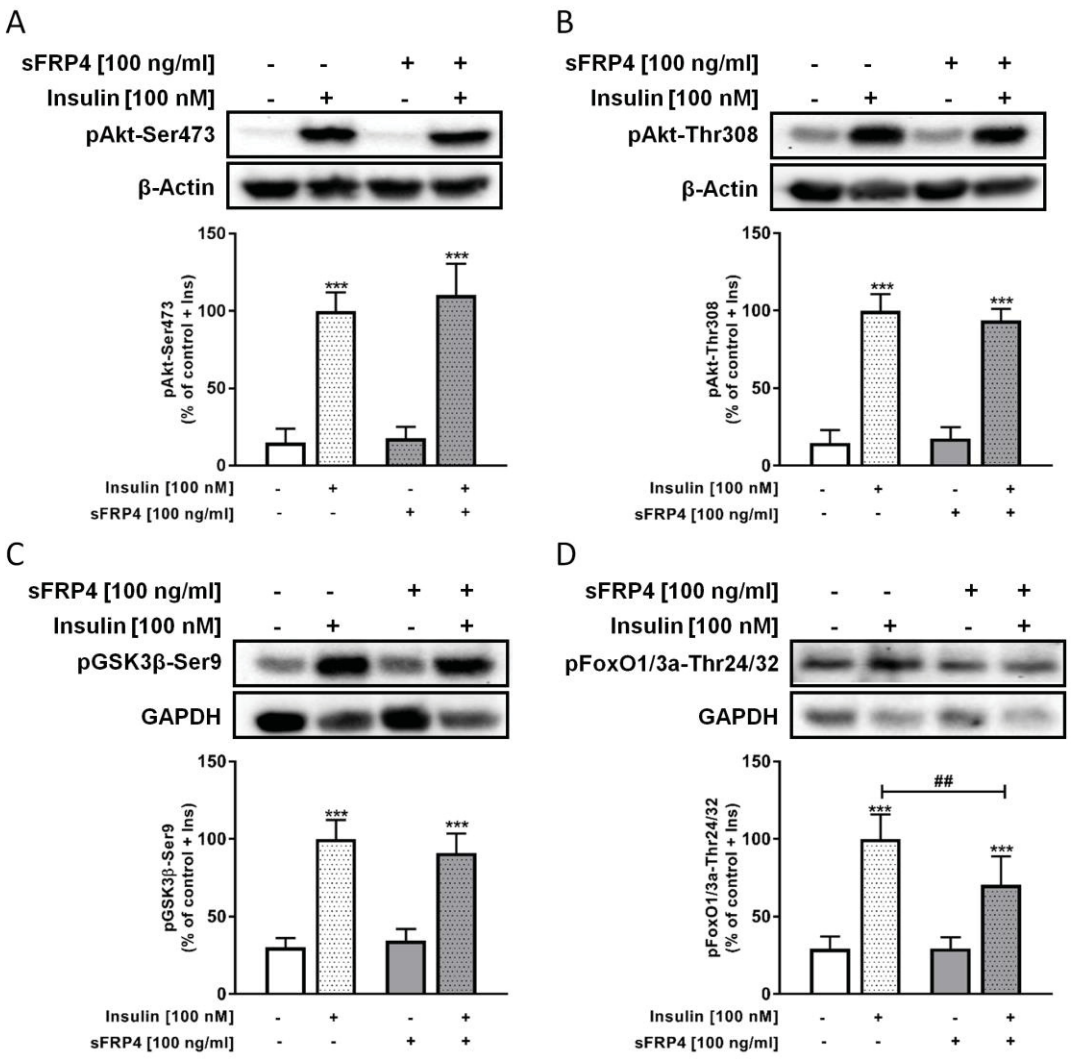

Figure 29. Effect of sFRP4 on insulin signaling in primary hSkMC. Primary hSkMC were treated with sFRP4 for 24h prior to insulin stimulation (10 min). Following cell lysis, protein lysates were analyzed for phosphorylation levels of Akt-Ser473 (**A**), Akt-Thr308 (**B**), GSK3β-Ser9 (**C**) and FoxO1/3a-Thr24/32 (**D**). The protein signals were normalized for the abundance of the loading control β-actin or GAPDH. Figures show representative Western blots and data are presented as mean ± SD of the phosphorylation levels of five independent experiments. The values obtained for sFRP4-untreated cells were considered as controls. All values were normalized to insulin-treated control cells (control + Ins) which were set as 100%. Differences among groups were calculated by two-way ANOVA analyses followed by the Sidak's multiple comparisons test. *p<0.05, **p<0.01, ***p<0.001 for insulin vs basal $^{\#}p$<0.05; $^{\#\#}p$<0.01; $^{\#\#\#}p$<0.001 for sFRP4-treated vs untreated cells.

The inhibitory effect of sFRP4 on insulin-mediated FoxO phosphorylation also was observed by using antibodies specific for either FoxO1-Ser256 phosphorylation or FoxO3a-Ser253 phosphorylation (Figure 30). Neither FoxO1 nor FoxO3a abundances were affected by sFRP4 (Figure 30B, D).

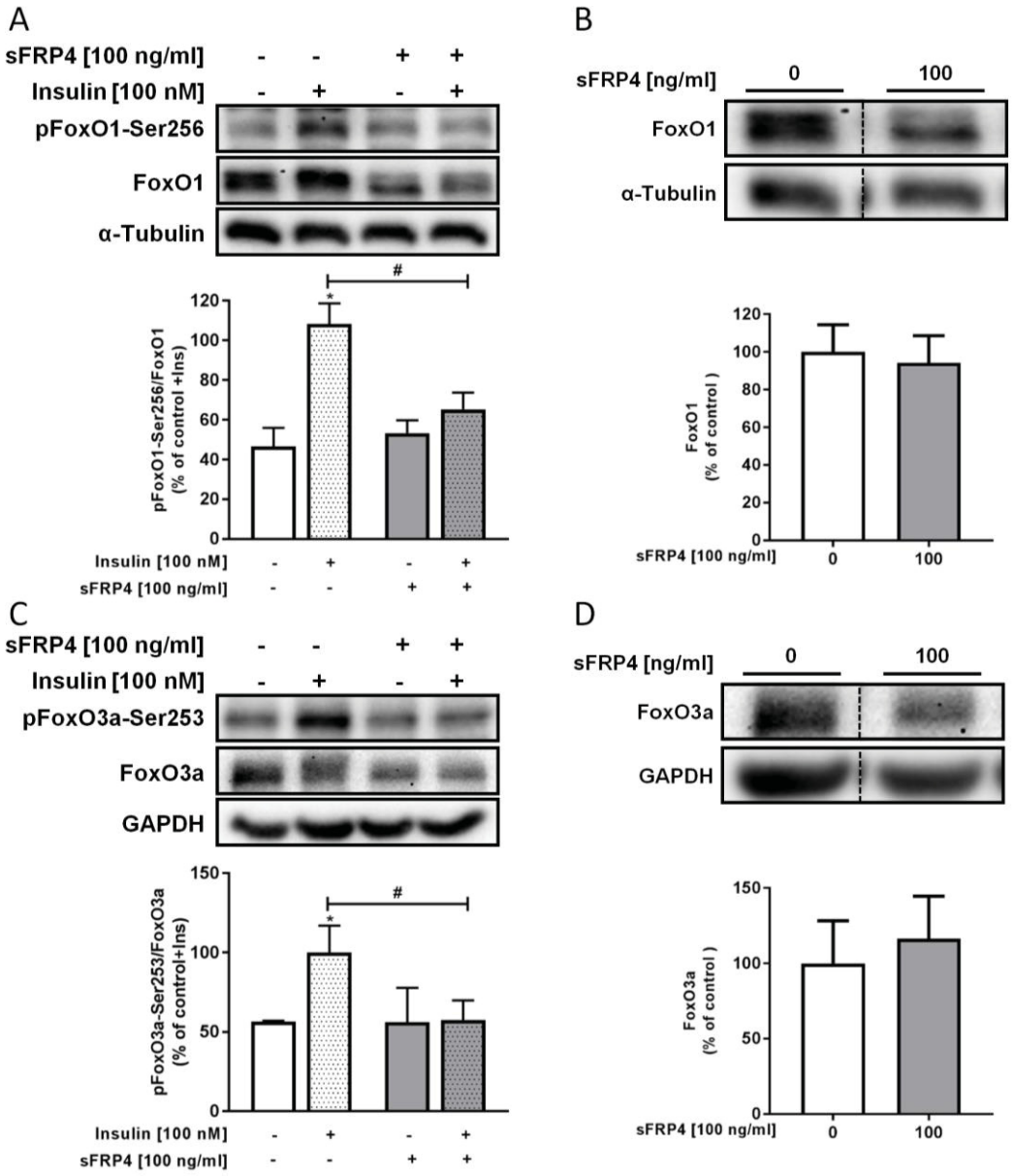

Figure 30. Impact of sFRP4 on insulin-induced phosphorylation of FoxOs in primary hSkMC. hSkMC were treated 24h with 100 ng/ml sFRP4 in the presence (+) or absence (-) of insulin (100 nM) (**A**-**D**). Signals for the phosphorylation levels of FoxO1-Ser256 (**A**) and FoxO3a-Ser253 (**C**) were normalized for the abundance of FoxO1 (**B**) and FoxO3a (**D**) and the loading control α-tubulin or GAPDH. Bar graphs represent data as mean ± SD of the phosphorylation levels or protein abundance of independent experiments using cells from different donors (n=3-4). The values obtained for sFRP4-untreated cells were considered as controls. All values were normalized to control cells in presence of insulin and set as 100%. Differences among groups were calculated by two-way ANOVA followed by Sidak's multiple comparisons test. **p*<0.05, ***p*<0.01, ****p*<0.001 for insulin versus basal.

The impaired insulin-mediated phosphorylation of FoxO1 did not result from the reduction in IRS-1 levels induced by sFRP4 (Figure 31). This was tested in more detail in cells that were pre-treated with BZ followed by sFRP4 exposure for 24h. Here, sFRP4 still decreased the insulin-

mediated phosphorylation of FoxO1-Ser256 in absence and presence of the inhibitor by 37% and 44% respectively (both $p<0.05$), compared to control cells (Figure 31A). BZ and sFRP4 exposure did not affect FoxO1 abundance (Figure 31B).

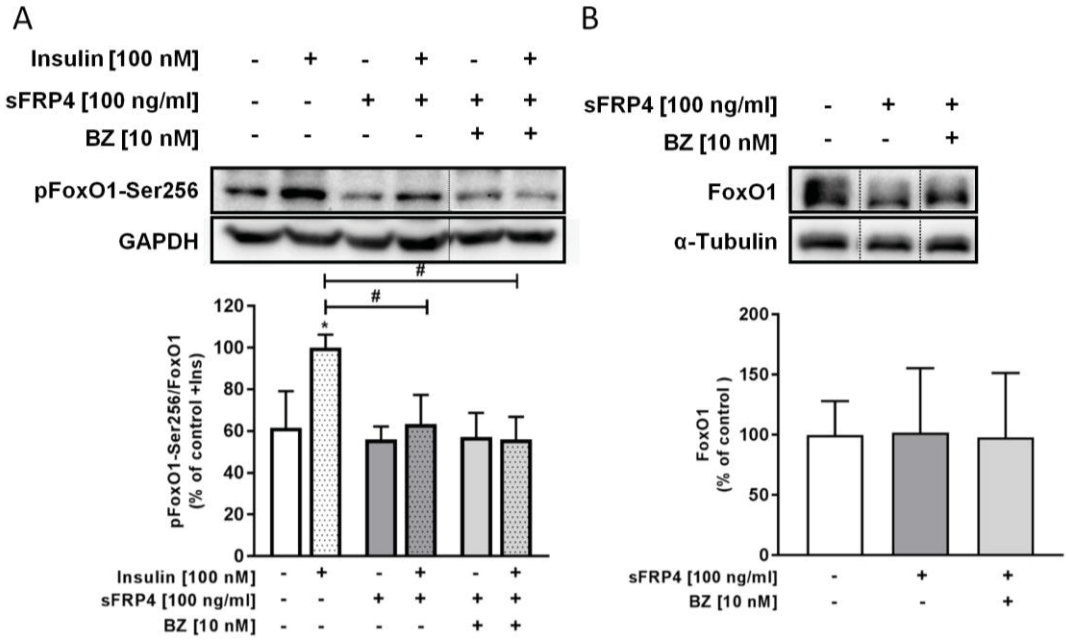

Figure 31. Effect of sFRP4 and BZ on insulin-mediated phosphorylation of FoxO in hSkMC. hSkMC were treated 24h with 100 ng/ml sFRP4 in the presence (+) or absence (-) of BZ prior to insulin stimulation (10 min, 100 nM). Phosphorylation levels of FoxO1-Ser256 and FoxO1 protein were normalized either for the abundance of FoxO1 protein and/or the loading control α-tubulin and GAPDH. Bar graphs represent data as mean ± SD of FoxO1-Ser256 phosphorylation levels (**A**) and FoxO1 protein abundance (**B**) of independent experiments using cells from different donors (n=3-4). The values obtained for sFRP4-untreated cells were considered as controls. All values were normalized to control cells in presence and set as 100%. Differences among groups were calculated by two-way ANOVA followed by Sidak's multiple comparisons test. *$p<0.05$ for insulin versus basal; $^{\#}p<0.05$ versus untreated cells.

3.4 Analysis of sFRP4 and isolation of primary hepatocytes from C57Bl6 and aP2-SREBP-1c mice

Given the hypothesis that sFRP4 acts as metabolic active adipokine, further analyses were focused on the role of sFRP4 on liver. The investigations in liver focused on two major points: i) the mechanistically action of sFRP4 on a metabolic healthy liver, and ii) alterations of the sFRP4 action on liver of lipodystrophic mice (aP2-SREBP-1c). The latter model is characterized by hepatic lipid accumulation and the complete loss of adipose tissue, so lacking VAT expressed sFRP4. To investigate predominant tissue expression and circulating levels of sfrp4 in mice, tissues biopsies and plasma samples were obtained from C57Bl6 and aP2-SREBP-1c

mice. To mimic the effect of the adipokine sFRP4 *in vitro* and to further examine whether sFRP4 affect hepatic energy homeostasis, lipid metabolism and insulin action in liver, primary hepatocytes were isolated from the phenotypical C57Bl6 control and diseased aP2-SREBP-1c mouse models.

3.4.1 Clinical characterization of C57Bl6 and aP2-SREBP-1c mice

The clinical parameters of the mice used for the study were summarized in Table 29. At 24 weeks of age, aP2-SREBP-1c mice had developed their full lipodystrophic phenotype with complete loss of white adipose tissue and enlarged fatty liver. This was determined in slightly increased overall body weight ($p<0.001$) compared to respective C57Bl6 control mice, due to massively increased liver weight ($p<0.001$), despite complete loss of visceral adipose tissue mass.

The clinical parameters of the aP2-SREBP-1c mice indicated dyslipidemia characterized by increased FFA ($p<0.001$), TG ($p<0.001$), and cholesterol ($p<0.01$) in plasma. Furthermore, aP2-SREBP-1c mice had a pronounced insulin resistance with increased plasma glucose ($p<0.001$) and insulin levels ($p<0.001$) in combination with elevated HOMA-IR ($p<0.001$) and compensatory increase in HOMA-%ß ($p<0.001$) in comparison to C57Bl6 mice. In concordance to the lipodystrophy phenotype, leptin levels were drastically reduced ($p<0.001$). Liver enzymes glutamat-oxalacetat-transaminase (GOT) ($p<0.001$) and glutamat-pyruvat-transaminase (GPT) ($p<0.001$) were increased, indicating liver functional impairment, but not liver injury yet, as glutamate dehydrogenase (GLDH) ($p=0.09$) was not significantly elevated.

Table 29. Clinical characteristics of C57Bl6 and aP2-SREBP-1c.

Variable	C57Bl6	aP2-SREBP-1c	*p*
N (male)	10	10	
Age (weeks)	24	24	
Weight (g)	30.67 (29.39-31.96)	36.29 (34.38-38.20)	<0.001
Liver (mg)	1835 (1747-1923)	3886 (3170-4602)	<0.001
Liver/weight (mg/g)	59.83 (58.25-61.41)	107.5 (86.74-128.20)	<0.001
VAT (g)	0.81 (0.74-0.88)	NA	<0.001
Metabolic variables			
TG (mg/dl)	124.5 (144.2-134.8)	302.3 (280-323.9)	<0.001
Cholesterol (mg/l)	106.5 (96.52-116.5)	127.9 (117.9-137.9)	<0.01
FFA (g/l)	1.00 (0.74-1.25)	6.23 (6.00-6.46)	<0.001
HOMA-IR	0.30 (0.21-0.40)	4.13 (3.45-4.81)	<0.001
Plasma glucose (mg/dl)	127 (116.3-137.7)	238.8 (219.8-257.8)	<0.001
Plasma insulin (µlU/ml)	0.94 (0.72-1.16)	6.95 (6.10-7.80)	<0.001
HOMA-%β	119.1 (93.51-144.7)	317.2 (273.9-360.40)	<0.001
Leptin (ng/ml)	15.88 (10.43-21.32)	1.04 (0.61-1.46)	<0.001
GOT (U/l)	36.60 (29.33-43.87)	329.7 (285.5-373.9)	<0.001
GPT (U/l)	35.40 (30.14-40.66)	131.2 (119.2-143.2)	<0.001
GLDH (U/l)	9.19 (3.99-14.40)	21.70 (11.58-31.82)	0.09

Data are presented as mean (95% CI). Significance differences were calculated by *t*-test and are stated by *p*-values. Triglycerides, TG; free fatty acids, FFA; glutamat-oxalacetat-transaminase, GOT; glutamat-pyruvat-transaminase, GPT; glutamate dehydrogenase, GLDH.

3.4.2 Expression and circulating levels of sfrp4 in metabolic healthy C57Bl6 mice and lipodystrophic aP2-SREBP1c mice

The predominant tissue-specific mRNA expression pattern of *sfrp4* was investigated in five different insulin-sensitive tissues including VAT, SAT, gastrocnemius (GAS) muscle, liver and pancreas. As Figure 32A shows, in C57Bl6 mice *sfrp4* mRNA expression was highest in VAT

(2.67 (0.98–4.37) AU) followed by GAS muscle (1.69 (1.24-2.13) AU). *Sfrp4* expression was also detectable in SAT (0.95 (0.72-2.61 AU), $p<0.05$) and to a minor extent in liver (0.03 (0.006-0.06) AU, $p<0.001$) and pancreas (0.08 (0.002-0.15) AU, $p<0.001$), but the expression levels were significantly lower than in VAT. In lipodystrophic aP2-SREBP-1c mice *sfrp4* expression was determined in GAS muscle, liver and pancreas (Figure 32B). *sfrp4* expression was highest in GAS muscle (1.87 (1.23-2.48) AU) and significantly lower expression levels were detected in liver (0.01 (0.001-0.03) AU, $p<0.001$) and pancreas (0.19 (0.10-0.47) AU, $p<0.001$) of aP2-SREBP-1c mice. Thus, expression levels of *sfrp4* in aP2-SREBP-1c mice in the examined tissues were similar to C57Bl6 mice.

Circulating sfrp4 levels in plasma of C57Bl6 control mice were 44.95 (40.29-49.61) ng/ml, whereas sfrp4 plasma levels in aP2-SREBP-1c mice were significantly lower 36.38 (33.24-39.51) ng/ml ($p=0.002$, Figure 32C).

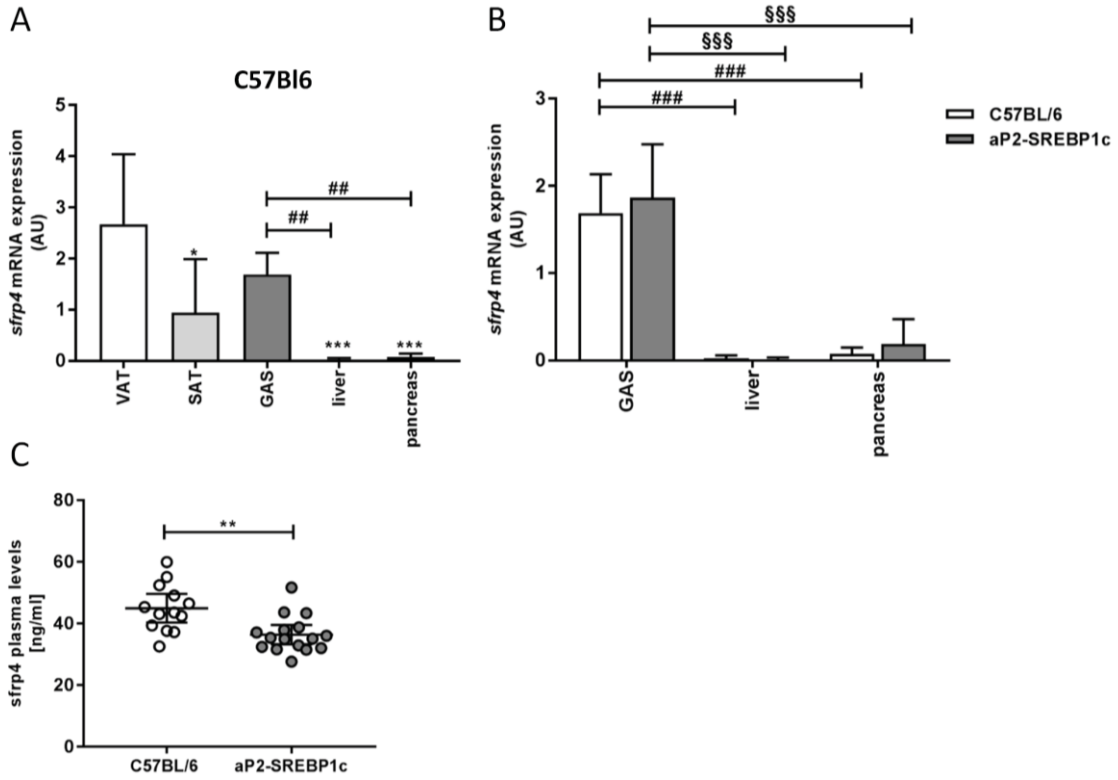

Figure 32. *sfrp4* mRNA expression in peripheral tissues and sfrp4 plasma levels in C57Bl6 and aP2-SREBP-1c mice. *Sfrp4* mRNA expressions in VAT and SAT (C57Bl6 n=4-5), gastrocnemius muscle (GAS) (C57Bl6 n=6, aP2-SREBP-1c n=4), liver (C57Bl6 n=6, aP2-SREBP-1c n=4) and pancreas (C57Bl6 n=6, aP2-SREBP-1c n=4) of C57Bl6 (**A**, **B**) and aP2-SREBP-1c mice (**B**) were obtained by qRT-PCR and analyzed by ΔCt method. Sfrp4 plasma levels were detected by ELISA in C57Bl6 (n=13) and aP2-SREBP-1c (n=16) (**C**). Data are given as mean (95% CI). Differences among groups were analyzed using one-way ANOVA following Tukey´s (**A**) or two-way ANOVA following Sidak´s (**B**) multiple post hoc comparisons test or *t*-test (**C**). $^{**}p<0.005$ (C); $^{*}p< 0.05$, $^{**}p< 0.005$, $^{***}p< 0.001$ vs VAT, $^{\#\#}p<0.005$ between tissues (**A**), $^{\#\#\#}p<0.001$ differences in C57Bl6, $^{\S\S\S}p<0.001$ differences in aP2-SREBP-1c (**B**).

3.4.3 Isolation of primary hepatocytes from C57Bl6 and lipodystrophic aP2-SREBP-1c mice

Primary hepatocytes of C57Bl6 and aP2-SREBP-1c mice were isolated from perfused livers from sacrificed mice via a two-step collagenase perfusion technique of the liver as previously described (Akie and Cooper, 2015). However, modifications to this protocol needed to be established for successful isolation of primary hepatocytes from C57Bl6 and aP2-SREBP-1C mice. Livers of aP2-SREBP-1c mice exhibited increased weight and pronounced elevated lipid accumulation compared to livers of C57Bl6 mice (3.4.1, Table 29). Therefore, time and flow rates of liver perfusion buffer and digestion buffer needed to be adopted from 3 ml/min (2-3 min) and 3.5 ml/min (6 min) for C57Bl6 to 5 ml/min (~4 min) and 5 ml/min (10 min) for aP2-SREBP-1c mice. Moreover, higher amounts of collagenase were used for the digestion of aP2-SREBP-1c livers with 120 U/ml compared to 100 U/ml for C57Bl6 livers to obtain full digestion of liver tissue. For successful isolation of primary hepatocytes from C57Bl6 and aP2-SREBP-1c mice, cell suspension was washed by centrifugation 50x g, 5 min and 4°C whereas separation from non-viable cells occurred by centrifugation with 90% Percoll gradient 50x g, 10 min, 4°c without brake (Figure 8). Although the overall viabilities of the isolated hepatocytes from C57Bl6 and aP2-SREBP-1c were similar, the isolation of primary hepatocytes from C57Bl6 yielded in average in higher amounts of viable cells than isolations of aP2-SREBP-1c hepatocytes.

3.4.4 Analysis of lipid accumulation in hepatocytes isolated of C57Bl6 mice and ap2-SREBP-1c mice

To verify that hepatocytes isolated of aP2-SREBP-1c mice maintained the ectopic lipid accumulation and a ´fatty liver´ phenotype when cultured *in vitro*, oil red O stainings were accomplished with hepatocytes isolated of control C57Bl6 and aP2-SREBP-1c mice after one day of culture. The phase-contrast microscopic images of hepatocytes after the oil red O staining showed that hepatocytes of C57Bl6 as well as of aP2-SREBP-1c exhibited a characteristic binucleated and hexagonal phenotype (Figure 33A, B). In contrast, aP2-SREBP-1c hepatocytes morphologically accumulated more cytosolic lipid droplets compared to control C57Bl6 hepatocytes as represented by the corresponding bright-field images of the oil red O stainings (Figure 33C, D).

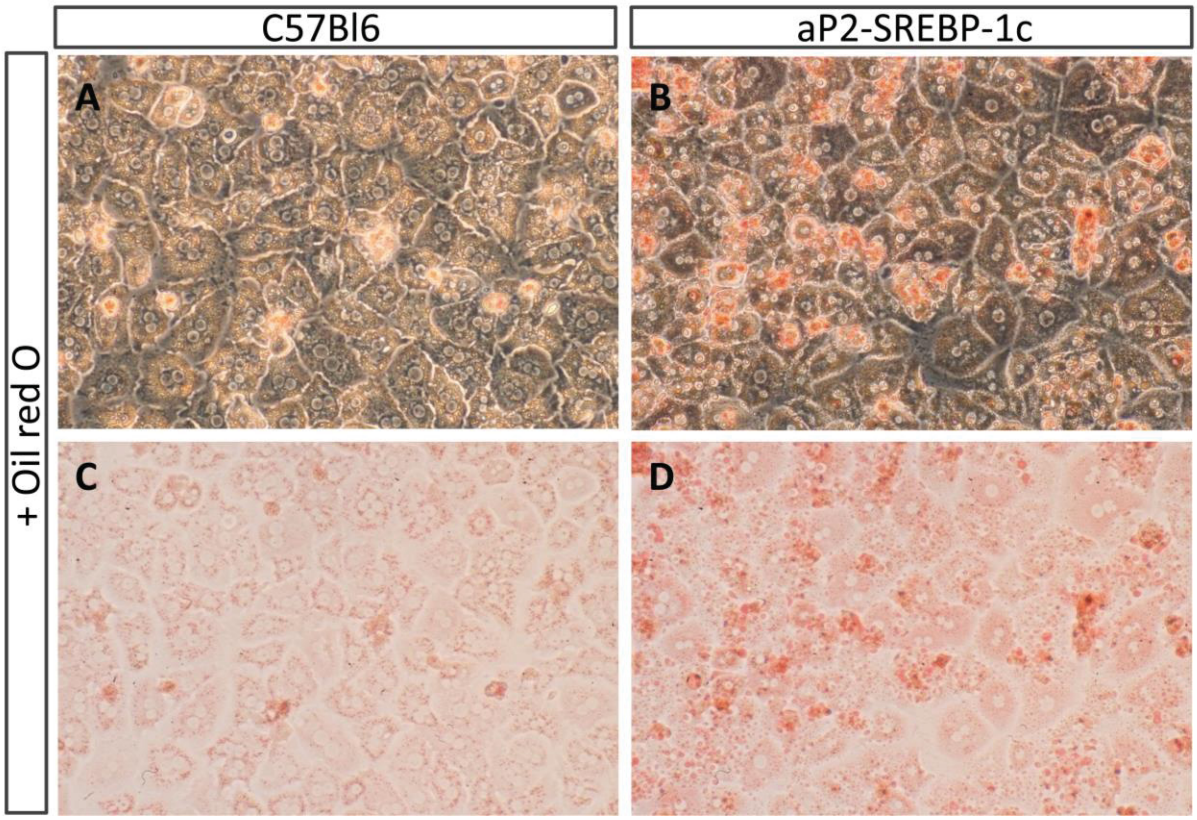

Figure 33. Lipid accumulation in hepatocytes of C57Bl6 (controls) and aP2-SREBP-1c mice. Representative phase-contrast microscopic (**A**, **B**) and corresponding bright-field (**C**, **D**) images (20x magnification) of fixed and oil red-O stained hepatocytes. Images show intracellular lipid accumulation in hepatocytes of C57Bl6 control mice (**A**, **C**) and aP2-SREBP1c (**B**, **D**) mice after one day in culture.

3.4.5 Investigation of insulin signaling in hepatocytes of C57Bl6 mice and ap2-SREBP-1c mice

As described in 3.4.1, the aP2-SREBP-1c mice developed pronounced insulin resistance. To assess whether primary hepatocytes isolated of aP2-SREBP-1c also exhibited impairments in insulin signaling *in vitro*, the phosphorylation levels of Akt-Ser473 and Akt-Thr308 in absence and presence of insulin in hepatocyte lysates of C57Bl6 and aP2-SREBP-1c mice were compared (Figure 34A, B). Although insulin was still able to increase phosphorylation of Akt-Ser473 and Akt-Thr308 in aP2-SREBP-1c hepatocytes, the insulin-mediated phosphorylation level of Akt-Ser473 and Akt-Thr308 were significantly reduced by 36.17% (p=0.03, Figure 34A) and 84.87% (p<0.001) respectively, compared to its phosphorylation levels in hepatocyte of C57Bl6 mice. Moreover, aP2-SREBP1-c hepatocytes had lower IRS-1 protein levels than hepatocyte of control mice, although this did not reach statistical significance (p=0.11) (Figure 34C).

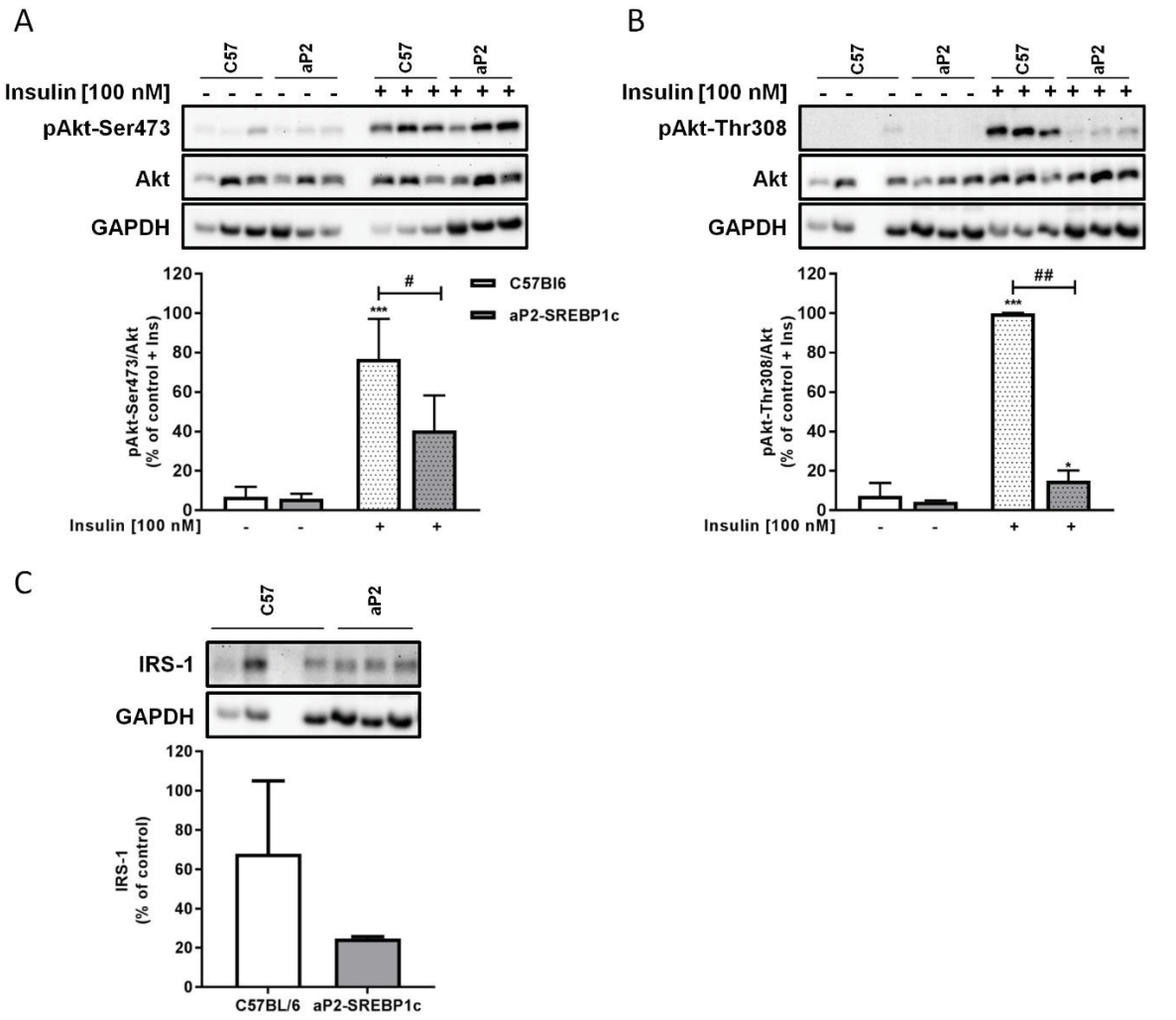

Figure 34. Insulin signaling in primary hepatocytes of C57Bl6 and aP2-SREBP-1c mice. Figures show representative Western blots and data are presented as mean ± SD for the phosphorylation levels of Akt-Ser473 (**A**), Akt-Thr308 (**B**) and protein abundance of IRS-1 (**C**) of three independent experiments (n=3). The protein signals were normalized for the abundance of non-phosphorylated protein and loading control GAPDH. The values obtained for insulin-unstimulated cells were considered as controls. All values were normalized to insulin-treated cells of C57Bl6 (control + Ins) which were set as 100%. Differences among groups were calculated by two-way ANOVA analyses followed by the Sidak's multiple comparisons test or *t*-test. **p*<0.05, ***p*<0.01, ****p*<0.001 for insulin versus basal; $^{\#}p$<0.05; $^{\#\#}p$<0.01; $^{\#\#\#}p$<0.001 for sFRP4-treated versus untreated cells. C57, C57Bl6 mice; aP2, aP2-SREBP-1c mice.

3.5 The role of sFRP4 in the regulation of insulin action, energy and lipid metabolism in primary hepatocytes of C57Bl6 and aP2-SREBP-1c mice

3.5.1 Effect of sFRP4 on primary hepatocytes of metabolic healthy C57Bl6 mice

The impact of sFRP4 and potential mechanisms of its action on energy and lipid metabolism and insulin signaling was investigated by using primary hepatocytes isolated from metabolic healthy C57Bl6 mice.

3.5.1.1 Analysis of sFRP4 on the regulation of glucose metabolism in primary hepatocytes of metabolic healthy C57Bl6

To examine whether sFRP4 affected gluconeogenesis in primary hepatocytes, cells were treated with 100 ng/ml sFRP4 for 4h or 24h followed by insulin stimulation for further 60 min. Figure 35A, B showed that insulin significantly suppressed the mRNA expression of *Pck1* and *G6pc* in untreated hepatocytes compared to basal conditions by 1.7-fold ($p<0.05$) and 2.2-fold ($p<0.01$), respectively. Whereas incubation of cells with sFRP4 for 4h or 24h, completely abrogated the insulin-mediated suppression of *Pck1* as well as *G6pc* expression compared to basal conditions. Further, 4h sFRP4 reduced *Pck1* ($p=0.05$) and *G6pc* ($p=0.07$) expression but without reaching statistical significance while 24h sFRP4 exposure significantly decreased *G6pc* expression under basal conditions compared to untreated control cells (1 ± 0.26 vs. 0.6 ± 0.05, $p<0.05$).

Next, it was determined in more detail whether the impaired insulin-mediated expression of gluconeogenic genes induced by sFRP4 also was associated with changes in glucose production in primary hepatocytes. The rate of hepatic glucose production via gluconeogenesis depends on the presence of gluconeogenic substrates including pyruvate and lactate. Therefore, cells were exposed to sFRP4 for 4h and 24h followed by stimulation with 2 mM sodium lactate and 2 mM sodium pyruvate for 4h in absence and presence of insulin. Incubation of hepatocytes with the gluconeogenic substrates significantly increased glucose release in the cell culture supernatant by 1.5-fold ($p<0.001$) compared to untreated cells under basal conditions (Figure 35C). Whereas insulin tended to decrease lactate- and pyruvate-stimulated glucose production in control cells by 1.2-fold ($p=0.1$), it failed to suppress glucose production in hepatocytes incubated with sFRP4 for 4h and 24h but without statistical

significance. However, sFRP4 did not affect lactate- and pyruvate-stimulated glucose production in absence of insulin compared to sFRP4-untreated cells.

To test the effect of sFRP4 on glycogen synthesis, primary hepatocytes were exposed to sFRP4 for 4h and 24h prior to incubation with ^{14}C-labeled glucose with or without insulin for 3h. Thereby, glycogen synthesis was represented by the incorporation of ^{14}C-glucose into glycogen. Insulin significantly induced glycogen synthesis in untreated hepatocytes and in cells pre-incubated with sFRP4 for 4h compared to basal conditions both by 1.4-fold (all p<0.01) (Figure 35D). However, insulin failed to promote glycogen synthesis in hepatocytes pre-incubated with sFRP4 for 24h. Therefore, the 24h sFRP4 incubation time of hepatocytes has been used for further analysis on lipid metabolism.

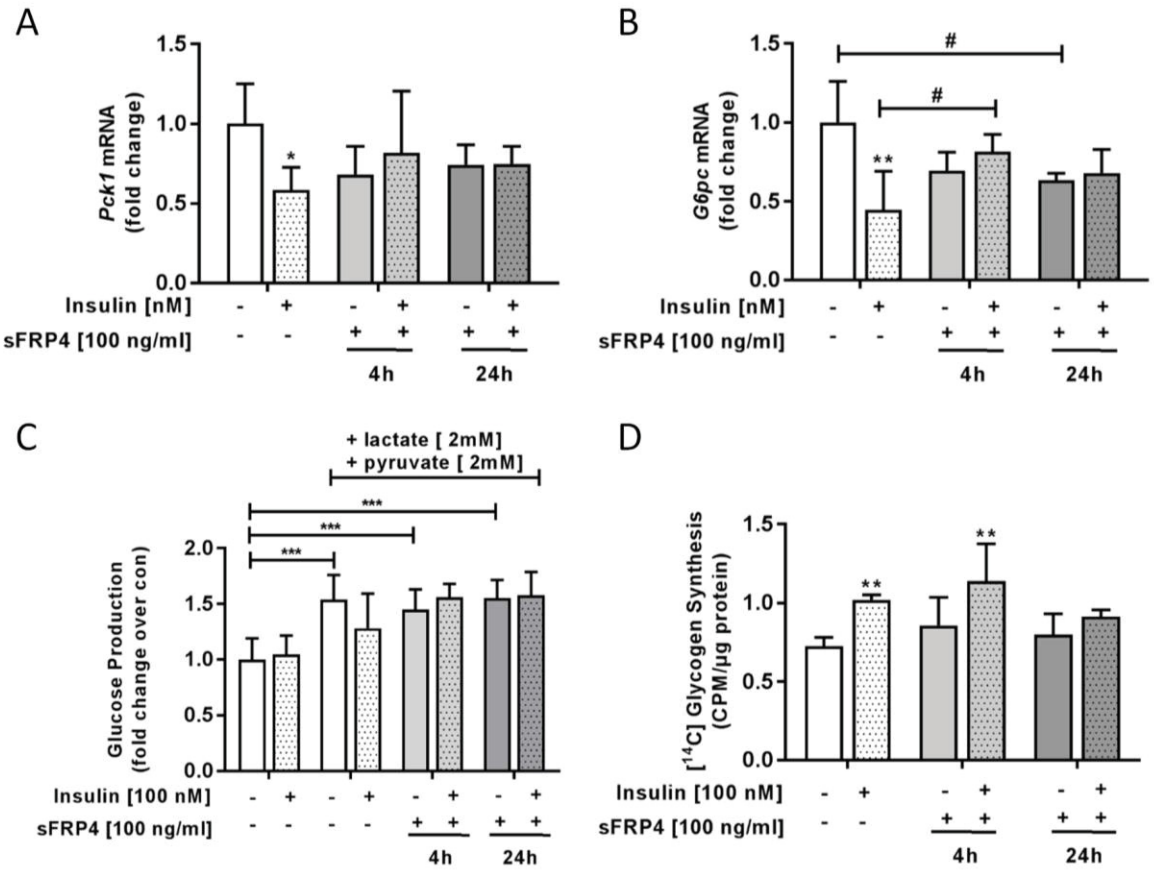

Figure 35. Impact of sFRP4 on insulin-mediated suppression of gluconeogenic genes, glucose production and glycogen synthesis in primary hepatocytes. Hepatocytes were exposed to sFRP4 (100 ng/ml) for 4h or 24h (**A**-**D**) in absence or presence of insulin (100 nM) for 60 min (**A**, **B**), 4h (**C**) or 3h (**D**) supplemented with the gluconeogenic substrates sodium lactate and pyruvate (each 2 mM) (**C**). *Pck1* (**A**) and *G6pc* (**B**) expression levels were assessed by quantitative RT-PCR and normalized to *18S*. Data represent mean ± SD of the expression levels of independent experiments (n=4-6). Hepatocyte culture supernatants were used for determination of glucose concentration. Glucose production was calculated by normalization of glucose concentration levels to protein content and presented as mean ± SD of independent experiments (n=4-8) (**C**). Glycogen synthesis was

determined as incorporation of D-[^{14}C(U)]-glucose into glycogen normalized to protein amount of independent experiments (n=6) (**D**) represented as mean ± SD. The values obtained for untreated cells without (**A-C**) or with insulin (**D**) were considered as controls and set as 1. Differences among conditions were calculated by two-way ANOVA analyses followed by the Sidak's multiple comparisons test. *p<0.05, **p<0.01, ***p<0.001 versus insulin; $^{\#}p$<0.05 control versus sFRP4.

3.5.1.2 Effect of sFRP4 on mitochondrial respiration in primary hepatocytes of metabolic healthy C57Bl6

To study the effect of sFRP4 on hepatic mitochondrial respiration, primary hepatocytes of C57Bl6 were exposed to sFRP4 (100 ng/ml) for 4h and 24h followed by extracellular flux analyzer measurements in the absence and presence of specific inhibitors and inducers of the mitochondrial respiratory chain (Figure 36A-G). The data showed that sFRP4 did not alter the mitochondrial bioenergetic profile in primary hepatocytes in regard to basal respiration, spare respiratory capacity, ATP production and proton leak.

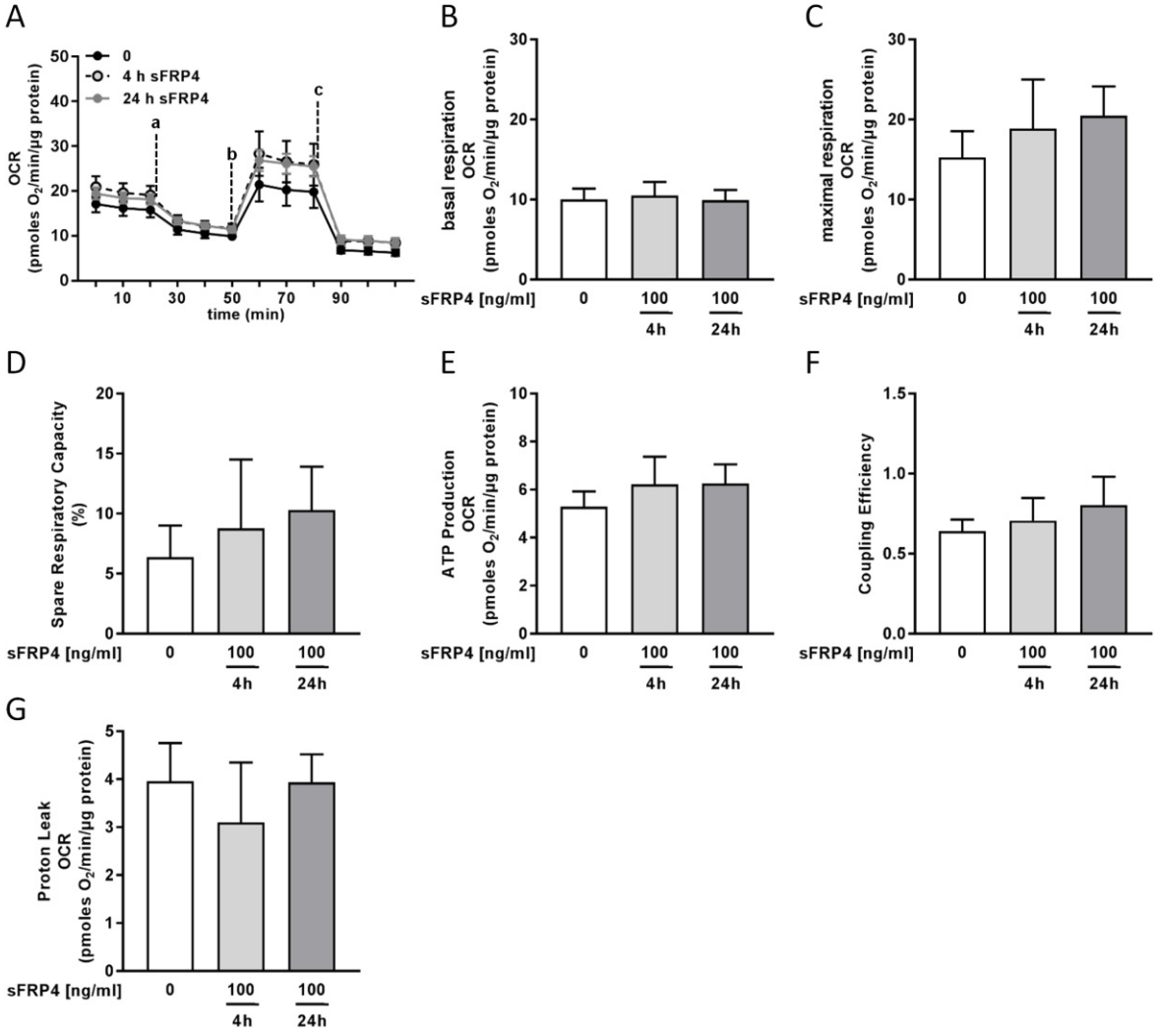

Figure 36. Effect of sFRP4 on mitochondrial respiration in primary hepatocytes. Hepatocytes were treated 4h and 24h with sFRP4. OCRs were measured in controls (0 ng/ml sFRP4) and sFRP4-treated cells (100 ng/ml) after sequential injection of oligomycin (1 µM, a), FCCP (0.5 µM, b) and antimycin A/rotenone (each 0.5 µM, c). Figure A show a representative graph of measured OCRs normalized to protein amount which were used for assessing basal respiration (**B**), maximal respiration (**C**), spare respiratory capacity (**D**), ATP production (**E**), coupling efficiency (**F**) and proton leak (**G**). The presented data are the mean ± SEM (**A**) or mean ± SD (**B**-**G**) of independent experiments (n=6-8). Differences among groups were calculated by one-way ANOVA following Tukey´s multiple comparison test. *p<0.05 for sFRP4 vs basal.

Only maximal respiration and coupling efficiency were increased in hepatocytes when incubated 24h with sFRP4 (20.48 ± 3.66 pmoles O_2/min/µg protein, p=0.07; 0.8 ± 0.18, p=0.07, respectively) compared to untreated cells (15.27 ± 3.27 pmoles O_2/min/µg protein; 0.63 ± 0.07, respectively), but these changes did not reach statistical sufgnificance (Figure 36C, F).

3.5.1.3 Effect of sFRP4 on energy metabolism in primary hepatocytes of metabolic healthy C57Bl6

The impact of sFRP4 on mitochondrial oxidation and uptake of palmitic acid was examined in primary hepatocytes. The release of produced [^{14}C]-CO_2 was determined in hepatocytes upon incubation with substances that promote or inhibit mitochondrial oxidation or after treatment with sFRP4, as already described for assessing the effect of sFRP4 on fatty acid oxidation in myotubes (Figure 37A). Incubation of hepatocytes with FCCP induced palmitic acid oxidation (182.2 ± 84.65 CPM/µg protein, p=0.2) compared to basal conditions (103.78 ± 27.89 CPM/µg protein) whereas oligomycin (30.35 ± 19.45 CPM/µg protein, p=0.02), antimycin/rotenone (42.86 ± 19.08 CPM/µg protein, p=0.04) and etomoxir (26.58 ± 18.63 CPM/µg protein, p=0.02) significantly inhibited fatty acid oxidation (Figure 37A, left panel). However, hepatocytes exposed to sFRP4 oxidized palmitic acids similar to untreated hepatocytes (Figure 37A, right panel). In addition, not only fatty acid oxidation but also uptake of fatty acids which was measured by cellular uptake of [^{3}H]-palmitic acid, was not altered after treatment of hepatocytes with sFRP4 (Figure 37B).

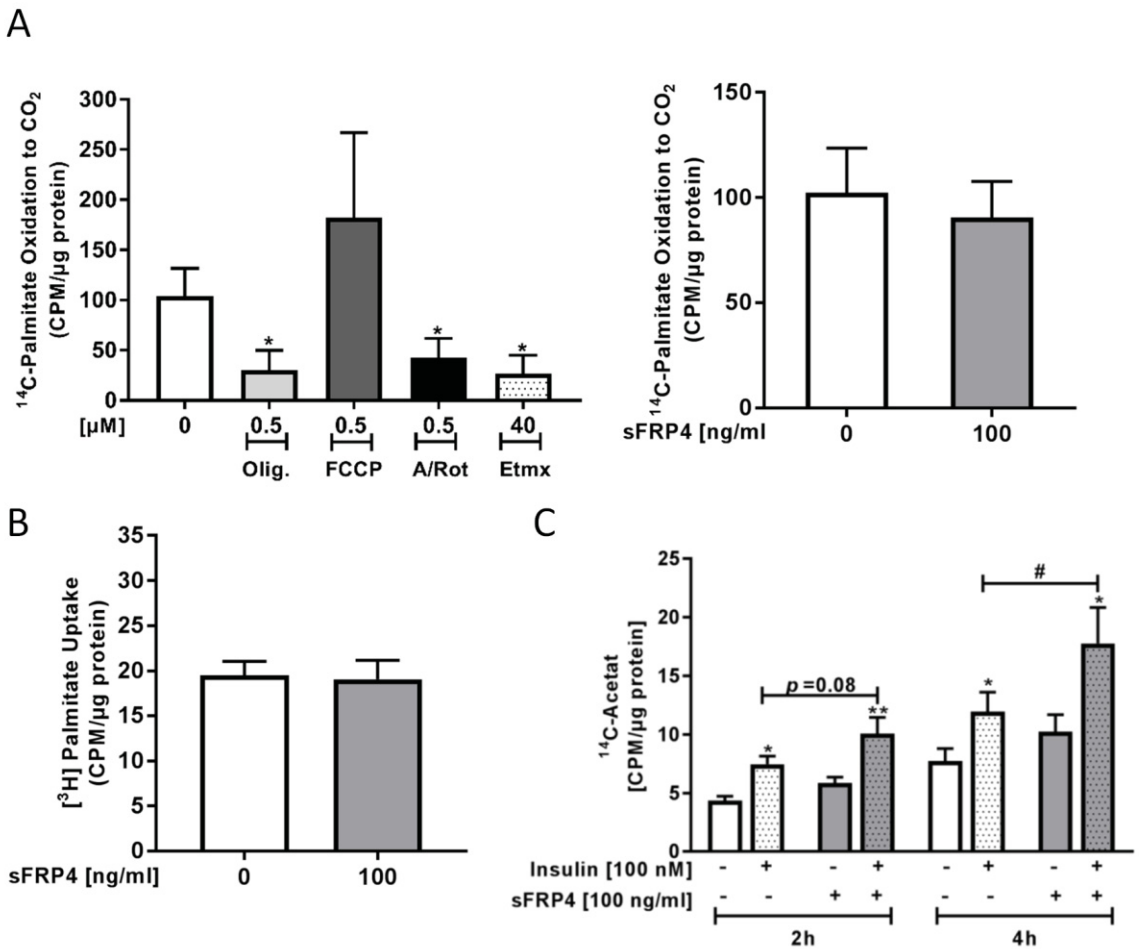

Figure 37. Effect of sFRP4 on fatty acid oxidation, uptake and DNL in primary hepatocytes. Hepatocytes were exposed to sFRP4 (100 ng/ml) for 24h (**A** right panel, **B**, **C**) or inducer (FCCP) or inhibitors of fatty acid β-oxidation (oligomycin, antimycin, rotenone, etomoxir) (**A** left panel). For DNL studies, cells were incubated with or without insulin (100 nM) during experiment. Cells were incubated with either ^{14}C-palmitate (**A**), ^{3}H-palmitate (**B**) for 15 min or with ^{14}C-acetate for 2h and 4h (**C**). Data show oxidation (**A**) or incorporation of isotopic labeled palmitate (**B**) or ^{14}C-acetate as lipogenic activity (**C**) of independent experiments (**A**, **B** n=3-5; C n=10-12) presented as mean ± SD in cultured hepatocytes. The values obtained for sFRP4-untreated cells were considered as controls (0 ng/ml). Differences among conditions were calculated by *t*-test (A, B) or two-way ANOVA analyses followed by Sidak's multiple comparisons test (**C**). **p*<0.05, ***p*<0.01, ****p*<0.001 versus control cells; $^{\#}$*p*<0.05 versus sFRP4 treated cells.

3.5.1.4 Effect of sFRP4 on lipid metabolism in hepatocytes of metabolic healthy C57Bl6 mice

For analysis of DNL, primary hepatocytes were treated with sFRP4 as indicated in Figure 37C in absence or presence of insulin followed by incubation with ^{14}C-labeled acetate for additional 2h and 4h. The assessed incorporation of ^{14}C-acetate during this time represented the cellular lipogenic activity. Figure 37C showed that insulin significantly increased hepatic lipogenic

activity after 2h (4.36 ± 1.2 vs 7.47 ± 2.15 CPM/µg protein, basal vs insulin, $p<0.05$) and 4h (7.74 ± 3.69 vs 11.97 ± 5.69 CPM/µg protein, basal vs insulin, $p<0.05$) in untreated hepatocytes. Moreover, a time-dependent increase in basal as well as insulin-stimulated lipogenic activity in untreated hepatocytes by 1.7- for 2h and 1.5-fold for 4h measurements could be observed. Hepatocytes exposed to sFRP4 did not synthesize statistically significant more lipids under basal (4.36 ± 1.2 vs. 5.87 ± 1.6 CPM/µg protein, control vs. sFRP4, $p=0.66$) and insulin-stimulated conditions (7.47 ± 2.15 vs. 10.07 ± 4.64 CPM/µg protein, control + Ins vs. sFRP4 + Ins, $p=0.47$) after a 2h measurement compared to untreated control cells. This effect became even more strikingly after a 4h measurement: sFRP4 significantly increased the insulin-mediated hepatic lipogenic activity in comparison to cells that were kept untreated (11.97 ± 5.69 vs. 17.78 ± 10.64 CPM/µg protein, control + Ins vs. sFRP4 + Ins, $p<0.05$).

3.5.1.5 Effect of sFRP4 on AMPK signaling in primary hepatocytes of metabolic healthy C57Bl6

To determine whether sFRP4 affect AMPK signaling in primary hepatocytes, cells were treated with sFRP4 (100 ng/ml) for 4h followed by analysis of the phosphorylation of AMPK at Thr172 and its substrate ACC at Ser79. Oligomycin, a potent activator of AMPK, was exposed to 4h and used as a positive control for AMPK phosphorylation in the performed experiments.

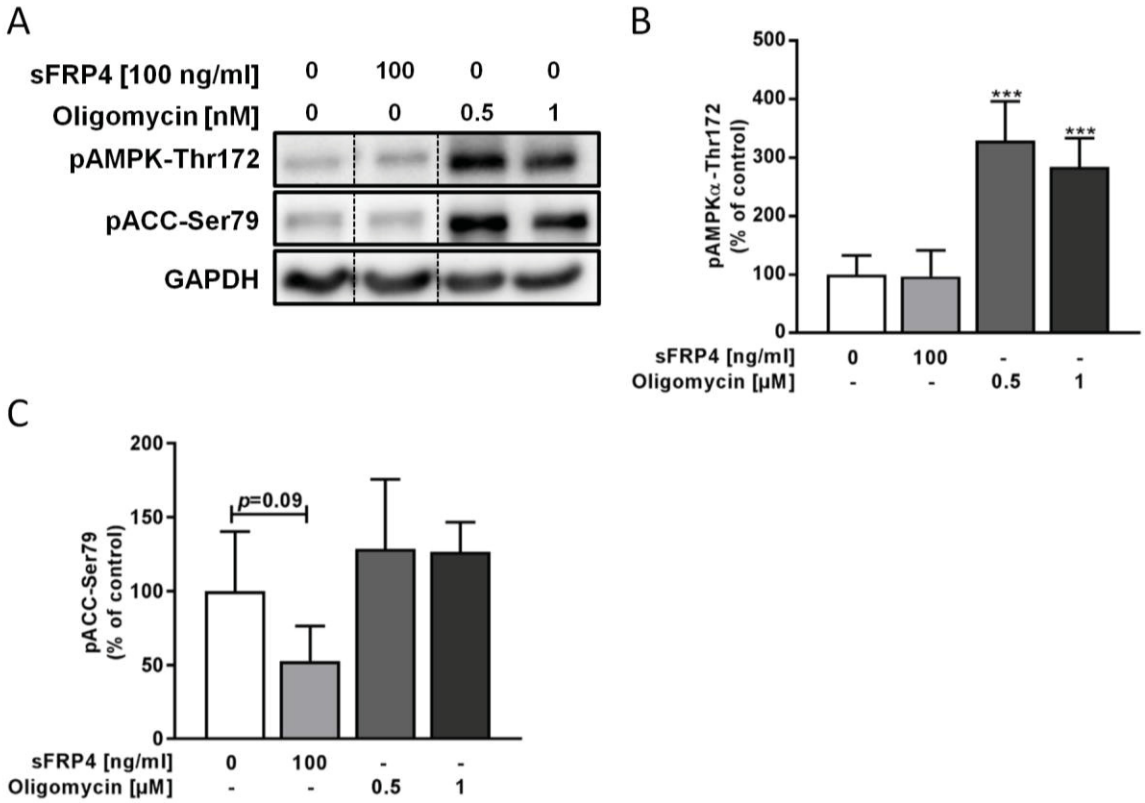

Figure 38. Effect of sFRP4 on AMPK signaling in primary hepatocytes. Hepatocytes were treated with 100 ng/ml sFRP4 or oligomycin (0.5 µM, 1 µM) for 4h. Following cell lysis, protein lysates were analyzed for phosphorylation levels of AMPKα-Thr172 and its substrate ACC-Ser79 (**A**-**C**). 4h oligomycin treatment of hepatocytes served as an activation control of AMPK signaling. The protein signals were normalized for the abundance of loading control GAPDH. Data show representative Western blots and bar graphs showing the mean ± SD of the phosphorylation levels of three independent experiments (n=3). The values obtained for sFRP4-untreated cells were considered as controls (0 ng/ml). Differences were calculated by *t*-test. ***$p<0.001$ versus control cells.

Exposing hepatocytes to sFRP4 for 4h did not affect the phosphorylation of AMPK, which was significantly increased in cells incubated with either 0.5 µM or 1 µM oligomycin by 3.3- and 2.8-fold, respectively (both $p<0.001$) (Figure 38A, B). Whereas the phosphorylation of ACC-Ser79 was decreased by ~48% ($p=0.09$) when cells were treated with sFRP4 although this did not reach statistical significance (Figure 38).

3.5.1.6 Analysis of sFRP4 in the regulation of insulin signaling in primary hepatocytes of metabolic healthy C57Bl6 mice

The correlation of sFRP4 with insulin resistance (Table 28) and the observed impairments mediated by sFRP4 on insulin regulated gluconeogenic gene expression, glycogen synthesis and *de novo* lipogenesis, strongly indicated that sFRP4 interferes with insulin signaling in primary hepatocytes. To study this in more detail, primary hepatocytes were exposed to sFRP4 for 24h prior to an acute insulin stimulus followed by analysis of the phosphorylation status of substrates belonging to the insulin signaling pathway. In accordance with the functional impairments of insulin action by sFRP4 in hepatocytes, the insulin-mediated phosphorylation of Akt-Ser 473 was significantly reduced in cells pre-incubated with sFRP4 for 24h by 46% ($p<0.01$) compared to untreated hepatocytes, whereas the phosphorylation of Akt at Thr308 was not affected by sFRP4 (Figure 39A, B). Additionally, the decrease in insulin-mediated phosphorylation of Akt-Ser473 was accompanied by impaired insulin-induced phosphorylation of its substrates GSK3β-Ser9 and FoxO1-Ser256 by 43% ($p<0.05$) and 46% ($p<0.05$) respectively, in cells exposed 24h to sFRP4 in comparison to cells that were kept untreated (Figure 39C, D). sFRP4 did not affect phosphorylation of Akt-Ser473, GSK3β-Ser9 and FoxO1-Ser256 under basal conditions.

The decrease in phosphorylation levels of Akt and GSK3β in cells treated 24h with sFRP4 could not be ascribed to changes in corresponding protein abundances (Figure 40A, B). However, the

decrease in insulin-mediated phosphorylation of FoxO1-Ser256 induced by sFRP4 coincided with a reduction in FoxO1 abundance by 55% (p=0.001) compared to untreated hepatocytes (Figure 40C).

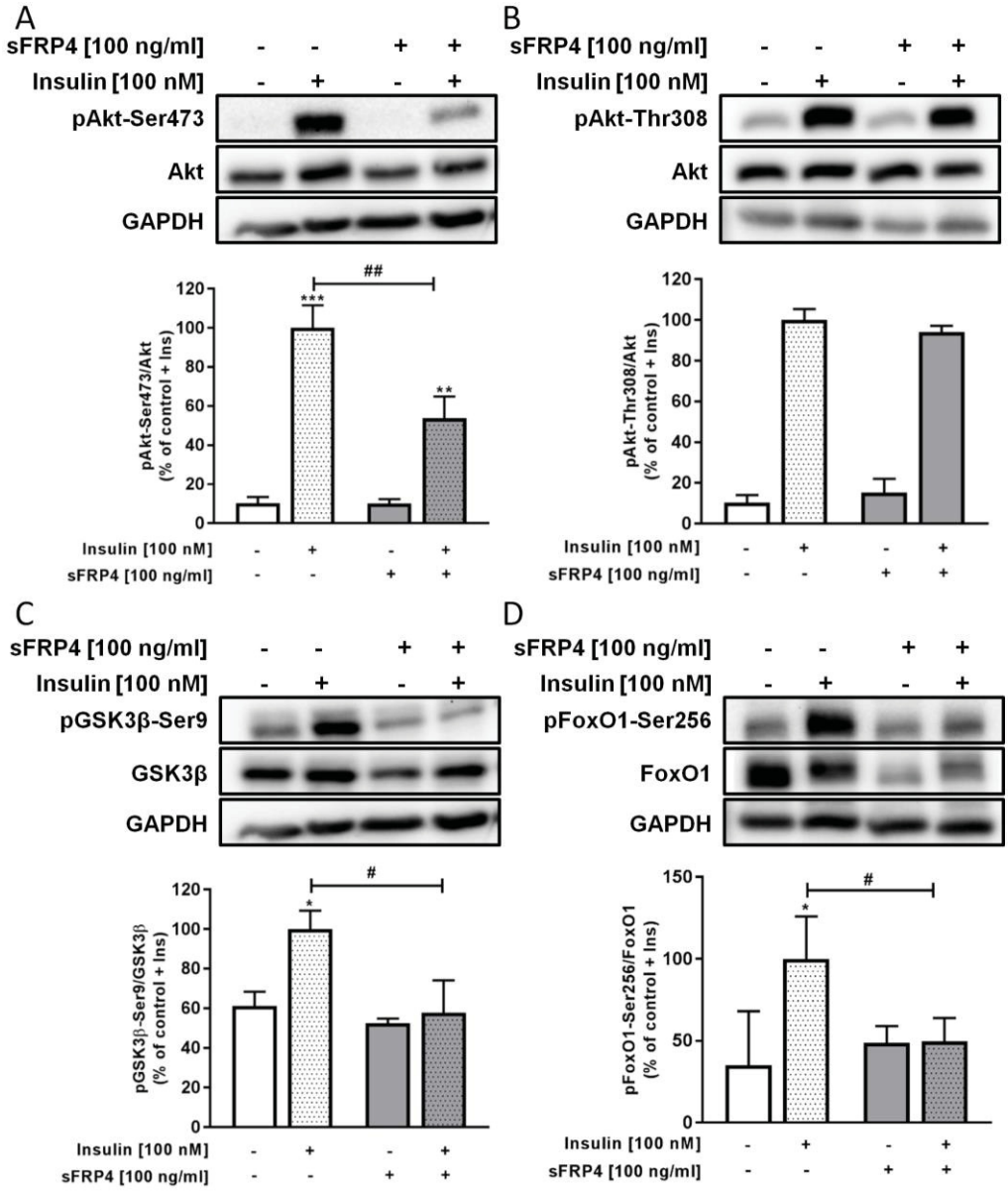

Figure 39. Effect of sFRP4 on insulin signaling in primary hepatocytes. Hepatocytes were treated with sFRP4 for 24h prior to insulin stimulation (10 min). Following cell lysis, protein lysates were analyzed for phosphorylation levels of Akt-Ser473 (**A**), Akt-Thr308 (**B**), GSK3β-Ser9 (**C**) and FoxO1-Ser256 (**D**). The protein signals were normalized for the abundance of the respective non-phosphorylated protein and the loading control GAPDH. Figures show representative Western blots and data are presented as mean ± SD of the phosphorylation levels of four independent experiments. The values obtained for sFRP4-untreated cells were considered as controls. All values were normalized to insulin-treated control cells (control + Ins) which were set as 100%. Differences among groups were calculated by two-way ANOVA analyses followed by the Sidak's multiple comparisons test. *p<0.05, **p<0.01, ***p<0.001 for insulin vs basal; $^{\#}p$<0.05; $^{\#\#}p$<0.01; $^{\#\#\#}p$<0.001 for sFRP4-treated vs untreated cells.

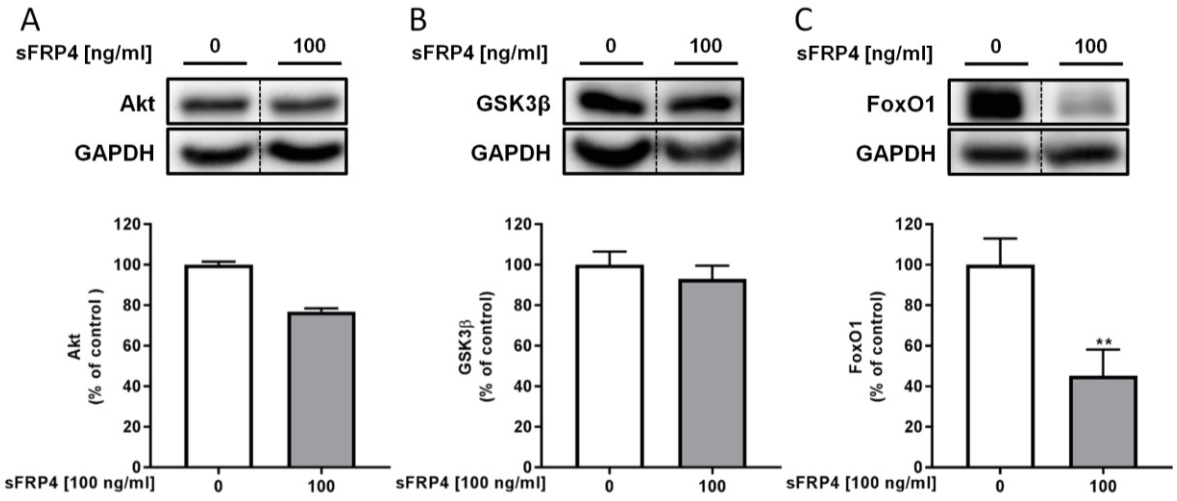

Figure 40. Effect of sFRP4 incubation on protein abundance of components of insulin action in primary hepatocytes. The Figure shows representative Western blots and data are presented as mean ± SD for the protein abundance of Akt (**A**), GSK3β (**B**), and FoxO1 (**C**) in four independent experiments. The protein signals were normalized for the abundance of the loading control GAPDH. The values obtained for sFRP4-untreated cells were considered as controls. All values were normalized to control cells which were set as 100%. Differences were calculated by *t*-test. ***p*<0.01 for sFRP4-treated versus untreated cells.

IRS-1/2 are key molecules more upstream of the insulin signaling cascade and direct intracellular substrates of the insulin receptor in liver. As Figure 41A illustrated, hepatocytes pre-incubated with sFRP4 for 4h had similar IRS-1 levels (p=0.5) whereas 24h sFRP4 treated cells had reduced IRS-1 protein levels by 35% (p<0.001) in comparison to control cells. As in muscle, *Irs1* mRNA expression was not altered by 24h sFRP4 exposure of cells (Figure 41B). 24h sFRP4 exposure of hepatocytes did not affect IRS-2 abundance (Figure 41C).

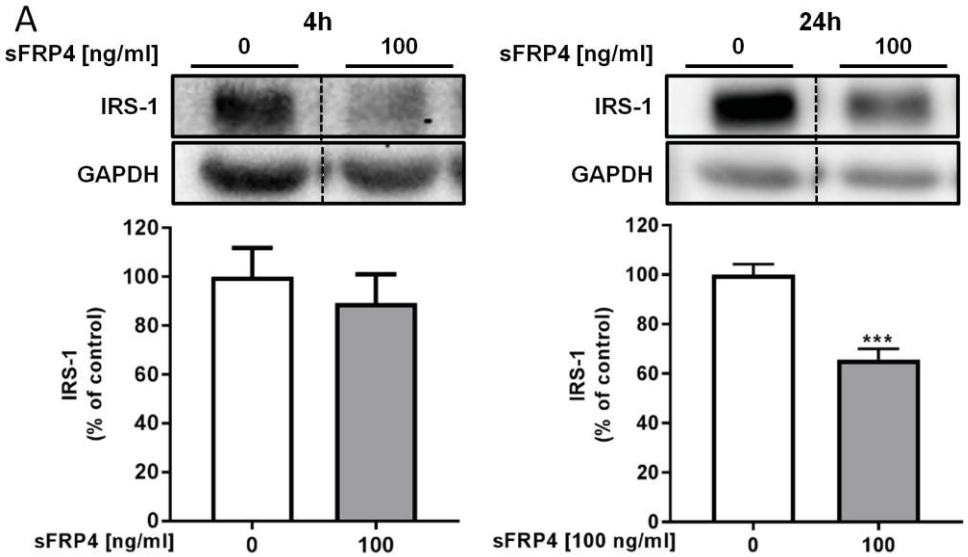

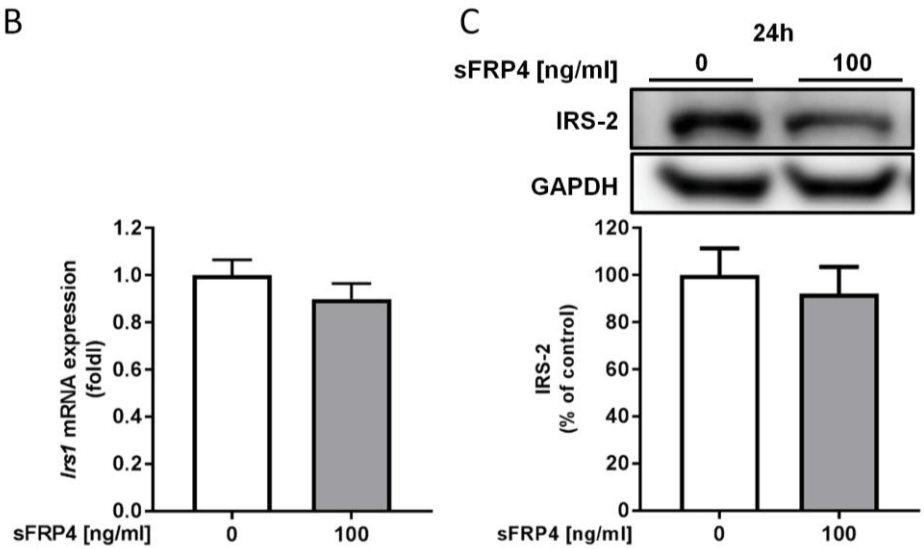

Figure 41. IRS-1 abundance was decreased by sFRP4 in primary hepatocytes. IRS-1 abundance (**A**) in hepatocytes were determined upon 4h and 24h sFRP4 treatment (100 ng/ml) (**A**), and *Irs1* expression (**B**) and IRS-2 abundance (**C**) after 24h sFRP4 exposure. IRS-1 and IRS-2 protein levels were assessed by Western blotting and normalized to GAPDH. *Irs1* mRNA expression levels were measured by quantitative RT-PCR and normalized to *Hprt1* and *Rps18*. Representative blots are shown. Bar graphs represent data as mean ± SD of the IRS-1 and IRS-2 levels of independent experiments using cells from different donors (n=3-9). The values obtained for sFRP4-untreated cells were considered as controls (0 ng/ml) and set as 1 or 100%. Differences among conditions were calculated by *t*-test. **p*<0.05, ***p*<0.01, ****p*<0.001 for sFRP4-treated versus control cells.

3.5.1.7 Impact of sFRP4 on IRS-1 degradation and proteasome activity in hepatocytes of metabolic healthy C57Bl6 mice

sFRP4 decreased IRS-1 abundance but not mRNA expression in hepatocytes which indicated a post-translational regulation of the IRS-1 protein induced by sFRP4 including proteasome-dependent degradation. To test this assumption in more detail, the proteasome inhibitor BZ was used in the experiments. To prevent that BZ affected viability of hepatocytes, first different concentrations of BZ [1-100 nM] were exposed for 24h to hepatocytes. Incubation of hepatocytes to 1 nM or 10 nM BZ did not affect metabolic activity, whereas 100 nM BZ remarkably reduced the cellular viability by ~65% (Figure 42A) compared to control cells. Therefore, 10 nM BZ have been used for further analysis. Primary hepatocytes were pre-incubated with 10 nM BZ for 30 min before sFRP4 was added to the cells for 24h followed by analysis of IRS-1 protein levels. As Figure 42B shows, sFRP4 significantly reduced IRS-1 levels (p=0.02) and this reduction was completely restored to similar levels observed in controls when cells were pre-incubated with BZ followed by sFRP4 exposure (100 ± 16.42% vs 89.13 ± 12.97%; basal vs sFRP4+BZ). BZ alone did not affect IRS-1 levels compared to control cells.

Moreover, the inhibitory effect of BZ and the impact of sFRP4 on chymotrypsin-like 26S proteasome activity in hepatocytes were examined. BZ incubation for 24h significantly reduced chymotrypsin-like activity of the proteasome by 43% (p=0.002) (Figure 42C). In contrast, 24h sFRP4 treatment did not affect proteasome activity in hepatocytes neither when added alone nor after 30 min pre-incubation with BZ for 24h.

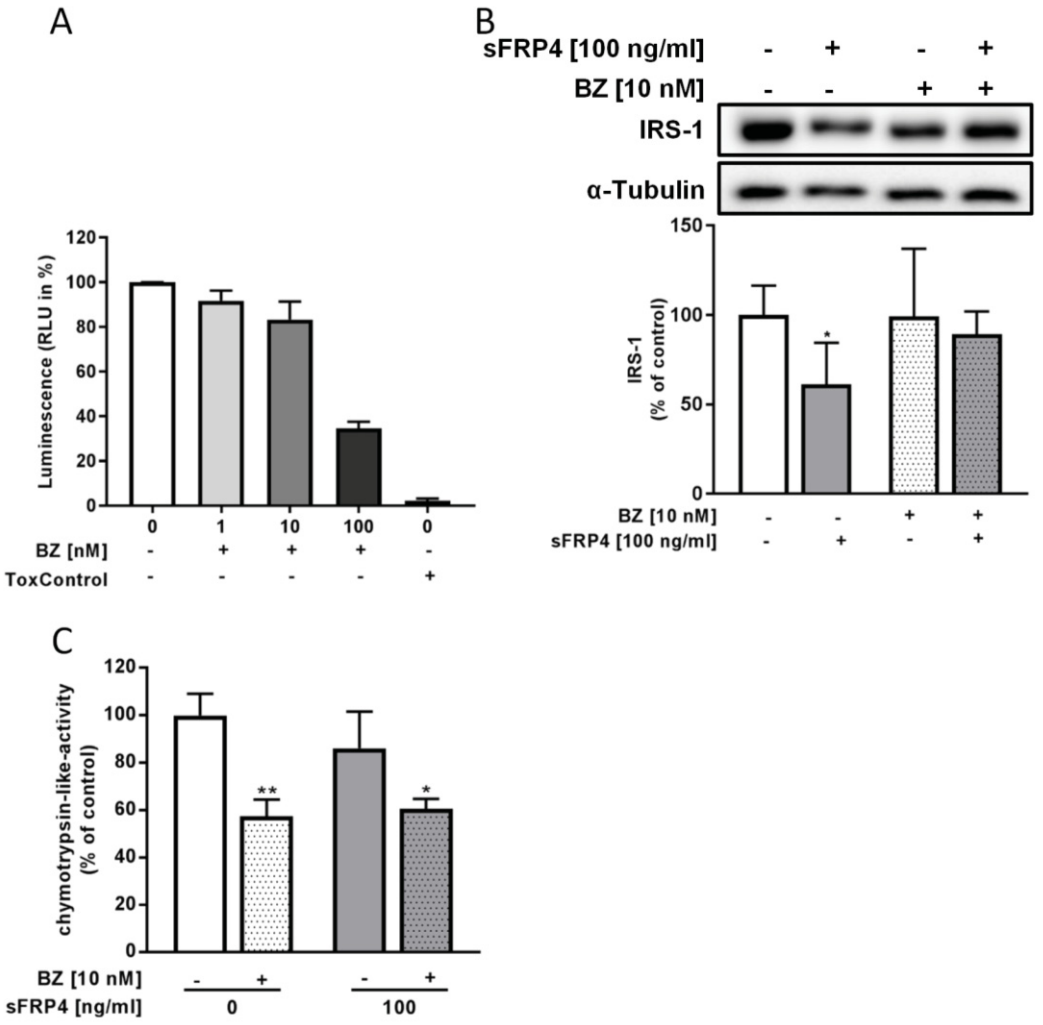

Figure 42. Impact of the proteasome on reduced IRS-1 levels induced by sFRP4 exposure in hepatocytes. Hepatocytes were exposed 24h to BZ (1-100 nM) to assess the effect of the used concentrations on metabolic cellular activity and thus viability using CellTiter-Glo® Luminescent Cell Viability Assay (**A**, n=2). 100 ng/ml sFRP4 for 24h with or without 10 nM BZ have been used to examine its impact on IRS-1 abundance **(B**) and proteasome activity (**C**). Data show the mean ± SD of three to six independent experiments (**B-C**). Data of untreated cells were regarded as controls and set as 100 %. Two-way ANOVA analyses followed by the Sidak's multiple comparisons test were performed. *p<0.05, **p<0.01*, ***p*<0.001 versus untreated cells.

Interestingly, in hepatocytes incubated with proteasome inhibitor BZ before sFRP4 exposure, the insulin-mediated phosphorylation levels of Akt-Ser473 (p<0.001) and GSK3β-Ser9 (p=0.02) were no further reduced as observed in cells treated with sFRP4 alone (Figure 43A, B). However, BZ treatment did not affect sFRP4-induced decrease on insulin-mediated phosphorylation of FoxO1-Ser256 (Figure 43C).

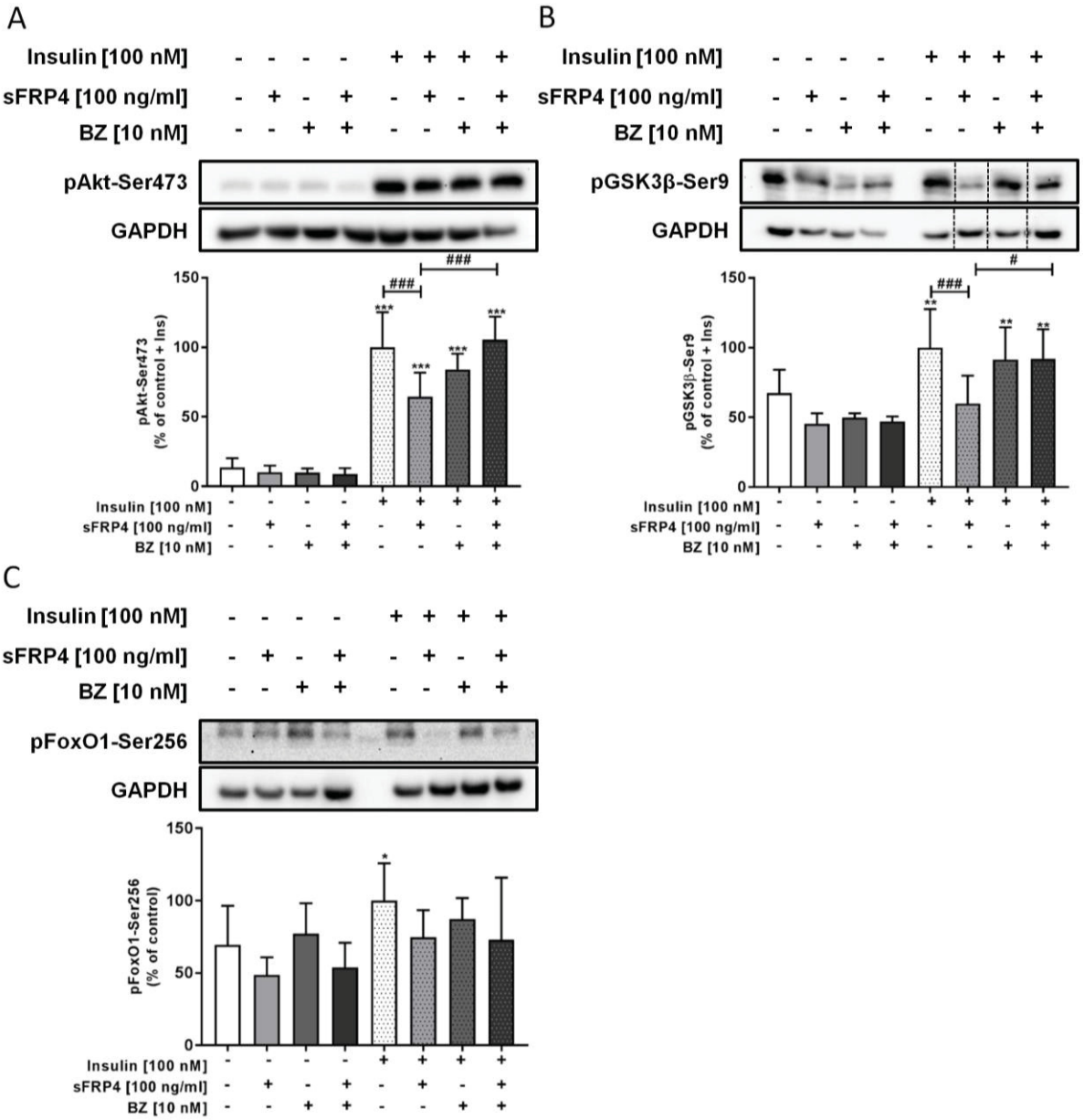

Figure 43. Effect of sFRP4 and BZ on insulin signaling in primary hepatocytes. Hepatocytes were treated 24h with 100 ng/ml sFRP4 in the presence (+) or absence (-) of BZ prior to insulin stimulation (10 min). Phosphorylation levels of pAkt-Ser473 (**A**), pGSK3β-Ser9 (**B**) and pFoxO1-Ser256 (**C**) were normalized for the loading control GAPDH. Bar graphs represent data as mean ± SD of phosphorylation levels of independent experiments using cells from different mice (n=5). The values obtained for sFRP4-untreated cells were considered as controls. All values were normalized to control cells in presence of insulin and set as 100%. Differences among

groups were calculated by two-way ANOVA followed by Sidak's multiple comparisons test. *p<0.05 for insulin versus basal; #p<0.05 versus sFRP4 treated cells.

Protein abundances of Akt and GSK3β were not altered in hepatocytes that were pre-incubated with BZ (Figure 44A, B). sFRP4 induced reduction of FoxO1 protein levels (p=0.003) were not completely restored with BZ treatment (p=0.08) compared to untreated control cells (Figure 44C).

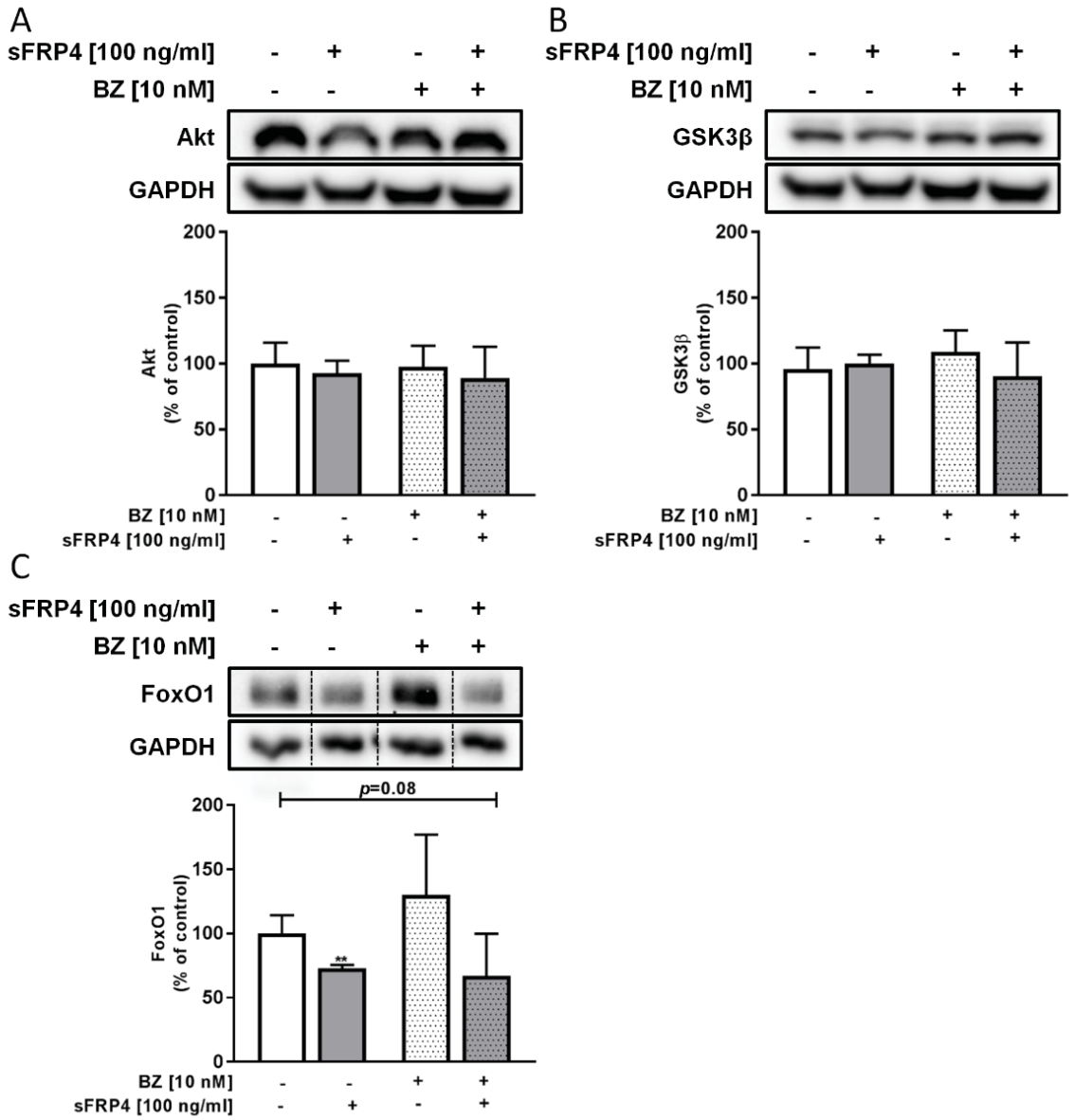

Figure 44. Effect of sFRP4 and BZ on protein abundance of components of insulin action in primary hepatocytes. Hepatocytes were treated 24h with 100 ng/ml sFRP4 in the presence (+) or absence (-) of BZ. Abundance of Akt (**A**), GSK3β (**B**) and FoxO1 (**C**) were normalized for the loading control GAPDH. Bar graphs represent data as mean ± SD of phosphorylation levels of independent experiments using cells from different mice (n=3). The values obtained for sFRP4-untreated cells were considered as controls. All values were normalized to control cells and set as 100%. Differences among groups were calculated by *t*-test. *p<0.05 versus basal.

3.5.1.8 Effect of sFRP4 on cellular sirtuin activity in primary hepatocytes of metabolic healthy C57Bl6 mice

To assess the effect of sFRP4 on sirtuin activity, primary hepatocytes were exposed 24h to 100 ng/ml sFRP4 followed by luminescence measurements which are directly proportional to relative sirtuin activity. As Figure 45 shows, sFRP4 significantly reduced SIRT activity in primary hepatocytes by 1.7-fold (p=0.03) in comparison to cells that were kept untreated.

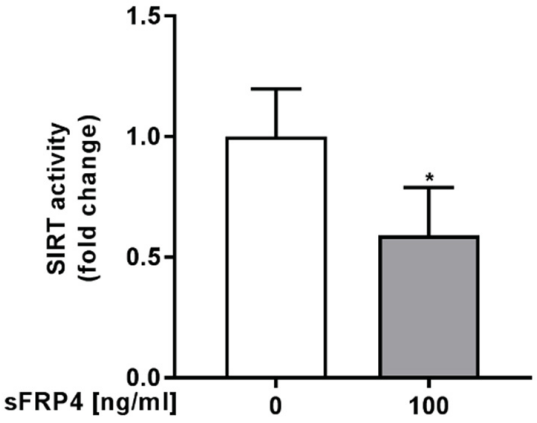

Figure 45. Effect of sFRP4 on sirtuin activity in primary hepatocytes of C57Bl6. Hepatocytes were exposed 24h to 100 ng/ml sFRP4 to assess its effect on cellular sirtuin activity using SIRT-Glo™. Data show the mean ± SD of four independent experiments using cells from different mice. Data of untreated cells were regarded as controls and set as 1. Differences between treatments were calculated by *t*-test. *p<0.05 versus untreated cells.

3.5.2 Effect of sFRP4 on primary hepatocytes isolated of lipodystrophic aP2-SREBP-1c mice

Next to the mechanistically investigations of the impact of sFRP4 in primary hepatocytes, further analyses focused on changes in the sFRP4 response on energy and lipid metabolism and insulin signaling in primary hepatocytes of aP2-SREBP-1c mice that exhibited diminished circulating sfrp4 levels and an increased hepatic lipid accumulation and impaired insulin signaling (Figures 33, 34).

3.5.2.1 Effect of sFRP4 on mitochondrial respiration in primary hepatocytes isolated of lipodystrophic aP2-SREBP-1c mice

The results from the oil red O stainings (Figure 33) confirmed an increased accumulation of lipids in aP2-SREBP-1c hepatocytes and also indicated an impaired cellular lipid metabolism *in vitro*. Based on the findings that sFRP4 affected lipogenesis and tended to increase

mitochondrial function in hepatocytes of C57Bl6 mice (Figures 36, 37), it should be clarified whether sFRP4 also modulated these processes in hepatocytes with an existing impaired insulin response, pronounced lipid accumulation and signs of functional impairments (Figures 33, 34).

For analysis of hepatic mitochondrial respiration in primary hepatocytes of aP2-SREBP-1c mice, cells were incubated with sFRP4 (100 ng/ml) for 24h before OCR measurements in the absence and presence of specific inhibitors and inducers of the mitochondrial respiratory chain. As illustrated in Figure 46A-G, the mitochondrial function here studied by mitochondrial respiration, spare respiratory capacity, coupling efficiency, ATP production and proton leak was not affected by sFRP4 in aP2-SREBP-1c hepatocytes. However, hepatocytes isolated of aP2-SREBP-1c mice showed lower OCR levels for basal as well as mitochondrial respiration (Figure 46B, C) in comparison to C57Bl6 hepatocytes (Figure 36B, C).

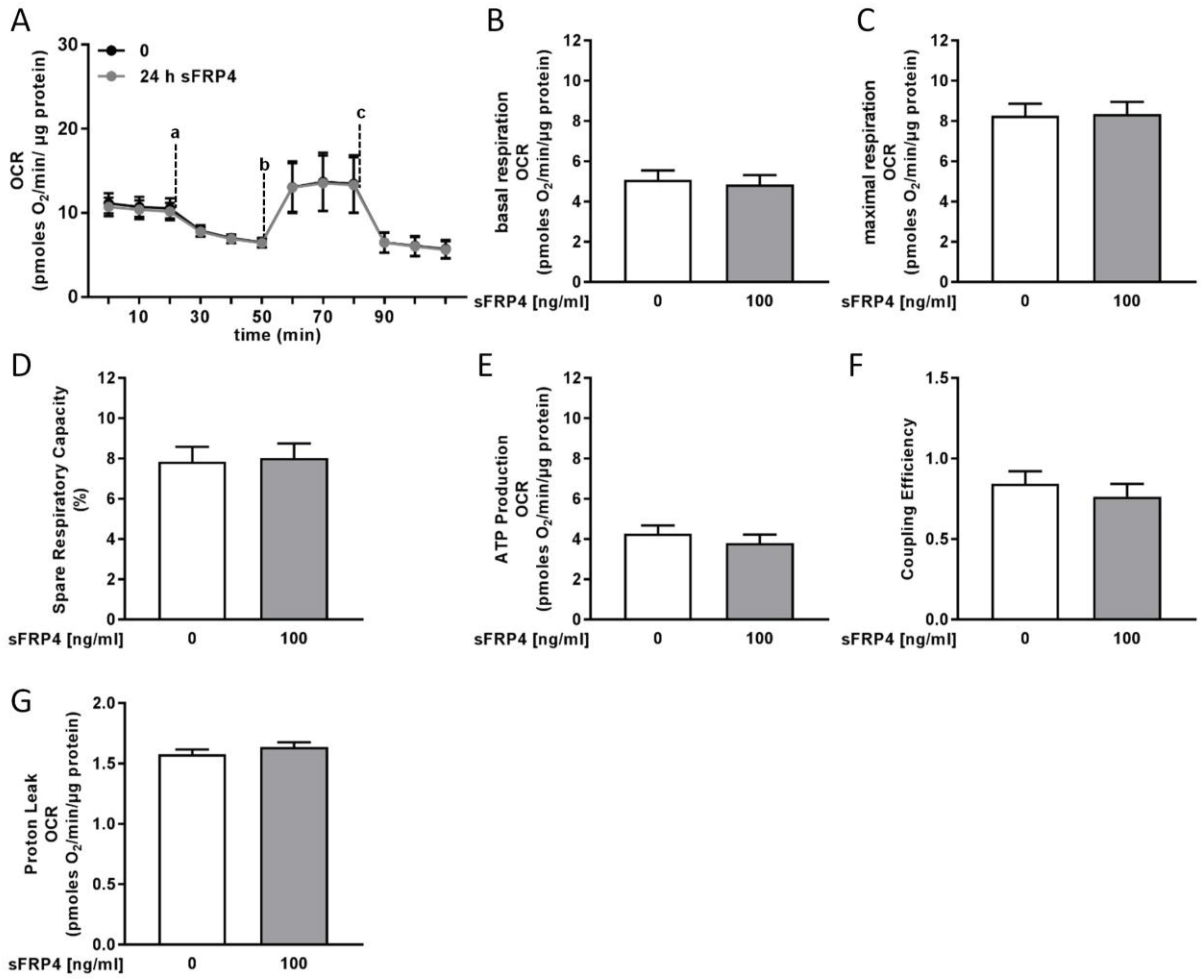

Figure 46. Effect of sFRP4 on mitochondrial respiration in primary hepatocytes of aP2-SREBP-1c mice. Hepatocytes were treated 24h with sFRP4. OCRs were measured in controls (0 ng/ml sFRP4) and sFRP4-treated cells (100 ng/ml) after sequential injection of oligomycin (1 µM, a), FCCP (0.5 µM, b) and antimycin A/rotenone

(each 0.5 µM, c). Figure show a representative graph (**A**) of measured OCRs normalized to protein amount which were used for assessing basal respiration (**B**), maximal respiration (**C**), spare respiratory capacity (**D**), ATP production (**E**), coupling efficiency (**F**) and proton leak (**G**). The presented data are the mean ± SEM (**A**) or mean ± SD (**B-G**) of independent experiments (n=6). Differences among groups were calculated by unpaired *t*-test.

3.5.2.2 Effect of sFRP4 on energy metabolism in primary hepatocytes of lipodystrophic aP2-SREBP-1c mice

The functionality of the aP2-SREBP-1c hepatocytes in mitochondrial fatty acid oxidation was verified by the observation of reduced palmitic acid oxidation following oligomycin (28.74 ± 19.26 CPM/µg protein, p=0.05), antimycin/rotenone (26.55 ± 10.51 CPM/µg protein, p=0.04) and etomoxir (29.87 ± 15.84 CPM/µg protein, p=0.06) incubation compared to untreated hepatocytes (Figure 47A, left panel). In line with the reduced induction of mitochondrial respiration by FCCP (Figure 47) in aP2-SREBP-1c hepatocytes compared to the levels in C57Bl6 hepatocytes (Figure 36), the palmitic acid oxidation also could not be promoted by addition of the uncoupling reagent FCCP in comparison to basal conditions (91.58 ± 41.55 CPM/µg protein vs. 82.24 ± 18.93 CPM/µg protein, FCCP vs. basal, p=0.97) (Figure 47A, left panel). Furthermore, administration of sFRP4 to aP2-SREBP-1c hepatocytes for 24h did not affect palmitic acid oxidation (Figure 47A, right panel). This observation was accompanied with no changes on fatty acid uptake in cells exposed 24h to sFRP4 compared to cells that were kept untreated (Figure 47B).

3.5.2.3 Effect of sFRP4 on lipid metabolism in primary hepatocytes of lipodystrophic aP2-SREBP-1c mice

Moreover, the effect of sFRP4 on hepatic DNL was determined in primary hepatocytes of aP2-SREBP-1c by 2h and 4h measurements of the incorporation of ^{14}C-labeled acetate which is directly proportional to hepatic lipogenic activity. As illustrated in Figure 47C insulin increased hepatic DNL after 2h and 4h measurement compared to basal conditions in untreated control cells but failed to achieve statistical significance (2h basal vs. insulin: 8.82 ± 3.36 CPM/µg protein vs 16.78 ± 11.06 CPM/µg protein, p=0.9; 4h basal vs. insulin: 19.55 ± 10.55 CPM/µg protein vs 30.69 ± 26.09 CPM/µg protein, p=0.8). Hepatic lipogenic activity in general was higher in aP2-SREBP-1c mice than in C57Bl6 hepatocytes as shown in Figure 37. No changes

on basal and insulin-stimulated hepatic lipogenic activity after 2h and 4h measurement were observed in hepatocytes pre-incubated 24h with sFRP4 compared to untreated control cells.

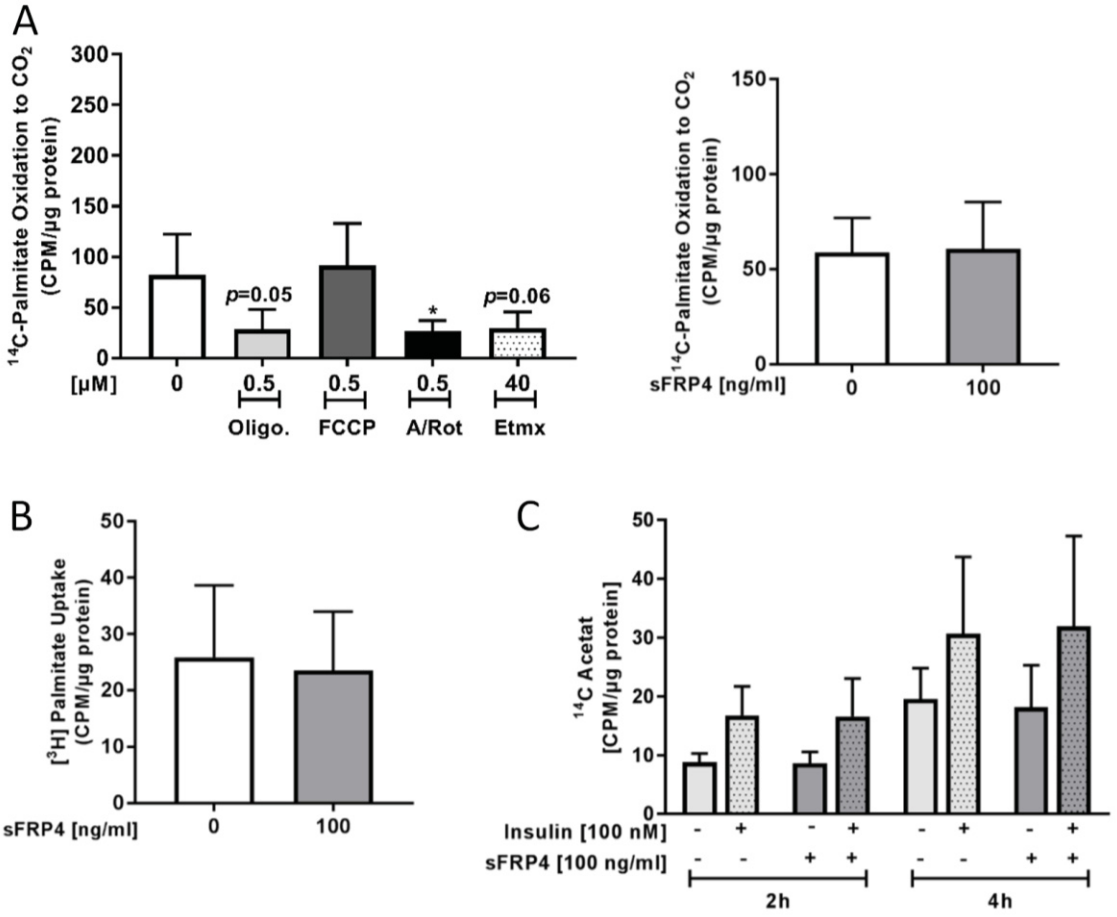

Figure 47. Effect of sFRP4 on fatty acid oxidation, uptake and DNL in primary hepatocytes of aP2-SREBP-1c. Hepatocytes were exposed to sFRP4 (100 ng/ml) for 24h (**A** right panel, **B**, **C**), inducer (FCCP) or inhibitors of fatty acid β-oxidation (oligomycin, antimycin, rotenone, etomoxir) (A left panel). For DNL studies, cells were incubated with or without insulin (100 nM) during experiment. Cells were incubated with either ^{14}C-palmitate (**A**), ^{3}H-palmitate (**B**) for 15 min or with ^{14}C-acetate for 2h and 4h (**C**). Data show oxidation (**A**) or incorporation of isotopic labeled palmitate (**B**) or ^{14}C-acetate as lipogenic activity (**C**) of independent experiments (n=3-5) presented as mean ± SD in cultured hepatocytes. The values obtained for sFRP4-untreated cells were considered as controls (0 ng/ml). Differences among conditions were calculated by *t*-test. *p<0.05 versus control or insulin-treated cells.

3.5.2.4 The impact of sFRP4 on insulin signaling in primary hepatocytes of lipodystrophic aP2-SREBP-1c mice

The findings that sFRP4 reduced insulin signaling on the levels of Akt, GSK3β and FoxO1 in hepatocytes of C57Bl6 mice that generally exhibit an intact metabolism, lead to the hypothesis that sFRP4 also might affect insulin action in hepatocytes that already have an impaired insulin sensitivity phenotype. To determine this in more detail, primary aP2-SREBP-1c hepatocytes

were exposed to sFRP4 for 24h prior to an acute insulin stimulus followed by analysis of the phosphorylation levels and protein abundances of Akt, GSK3β and FoxO1 (Figure 48). Similar to the effects of sFRP4 on Akt phosphorylation in hepatocytes of C57Bl6 but even more strikingly, sFRP4 significantly decreased the insulin-induced phosphorylation of Akt-Ser473 and Akt-Thr308 by 55% (p<0.001) and 69% (p<0.001) in comparison to untreated cells (Figure 48A, B). These observed reductions on Akt phosphorylation induced by sFRP4 coincided with a significant decrease in the insulin-mediated phosphorylation of GSK3β-Ser9 by 76% (p<0.001) in cells pre-incubated with sFRP4 for 24 h compared to cells that were kept untreated (Figure 48C).

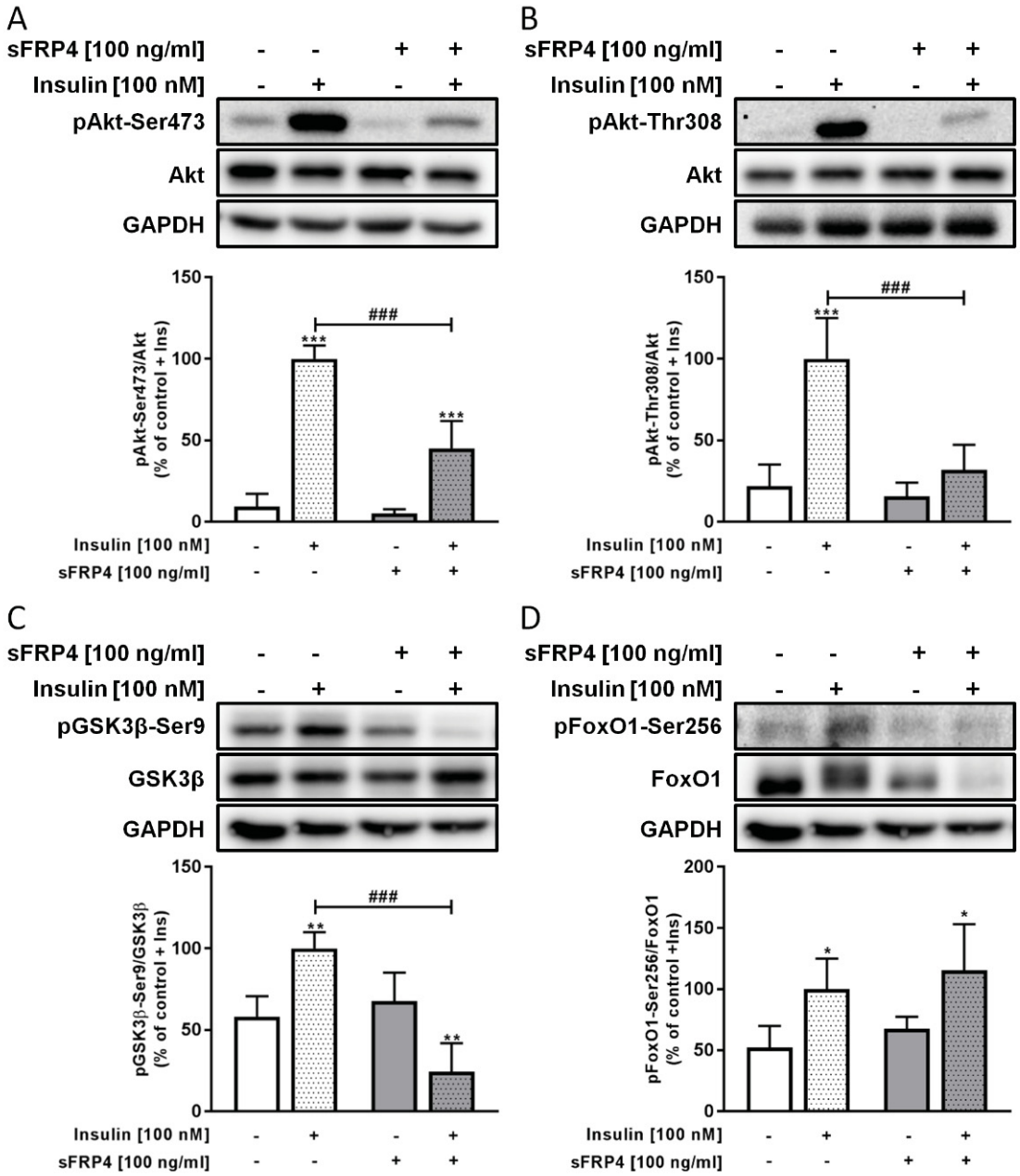

Figure 48. Effect of sFRP4 on insulin signaling in primary hepatocytes of aP2-SREBP-1c. Figures show representative Western blots and data are presented as mean ± SD for the protein abundance of Akt (**A**), GSK3β-Ser9 (**B**), and FoxO1(**C**) of four independent experiments. The protein signals were normalized for the abundance of the non-phosphorylated protein and the loading control GAPDH. The values obtained for sFRP4-untreated cells were considered as controls. All values were normalized to insulin-treated control cells (control + Ins) which were set as 100%. Differences among groups were calculated by two-way ANOVA analyses followed by the Sidak's multiple comparisons test. *p<0.05, **p<0.01, ***p<0.001 for insulin versus basal $^{\#}p$<0.05; $^{\#\#}p$<0.01; $^{\#\#\#}p$<0.001 for sFRP4-treated versus untreated cells.

As Figure 48D shows, sFRP4 did not affect the ratio of phosphorylated FoxO1-Ser256 to FoxO1 protein in cells stimulated with insulin compared to the ratio in respective control cells. However, the phosphorylation status of FoxO1-Ser256 itself as well as FoxO1 protein abundance were reduced by 25.5% (p=0.18) and by 69% (p<0.001) respectively, by sFRP4 under basal conditions compared to untreated cells (Figure 49A). These reductions became even more strikingly in cells exposed to sFRP4 followed by an acute insulin stimulus. Here, sFRP4 reduced the phosphorylation of FoxO1-Ser256 and FoxO1 protein by 68% (p<0.001) and 83% (p<0.001), respectively. Further, it is to note that insulin failed to significantly induce phosphorylation of FoxO1-Ser256 (p=0.1) whereas reduced FoxO1 protein by 33% (p=0.04) in untreated control cells (Figure 49A). IRS-1 abundance was not significantly affected by sFRP4 in aP2-SREBP-1c hepatocytes (p=0.26) (Figure 49B). Although the impaired phosphorylation of Akt in cells exposed to sFRP4 could not be ascribed to changes in Akt abundance, GSK3β levels were reduced by 30% (p<0.05) by sFRP4 (Figure 49C, D).

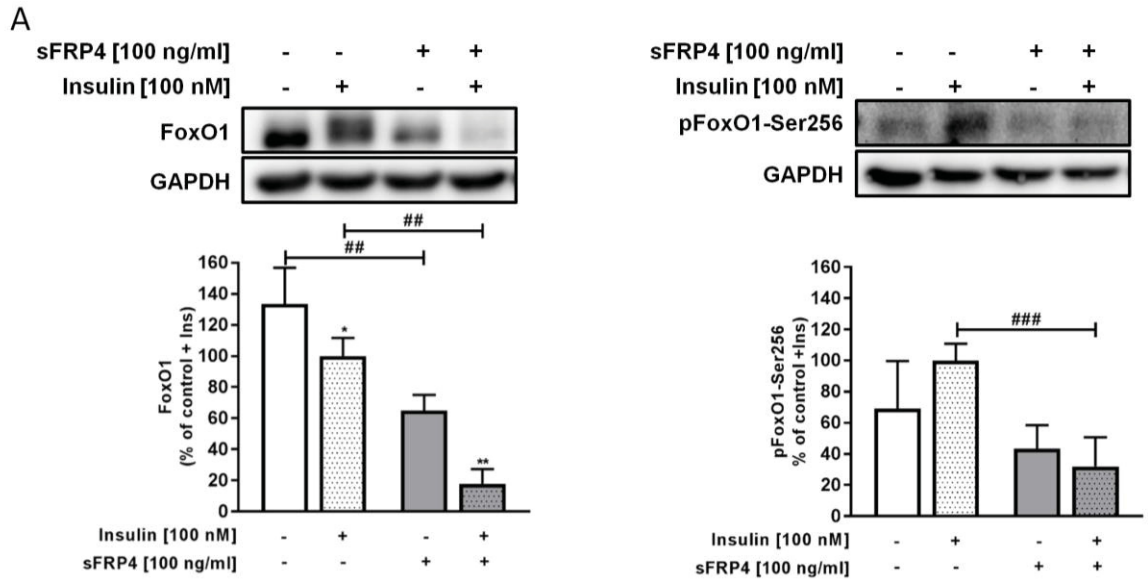

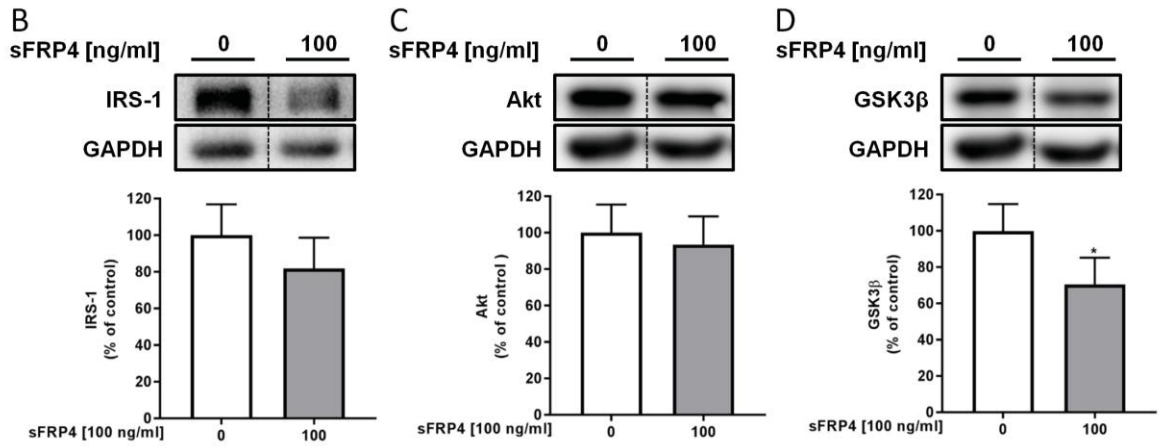

Figure 49. Effect of sFRP4 on phosphorylation level and protein abundance of components of insulin action in primary hepatocytes of aP2-SREBP-1c. The figures show representative Western blots and data are presented as mean ± SD for the protein abundance of FoxO1 and pFoxO1-Ser256 (**A**), IRS-1 (**B**), Akt (**C**), GSK3β (**D**) of four independent experiments (n=4). The protein signals were normalized for the abundance of the loading control GAPDH. The values obtained for sFRP4-untreated cells were considered as controls. Values were normalized to insulin-untreated (**B-D**) or insulin-treated control cells (control + Ins) (**A**) which were set as 100%. Differences among conditions were calculated by two-way ANOVA analyses followed by the Sidak's multiple comparisons test (**A**) or *t*-test (**B-D**). **p*<0.05, ***p*<0.01, ****p*<0.001 for insulin/sFRP4 versus basal; $^{\#}p$<0.05, $^{\#\#\#}p$<0.001 versus sFRP4-treated cells.

3.5.2.5 Effect of sFRP4 on cellular sirtuin activity in primary hepatocytes of lipodystrophic aP2-SREBP-1c mice

To observe the effect of sFRP4 on sirtuin activity in metabolic dysfunctional hepatocytes of aP2-SREBP-1c, cells were exposed 24h to 100 ng/ml sFRP4 followed by measurements of sirtuin activity. The data show that sFRP4 did not affect SIRT activity in primary hepatocytes of aP2-SREBP-1c compared to untreated cells. (Figure 50).

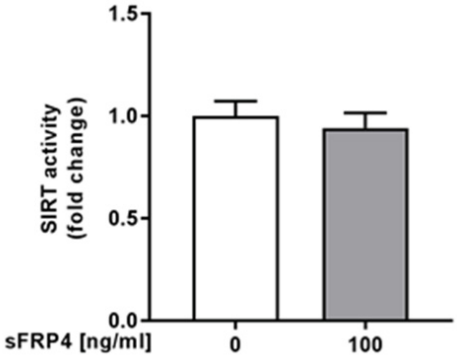

Figure 50. Effect of sFRP4 on sirtuin activity in primary hepatocytes of aP2-SREBP-1c. Hepatocytes were exposed 24h to 100 ng/ml sFRP4 to assess its effect on cellular sirtuin activity using SIRT-Glo™. Data show the mean ± SD of three independent experiments using cells from different mice. Data of untreated cells were regarded as controls and set as 1.

3.6 Impact of sFRP4 on the secretome of hepatocytes from C57Bl6 and aP2-SREBP-1c mice

Secreted molecules are important mediators in the inter-organ communication and enable systemic reactions to environmental, e.g. nutritional, conditions, or alterations in tissues metabolism. To mimic inter-organ communication of the adipokine sFRP4 on a metabolic healthy liver and a liver with pronounced hepatic lipid accumulation and an insulin resistant phenotype, primary hepatocytes isolated from C57Bl6 and aP2-SREBP-1c mice were either left untreated or treated with sFRP4 (100 ng/ml) for 24h. Hepatic secretomes of these four conditions were analyzed by untargeted proteome analyses with consecutive mass spectrometry for protein identification (appendix, Table 30). The comparisons identified 48 differential secreted proteins (6 up and 42 down in C57Bl6) in the comparison C57Bl6 vs aP2-SREBP-1c. Of these, 19 proteins were assigned as secreted (SP+/SP-) and 29 as non-secreted (NP) proteins. If cells of both models were treated with sFRP4, the analysis revealed 58 differential secreted proteins (29 up and 29 down in C57Bl6 sFRP4) in the comparison C57Bl6 sFRP4 vs aP2-SREBP-1c sFRP4. Of these, 22 were assigned as SP+/SP- and 36 as NP proteins. The administration of sFRP4 on primary hepatocytes of the healthy C57BL6 mice resulted in 29 differential secreted proteins compared to untreated cells (22 up and 7 down in C57Bl6 sFRP4). Of these, 5 were assigned as SP+/SP- and 24 as NP proteins. If cells of the lipodystrophic mice were treated with sFRP4, the comparison to untreated cells revealed 29 differential secreted proteins (13 up and 16 down in aP2-SREBP-1c sFRP4). Of these 12 were assigned as SP+/SP- and 17 as NP proteins (appendix, Table 30). An overall secretion network can be generated from the secreted molecules that emphasizes the interaction and the specificity of secreted proteins for the respective comparison (Figure 51). The Figure 51 shows that the differential secreted proteins are rather specific for each of all four comparisons.

Knowledge-based functional annotation with such limited numbers of molecules may not be informative. The differences observed in both of these comparisons involving C57Bl6 and aP2-SREBP-1c were mainly due to the different genotypes and not to the application of sFRP4, indicated e.g. by interactions with lipid metabolism, directly (Appendix, Table 31).

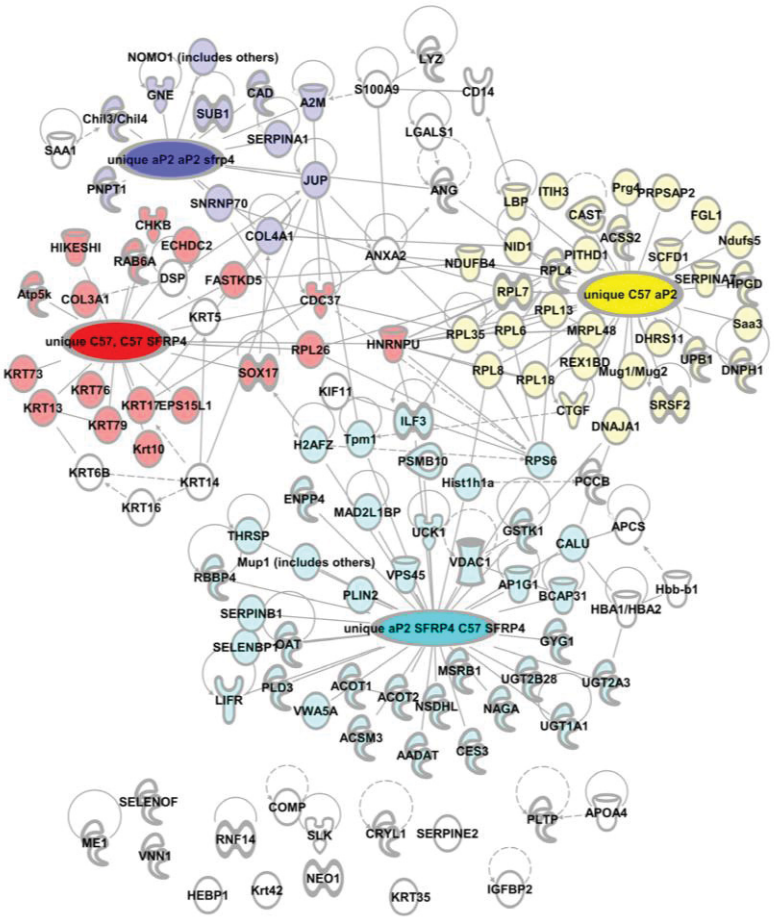

Figure 51. Interaction of differential secreted proteins. Differential secreted proteins (determined with Spectronaut® v11; >1.5-fold, *p*-value <0.05, *t*-test) were used to generate an interaction Network (IPA®). Color code indicates proteins that were unique in either comparison, connecting lines indicate direct or indirect (dotted line) knowledge-based interaction of the molecules.

The secretome analyses focused on the specific action of sFRP4 on healthy and metabolically diseased hepatocytes.

In the analyses the effect of sFRP4 stimulation of C57Bl6 pointed to KRT14 as the predominant regulator molecule (*p*-value of overlap, 1.67 x 10^{-5}) that is also differentially regulated (2.016-fold regulated in the comparison). In the C57Bl6 mice, the analyses revealed further keratins involved in intracellular signal transduction, e.g. KRT76, KRT79, KRT17 and KRT13 (Figure 52). In the lipodystrophic fatty liver model, sFRP4 exposure resulted in the differential regulation of alpha 2 macroglobulin (A2M), which is involved in the inhibition of all known classes of proteinases, as well as the enzyme PLA2G2E (p-value of overlap, 1.98 x 10^{-9}) that was the key upstream activator deduced from the differential secreted proteins (Appendix, Table 31). In these comparisons, molecular links to hepatic fibrosis (*p*-value of enrichment: 8.71 x 10^{-3}, in

aP2-SREBP-1c; 1.91 x 10^{-2} in C57Bl6), but also to molecules and interaction networks with impact activities on other tissues like heart or kidney can be observed in C57Bl6 e.g. proteins related to renal ischemia (7.59 x 10^{-4}) or renal failure (2.88 x 10^{-3}), or cardiac fibrosis (3.98 x 10^{-2}) (Appendix, Table 31). In aP2-SREBP-1c, e.g. proteins related to renal failure (2.88 x 10^{-3}) were enriched as well as LXR/RXR activation (1.20 x 10^{-2}) involved in metabolic lipid and cholesterol clearance.

In regard to pathway activation, components of the glucocorticoid receptor signaling pathway were the highest regulated once in both cell systems (8.9 x 10^{-9}) in C57Bl6 and to lower extend (5.37 x 10^{-6}) in aP2-SREBP-1c derived hepatocytes. The enrichment was mainly due to the various keratin protein family members, involved in intracellular filament formation (Figure 52).

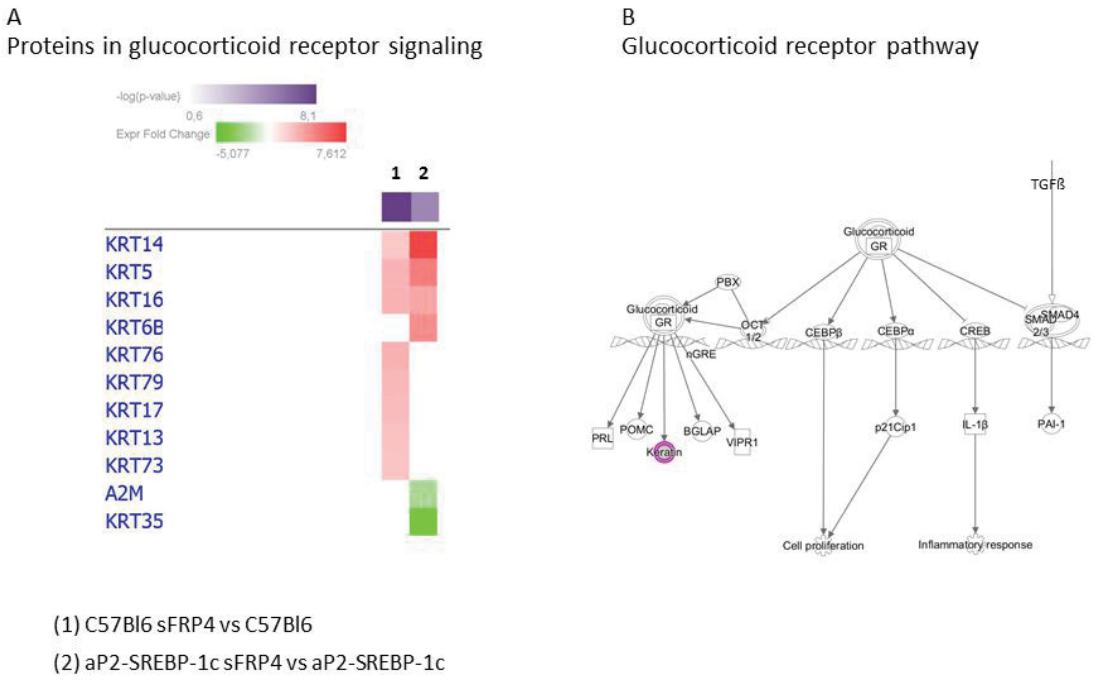

Figure 52. Components of glucocorticoid signaling in sFRP4-induced secretion in healthy and metabolic diseased hepatocytes. Proteins with differential secretion (1.5-fold, *p*-value <0.05) were used for IPA® core analyses (**A**). Color code indicates different abundance (red: increase in condition 1, green: decrease in condition 1) based on fold change level. Different abundance of network protein is indicated in detail in the hierarchical cluster. Scheme of glucocorticoid receptor signaling (**B**). Location of secreted molecules is highlighted.

4 Discussion

The health burden of obesity and obesity-related metabolic diseases is based on increased fat mass, mainly the metabolically active visceral fat. Next to the surplus of metabolites and an increased risk for oxidative stress, an alteration in the amount and composition of secreted adipokines is specific for obese compared to lean conditions and crucial for alterations in adipose tissue function, metabolic flexibility and adipose tissue health.

Furthermore, adipokines regulate whole-body energy homeostasis by interference with distinct tissues, even in a tissue-specific manner and dependent on each adipokine´s specific nature. This thesis focused on the functional characterization of two recently identified adipokines i.e. WISP1 and sFRP4 (Lehr et al., 2012; Murahovschi et al., 2015) and aimed to explore the role of WISP1 and sFRP4 in the context of obesity and type 2 diabetes and their function in the regulation of energy metabolism and insulin action in two major insulin-responsive tissues, skeletal muscle and liver.

Recent studies indicate an association of WISP1 and sFRP4 with obesity and metabolic impairments present in T2D (Anand et al., 2016; Barchetta et al., 2017; Brix et al., 2016; Ehrlund er al., 2013; Mahdi et al., 2012; Murahovschi et al., 2015; Tacke et al., 2017). Whilst the present thesis further supports an association of WISP1 with inflammation, insulin resistance and obesity independent of T2D, sFRP4 turned out to be a factor implicated in obesity and T2D that associated with lipidemia. Functional, the thesis provides evidence for the specific actions of the two adipokines, while WISP1 abrogated insulin action *in vitro* in skeletal muscle and liver, sFRP4 promoted protein breakdown along with IRS-1 degradation and might be linked to cellular stress response in skeletal muscle cells while strongly impaired insulin action in hepatocytes resulting in reduced insulin signaling but increased lipid synthesis. The results obtained for both adipokines are further discussed separately.

4.1 The novel adipokine WISP1 associated with insulin resistance and impaired insulin action in human myotubes and mouse hepatocytes

Like in the results section, parts of the discussion on page 124 to 130 have been taken over from the manuscript cited under *References* and *Appendix* (Hörbelt et al., 2018).

4.1.1 WISP1 associated with visceral adiposity and insulin resistance independent of glycemic status

The data described in this thesis showed that both circulating levels of WISP1 and expression of *WISP1* mRNA in VAT were increased in obese men, irrespective of type 2 diabetes status. Regression analysis showed that *WISP1* expression and circulating levels of WISP1 were associated with variables reflecting insulin resistance and adipose tissue inflammation, even after adjusting for age and BMI. *In vitro* studies on primary hSkMCs as well as the mouse hepatocyte cell line AML12 showed that recombinant WISP1 directly impaired insulin action by inhibiting the Akt signaling pathway.

The reported data on VAT and SAT explants revealed visceral adipose tissue as a major depot for WISP1. The increased *WISP1* expression in VAT of obese men is in line with previous reports (Barchetta et al., 2017; Murahovschi et al., 2015; Sahin Ersoy et al., 2016; Tacke et al., 2017) suggesting that *WISP1* expression is regulated by body weight. High-fat feeding in mice increased the expression of *WISP1* in adipose tissue (Ferrand et al., 2017; Murahovschi et al., 2015) while diet-induced weight loss in humans lowered *WISP1* expression in adipose tissue (Murahovschi et al., 2015). Further, these findings strongly suggest WISP1 as a factor associated with visceral adiposity and the onset of T2D. During obesity-related adipose tissue dysfunctions, visceral adipose tissue has been characterized as the depot of WAT with more hypertrophic properties, higher metabolic activity, pronounced inflammatory response and expression of lipogenic and lipolytic genes compared to SAT (Ibrahim et al., 2010; Komolka et al., 2014; Weisberg et al., 2003). In the onset of obesity, increased VAT accumulation as well as ectopic lipid accumulation in peripheral tissue including liver and skeletal muscle may occur when energy storage capacity of SAT is exceeded (Cuthbertson et al., 2017; Jensen et al., 2008). Hence, visceral abdominal adiposity rather than peripheral adiposity has been mainly associated with dysregulations in glucose and lipid metabolism and T2D (Ibrahim et al., 2010). The present study also detailed the relationship between WISP1 and insulin sensitivity. In individuals with normal glucose tolerance, *WISP1* expression in adipose tissue is related to

determinants of insulin sensitivity (Murahovschi et al., 2015; Tacke et al., 2017). The data reported in the present work additionally showed that circulating levels of WISP1 were negatively associated with insulin sensitivity. Although the associations with fasting glucose and insulin levels as well as HOMA-IR in this cohort of obese men were confounded by BMI, this was not the case when considering glucose clearance after an OGTT. The association between circulating WISP1 and post-load glucose levels was not affected by adjustments for age and BMI, strongly suggesting that WISP1 may interfere with insulin signaling in target tissues for insulin action.

Another interesting finding is that circulating WISP1 level was positively associated with plasma glucose in the OGTT (independent of BMI) and negatively with the Gutt index of insulin sensitivity, confirming the association of WISP1 with insulin resistance. However, circulating WISP1 was not further increased in obese individuals with diabetes and showed no association with HOMA-IR after adjustment for BMI. It should be noted that in the analysis of glucose in the OGTT, HOMA-IR and Gutt index, individuals treated with insulin were excluded from the analysis. In the described cohort (Table 22), all individuals with diabetes were treated with insulin, so that all those with diabetes were completely excluded from the analysis. For the correct analysis of WISP1 association with plasma glucose in future studies, drug-naive individuals with diabetes should be investigated. Nevertheless, the mentioned results confirm that WISP1 level is directly related to adiposity independent of glycemic status. This is in agreement with previously published data of Barchetta et al. and Tacke et al., who also found no difference in plasma WISP1 levels between diabetic and non-diabetic individuals (Barchetta et al., 2017; Tacke et al., 2017).

Beyond obesity, recent studies linked WISP1 to the onset of hepatic steatosis in mice by reporting that the knockdown of WISP1 in obese mice reduced lipid accumulation and the lipogenesis-associated proteins SREBP-1c, stearoyl-CoA desaturase-1 (SCD1) and fatty acid synthase (FAS) (Jung et al., 2018). However so far, these findings could not be validated in human studies, since no differences of *WISP1* expression in livers of individuals with NAFLD and no associations with NAFLD activity score (NAS) and liver fat content were found (Murahovschi et al., 2015). Additionally, no correlation of WISP1 plasma levels with NAFLD were detectable (Barchetta et al., 2017).

4.1.2 WISP1 impaired insulin signaling and insulin action on glucose metabolism in myotubes and hepatocytes

The *in vitro* data reported in this study corroborate the suggestion that WISP1 may interfere with insulin signaling in insulin target tissues (Figure 53). Recombinant WISP1 was found to impair insulin signaling in two different cell types, namely primary hSkMCs and murine AML12 hepatocytes. The skeletal muscle accounts for around 45% to 55% of the body weight in normal-weight adults (Janssen et al., 2000; Zurlo et al., 1990). The skeletal muscle is the largest insulin-responsive organ and with a contribution of over 80%, the primary site for insulin-stimulated glucose uptake and thus crucial for systemic glucose disposal (Ferrannini et al., 1988; Thiebaud et al., 1982). Additionally, the skeletal muscle is the major tissue for glycogen storage with an approximately 4 times higher capability than the liver (Egan and Zierath, 2013). In muscle, satellite cells proliferate into myoblasts that differentiate into multi-nucleated myotubes to form myofibers by fusion with other myotubes. The insulin-responsive myotubes are essential for the regulation of skeletal muscle function (Eckstein et al., 2017). The liver plays a crucial role in systemic glucose and lipid homeostasis by regulating production, storage, consumption, disposal and delivery of lipids, glucose and proteins. The liver predominantly contains hepatocytes (60%-70%), the major site for energy homeostasis, but also non-parenchymal cells (30%-40%) including liver sinusoidal endothelial cells (LSEC), Kupffer cells, lymphocytes, and to a minor extent biliary cells and hepatic stellate cells (HSCs) (Gao et al., 2008; Racanelli et al., 2006).

In both, skeletal muscle cells and hepatocytes, WISP1 inhibited the insulin-mediated phosphorylation of Akt, an important regulator of multiple aspects of glucose metabolism, such as glucose uptake, glycogen synthesis and suppression of hepatic glucose production by insulin.

The interaction of WISP1 with the Akt signaling pathway has been observed in different cell types in previous studies. *In vitro*, WISP1 has been shown to inhibit apoptosis by suppressing mitochondrial release of cytochrome C and inducing antiapoptotic Bcl-X_L via activation of Akt signaling pathway (Su et al., 2002). In cardiomyocytes, WISP1 prevented cell death via dual activation of Akt and canonical β-catenin signaling (Venekatesan et al., 2010). Further, WISP1 induced hypertrophy in cardiomyocytes via activation of Akt signaling (Colston et al., 2007). Recent studies reported that WISP1 impaired insulin-mediated phosphorylation of Akt by activation of NFκB and c-Jun N-terminal kinases (JNK) signaling in C2C12 myotubes (Jung et

al., 2018) while WISP1 exposure exerted no effects on Akt signaling in human mesenchymal stem cell-derived adipocytes (Murahovschi et al., 2015).

Moreover, the data presented in this study demonstrate the functional relevance of the reduced insulin signaling in both cell types. Human myotubes pre-incubated with WISP1 displayed impaired insulin-stimulated glycogen synthesis and exposure to WISP1 abrogated the insulin-mediated suppression of the gluconeogenic genes *Pck1* and *G6pc* in mouse primary hepatocytes.

WISP1 deficiency in mice leads to a slightly lower body weight than found in wild-type animals but unfortunately no data on glucose traits or insulin sensitivity are available yet (Maeda et al., 2015). In contrast, WISP1 did not interfere with insulin-mediated Akt phosphorylation in 3T3L1 adipocytes (Murahovschi et al., 2015). Apart from potential tissue-specific effects, other possible reasons for this difference may include the duration of WISP1 exposure (24h in the present study vs 30 min in the 3T3-L1 experiment) as well as the concentration of WISP1 applied. The WISP1 concentrations used in the experiments reported in this work were representative of the levels found in the circulation whereas the 3T3-L1 adipocytes were exposed to supra-physiological concentrations of WISP1. Moreover, different signaling pathways might be involved in the actions of WISP1 in various cell types (Ferrand et al., 2017).

Importantly, the impaired insulin-mediated Akt phosphorylation in primary hSkMCs and AML12 hepatocytes was accompanied by inhibition of the phosphorylation of several of its well-characterized substrates. In myotubes, reductions in the insulin-mediated phosphorylation of GSK3β and p70S6K paralleled the inhibition of Akt phosphorylation. Strikingly, in AML12 hepatocytes, the insulin-mediated phosphorylation of GSK3β was not impaired by recombinant WISP1, whereas the phosphorylation of p70S6K and FoxO1 were markedly reduced or even abrogated. Tissue-specific differences in the phosphorylation of Akt substrates have also been reported by others (Bouzakri et al., 2006; Gonzalez and McGraw, 2009). Gene silencing experiments in cultured cells as well as studies on mouse models suggest that tissue-specific changes in the abundance of Akt isoforms as well as the insulin receptor substrates IRS-1 and IRS-2 contribute to Akt substrate selection (Bouzakri et al., 2006; Gonzalez and McGraw, 2009),

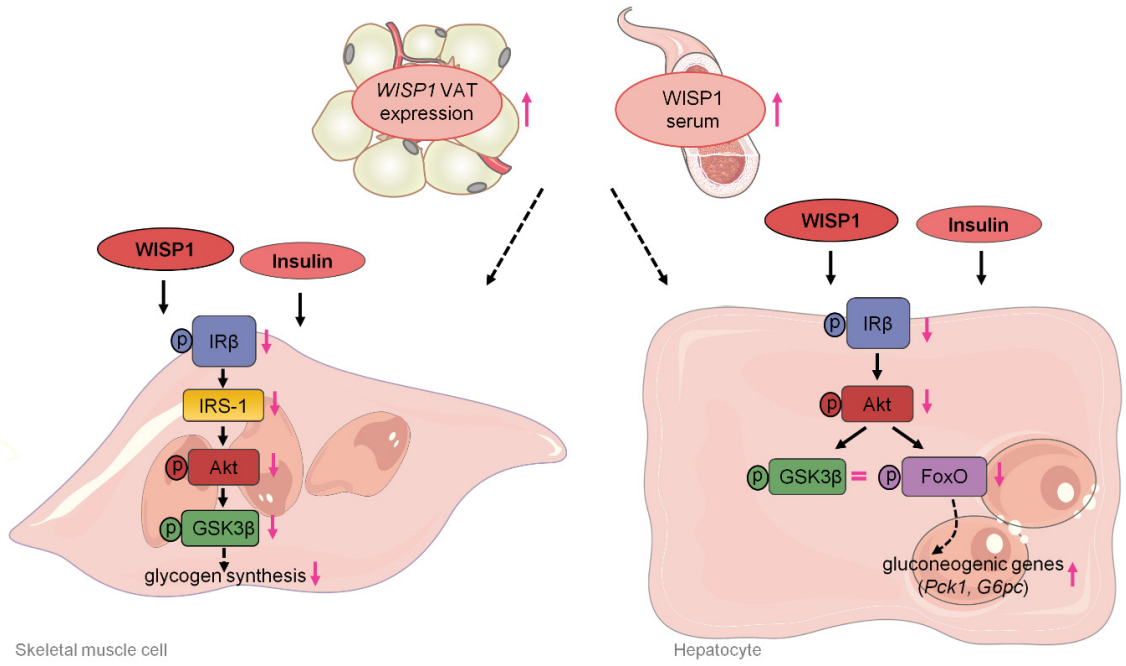

Figure 53. Schematic diagram showing how WISP1 impaired insulin action in skeletal muscle cells and hepatocytes. During obesity, *WISP1* VAT expression and WISP1 serum levels increased. *In vitro*, physiological concentrations of WISP1 impaired insulin action on phosphorylation of IRβ, Akt and GSK3β and reduced IRS-1 protein in myotubes while reduced insulin-mediated phosphorylation of IRβ, Akt, GSK3β and FoxO1 in hepatocytes (pink arrow downwards). WISP1 abrogated insulin-mediated induction of glycogen synthesis in myotubes (pink arrow downwards) and insulin-induced suppression of gluconeogenic gene expression (pink arrow upwards). Examined effects (solid arrow), potential effects (dotted arrow). GSK3β, glycogen synthase kinase 3β; FoxO1, forkhead box protein O1; IRβ, insulin receptor β; VAT, visceral adipose tissue.

4.1.3 WISP1 associated with adipose tissue and systemic inflammation

As previously mentioned, WISP1 is a proinflammatory adipokine (Murahovschi et al., 2015) and circulating WISP1 showed an association with systemic levels of IL-8 levels in a cohort of non-diabetic and diabetic individuals linking WISP1 to inflammation (Barchetta et al., 2017). Multiple studies demonstrated an association of WISP1 with inflammatory events in different tissues and cell types. WISP1 levels were enhanced in human intestine of individuals with inflammatory bowel disease and further induced by TNF-α (Zhang et al., 2016). Moreover, Chen et al. reported that WISP1 induced the pro-inflammatory cytokine TNF-α via binding to αvβ3 integrin and activation of *toll-like receptor* (TLR)-4/cluster of differentiation (CD)-14 in lung-derived macrophages of mice after sepsis (Chen et al., 2016). *In vivo*, ablation of WISP1 reduced serum levels of the inflammatory proteins MCP-1 and TNF-α and JNK phosphorylation in skeletal muscle and liver in high-fat diet-induced obese mice (Jung et al., 2018). In line with

that, WISP1 exposure increased JNK phosphorylation in cultured mouse hepatocytes and C2C12 myotubes (Jung et al., 2018).

The data of this thesis further revealed the association between circulating WISP1 and markers of adipose tissue and systemic inflammation. Interestingly, the serum HO-1 level was the strongest predictor of circulating WISP1, even after adjustment for age and BMI. HO-1, encoded by *HMOX1*, is a stress-induced protein that is critical for stem cell differentiation (Kozakowska et al., 2014). Induction of the *Hmox1* gene in mice is protective against deleterious obesity phenotype as characterized by a reduced number of enlarged adipocytes, an increased number of small adipocytes and a higher adiponectin concentration (Li et al., 2008). Moreover, increased *HO-1* expression in human mesenchymal stem cell-derived adipocytes decreases differentiation and lipid accumulation of adipocytes via upregulation of the Wnt signaling cascade (Vanella et al., 2013). These data allow to speculate that upregulation of Wnt signaling by HO-1 leads to higher expression levels and possibly production of WISP1 from younger adipocytes. This, in turn, might result in tissue remodelling characterized by the redistribution of in-tissue and in-body insulin sensitivity and an increased insulin resistance in older cells (i.e. redistribution of glucose and other substrates with better supply of young and proliferating cells). Several studies linked WISP1 to aberrant tissue remodelling that entailed fibrotic events. Königshoff et al. reported that WISP1 expression associated with pulmonary fibrosis in mice and human and WISP1 induced remodeling of ECM components and expression of fibrosis-specific genes in lung fibroblast (Königshoff et al., 2009). In cardiomyocytes, WISP1 has been shown to induce hypertrophy, fibroblast proliferation and expression of components of the ECM (Bernscheider and Konigshoff, 2011; Colston et al., 2007; Venkatachalam et al., 2009). *WISP1* expression was enhanced in fibrotic rat livers and induced by TNF-a and TGF-β in hepatic stellate cells (Jian et al., 2014). Moreover, in cohort of individuals with type 2 diabetes, circulating WISP1 was found to associate with procollagen-III peptide (PIIINP), an established marker for cardiac and hepatic fibrosis (Barchetta et al., 2018). Hence, the participation of WISP1 as an extracellular matrix protein in fibrotic events in skeletal muscle and liver should be addressed in future studies.

A limitation of the present study is that it could not be detailed the mechanism by which WISP1 inhibits insulin action especially because of the high complexity of the Wnt signaling pathway (Niehrs et al., 2012). Based on the modular structure of WISP1, several functional receptors have been identified. Previous studies showed that WISP1 interacted with integrin α(5)β in

human bone marrow stromal cells (Ono et al., 2011). Furthermore, WISP1 has been shown to bind decorin and biglycan in the extracellular matrix of fibroblasts (Desnoyers et al, 2001). The presence of an IGF binding protein domain in CCN proteins including WISP1 suggests an interference with the IGF and insulin signalling pathway (Lorenzatti et al., 2011; Lopez-Bermejo et al., 2006; Yamanaka et al., 1997). Our observations showed a decrease in the insulin-mediated tyrosine phosphorylation of insulin receptor-β/IGF-1 receptor by WISP1, indicating that WISP1 might act by interfering with these receptors or insulin in myotubes and hepatocytes. The inhibition of insulin action by adipo(cyto)kines is frequently associated with a decreased protein abundance of IRS-1 (Eckstein et al., 2017; Wiza et al., 2013). Although WISP1 was found to decrease the abundance of IRS-1 in myotubes, this was not the case in AML12 hepatocytes. The latter cell line even displayed an increase in IRS-1 protein levels following WISP1 exposure, whereas the abundance of IRS-2 was unaltered by WISP1 treatment. This raises the possibility that WISP1 may use alternative mechanisms to impair insulin action in myotubes and hepatocytes. The second limitation of this study is that it was conducted in men (but not in women), and that the OGTT data were collected in a subgroup of the obese men. Without additional studies, caution should be taken when generalising these findings to the entire population.

4.2 *sFRP4* mRNA expression was enhanced in VAT of obese men with and without T2D and associated with triglycerides and markers of insulin resistance

Recent studies identified sFRP4 as a novel adipokine, expressed and secreted by WAT in rodents and humans (Ehrlund et al., 2013; Lehr et al., 2012; Mastaitis et al., 2015). However, WAT-depot specific expression of *sFRP4* in obese individuals without and with type 2 diabetes and the functional role of sFRP4 in the regulation of insulin action and energy metabolism in pivotal insulin-responsive target cell types, i.e. skeletal muscle cells and hepatocytes, have not been elucidated so far.

The findings of the present thesis revealed that *sFRP4* was rather expressed in VAT than in SAT and *sFRP4* mRNA levels were significant higher in obese men compared to normal-weight men. Interestingly, *sFRP4* expression in VAT was even higher in obese men with type 2 diabetes compared to obese men without type 2 diabetes emphasizing the novelty of this work. Furthermore, *sFRP4* VAT mRNA associated with fasting insulin and glucose levels, HOMA-IR and strongly correlated with triglycerides and adiponectin levels. These findings

strongly suggest sFRP4 as a factor associated with visceral adiposity, peripheral insulin resistance and the onset of T2D and emphasized the role of sFRP4 as an adipokine and its potential involvement in lipid homeostasis.

These observations are in line with recent studies that suggest increased serum sFRP4 as a biomarker for obesity and type 2 diabetes in humans, even prior their diabetes diagnosis and linked sFRP4 to the onset of insulin resistance (Anand et al., 2016; Brix et al., 2016; Ehrlund et al., 2013; Garufi et al., 2015; Mahdi et al., 2012). Further analyses showed increased circulating sFRP4 in individuals with obesity independent of type 2 diabetes and demonstrated an association of sFRP4 serum levels with insulin sensitivity, body fat mass and adipose tissue vascularization (Garufi et al., 2014). In a cross-sectional study, circulating sFRP4 levels were positively correlated with fasting glucose levels, insulin levels, glycated hemoglobin and HOMA-IR (Anand et al., 2016). In addition, BMI, triglycerides and HDL-cholesterol were found to be major predictors for sFRP4 (Brix et al., 2016). Although the reported ranges of physiological sFRP4 serum levels slightly differed between the examined cohorts in dependence of ethnical background of the study participants, all cited studies demonstrated significantly increased circulating sFRP4 levels with obesity and/or diabetes. The observations presented in this work complement the previous findings by verifying increased *sFRP4* also on mRNA level in VAT of obese, type 2 diabetic men.

4.3 The adipokine sFRP4 impaired insulin action and energy metabolism in human myotubes and mouse hepatocytes

The findings presented in this work hypothesized an interference of the adipokine sFRP4 with insulin action and lipid metabolism in insulin-responsive target tissues. Hence, *in vitro* studies aimed at elucidating the impact of sFRP4 in skeletal muscle cells and hepatocytes. Thereby *in vitro* concentrations of sFRP4 were used that were in the reported range found in the circulation (Anand et al., 2016; Garufi et al., 2015).

4.3.1 sFRP4 increased mitochondrial respiration and AMPK phosphorylation in myotubes

Under resting conditions, the skeletal muscle accounts for around 30% of whole body energy metabolism (Egan and Zierath, 2013). During fasting, the skeletal muscle induces fatty acid

oxidation whereas suppresses glycolysis and glucose oxidation to provide energy for maintenance of whole body energy homeostasis (Houmard et al., 2008; Kiens et al., 2006).
Due to the crucial role of skeletal muscle in metabolic adaptions and glycemic control, metabolic impairments of skeletal muscle are frequently associated with the onset of obesity and the development of T2D (Kelley and Mandarion, 2000; Storlien et al., 2004).
sFRP4 did not affect glycolysis and fatty acid oxidation whereas it induced basal as well as maximal mitochondrial respiration in myotubes. Mitochondria are the primary site for oxidative ATP generation via the electron transport chain. Hence, metabolic dysfunctions in mitochondria in skeletal muscle have been linked to impaired metabolite oxidation, intracellular lipid accumulation and the development of insulin resistance and T2D (Kim et al., 2008b; Lowell and Shulman 2005; Samuel and Shulman 2012; Turner and Heilbronn 2008), and have been observed in skeletal muscles of obese, insulin-resistant individuals with or without T2D (Morino et al., 2005; Ritov et al., 2010). Beyond their function in ATP generation, mitochondria are a major site for production of reactive oxygen species (ROS). Multiple studies demonstrated an association of increased ROS production in skeletal muscle with impaired mitochondrial function and the onset of insulin resistance (Anderson et al., 2009; Fisher-Wellmann et al., 2013). The data reported in this work showed that sFRP4 tended to increase proton leak across the mitochondrial membrane of myotubes. Increased proton leak leads to incomplete coupling of the substrate oxygen to ATP production and has been found to be promoted by increased ROS production (Brookes et al., 2005). Thus, the data of this thesis indicate that sFRP4 may challenge the anti-oxidant defense capacity in myotubes.
The observed increase in mitochondrial respiration in C2C12 myotubes induced by sFRP4 was accompanied by an enhanced ratio of AMPK phosphorylation to AMPK protein indicating an increase in AMPK activity. AMPK suppresses ACC by phosphorylation at Ser-79 that results in increased fatty acid oxidation, since ACC inhibits via induced malonyl-CoA the carnitine palmitoyltransferase 1 (CPT1) and thus the mitochondrial transport of fatty acids for β-oxidation (Fediuc et al., 2006; Munday et al., 1988). However, sFRP4-induced AMPK phosphorylation in myotubes did not entail an inhibition of ACC. The increase in AMPK phosphorylation along with delayed increased mitochondrial respiration induced by sFRP4 might be a response to cellular stress that limits damage to mitochondria and thus sustains mitochondrial homeostasis and cell survival.

The presented data suggest a minor role of sFRP4 in the regulation of glucose and fatty acid metabolism in skeletal muscle under basal insulin-unstimulated conditions. These findings might indicate that the interaction of sFRP4 and skeletal muscle likely did not account for or just play a minor role in the observed correlation of *sFRP4* VAT expression and fasting glucose levels and thus systemic glucose homeostasis. However, to gain more insight, further investigations are needed.

4.3.1.1 sFRP4 induced abundance of E3 ubiquitin ligases via AMPK-FoxO3a signaling in primary hSkMC

The FoxO transcription factors are crucial mediators in the regulation of cellular stress response, apoptosis, mitochondrial function, lipid and glucose metabolism in skeletal muscle and direct transcriptional and posttranscriptional substrates of AMPK (Calnan and Brunet, 2008; Canto et al., 2009; Greer et al., 2007; Tong et al., 2009; Sanchez et al., 2014). Phosphorylation of FoxO3a at Ser253 and Thr32 has been identified to be essential for its nuclear exclusion and inhibition of its transcriptional activity (Salih and Brunet, 2008). sFRP4 reduced the inhibitory phosphorylation of FoxO3a at Ser235 in primary hSkMC by induction of AMPK signaling. AMPK-dependent activation of FoxO3a has been implicated in the modulation of muscle protein breakdown by induction of the E3 ubiquitin ligases MuRF1 and MAFbx/atrogin-1 (Bodine et al., 2001; Gomes et al., 2001; Nakashima and Yakabe., 2007; Krawiec et al., 2007; Sandri et al., 2004; Tong et al., 2009;). MuRF1 and MAFbx/atrogin-1 were elevated under catabolic conditions along with oxidative stress or inflammation in skeletal muscle and found to regulate skeletal muscle proteolysis (Bodine et al., 2001; Gomes et al., 2001). FoxO3a but also FoxO1 are direct transcription regulators of MuRF1 and MAFbx/atrogin-1 (Sandri et al., 2004; Stitt et al., 2004; Wadell et al., 2008). AMPK activation e.g. by AICAR resulted in increased expression of *Foxo1* and *Foxo3a* along with increased *MuRF1* and *MAFbx* expression and enhanced protein degradation (Nakashima and Yakabe., 2007) while inhibition of activated AMPK resulted in the suppression of *MuRF1* and *MAFbx* expression in myotubes. (Krawiec et al., 2007).

sFRP4 exposure significantly induced the abundances of MuRF1 and MAFbx/atrogin-1 by AMPK-FoxO3a signaling in primary hSkMC while the inhibition of AMPK prevented the sFRP4 mediated increase in MuRF1 and MAFbx levels. However, the underlying mechanism entailing

the AMPK-mediated suppression of inhibitory FoxO3a phosphorylation at Ser256 in cells treated with sFRP4 remains unclear.

Akt has been described to be the specific kinase for phosphorylation of FoxO3a at Ser253 and Thr32 resulting in the nuclear exclusion and transcriptional inhibition of the transcription factor (Brunet et al., 1999). In contrast, AMPK-mediated phosphorylation of FoxO3 at six distinct sites was associated with its transcriptional activation (Greer et al., 2007). Thus, the reduced phosphorylation of FoxO3a at Ser253 by sFRP4 might be accompanied by AMPK-specific phosphorylation of FoxO3a leading to an inhibition of FoxO3a phosphorylation by Akt via potential processes that impair the access of Akt to its corresponding phosphorylation site (Ser253) in FoxO3a. This hypothesis is supported by findings of Tong et al. who showed that AICAR-activated AMPK mediated a reduction in the inhibitory phosphorylation of FoxO3a at other Akt associated sites in C2C12 myotubes while induced FoxO3a nuclear transport and activity via direct phosphorylation of FoxO3 at the specific sites Ser412/588 that entailed increased abundance of MuRF1 and MAFbx (Tong et al., 2009). Thus, to gain further mechanistic insight of the sFRP4-AMPK-FoxO3a interaction, it would be interesting to examine in future studies whether the activating AMPK phosphorylation induced by sFRP4 results in an increased stimulatory phosphorylation of FoxO3a at AMPK specific sites.

In addition, AMPK has been shown to induce the activity of NAD^+-dependent deacetylase SIRT1 along with increased transcriptional activity of FoxO1 and FoxO3a in skeletal muscle (Canto et al., 2009). Besides phosphorylation, FoxO transcription factors are posttranslational de-/acetylated to modulate their stability and transcriptional activity (Boccitto and Kalb, 2011). Several studies demonstrated that SIRTs deacetylated and activated FoxO3a which resulted in its nuclear translocation and target gene expression (Brunet et al., 2004; Ferguson et al., 2015; Wang et al., 2007). Moreover, synergistical regulation of FoxO3a by phosphorylation and de-/acetylation events led to alterations in its subcellular localization and transcriptional activity (Matsuzaki et al., 2005; Senf et al., 2011). These studies indicate further potential mechanisms via which sFRP4 induction of AMPK might result in a reduced inhibitory phosphorylation of FoxO3a at Ser253 and increased MuRF1 and MAFbx levels as observed in primary hSkMC. However, while AMPK inhibition significantly reduced SIRT activity in primary hSkMC, sFRP4 did not affect SIRT activity, providing a basic proof that the observed sFRP4-induced effects in skeletal muscle cells were independent of sirtuin activity and thus deacetylation events.

4.3.1.2 sFRP4 activated the proteasome in primary hSkMC

The E3 ubiquitin ligases MuRF1 and MAFbx/atrogin-1 are important mediators of the ATP-dependent ubiquitin proteasome pathway that exhibits the major site for the degradation of intracellular proteins in skeletal muscle (Lecker et al., 1999). Further, MuRF1 and MAFbx levels have been found to be remarkably increased during skeletal muscle protein degradation linking them to enhanced proteasome activity, loss of muscle mass and decreased muscle fiber size, a condition known as skeletal muscle atrophy (Bodine et al., 2001; Gomes et al., 2001).

The observed findings that sFRP4 induced the E3 ubiquitin ligases MuRF1 and MAFbx/atrogin-1 in hSkMC via AMPK-FoxO3 signaling strongly suggested that it also modulate the activity of the ubiquitin-dependent proteasome system. The first and so far only therapeutically applicated proteasome inhibitor in humans is the dipeptide boronate BZ (Adams et al., 1998; Chauhan et al., 2008; Kisselev and Goldberg, 2001). BZ is cell permeable and selectively inhibits the β subunit of the catalytic 20S core of the proteasome with a substantial higher potency for the chymotrypsin-like activity than the trypsin- or caspase-like activity and 10 nM BZ have been used for effective inhibition of the proteasome activity in primary skeletal muscle cells (Crawford et al., 2006; Jager et al., 1999; Körner et al., 2014). While BZ alone or in combination with sFRP4 reduced the chymotrypsin-like activity of the proteasome, sFRP4 administration alone significantly increased proteasome activity.

The proteasomal degradation of misfolded and damaged proteins is crucial to regulate inflammatory responses, cell development and cell cycle control. However, increased proteasome activity and protein catabolism over a long time is strongly associated with the onset of excessive muscle loss and diabetes (Franch et al., 2005; Lecker et al., 2006). Increased proteasome activity has been observed in cultured primary skeletal muscle cells isolated from morbidly obese individuals (Bollinger et al., 2015).

The observed data provide evidence that the sFRP4-mediated increase in MuRF1 and MAFbx/atrogin-1 abundance induced by AMPK-FoxO3a signaling associated with an increase in proteasomal activity in primary human skeletal muscle cells. In line with this, sFRP4 exposure increased mitochondrial respiration in myotubes and thus cellular ATP, the indispensable fuel for the proteasome. Therefore, one can speculate that sFRP4 might induce mitochondrial respiration to provide sufficient energy for enhanced proteasome activity. Along with the increased abundance of MuRF1 and MAFbx/atrogin-1, the observations linked sFRP4 to impaired proteolysis in skeletal muscle that might cause skeletal muscle atrophy

which has been found in skeletal muscles of older individuals with type 2 diabetes (Kim et al., 2014; Leenders et al., 2013; Park et al., 2009). Moreover, enhanced FoxO activity, increased abundance of MuRF1 and MAFbx and proteasome activity have been associated with the onset of insulin resistance in skeletal muscle (Ostler et al., 2014; Woodworth-Hobbs et al., 2014).

4.3.1.3 sFRP4 mediated IRS1 degradation by the proteasome and reduced insulin-induced phosphorylation of FoxO independent of Akt in primary human skeletal muscle cells

Appropriate IRS-1 level in skeletal muscle are essential for differentiation, growth, glucose and lipid metabolism and thus maintenance of health (Eckstein et al., 2017). In contrast, reduced IRS-1 protein levels have been found in skeletal muscles of obese, insulin-resistant humans (Goodyear et al., 1995). The exposure of 24h sFRP4 to primary human skeletal muscle cells significantly reduced IRS-1 abundance without affecting *IRS1* gene expression suggesting posttranslational modifications i.e. proteasomal degradation. Reduced IRS-1 levels induced by sFRP4 were completely restored to normal levels when the proteasome was inhibited providing proof for the proteasome-dependent degradation of IRS-1 by sFRP4 in primary hSkMC. Proteasomal degradation of the IRS-1 protein has been linked to impaired insulin signaling and the onset of insulin resistance (Carvalho et al., 1999; Greene et al., 2003; Shah et al., 2004). Thus, reduced IRS-1 levels were accompanied by diminished insulin-mediated Akt phosphorylation and glucose uptake in skeletal muscles of insulin-resistent or T2D individuals (Krook et al., 1998; Takano et al., 2001).

Mechanistically, hyperinsulemia and chronic insulin exposure have been shown to induce proteasomal IRS-1 degradation via the PI3K/Akt/mTOR pathway (Berg et al., 2002; Greene et al., 2003).

However, the reduction of IRS-1 levels by sFRP4 was not accompanied by an impaired insulin-mediated phosphorylation of Akt and GSK3β, although the insulin-induced phosphorylation levels of FoxO1-Thr24/Ser256 as well as of FoxO3a-Thr32/Ser253 were significantly reduced. This investigation excluded that the degradation of IRS-1 entailed with an impaired Akt and GSK3β singling in primary human skeletal muscle cells.

Additionally, the insulin-mediated inhibitory phosphorylation of FoxO1 in response to 24h sFRP4 administration was not dependent on proteasome activity. These data confirmed that

the decrease in FoxO1 phosphorylation did not result from reductions in IRS-1 protein and thus is not associated with impaired IRS-1 downstream signaling. More likely, these observations suggest an IRS-1 and Akt independent mechanism causing a reduction in the inhibitory phosphorylation of FoxO in response to sFRP4 under an acute insulin stimulus. Hence, these data may provide evidence that FoxO1 and FoxO3a might be targeted by other kinases or protein phosphatases for instance by the mammalian STE20-like protein kinase-1 (MST-1) or the protein phosphatase 2A (Lehtinen et al., 2006; Singh et al., 2010) in response to sFRP4, causing the observed decrease in the inhibitory insulin-mediated phosphorylation of the transcription fators.

Distinct IRS-1 specific E3 ubiquitin ligases have yet been identified that mediate IRS1-degradation including SOCS-1/3, Cbl-b and F-box only protein (FBxo40) (Nakao et al., 2009; Rui et al., 2002; Shi et al., 2011). Studies providing precise evidence that MuRF1 and MAFbx/atrogin-1 are specific E3 ligases for IRS-1 do not exist so far, thus raises another issue that needs to be clarified in future investigations. Taken together, the described findings suggest sFRP4 as a potential biomarker for visceral adiposity before and during the onset of T2D. Moreover, the *in vitro* observations indicate that sFRP4 might be involved in impaired insulin action in skeletal muscle and atrophic conditions by promoting mitochondrial respiration and proteasome activity along with IRS-1 degradation related to the activation of AMPK-FoxO3a signaling in primary human skeletal muscle cells (Figure 54).

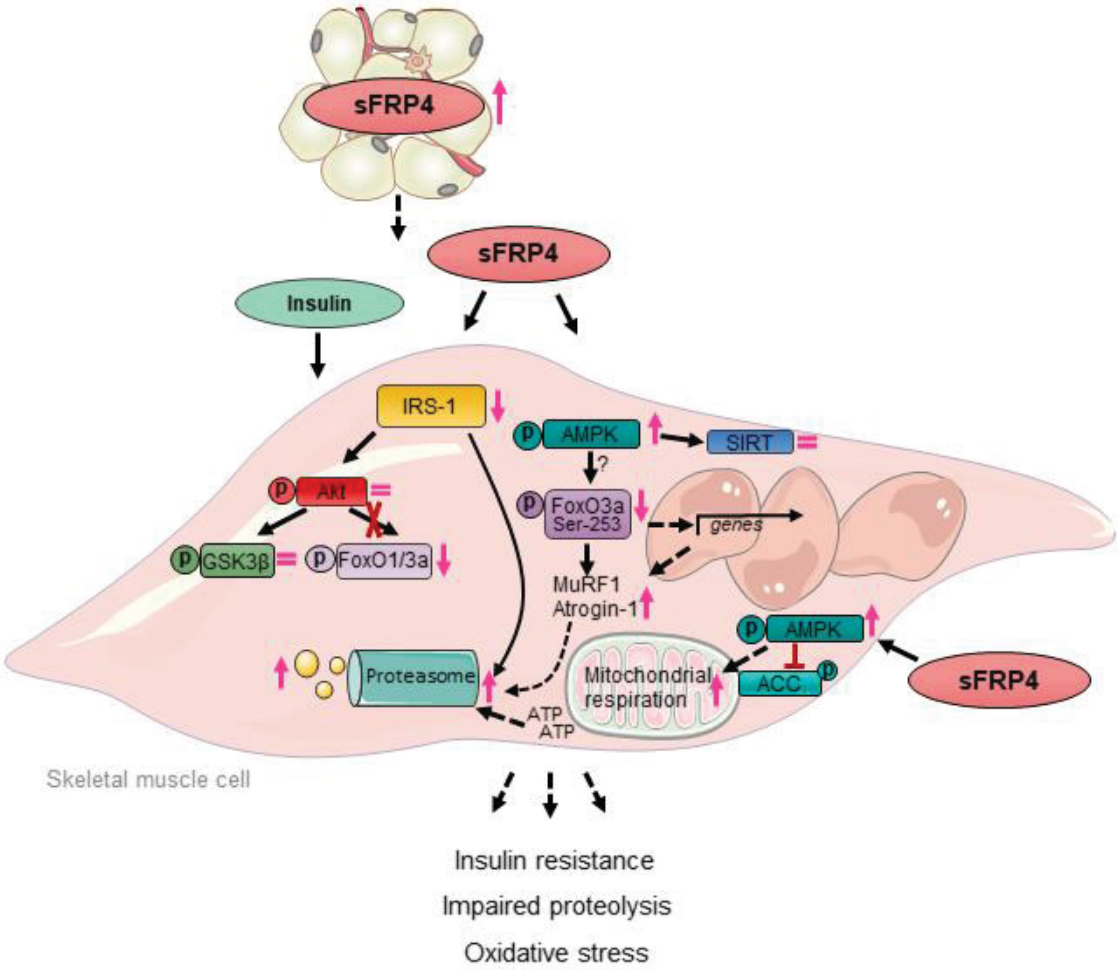

Figure 54. Effect of sFRP4 on insulin action and energy metabolism in primary hSkMC. *sFRP4* expression in VAT was increased with obesity and type 2 diabetes. *In vitro*, sFRP4 induced the proteasome activity and IRS-1 degradation in skeletal muscle cells (pink arrow upwards). Moreover, sFRP4 promoted mitochondrial respiration and induced phosphorylation of AMPK that resulted in reduced inhibitory FoxO3a phosphorylation (pink arrow downwards) and increased abundance of MuF1 and MAFbx/atrogin-1 linking sFRP4 to impaired proteolysis, stress response and insulin resistance in skeletal muscle. However, sFRP4 did not affect phosphorylation of Akt, GSK3β and SIRT activity in skeletal muscle cells (equal sign). Examined effects (solid arrow), potential effects (dotted arrow). AMPK, AMP-activated protein kinas; ACC, acetyl-CoA carboxylase; FoxO1/3a, forkhead box protein O1/3a; GSK3β, glycogen synthase kinase 3β; IRS-1, insulin receptor substrate-1; SIRT, sirtuin.

4.3.2 *sFRP4* expression was not restricted to visceral adipose tissue in mice

The data presented in this thesis are in line with previous studies that identified VAT as a major depot for the expression and secretion of the adipokine sFRP4 in humans (Ehrlund et al., 2013; Visweswaran et al., 2015). However, sFRP4 also has been described to be expressed and secreted from pancreatic islets and serum sFRP4 was higher in individuals with T2D (Mahdi et al., 2012; Taneera et al., 2012). Accompanying with this, *in vitro* and *in vivo* studies showed

that sFRP4 was associated with inflammation, insulin resistance and β-cell dysfunction (Mahdi et al., 2012; Taneera et al., 2012). In mice, *sfrp4* expression was mainly found in VAT but also in gastrocnemius (GAS) muscle but not in pancreatic islets (Mastaitis et al., 2015). To gain further insight how adipose tissue accounts for the sFRP4 levels that are present in the circulation, comparative tissue expression and plasma analyses of sfrp4 has been accomplished in C57Bl6 mice and in lipodystrophic aP2-SREBP-1c mice. Although circulating sfrp4 was significantly lower in plasma of aP2-SREBP-1c mice compared to C57Bl6 mice, sfrp4 was still detectable with a substantial amount, verified adipose tissue as an important source for systemic sfrp4 but also give proof that it is not the only sfrp4 releasing tissue in lipodystrophic mice. In accordance with previous findings (Mastaitis et al., 2015), the present data also showed that the *sfrp4* expression was mainly restricted to VAT in C57Bl6 mice. Besides VAT, GAS muscle showed the highest *sfrp4* expression suggesting the skeletal muscle as a further site for sfrp4 secretion. In humans, sFRP4 is also expressed and secreted from primary skeletal muscle cells. Studies by Hartwig et al. identified sFRP4 as a myokine, (Hartwig et al., 2014) confirming the skeletal muscle as an important source for sFRP4 beyond adipose tissue. Although the expression levels of *sfrp4* in GAS muscle of C57Bl6 and aP2-SREBP-1c mice were similar, it remains unclear whether sfrp4 abundance and release are altered in skeletal muscles between the two genotypes.To rule out whether the loss of adipose tissue in aP2-SREBP-1c results in an altered sfrp4 expression and secretion profile by other tissues e.g. skeletal muscle which may entail changes in systemic sfrp4 levels, sfrp4 protein abundance and secretion from different tissues than VAT should be examined in further studies. In conclusion, the presented data give evidence that even though VAT is one major source for sFRP4, the circulating sFRP4 pool does not seem to be restricted by VAT but also determined by other peripheral tissues, among them most likely the skeletal muscle.

4.3.2.1 sFRP4 impaired suppression of gluconeogenic genes, insulin-mediated glycogen synthesis and insulin signaling in hepatocytes of healthy C57Bl6

The observed strong associations of sFRP4 in VAT with serum triglycerides even after adjustment for age and BMI, hypothesized that sFRP4 might be involved in the control of lipid metabolism next to insulin action. Further, VAT-derived adipokines are directly secreted into the portal vein system and thus delivered to the liver, linking sFRP4 to a potential function in the regulation of glucose and lipid metabolism in liver.

An imbalance in the regulation of hepatic energy metabolism is crucial in the development of pathophysiological changes including insulin resistance, type 2 diabetes and NAFLD (Bechmann et al., 2012). Approximately 90% of the systemic glucose production is derived and synthesized by the liver (Ekberg et al., 1999; Petersen et al., 2017; Moore et al., 2012). The overall glucose production and disposal by the liver are pivotal for the peripheral glucose homeostasis and are driven by processes including gluconeogenesis, glycogenolysis and glycogen synthesis, and rates of these processes were increased in individuals with type 2 diabetes causing increased systemic blood glucose that manifests in hyperglycemia and insulin resistance (Basu et al., 2005; Boden et al. 2001; Magnusson et al., 1992; Petersen et al., 2017). Insulin regulates hepatic gluconeogenesis by suppression of the expression of the key gluconeogenic enzymes *Pck1* and *G6pc* to sustain glucose homeostasis. As described in the present thesis, elongated sFRP4 exposure reduced the basal and abrogated the insulin-mediated suppression of *Pck1* and *G6pc* expression. Interstingly, sFRP4 seemed to uncouple impairments on gluconeogenic gene expression from hepatic glucose production in presence of gluconeogenic substrates. Moreover, prolonged sFRP4 exposure blunted the insulin-induced stimulation of glycogen synthesis. Hence, the observations give evidence that sFRP4 impaired insulin action in primary hepatocytes which resulted in dysregulated gluconeogenesis and glycogen synthesis and thus might be involved in impaired glucose disposal. In line with this, reduced hepatic glycogen synthesis along with decreased liver glycogen content was described to be associated with reduced insulin sensitivity and an impaired overall glucose disposal in individuals with type 2 diabetes (Krssak et al., 2004; Solini et al., 2001). In addition, mice deficient for liver glycogen synthase, the key enzyme in glycogen synthesis, exhibited impaired hepatic glucose disposal and insulin signaling (Irimia et al., 2017).

In accordance with the reported functional findings, sFRP4 exposure remarkably impaired insulin signaling on level of Akt, GSK3β and FoxO1 in primary hepatocytes, thus linking sFRP4 to hepatic insulin resistance. FoxO1 is a master mediator of the expression of the gluconeogenic genes *G6Pc* and *PCK1* and thus hepatic glucose production, activated during fasting and suppressed postprandially by insulin-dependent activation of Akt (Matsumoto et al., 2007; Puigserver et al., 2003). Mice with liver specific loss of either the insulin receptor, Akt or IRS-1/IRS-2 displayed increased FoxO1-mediated hepatic glucose production along with severe insulin resistance and glucose intolerance while metabolic impairments were restored

if combined with ablation of FoxO1 in liver (Dong et al., 2008; Lu et al., 2012; Matsumoto et al., 2007; Titchenell et al., 2015). These studies suggested an alternative, IR-, IRS- and Akt-independent mechanism via which FoxO1 regulates hepatic glucose production (Titchenell et al., 2015). The decrease in insulin-mediated phosphorylation of FoxO1 in response to sFRP4 could in part be ascribed to the reduced FoxO1 protein abundance. This reduction might indicate a cellular attempt to compensate for the impaired insulin effect on FoxO1 induced by sFRP4. Constitutively active hepatic FoxO1 has been associated with impaired fasting glucose, hyperinsulinemia and increased TG levels and steatosis in mice while liver specific deletion of FoxO1 was found to decrease gluconeogenesis and restore hyperglycemia in ob/ob mice (Altomonte et al., 2003, 2004; Nakae et al., 2001, 2002; Zhang et al., 2006). In addition, previous studies demonstrated that the hepatic gain of function of FoxO1 promoted insulin signaling via positive feedback mechanisms amongst others by stimulation of *Irs2* expression and suppression of Akt inhibiting kinases (Ide et al., 2004; Matsumoto et al., 2006). Hence, the above described reductions in *Pck1* and *G6pc* expression might be a result of reduced FoxO1 protein concomitant with impaired insulin signaling in response to sFRP4.

Phosphorylation of glycogen synthase (GS) by GSK3 results in its inhibition and subsequent suppression of glycogen synthesis (Roach et al., 2002). sFRP4 administration decreased the ratio of the insulin-mediated inhibitory phosphorylation of GSK3β-Ser9 to GSK3β protein which might further be involved in the observed inhibition of the insulin-mediated glycogen synthesis. Although increased GSK3 activity in obesity and diabetes associated with impaired hepatic glucose disposal and insulin resistance (Eldar-Finkelmann 1999; Nikoulina et al., 2000), recent studies in GSK deficient mice suggested that stimulation of hepatic glycogen synthesis by insulin can also occur independent of GSK3 (Wan et al., 2013).

Thus, the data reported in the present thesis suggest an association of sFRP4 with an impaired glucose disposal in response to insulin at site of liver.

4.3.2.2 sFRP4 impaired insulin signaling via proteasomal degradation of IRS-1 in primary hepatocytes

IRS-1/2 are crucial regulators of hepatic insulin signaling, glucose metabolism and growth (Dong et al., 2006). Moreover, similar to skeletal muscle, reduced IRS-1 levels in liver have been associated with insulin resistance and hyperinsulinemia as reported in ob/ob mice (Saad et al., 1992).

sFRP4 exposure to primary hepatocytes resulted in a significant reduction of IRS-1 protein without affecting IRS-2 indicating that the decreased IRS-1 levels accounted for the impaired insulin signaling that was not compensated by the IRS-2 isoform. This is in line with observations in obese human with and without T2D who had reduced IRS-1 levels in liver accompanied with reduced insulin signaling while hepatic IRS-2 levels were not affected (Sajan et al., 2015). Moreover, sFRP4 mediated the posttranslational degradation of IRS-1 by the proteasome as observed in skeletal muscle cells. However, in contrast to skeletal muscle cells, sFRP4 did not induce the overall chymotrypsin-like activity of the proteasome in hepatocytes suggesting that sFRP4 just promoted the proteasomal degradation of particular proteins in primary hepatocytes. FoxO1 protein levels and phosphorylation were reduced in response to sFRP4, and not fully restored to levels of untreated cells upon inhibition of the proteasome. Ubiquitination of FoxO transcription factors and their subsequent proteasomal degradation have been reported to be promoted by deacetylation (Wang et al., 2012; Kitamura et al., 2005). Contradictory, FoxO1 deacetylation by SIRT1 prevented Akt-dependent inhibitory phosphorylation of FoxO1 and has been reported to induce FoxO1-mediated gluconeogenic gene expression, gluconeogenesis and thus glucose release from hepatocytes while the loss of SIRT1 has been associated with reduced gluconeogenesis (Erion et al., 2009; Frescas et al., 2005). Hence, the observed reduction of SIRT activity in primary hepatocytes in response to sFRP4 might be a cause or a consequence of the mentioned decrease in FoxO1 protein and the observed changes in gluconeogenic gene expression.

Beyond the restored IRS1-levels, proteasome inhibition restored insulin signaling on Akt and GSK3β phosphorylation in hepatocytes confirming that sFRP4 impaired insulin signaling in part via proteasome dependent degradation of IRS-1.

4.3.2.3 Mitochondrial energy metabolism was not affected by sFRP4 in primary hepatocytes

In liver, mitochondria are the key regulators of β-oxidation, tricarboxylic acid cycle (TCA), ATP generation via oxidative phosphorylation and formation of ROS (Bechmann et al., 2012; Li et al., 2015). The role of impaired mitochondrial function in the onset of hepatic insulin resistance, type 2 diabetes and/or NAFLD remains uncertain. Some reports associated mitochondrial dysfunctions in liver with reduced insulin sensitivity and T2D, whereas accumulating studies demonstrated increased hepatic mitochondrial respiration in obese,

insulin-resistant humans with and without NAFLD as well as in diabetic mice with severe hyperglycemia (Franko et al., 2014; Koliaki et al., 2015; Schmid et al., 2011; Sunny et al., 2011; Szendroedi et al., 2009). However, mitochondrial respiration and function were not affected by sFRP4 in hepatocytes of C57Bl6.

Hepatic fatty acid metabolism is stimulated by either dietary circulating fatty acid or fatty acids derived from extrahepatic tissues. In dependence of cellular energy level and metabolic conditions, fatty acids are either metabolized for ATP supply via mitochondrial fatty acid β-oxidation in hepatocytes during fasting or esterified to TAG for hepatic storage in lipid droplets or packed into VLDL particles for secretion into the bloodstream (Bechmann et al., 2012; Rui et al., 2014). Long-chain fatty acids like palmitic acids need to be activated by cytosolic acyl-CoA-synthase to acyl-CoA before they are actively transported into mitochondria, in a substrate-inhibitory process (Bechmann et al., 2012; Rui et al., 2014; Abu-Elheiga et al., 2000). Concomitant with unaltered mitochondrial respiration, sFRP4 did not interfere with mitochondrial palmitic acid oxidation in primary murine hepatocytes.

In the fasted state, adipocytes supply lipolysis-derived NEFAs for uptake and metabolization in hepatocytes while dietary fats were packed in chylomicrons and delivered to the liver (Bechmann et al., 2012; Rui et al., 2014). Hepatocytes actively take up fatty acids predominantly via fatty acid transporter 2/5 and the membrane-bounded glycoprotein fatty acid translocase (CD36/FAT), a process that is tightly regulated by glucagon and insulin (Arner et al., 2005). Along with unaltered mitochondrial β-oxidation, sFRP4 also did not affect palmitate uptake. In conclusion, the mentioned data give evidence that sFRP4 is likely not involved in the regulation of mitochondrial energy metabolism in primary hepatocytes of healthy C57Bl6 mice.

4.3.2.4 sFRP4 induced a selective insulin resistant state in primary hepatocytes of C57Bl6 mice

The key observations of sFRP4 action in primary hepatocytes were the significant increase of the insulin-mediated *de novo* lipid synthesis while the insulin-induced glycogen synthesis and gluconeogenic gene expression was abrogated along with an induction of IRS-1 degradation that resulted in impaired insulin signaling. Increased hepatic *de novo* lipogenesis is frequently associated with the onset of insulin resistance (Kawano and Cohen 2013). Excessive energy intake from diet along with dysfunction and insulin resistance in adipose tissue and/or skeletal

muscle impede the disposal of ingested nutrients by extrahepatic tissues. Hence, the liver attempts to compensate the surplus of energy by metabolizing that entails increased hepatic glucose production, triglyceride accumulation and hepatic insulin resistance (Samuel and Shulman, 2018). Extrahepatic-derived glucose and NEFAs promote hepatic DNL independently of insulin by providing metabolic substrates that are converted and esterified resulting in hepatic DAG and TAG accumulation. The surplus of glucose delivery into liver functions as activator of hepatic carbohydrate-responsive element-binding protein (ChREBP), while the increased lipid components release and activate SREBP-1c transcription factors that further fuel glycolysis and DNL in liver (Samuel and Shulman, 2018). Besides increased lipogenesis, hepatic insulin resistance results in reduced glycogen synthesis while hepatic glucose production is enhanced paving the way to metabolic liver pathologies such as NAFLD (Kawano and Cohen 2013; Ameer et al., 2014; Jelenik et al., 2017). However, it still remains to be elucidated what is cause and consequence in the interaction of hepatic insulin resistance and metabolic impairments associated with the development of NAFLD. Although previous studies did not find associations for circulating sFRP4 or *sFRP4* VAT expression with histopathological liver parameters related to NAFLD, *sFRP4* expression was significantly increased in VAT of obese individuals with NAFLD (Bekaert et al., 2016).

In vitro, sFRP4 increased insulin responsiveness on hepatic lipogenesis while abrogated insulin action on hepatic glucose metabolism suggesting the contribution of distinct insulin-mediated pathways that independently control lipid synthesis and glucose metabolism in liver. The action of sFRP4 therefore mimics the paradox phenomenon of selective insulin resistance on lipid metabolism in liver, initially described by Goldstein und Brown (Goldstein und Brown, 2008). This model hypothesizes that insulin signaling via the Akt/FoxO1 pathway is impaired and thus the suppression of gluconeogenesis and hepatic glucose output whereas SREBP-1c-mediated DNL is promoted in response to insulin causing hyperglycemia, hypertriglyceridemia and hyperinsulinemia, the hallmarks of type 2 diabetes (Goldstein and Brown, 2008). Thereby, reduced IRS-1 protein might entail impaired insulin signaling induced by sFRP4 while unaffected IRS-2 protein might be involved in the maintenance or even increase of insulin action on lipid synthesis in hepatocytes in response to sFRP4. The question whether sFRP4 induced hepatic lipogenesis that entails increased triglyceride accumulation in hepatocytes or enhanced secretion of lipids should be addressed in future investigations. Deacetylation of SREBP-1c, the key regulator of lipid synthesis, by SIRT1 has been shown to result in the

suppression of hepatic DNL (Ponugoti et al., 2010) whereas deletion of SIRT1 in hepatocytes has been found to associate with the onset of hepatic steatosis (Purushotham et al., 2009). Thus, the sFRP4-induced reduction in the activity of sirtuins further supports a role of sFRP4 in promoting dysregulations of hepatic lipid metabolism in hepatocytes. In conclusion, the described observations provide evidence that sFRP4 impaired insulin signaling and glucose disposal while favoured lipid synthesis in hepatocytes linking it to hepatic selective insulin resistance and the onset of NAFLD and/ or T2D (Figure 55).

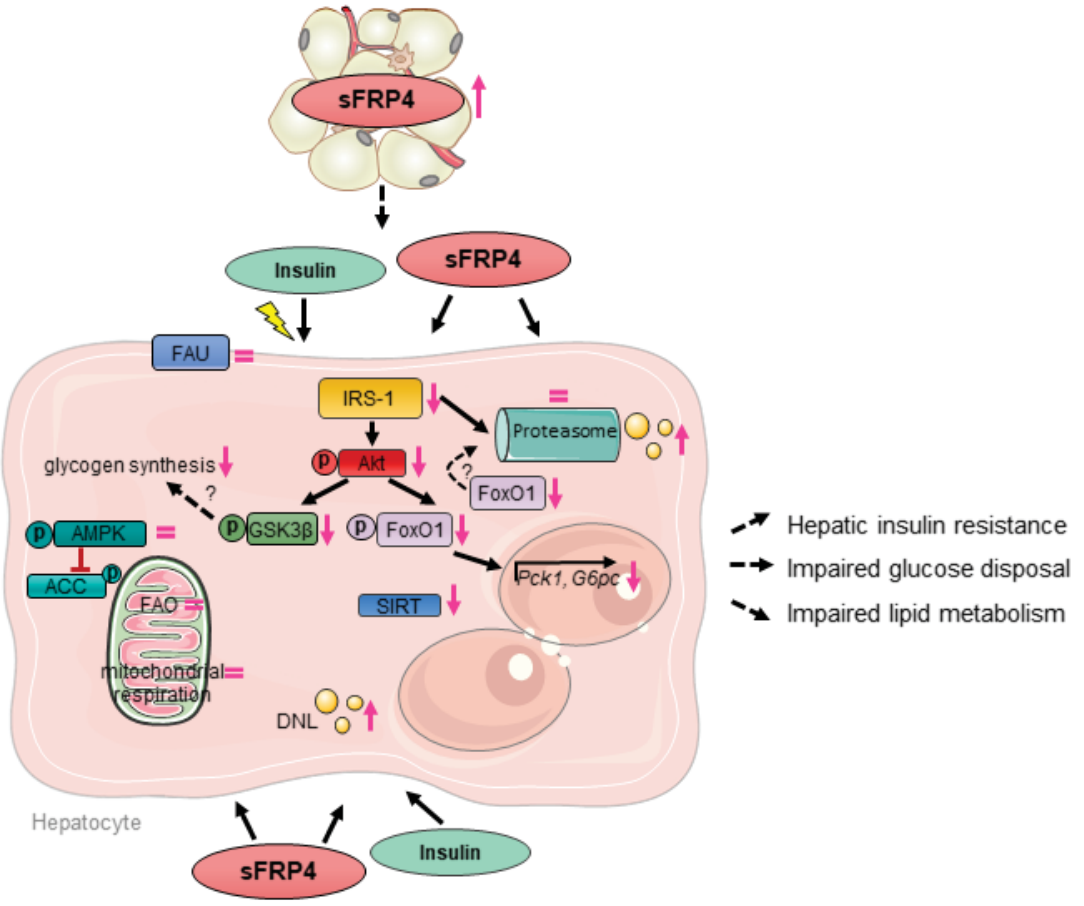

Figure 55. Effect of sFRP4 on insulin action, energy and lipid metabolism in primary murine hepatocytes. sFRP4 impaired insulin signaling, glucose and lipid metabolism in hepatocytes. With obesity and the onset of type 2 diabetes, *sFRP4* VAT expression increased. *In vitro*, sFRP4 induced IRS-1 degradation and abrogated insulin action on phosphorylation of Akt, GSK3β and FoxO1, glycogen synthesis and gluconeogenic gene expression in hepatocytes while promoted insulin-mediated lipid synthesis (pink arrow upwards) linking sFRP4 to hepatic insulin resistance, impaired glucose disposal and lipid metabolism. Moreover, sFRP4 decreased FoxO1 protein and SIRT activity in hepatocytes (pink arrow downwards). However, neither fatty acid uptake (FAU), fatty acid oxidation (FAO) nor mitochondrial respiration and AMPK phosphorylation were affected in response to sFRP4 (equal sign). Examined effects (solid arrow), potential effects (dotted arrow). AMPK, AMP-activated protein kinas; ACC, acetyl-CoA carboxylase; DNL, *de novo* lipogenesis; FoxO1, forkhead box protein O1; G6pc, glucose-6-

phosphatase c; GSK3β, glycogen synthase kinase 3β; IRS-1, insulin receptor substrate-1; Pck1, phosphoenolpyruvate carboxykinase 1; SIRT, sirtuin.

4.3.2.5 sFRP4 severely diminished insulin signaling and reduced FoxO1 in metabolic, dysfunctional hepatocytes of lipodystrophic aP2-SREBP-1c mice

The conditions of selective insulin resistance have been observed in humans and rodents with lipodystrophy. Due to the loss of adipose tissue, lipodystrophy causes excessive ectopic storage of fat in liver concomitant with enhanced hepatic DNL that in humans likely entails severe hepatic insulin resistance, dyslipidemia, hyperglycemia, hypertriglyceridemia, hyperinsulinemia and/or NAFLD that might progress to NASH (Garg et al., 2000; Kim et al., 2000; Petersen et al., 2002; Garg et al., 2000; Semple et al., 2009). Lipodystrophic aP2-SREBP-1c mice lack adipose tissue. Thus, these mice display e.g. increased insulin secretion, ectopic lipid accumulation and increased gluconeogenesis in liver and skeletal muscle in concert with hepatic and whole-body insulin resistance (Shimomura et al., 1998, 1999). Hepatic insulin resistance in aP2-SREBP-1c has been reported to manifest in impaired insulin signaling and abrogated insulin-induced suppression of gluconeogenesis but increased SREBP-1c-mediated lipid synthesis (Shimomura 1998, 1999). Thus, with lipodystrophy, the onset of hepatic insulin resistance is dissociated from severe visceral adiposity while confirming hepatic lipid accumulation as a leading cause. Hence, investigations of sFRP4 exposure to hepatocytes isolated from lipodystrophic mice provided insight into sFRP4 associated impairments on insulin action. The aP2-SREBP-1c mice used in this thesis completely lacked WAT and displayed dyslipidemia, pronounced insulin resistance, dramatically reduced plasma leptin and liver dysfunction. Hepatocytes isolated of aP2-SREBP-1c mice exhibited impaired insulin signaling while displayed larger and more lipid droplets and increased lipogenic activity than hepatocytes of corresponding C57Bl6 mice providing evidence that these cells maintained their insulin resistant phenotype in culture. Although sFRP4 exposure did neither affect energy metabolism nor lipid synthesis in primary hepatocytes of aP2-SREBP-1c mice, it dramatically reduced insulin responsiveness on Akt and GSK3β phosphorylation indicating that sFRP4 has the ability to even worsen the insulin resistant conditions present in hepatocyte of lipodystrophic mice. Moreover, sFRP4 alone and in concomitant with insulin dramatically reduced FoxO1 protein and sFRP4 decreased GSK3β. In contrast to hepatocytes of healthy C57Bl6 mice, sFRP4 did not affect IRS-1 in hepatocytes of lipodystrophic mice. However, these

findings do not exclude that sFRP4 may exert changes in IRS-1 serine/threonine phosphorylation that has been shown to result in inhibition of IRS-1 signal transduction (Copps and White, 2012). Although sFRP4 impaired insulin signaling, the reduction of hepatic FoxO1 in response to sFRP4 suggests that sFRP4 might compensate for the displayed insulin resistance and nutrient overflow to sustain glucose levels and thus counteract hyperglycemia. Hence, sFRP4 impaired insulin responsiveness on the levels of Akt and GSK3β phosphorylation while maintained insulin action on lipogenesis in hepatocytes with an existing disrupted insulin sensitivity and elevated lipid synthesis linking sFRP4 to the induction of hepatic insulin resistance.

4.4 sFRP4 induced the secretion of factors from hepatocytes that are involved in glucocorticoid receptor signaling

Proteins that are secreted from the liver have been implicated in the regulation of glucose and lipid metabolism in an auto-/para- and endocrine fashion. The proteome and bioinformatic approaches of the secretomes of metabolic intact and impaired hepatocytes isolated from C57Bl6 and lipodystrophic aP2-SREBP-1c mice treated with sFRP4 revealed that sFRP4 associated with hepatic fibrosis on molecular level in hepatocytes of both genotypes. Further, hints for molecular interactions with cardiac fibrosis and renal ischemia and failure could be observed. Besides hepatic insulin resistance and ectopic lipid accumulation in liver, fibrosis is a crucial characteristic of NASH (Brunt et al., 2004) supporting a potential association of sFRP4 with NASH related pathophysiological metabolic alterations in liver. In the secretome of hepatocytes of both genotype, sFRP4 mediated the enrichment of proteins associated with LXR/RXR activation. The nuclear receptor liver X receptor (LXR) along with the retinoid X receptor (RXR) are important regulators of hepatic lipid metabolism and have been reported to be activated by Akt and induce hepatic lipogenesis by promoting SREBP-1c expression and proteolytic activation (Chawla et al., 2001; Fon Tacer and Rozman, 2011; Yoshikawa et al., 2001). In aP2-SREBP-1c hepatocytes, the bioinformatic analyses revealed PLA2G2E as the major regulator molecule that encoded for the phospholipase group IIE secretory phospholipase A2. The enzyme phospholipase A2 hydrolyzes phospholipids into lysophospholipids and free fatty acids. Another phospholipase, the secreted PLA2G1B, has been reported to induce lysophospholipid absorption and hepatic lipogenesis while inhibited hepatic fatty acid oxidation that entail hyperlipidemia (Hollie and Hui, 2011). The enrichment

analyses of secretomes of sFRP4 treated hepatocytes from C57Bl6, pointed to keratin 14 (KRT14) as the major upstream regulator. Keratins are intermediate filaments of the cytoskeleton of hepatocytes, displaying structural roles by ensuring mechanical stability but also cytoprotective capabilities by regulating cellular stress response. Alterations of the keratin cytoskeleton leading to misfolding or keratin aggregation and have been associated with pathological impairments in liver during NASH (Zatlouka et al., 2006). However, so far only keratin 8 and keratin 18 have been identified in hepatocytes (Tao et al., 2009). Moreover, web-based analyses of secretome data of hepatocytes of both genotypes revealed that components of the glucocorticoid receptor signaling pathway are differentially enriched suggesting pathway activation, predominantly due to keratin gene family members.

The nuclear glucocorticoid receptor regulates transcription in response to glucocortides that are syntethized from the acetly-CoA-mevalonate-cholesterol biosynthesis pathway. Glucocorticoid receptor signaling plays a pivotal role in lipid metabolism in adipose tissue and liver. In adipose tissue glucocorticoid receptor activation induced lipolysis, fatty acid release but decreased lipogenesis (Divertie et al., 1991; Gathercole et al., 2011; Wang et al., 2015). In liver glucocorticoide signaling promotes lipogenic gene expression, gluconeogenesis and glycogenolysis and thus lipid synthesis and accumulation, hence it has been implicated in the development of NAFLD (Canalis et al., 1983; Dich et al., 1983; Dolinsky et al., 2004; Mueller et al., 2012). Thus, the differential effects of sFRP4 on DNL observed in metabolic healthy and diseased hepatocytes were accompanied by differential secretion profiles of these cells. Further, the analyses indicate that beyond the here reported findings, sFRP4 may exerts distinct effects even on other tissues including heart and kidney, by modulating the secretion of proteins from hepatocytes that amongst others are involved in glucocorticoid receptor signaling.

4.5 Conclusion and perspectives

The present thesis aimed to explore the role of the adipokines WISP1 and sFRP4 in the context of obesity and type 2 diabetes and their function in the regulation of energy metabolism and insulin action in two major insulin-responsive tissues, skeletal muscle and liver. Previous studies predominately are based on the impact of sFRP4 and WISP1 on adipose tissue, whilst their roles in skeletal muscle and liver are largely obscure yet, thus supporting the novelty of the findings reported in this thesis.

The first part of this thesis focused on the role of WISP1 in the proposed issues. The findings of this work identified WISP1 as a determinant of obesity in men. The increases in circulating WISP1 levels associated with variables reflecting insulin resistance *in vivo* in individuals with obesity. *In vitro* studies corroborate the associations observed in the clinical study by showing that recombinant WISP1 impaired insulin signaling in both insulin-sensitive cell types, i.e. myotubes and hepatocytes with consequent impaired gluconeogenesis and glycogen synthesis. The data provide evidence that WISP1 may regulate whole-body insulin sensitivity and glucose uptake due to its effects on insulin signaling in liver and muscle and thus may be a promising target for the prevention and treatment of obesity and diabetes.

As a perspective of the findings of the thesis, further investigations might focus on the detailed mechanism via which WISP1 inhibits insulin action. Furthermore, the *in vitro* observations may be target for validation in *in vivo* animal studies to determine phenotypical effects of WISP1 on whole-body glucose disposal, insulin resistance and the development of diabetes and obesity. The described studies were conducted in men only. In regard to the clinical consideration of WISP1 and its utilization as a biomarker for obesity and T2D in humans, an extension of the study cohort including women would be needed to provide an approach for the generalization of the findings to entire population.

The second part of this work reported the impact of sFRP4 as a potential biomarker for adiposity and T2D in men since the clinical associations corroborate an interference of sFRP4 with insulin action, glucose and lipid metabolism. Functional investigations revealed that in primary human skeletal muscle cells sFRP4 induced mitochondrial respiration and promoted proteasome activity and degradation of IRS-1 likely via activation of AMPK-FoxO3a signaling and sFRP4 may impede insulin action apart from Akt signaling transduction. In conclusion, the present data suggest sFRP4 as a promotor of cellular stress response, impaired insulin signaling and atrophic conditions in skeletal muscle.

The strong association of *sFRP4* in VAT with circulating triglycerides indicated a potential role of sFRP4 in liver metabolism that was confirmed *in vitro*. sFRP4 impaired the insulin response on molecular level and on glycogen synthesis and induced IRS-1 degradation while enhanced insulin action on DNL and thus promoted lipid synthesis in primary murine hepatocytes. In addition, sFRP4 further impeded the insulin action on molecular level but did not affect insulin-mediated lipid synthesis in metabolic dysfunctional hepatocytes. These findings

support the role of sFRP4 as mediator of impaired glucose disposal and selective insulin resistance in hepatocytes.

Taken together, this thesis provides first evidence that sFRP4 may modulate systemic insulin sensitivity, glucose disposal and lipidemia based on the reported findings in skeletal muscle and liver, justifying sFRP4 to be considered in future research as a potential target for the prevention of T2D and NAFLD.

As a perspective, an investigation of the impact of sFRP4 on insulin-mediated metabolic pathways including glycogen synthesis and glucose uptake but also fatty acid uptake, lipid synthesis and storage, would provide important functional insight for the interference of sFRP4 with insulin action on skeletal muscle. Further investigations ought to target the mechanism via which sFRP4 exerts its effects in skeletal muscle and liver, to unravel the potential role of sFRP4 in the development of whole-body insulin resistance. One promising target might be the effect of sFRP4 on FoxO, as it turned out to be a common substrate of sFRP4 in skeletal muscle and liver and thus providing an approach for further studies in this direction. Investigations of sFRP4 action on hepatic lipid accumulation and secretion would be important to get detailed insight whether sFRP4 contributes to a fatty liver phenotype and/or a state of dyslipidemia and thus the development of T2D and NAFLD. For consideration of sFRP4 as a clinical indicator for obesity and T2D in humans, an extension of the study cohort including women as proposed for WISP1, might allow a generalization of the describes observations.

The investigations described in this thesis identified the adipokines WISP1 and sFRP4 as effectors in the inter-organ communication that directly interfere with metabolic events in skeletal muscle cells and hepatocytes in a cell-type specific manner. The elucidation of adipokine secretion patterns and translational studies as performed in this thesis will help to better understand the complex interaction network of distinct metabolic tissues and provide insight in metabolic alterations related to health and disease.

5 References

Abiola, M., Favier, M., Christodoulou-Vafeiadou, E., Pichard, A.L., Martelly, I., and Guillet-Deniau, I. (2009). Activation of Wnt/beta-catenin signaling increases insulin sensitivity through a reciprocal regulation of Wnt10b and SREBP-1c in skeletal muscle cells. PloS one *4*, e8509.

Abu-Elheiga, L., Brinkley, W.R., Zhong, L., Chirala, S.S., Woldegiorgis, G., and Wakil, S.J. (2000). The subcellular localization of acetyl-CoA carboxylase 2. Proceedings of the National Academy of Sciences of the United States of America *97*, 1444-1449.

Adachi, M., and Brenner, D.A. (2008). High molecular weight adiponectin inhibits proliferation of hepatic stellate cells via activation of adenosine monophosphate-activated protein kinase. Hepatology (Baltimore, Md.) *47*, 677-685.

Adams, J., Behnke, M., Chen, S., Cruickshank, A.A., Dick, L.R., Grenier, L., Klunder, J.M., Ma, Y.T., Plamondon, L., and Stein, R.L. (1998). Potent and selective inhibitors of the proteasome: dipeptidyl boronic acids. Bioorganic & medicinal chemistry letters *8*, 333-338.

Adams, L.A., Lymp, J.F., St Sauver, J., Sanderson, S.O., Lindor, K.D., Feldstein, A., and Angulo, P. (2005). The natural history of nonalcoholic fatty liver disease: a population-based cohort study. Gastroenterology *129*, 113-121.

Ahima, R.S., and Flier, J.S. (2000). Adipose tissue as an endocrine organ. Trends in endocrinology and metabolism: TEM *11*, 327-332.

Akie, T.E., and Cooper, M.P. (2015). Determination of Fatty Acid Oxidation and Lipogenesis in Mouse Primary Hepatocytes. Journal of visualized experiments : JoVE, e52982.

Altomonte, J., Cong, L., Harbaran, S., Richter, A., Xu, J., Meseck, M., and Dong, H.H. (2004). Foxo1 mediates insulin action on apoC-III and triglyceride metabolism. The Journal of clinical investigation *114*, 1493-1503.

Altomonte, J., Richter, A., Harbaran, S., Suriawinata, J., Nakae, J., Thung, S.N., Meseck, M., Accili, D., and Dong, H. (2003). Inhibition of Foxo1 function is associated with improved fasting glycemia in diabetic mice. American journal of physiology. Endocrinology and metabolism *285*, E718-728.

Ameer, F., Scandiuzzi, L., Hasnain, S., Kalbacher, H., and Zaidi, N. (2014). De novo lipogenesis in health and disease. Metabolism: clinical and experimental *63*, 895-902.

American Diabetes Association (ADA) (2017). 2. Classification and Diagnosis of Diabetes. Diabetes care *40(Supplement 1)*, S11-S24.

Anand, K., Vidyasagar, S., Lasrado, I., Pandey, G.K., Amutha, A., Ranjani, H., Mohan Anjana, R., Mohan, V., and Gokulakrishnan, K. (2016). Secreted Frizzled-Related Protein 4 (SFRP4): A Novel Biomarker of beta-Cell Dysfunction and Insulin Resistance in Individuals With Prediabetes and Type 2 Diabetes. Diabetes care *39*, e147-148.

Anderson, E.J., Lustig, M.E., Boyle, K.E., Woodlief, T.L., Kane, D.A., Lin, C.T., Price, J.W., 3rd, Kang, L., Rabinovitch, P.S., Szeto, H.H., et al. (2009). Mitochondrial H2O2 emission and cellular redox state link excess fat intake to insulin resistance in both rodents and humans. The Journal of clinical investigation *119*, 573-581.

Arner, P. (2005). Human fat cell lipolysis: biochemistry, regulation and clinical role. Best practice & research. Clinical endocrinology & metabolism *19*, 471-482.

Badman, M.K., Pissios, P., Kennedy, A.R., Koukos, G., Flier, J.S., and Maratos-Flier, E. (2007). Hepatic fibroblast growth factor 21 is regulated by PPARalpha and is a key mediator of hepatic lipid metabolism in ketotic states. Cell metabolism *5*, 426-437.

Bafico, A., Gazit, A., Pramila, T., Finch, P.W., Yaniv, A., and Aaronson, S.A. (1999). Interaction of frizzled related protein (FRP) with Wnt ligands and the frizzled receptor suggests alternative mechanisms for FRP inhibition of Wnt signaling. The Journal of biological chemistry *274*, 16180-16187.

Baldry, E.L., Aithal, G.P., Kaye, P., Idris, I.R., Bennett, A., Leeder, P.C., and Macdonald, I.A. (2017). Effects of short-term energy restriction on liver lipid content and inflammatory status in severely obese adults: Results of a randomized controlled trial using 2 dietary approaches. Diabetes, obesity & metabolism *19*, 1179-1183.

Barchetta, I., Cimini, F.A., Capoccia, D., De Gioannis, R., Porzia, A., Mainiero, F., Di Martino, M., Bertoccini, L., De Bernardinis, M., Leonetti, F., et al. (2017). WISP1 Is a Marker of Systemic and Adipose Tissue Inflammation in Dysmetabolic Subjects With or Without Type 2 Diabetes. Journal of the Endocrine Society *1*, 660-670.

Barzilai, N., Wang, J., Massilon, D., Vuguin, P., Hawkins, M., and Rossetti, L. (1997). Leptin selectively decreases visceral adiposity and enhances insulin action. The Journal of clinical investigation *100*, 3105-3110.

Bastie, C.C., Nahle, Z., McLoughlin, T., Esser, K., Zhang, W., Unterman, T., and Abumrad, N.A. (2005). FoxO1 stimulates fatty acid uptake and oxidation in muscle cells through CD36-dependent and -independent mechanisms. The Journal of biological chemistry *280*, 14222-14229.

Basu, R., Chandramouli, V., Dicke, B., Landau, B., and Rizza, R. (2005). Obesity and type 2 diabetes impair insulin-induced suppression of glycogenolysis as well as gluconeogenesis. Diabetes *54*, 1942-1948.

Bataller, R., Rombouts, K., Altamirano, J., and Marra, F. (2011). Fibrosis in alcoholic and nonalcoholic steatohepatitis. Best practice & research. Clinical gastroenterology *25*, 231-244.

Bechmann, L.P., Hannivoort, R.A., Gerken, G., Hotamisligil, G.S., Trauner, M., and Canbay, A. (2012). The interaction of hepatic lipid and glucose metabolism in liver diseases. Journal of hepatology *56*, 952-964.

Bekaert, M., Ouwens, D.M., Horbelt, T., Van de Velde, F., Fahlbusch, P., Herzfeld de Wiza, D., Van Nieuwenhove, Y., Calders, P., Praet, M., Hoorens, A., et al. (2016). Reduced expression of chemerin in visceral adipose tissue associates with hepatic steatosis in patients with obesity. Obesity (Silver Spring, Md.) *24*, 2544-2552.

Bellentani, S. (2017). The epidemiology of non-alcoholic fatty liver disease. Liver international : official journal of the International Association for the Study of the Liver *37 Suppl 1*, 81-84.

Bendtsen, J.D., Jensen, L.J., Blom, N., Von Heijne, G., and Brunak, S. (2004). Feature-based prediction of non-classical and leaderless protein secretion. Protein engineering, design & selection : PEDS *17*, 349-356.

Bennett, C.N., Ross, S.E., Longo, K.A., Bajnok, L., Hemati, N., Johnson, K.W., Harrison, S.D., and MacDougald, O.A. (2002). Regulation of Wnt signaling during adipogenesis. The Journal of biological chemistry *277*, 30998-31004.

Berg, C.E., Lavan, B.E., and Rondinone, C.M. (2002). Rapamycin partially prevents insulin resistance induced by chronic insulin treatment. Biochemical and biophysical research communications *293*, 1021-1027.

Berschneider, B., and Konigshoff, M. (2011). WNT1 inducible signaling pathway protein 1 (WISP1): a novel mediator linking development and disease. The international journal of biochemistry & cell biology *43*, 306-309.

Billeter, A.T., Senft, J., Gotthardt, D., Knefeli, P., Nickel, F., Schulte, T., Fischer, L., Nawroth, P.P., Buchler, M.W., and Muller-Stich, B.P. (2016). Combined Non-alcoholic Fatty Liver Disease and Type 2 Diabetes Mellitus: Sleeve Gastrectomy or Gastric Bypass?-a Controlled Matched Pair Study of 34 Patients. Obesity surgery *26*, 1867-1874.

Blumensatt, M., Fahlbusch, P., Hilgers, R., Bekaert, M., Herzfeld de Wiza, D., Akhyari, P., Ruige, J.B., and Ouwens, D.M. (2017). Secretory products from epicardial adipose tissue from patients with type 2 diabetes impair mitochondrial beta-oxidation in cardiomyocytes via activation of the cardiac renin-angiotensin system and induction of miR-208a. Basic research in cardiology *112*, 2.

Boccitto, M., and Kalb, R.G. (2011). Regulation of Foxo-dependent transcription by post-translational modifications. Current drug targets *12*, 1303-1310.

Boden, G., Chen, X., and Stein, T.P. (2001). Gluconeogenesis in moderately and severely hyperglycemic patients with type 2 diabetes mellitus. American journal of physiology. Endocrinology and metabolism *280*, E23-30.

Bodine, S.C., Latres, E., Baumhueter, S., Lai, V.K., Nunez, L., Clarke, B.A., Poueymirou, W.T., Panaro, F.J., Na, E., Dharmarajan, K., et al. (2001). Identification of ubiquitin ligases required for skeletal muscle atrophy. Science (New York, N.Y.) *294*, 1704-1708.

Bollinger, L.M., Powell, J.J., Houmard, J.A., Witczak, C.A., and Brault, J.J. (2015). Skeletal muscle myotubes in severe obesity exhibit altered ubiquitin-proteasome and autophagic/lysosomal proteolytic flux. Obesity (Silver Spring, Md.) *23*, 1185-1193.

Boushel, R., Gnaiger, E., Schjerling, P., Skovbro, M., Kraunsoe, R., and Dela, F. (2007). Patients with type 2 diabetes have normal mitochondrial function in skeletal muscle. Diabetologia *50*, 790-796.

Bovolenta, P., Esteve, P., Ruiz, J.M., Cisneros, E., and Lopez-Rios, J. (2008). Beyond Wnt inhibition: new functions of secreted Frizzled-related proteins in development and disease. Journal of cell science *121*, 737-746.

Bray, G.A., and Popkin, B.M. (2014). Dietary sugar and body weight: have we reached a crisis in the epidemic of obesity and diabetes?: health be damned! Pour on the sugar. Diabetes care *37*, 950-956.

Brigstock, D.R. (2003). The CCN family: a new stimulus package. The Journal of endocrinology *178*, 169-175.

Brix, J.M., Krzizek, E.C., Hoebaus, C., Ludvik, B., Schernthaner, G., and Schernthaner, G.H. (2016). Secreted Frizzled-Related Protein 4 (SFRP4) is Elevated in Patients with Diabetes Mellitus. Hormone and metabolic research = Hormon- und Stoffwechselforschung = Hormones et metabolisme *48*, 345-348.

Brookes, P.S. (2005). Mitochondrial H(+) leak and ROS generation: an odd couple. Free radical biology & medicine *38*, 12-23.

Brown, M.S., and Goldstein, J.L. (2008). Selective versus total insulin resistance: a pathogenic paradox. Cell metabolism *7*, 95-96.

Brunt, E.M. (2004). Nonalcoholic steatohepatitis. Seminars in liver disease *24*, 3-20.

Brunet, A., Bonni, A., Zigmond, M.J., Lin, M.Z., Juo, P., Hu, L.S., Anderson, M.J., Arden, K.C., Blenis, J., and Greenberg, M.E. (1999). Akt promotes cell survival by phosphorylating and inhibiting a Forkhead transcription factor. Cell *96*, 857-868.

Brunet, A., Sweeney, L.B., Sturgill, J.F., Chua, K.F., Greer, P.L., Lin, Y., Tran, H., Ross, S.E., Mostoslavsky, R., Cohen, H.Y., et al. (2004). Stress-dependent regulation of FOXO transcription factors by the SIRT1 deacetylase. Science (New York, N.Y.) *303*, 2011-2015.

Burcelin, R., Kamohara, S., Li, J., Tannenbaum, G.S., Charron, M.J., and Friedman, J.M. (1999). Acute intravenous leptin infusion increases glucose turnover but not skeletal muscle glucose uptake in ob/ob mice. Diabetes *48*, 1264-1269.

Burgess, A., Li, M., Vanella, L., Kim, D.H., Rezzani, R., Rodella, L., Sodhi, K., Canestraro, M., Martasek, P., Peterson, S.J., et al. (2010). Adipocyte heme oxygenase-1 induction attenuates metabolic syndrome in both male and female obese mice. Hypertension (Dallas, Tex. : 1979) *56*, 1124-1130.

Calnan, D.R., and Brunet, A. (2008). The FoxO code. Oncogene *27*, 2276-2288.

Calvisi, D.F., Conner, E.A., Ladu, S., Lemmer, E.R., Factor, V.M., and Thorgeirsson, S.S. (2005). Activation of the canonical Wnt/beta-catenin pathway confers growth advantages in c-Myc/E2F1 transgenic mouse model of liver cancer. Journal of hepatology *42*, 842-849.

Canto, C., Gerhart-Hines, Z., Feige, J.N., Lagouge, M., Noriega, L., Milne, J.C., Elliott, P.J., Puigserver, P., and Auwerx, J. (2009). AMPK regulates energy expenditure by modulating NAD+ metabolism and SIRT1 activity. Nature *458*, 1056-1060.

Canalis, E. (1983). Effect of glucocorticoids on type I collagen synthesis, alkaline phosphatase activity, and deoxyribonucleic acid content in cultured rat calvariae. Endocrinology *112*, 931-939.

Carey, A.L., Steinberg, G.R., Macaulay, S.L., Thomas, W.G., Holmes, A.G., Ramm, G., Prelovsek, O., Hohnen-Behrens, C., Watt, M.J., James, D.E., et al. (2006). Interleukin-6 increases insulin-stimulated glucose disposal in humans and glucose uptake and fatty acid oxidation in vitro via AMP-activated protein kinase. Diabetes *55*, 2688-2697.

Carmon K.S., L.D.S. (2010). SFRP4 [secreted frizzled-related protein 4] Atlas. Genet. Cytogenet. Oncol, Haematol., 14 (3) 296-300.

Carmon, K.S., and Loose, D.S. (2008). Secreted frizzled-related protein 4 regulates two Wnt7a signaling pathways and inhibits proliferation in endometrial cancer cells. Molecular cancer research : MCR *6*, 1017-1028.

Carvalho, E., Jansson, P.A., Axelsen, M., Eriksson, J.W., Huang, X., Groop, L., Rondinone, C., Sjostrom, L., and Smith, U. (1999). Low cellular IRS 1 gene and protein expression predict insulin resistance and NIDDM. FASEB journal : official publication of the Federation of American Societies for Experimental Biology *13*, 2173-2178.

Chawla, A., Repa, J.J., Evans, R.M., and Mangelsdorf, D.J. (2001). Nuclear receptors and lipid physiology: opening the X-files. Science (New York, N.Y.) *294*, 1866-1870.

Ceddia, R.B., William, W.N., Jr., and Curi, R. (1998). Leptin increases glucose transport and utilization in skeletal muscle in vitro. General pharmacology *31*, 799-801.

Ceddia, R.B., William, W.N., Jr., Lima, F.B., Flandin, P., Curi, R., and Giacobino, J.P. (2000). Leptin stimulates uncoupling protein-2 mRNA expression and Krebs cycle activity and inhibits lipid synthesis in isolated rat white adipocytes. European journal of biochemistry *267*, 5952-5958.

Cernea, M., Tang, W., Guan, H., and Yang, K. (2016). Wisp1 mediates Bmp3-stimulated mesenchymal stem cell proliferation. Journal of molecular endocrinology *56*, 39-46.

Charlton, M., Krishnan, A., Viker, K., Sanderson, S., Cazanave, S., McConico, A., Masuoko, H., and Gores, G. (2011). Fast food diet mouse: novel small animal model of NASH with ballooning, progressive fibrosis, and high physiological fidelity to the human condition. American journal of physiology. Gastrointestinal and liver physiology *301*, G825-834.

Chauhan, D., Bianchi, G., and Anderson, K.C. (2008). Targeting the UPS as therapy in multiple myeloma. BMC biochemistry *9 Suppl 1*, S1.

Chen, C.C., and Lau, L.F. (2009). Functions and mechanisms of action of CCN matricellular proteins. The international journal of biochemistry & cell biology *41*, 771-783.

Chen, Z., Ding, X., Jin, S., Pitt, B., Zhang, L., Billiar, T., and Li, Q. (2016). WISP1-alphavbeta3 integrin signaling positively regulates TLR-triggered inflammation response in sepsis induced lung injury. Scientific reports *6*, 28841.

Chong, J.M., Uren, A., Rubin, J.S., and Speicher, D.W. (2002). Disulfide bond assignments of secreted Frizzled-related protein-1 provide insights about Frizzled homology and netrin modules. The Journal of biological chemistry *277*, 5134-5144.

Cohen, P. (1999). The Croonian Lecture 1998. Identification of a protein kinase cascade of major importance in insulin signal transduction. Philosophical transactions of the Royal Society of London. Series B, Biological sciences *354*, 485-495.

Coleman, R.A., and Lee, D.P. (2004). Enzymes of triacylglycerol synthesis and their regulation. Progress in lipid research *43*, 134-176.

Colston, J.T., de la Rosa, S.D., Koehler, M., Gonzales, K., Mestril, R., Freeman, G.L., Bailey, S.R., and Chandrasekar, B. (2007). Wnt-induced secreted protein-1 is a prohypertrophic and profibrotic growth factor. American journal of physiology. Heart and circulatory physiology *293*, H1839-1846.

Combs, T.P., Berg, A.H., Obici, S., Scherer, P.E., and Rossetti, L. (2001). Endogenous glucose production is inhibited by the adipose-derived protein Acrp30. The Journal of clinical investigation *108*, 1875-1881.

Copps, K.D., and White, M.F. (2012). Regulation of insulin sensitivity by serine/threonine phosphorylation of insulin receptor substrate proteins IRS1 and IRS2. Diabetologia *55*, 2565-2582.

Constantinou, T., Baumann, F., Lacher, M.D., Saurer, S., Friis, R., and Dharmarajan, A. (2008). SFRP-4 abrogates Wnt-3a-induced beta-catenin and Akt/PKB signalling and reverses a Wnt-3a-imposed inhibition of in vitro mammary differentiation. Journal of molecular signaling *3*, 10.

Corton, J.M., Gillespie, J.G., and Hardie, D.G. (1994). Role of the AMP-activated protein kinase in the cellular stress response. Current biology : CB *4*, 315-324.

Crawford, L.J., Walker, B., Ovaa, H., Chauhan, D., Anderson, K.C., Morris, T.C., and Irvine, A.E. (2006). Comparative selectivity and specificity of the proteasome inhibitors BzLLLCOCHO, PS-341, and MG-132. Cancer research *66*, 6379-6386.

Cross, D.A., Alessi, D.R., Cohen, P., Andjelkovich, M., and Hemmings, B.A. (1995). Inhibition of glycogen synthase kinase-3 by insulin mediated by protein kinase B. Nature *378*, 785-789.

Cuthbertson, D.J., Steele, T., Wilding, J.P., Halford, J.C., Harrold, J.A., Hamer, M., and Karpe, F. (2017). What have human experimental overfeeding studies taught us about adipose tissue expansion and susceptibility to obesity and metabolic complications? International journal of obesity (2005) *41*, 853-865.

Czech, M.P. (2017). Insulin action and resistance in obesity and type 2 diabetes. Nature medicine *23*, 804-814.

Dahlman, I., Elsen, M., Tennagels, N., Korn, M., Brockmann, B., Sell, H., Eckel, J., and Arner, P. (2012). Functional annotation of the human fat cell secretome. Archives of physiology and biochemistry *118*, 84-91.

Das, S.K., and Elbein, S.C. (2006). The Genetic Basis of Type 2 Diabetes. Cellscience *2*, 100-131.

De Feyter, H.M., Lenaers, E., Houten, S.M., Schrauwen, P., Hesselink, M.K., Wanders, R.J., Nicolay, K., and Prompers, J.J. (2008). Increased intramyocellular lipid content but normal skeletal muscle mitochondrial oxidative capacity throughout the pathogenesis of type 2 diabetes. FASEB journal : official publication of the Federation of American Societies for Experimental Biology *22*, 3947-3955.

de Luca, C., and Olefsky, J.M. (2006). Stressed out about obesity and insulin resistance. Nature medicine *12*, 41-42; discussion 42.

DeFronzo, R.A. (1992). Pathogenesis of type 2 (non-insulin dependent) diabetes mellitus: a balanced overview. Diabetologia *35*, 389-397.

del Pozo, C.H., Calvo, R.M., Vesperinas-Garcia, G., Gomez-Ambrosi, J., Fruhbeck, G., Rubio, M.A., and Obregon, M.J. (2011). Expression profile in omental and subcutaneous adipose tissue from lean and obese subjects. Repression of lipolytic and lipogenic genes. Obesity surgery *21*, 633-643.

Desnoyers, L., Arnott, D., and Pennica, D. (2001). WISP-1 binds to decorin and biglycan. The Journal of biological chemistry *276*, 47599-47607.

Dietze, D., Koenen, M., Rohrig, K., Horikoshi, H., Hauner, H., and Eckel, J. (2002). Impairment of insulin signaling in human skeletal muscle cells by co-culture with human adipocytes. Diabetes *51*, 2369-2376.

Dich, J., Bro, B., Grunnet, N., Jensen, F., and Kondrup, J. (1983). Accumulation of triacylglycerol in cultured rat hepatocytes is increased by ethanol and by insulin and dexamethasone. The Biochemical journal *212*, 617-623.

Divertie, G.D., Jensen, M.D., and Miles, J.M. (1991). Stimulation of lipolysis in humans by physiological hypercortisolemia. Diabetes *40*, 1228-1232.

Dolinsky, V.W., Douglas, D.N., Lehner, R., and Vance, D.E. (2004). Regulation of the enzymes of hepatic microsomal triacylglycerol lipolysis and re-esterification by the glucocorticoid dexamethasone. The Biochemical journal *378*, 967-974.

Dong, X., Park, S., Lin, X., Copps, K., Yi, X., and White, M.F. (2006). Irs1 and Irs2 signaling is essential for hepatic glucose homeostasis and systemic growth. The Journal of clinical investigation *116*, 101-114.

Dong, X.C., Copps, K.D., Guo, S., Li, Y., Kollipara, R., DePinho, R.A., and White, M.F. (2008). Inactivation of hepatic Foxo1 by insulin signaling is required for adaptive nutrient homeostasis and endocrine growth regulation. Cell metabolism *8*, 65-76.

Donnelly, K.L., Smith, C.I., Schwarzenberg, S.J., Jessurun, J., Boldt, M.D., and Parks, E.J. (2005). Sources of fatty acids stored in liver and secreted via lipoproteins in patients with nonalcoholic fatty liver disease. The Journal of clinical investigation *115*, 1343-1351.

Eckstein, S.S., Weigert, C., and Lehmann, R. (2017). Divergent Roles of IRS (Insulin Receptor Substrate) 1 and 2 in Liver and Skeletal Muscle. Current medicinal chemistry *24*, 1827-1852.

Egan, B., and Zierath, J.R. (2013). Exercise metabolism and the molecular regulation of skeletal muscle adaptation. Cell metabolism *17*, 162-184.

Ehrlund, A., Mejhert, N., Lorente-Cebrian, S., Astrom, G., Dahlman, I., Laurencikiene, J., and Ryden, M. (2013). Characterization of the Wnt inhibitors secreted frizzled-related proteins (SFRPs) in human adipose tissue. The Journal of clinical endocrinology and metabolism *98*, E503-508.

Ekberg, K., Landau, B.R., Wajngot, A., Chandramouli, V., Efendic, S., Brunengraber, H., and Wahren, J. (1999). Contributions by kidney and liver to glucose production in the postabsorptive state and after 60 h of fasting. Diabetes *48*, 292-298.

Eldar-Finkelman, H., Schreyer, S.A., Shinohara, M.M., LeBoeuf, R.C., and Krebs, E.G. (1999). Increased glycogen synthase kinase-3 activity in diabetes- and obesity-prone C57BL/6J mice. Diabetes *48*, 1662-1666.

European Association for the Study of the Liver (EASL), European Association for the Study of Diabetes (EASD) and European Association for the Study of Obesity (EASO) (2016). Clinical Practice Guidelines for the management of non-alcoholic fatty liver disease. Journal of hepatology *64*, 1388-1402.

Fabbrini, E., Sullivan, S., and Klein, S. (2010). Obesity and nonalcoholic fatty liver disease: biochemical, metabolic, and clinical implications. Hepatology (Baltimore, Md.) *51*, 679-689.

Fasshauer, M., and Bluher, M. (2015). Adipokines in health and disease. Trends in pharmacological sciences *36*, 461-470.

Fawcett, J., Sang, H., Permana, P.A., Levy, J.L., and Duckworth, W.C. (2010). Insulin metabolism in human adipocytes from subcutaneous and visceral depots. Biochemical and biophysical research communications *402*, 762-766.

Febbraio, M.A., and Pedersen, B.K. (2005). Contraction-induced myokine production and release: is skeletal muscle an endocrine organ? Exercise and sport sciences reviews *33*, 114-119.

Fediuc, S., Gaidhu, M.P., and Ceddia, R.B. (2006). Regulation of AMP-activated protein kinase and acetyl-CoA carboxylase phosphorylation by palmitate in skeletal muscle cells. Journal of lipid research *47*, 412-420.

Ferguson, D., Shao, N., Heller, E., Feng, J., Neve, R., Kim, H.D., Call, T., Magazu, S., Shen, L., and Nestler, E.J. (2015). SIRT1-FOXO3a regulate cocaine actions in the nucleus accumbens. The Journal of neuroscience : the official journal of the Society for Neuroscience *35*, 3100-3111.

Ferrand, N., Bereziat, V., Moldes, M., Zaoui, M., Larsen, A.K., and Sabbah, M. (2017). WISP1/CCN4 inhibits adipocyte differentiation through repression of PPARgamma activity. Scientific reports *7*, 1749.

Ferrannini, E., Simonson, D.C., Katz, L.D., Reichard, G., Jr., Bevilacqua, S., Barrett, E.J., Olsson, M., and DeFronzo, R.A. (1988). The disposal of an oral glucose load in patients with non-insulin-dependent diabetes. Metabolism: clinical and experimental *37*, 79-85.

Ferrari, S.L., Deutsch, S., Choudhury, U., Chevalley, T., Bonjour, J.P., Dermitzakis, E.T., Rizzoli, R., and Antonarakis, S.E. (2004). Polymorphisms in the low-density lipoprotein receptor-related protein 5 (LRP5) gene are associated with variation in vertebral bone mass, vertebral bone size, and stature in whites. American journal of human genetics *74*, 866-875.

Fisher-Wellman, K.H., Gilliam, L.A., Lin, C.T., Cathey, B.L., Lark, D.S., and Neufer, P.D. (2013). Mitochondrial glutathione depletion reveals a novel role for the pyruvate dehydrogenase complex as a key H2O2-emitting source under conditions of nutrient overload. Free radical biology & medicine *65*, 1201-1208.

Fisher, F.M., Chui, P.C., Nasser, I.A., Popov, Y., Cunniff, J.C., Lundasen, T., Kharitonenkov, A., Schuppan, D., Flier, J.S., and Maratos-Flier, E. (2014). Fibroblast growth factor 21 limits lipotoxicity by promoting hepatic fatty acid activation in mice on methionine and choline-deficient diets. Gastroenterology *147*, 1073-1083.e1076.

Fon Tacer, K., and Rozman, D. (2011). Nonalcoholic Fatty liver disease: focus on lipoprotein and lipid deregulation. Journal of lipids *2011*, 783976.

Franch, H.A., and Price, S.R. (2005). Molecular signaling pathways regulating muscle proteolysis during atrophy. Current opinion in clinical nutrition and metabolic care *8*, 271-275.

Franke, T.F., Kaplan, D.R., Cantley, L.C., and Toker, A. (1997). Direct regulation of the Akt proto-oncogene product by phosphatidylinositol-3,4-bisphosphate. Science (New York, N.Y.) *275*, 665-668.

Franko, A., von Kleist-Retzow, J.C., Neschen, S., Wu, M., Schommers, P., Bose, M., Kunze, A., Hartmann, U., Sanchez-Lasheras, C., Stoehr, O., et al. (2014). Liver adapts mitochondrial function to insulin resistant and diabetic states in mice. Journal of hepatology *60*, 816-823.

Freedland, E.S. (2004). Role of a critical visceral adipose tissue threshold (CVATT) in metabolic syndrome: implications for controlling dietary carbohydrates: a review. Nutrition & metabolism *1*, 12.

Frescas, D., Valenti, L., and Accili, D. (2005). Nuclear trapping of the forkhead transcription factor FoxO1 via Sirt-dependent deacetylation promotes expression of glucogenetic genes. The Journal of biological chemistry *280*, 20589-20595.

Froylich, D., Corcelles, R., Daigle, C., Boules, M., Brethauer, S., and Schauer, P. (2016). Effect of Roux-en-Y gastric bypass and sleeve gastrectomy on nonalcoholic fatty liver disease: a comparative study. Surgery for obesity and related diseases : official journal of the American Society for Bariatric Surgery *12*, 127-131.

Fruhbeck, G., Toplak, H., Woodward, E., Yumuk, V., Maislos, M., and Oppert, J.M. (2013). Obesity: the gateway to ill health - an EASO position statement on a rising public health, clinical and scientific challenge in Europe. Obesity facts *6*, 117-120.

Furuyama, T., Kitayama, K., Yamashita, H., and Mori, N. (2003). Forkhead transcription factor FOXO1 (FKHR)-dependent induction of PDK4 gene expression in skeletal muscle during energy deprivation. The Biochemical journal *375*, 365-371.

Gao, B., Jeong, W.I., and Tian, Z. (2008). Liver: An organ with predominant innate immunity. Hepatology (Baltimore, Md.) *47*, 729-736.

Garg, A. (2000). Lipodystrophies. The American journal of medicine *108*, 143-152.
Gathercole, L.L., Morgan, S.A., Bujalska, I.J., Hauton, D., Stewart, P.M., and Tomlinson, J.W. (2011). Regulation of lipogenesis by glucocorticoids and insulin in human adipose tissue. PloS one *6*, e26223.

Garcia-Hoyos, M., Cantalapiedra, D., Arroyo, C., Esteve, P., Rodriguez, J., Riveiro, R., Trujillo, M.J., Ramos, C., Bovolenta, P., and Ayuso, C. (2004). Evaluation of SFRP1 as a candidate for human retinal dystrophies. Molecular vision *10*, 426-431.

Garufi, G., Seyhan, A.A., and Pasarica, M. (2015). Elevated secreted frizzled-related protein 4 in obesity: a potential role in adipose tissue dysfunction. Obesity (Silver Spring, Md.) *23*, 24-27.

Ge, X., Chen, C., Hui, X., Wang, Y., Lam, K.S., and Xu, A. (2011). Fibroblast growth factor 21 induces glucose transporter-1 expression through activation of the serum response factor/Ets-like protein-1 in adipocytes. The Journal of biological chemistry *286*, 34533-34541.

Ge, F., Zhou, S., Hu, C., Lobdell, H.t., and Berk, P.D. (2010). Insulin- and leptin-regulated fatty acid uptake plays a key causal role in hepatic steatosis in mice with intact leptin signaling but not in ob/ob or db/db mice. American journal of physiology. Gastrointestinal and liver physiology *299*, G855-866.

Gimeno, R.E., and Moller, D.E. (2014). FGF21-based pharmacotherapy--potential utility for metabolic disorders. Trends in endocrinology and metabolism: TEM *25*, 303-311.

Gomes, M.D., Lecker, S.H., Jagoe, R.T., Navon, A., and Goldberg, A.L. (2001). Atrogin-1, a muscle-specific F-box protein highly expressed during muscle atrophy. Proceedings of the National Academy of Sciences of the United States of America *98*, 14440-14445.

Gonzalez, E., and McGraw, T.E. (2009). The Akt kinases: isoform specificity in metabolism and cancer. Cell cycle (Georgetown, Tex.) *8*, 2502-2508.

Goodyear, L.J., Giorgino, F., Sherman, L.A., Carey, J., Smith, R.J., and Dohm, G.L. (1995). Insulin receptor phosphorylation, insulin receptor substrate-1 phosphorylation, and phosphatidylinositol 3-kinase activity are decreased in intact skeletal muscle strips from obese subjects. The Journal of clinical investigation *95*, 2195-2204.

Goralski, K.B., McCarthy, T.C., Hanniman, E.A., Zabel, B.A., Butcher, E.C., Parlee, S.D., Muruganandan, S., and Sinal, C.J. (2007). Chemerin, a novel adipokine that regulates adipogenesis and adipocyte metabolism. The Journal of biological chemistry *282*, 28175-28188.

Grant, S.F., Thorleifsson, G., Reynisdottir, I., Benediktsson, R., Manolescu, A., Sainz, J., Helgason, A., Stefansson, H., Emilsson, V., Helgadottir, A., et al. (2006). Variant of transcription factor 7-like 2 (TCF7L2) gene confers risk of type 2 diabetes. Nature genetics *38*, 320-323.

Greer, E.L., Dowlatshahi, D., Banko, M.R., Villen, J., Hoang, K., Blanchard, D., Gygi, S.P., and Brunet, A. (2007). An AMPK-FOXO pathway mediates longevity induced by a novel method of dietary restriction in C. elegans. Current biology : CB *17*, 1646-1656.

Greene, M.W., Sakaue, H., Wang, L., Alessi, D.R., and Roth, R.A. (2003). Modulation of insulin-stimulated degradation of human insulin receptor substrate-1 by Serine 312 phosphorylation. The Journal of biological chemistry *278*, 8199-8211.

Gurbuz, I., and Chiquet-Ehrismann, R. (2015). CCN4/WISP1 (WNT1 inducible signaling pathway protein 1): a focus on its role in cancer. The international journal of biochemistry & cell biology *62*, 142-146.

Gustafson, B., Hammarstedt, A., Hedjazifar, S., and Smith, U. (2013). Restricted adipogenesis in hypertrophic obesity: the role of WISP2, WNT, and BMP4. Diabetes *62*, 2997-3004.

Hamrick, M.W., Herberg, S., Arounleut, P., He, H.Z., Shiver, A., Qi, R.Q., Zhou, L., Isales, C.M., and Mi, Q.S. (2010). The adipokine leptin increases skeletal muscle mass and significantly alters skeletal muscle miRNA expression profile in aged mice. Biochemical and biophysical research communications *400*, 379-383.

Hanke, S., and Mann, M. (2009). The phosphotyrosine interactome of the insulin receptor family and its substrates IRS-1 and IRS-2. Molecular & cellular proteomics : MCP *8*, 519-534.

Hardie, D.G., Ross, F.A., and Hawley, S.A. (2012). AMPK: a nutrient and energy sensor that maintains energy homeostasis. Nature reviews. Molecular cell biology *13*, 251-262.

Hartwig, S., Raschke, S., Knebel, B., Scheler, M., Irmler, M., Passlack, W., Muller, S., Hanisch, F.G., Franz, T., Li, X., et al. (2014). Secretome profiling of primary human skeletal muscle cells. Biochimica et biophysica acta *1844*, 1011-1017.

Hessvik, N.P., Bakke, S.S., Fredriksson, K., Boekschoten, M.V., Fjorkenstad, A., Koster, G., Hesselink, M.K., Kersten, S., Kase, E.T., Rustan, A.C., et al. (2010). Metabolic switching of human myotubes is improved by n-3 fatty acids. Journal of lipid research *51*, 2090-2104.

Hoang, B., Moos, M., Jr., Vukicevic, S., and Luyten, F.P. (1996). Primary structure and tissue distribution of FRZB, a novel protein related to Drosophila frizzled, suggest a role in skeletal morphogenesis. The Journal of biological chemistry *271*, 26131-26137.

Holbourn, K.P., Acharya, K.R., and Perbal, B. (2008). The CCN family of proteins: structure-function relationships. Trends in biochemical sciences *33*, 461-473.

Holland, W.L., Miller, R.A., Wang, Z.V., Sun, K., Barth, B.M., Bui, H.H., Davis, K.E., Bikman, B.T., Halberg, N., Rutkowski, J.M., et al. (2011). Receptor-mediated activation of ceramidase activity initiates the pleiotropic actions of adiponectin. Nature medicine *17*, 55-63.

Hollie, N.I., and Hui, D.Y. (2011). Group 1B phospholipase A(2) deficiency protects against diet-induced hyperlipidemia in mice. Journal of lipid research *52*, 2005-2011.

Hörbelt, T., Tacke, C., Markova, M., Herzfeld de Wiza, D., Van de Velde, F., Bekaert, M., Van Nieuwenhove, Y., Hornemann, S., Rodiger, M., Seebeck, N., et al. (2018). The novel adipokine WISP1 associates with insulin resistance and impairs insulin action in human myotubes and mouse hepatocytes. Diabetologia.

Houmard, J.A. (2008). Intramuscular lipid oxidation and obesity. American journal of physiology. Regulatory, integrative and comparative physiology *294*, R1111-1116.

Hoyumpa, A.M., Jr., Greene, H.L., Dunn, G.D., and Schenker, S. (1975). Fatty liver: biochemical and clinical considerations. The American journal of digestive diseases *20*, 1142-1170.

Huang, H., Regan, K.M., Wang, F., Wang, D., Smith, D.I., van Deursen, J.M., and Tindall, D.J. (2005). Skp2 inhibits FOXO1 in tumor suppression through ubiquitin-mediated degradation. Proceedings of the National Academy of Sciences of the United States of America *102*, 1649-1654.

Ibrahim, M.M. (2010). Subcutaneous and visceral adipose tissue: structural and functional differences. Obesity reviews : an official journal of the International Association for the Study of Obesity *11*, 11-18.

Ide, T., Shimano, H., Yahagi, N., Matsuzaka, T., Nakakuki, M., Yamamoto, T., Nakagawa, Y., Takahashi, A., Suzuki, H., Sone, H., et al. (2004). SREBPs suppress IRS-2-mediated insulin signalling in the liver. Nature cell biology *6*, 351-357.

Inkson, C.A., Ono, M., Kuznetsov, S.A., Fisher, L.W., Robey, P.G., and Young, M.F. (2008). TGF-beta1 and WISP-1/CCN-4 can regulate each other's activity to cooperatively control osteoblast function. Journal of cellular biochemistry *104*, 1865-1878.

International Diabetes Federation (IDF) (2010). Diabetes Atlas. Eighth Edition.

Irimia, J.M., Meyer, C.M., Segvich, D.M., Surendran, S., DePaoli-Roach, A.A., Morral, N., and Roach, P.J. (2017). Lack of liver glycogen causes hepatic insulin resistance and steatosis in mice. The Journal of biological chemistry *292*, 10455-10464.

Itoh, N. (2014). FGF21 as a Hepatokine, Adipokine, and Myokine in Metabolism and Diseases. Frontiers in endocrinology *5*, 107.

Iwabu, M., Yamauchi, T., Okada-Iwabu, M., Sato, K., Nakagawa, T., Funata, M., Yamaguchi, M., Namiki, S., Nakayama, R., Tabata, M., et al. (2010). Adiponectin and AdipoR1 regulate PGC-1alpha and mitochondria by Ca(2+) and AMPK/SIRT1. Nature *464*, 1313-1319.

Jager, S., Groll, M., Huber, R., Wolf, D.H., and Heinemeyer, W. (1999). Proteasome beta-type subunits: unequal roles of propeptides in core particle maturation and a hierarchy of active site function. Journal of molecular biology *291*, 997-1013.

Janssen, I., Heymsfield, S.B., Baumgartner, R.N., and Ross, R. (2000). Estimation of skeletal muscle mass by bioelectrical impedance analysis. Journal of applied physiology (Bethesda, Md. : 1985) *89*, 465-471.

Jelenik, T., Kaul, K., Sequaris, G., Flogel, U., Phielix, E., Kotzka, J., Knebel, B., Fahlbusch, P., Horbelt, T., Lehr, S., et al. (2017). Mechanisms of Insulin Resistance in Primary and Secondary Nonalcoholic Fatty Liver. Diabetes *66*, 2241-2253.

Jensen, M.D. (2008). Role of body fat distribution and the metabolic complications of obesity. The Journal of clinical endocrinology and metabolism *93*, S57-63.

Jho, E.H., Zhang, T., Domon, C., Joo, C.K., Freund, J.N., and Costantini, F. (2002). Wnt/beta-catenin/Tcf signaling induces the transcription of Axin2, a negative regulator of the signaling pathway. Molecular and cellular biology *22*, 1172-1183.

Jian, Y.C., Wang, J.J., Dong, S., Hu, J.W., Hu, L.J., Yang, G.M., Zheng, Y.X., and Xiong, W.J. (2014). Wnt-induced secreted protein 1/CCN4 in liver fibrosis both in vitro and in vivo. Clinical laboratory *60*, 29-35.

Jun, J.I., and Lau, L.F. (2011). Taking aim at the extracellular matrix: CCN proteins as emerging therapeutic targets. Nature reviews. Drug discovery *10*, 945-963.

Jung, T.W., Kang, C., Goh, J., Chae, S.I., Kim, H.C., Lee, T.J., Abd El-Aty, A.M., and Jeong, J.H. (2018). WISP1 promotes non-alcoholic fatty liver disease and skeletal muscle insulin resistance via TLR4/JNK signaling. Journal of cellular physiology.

Kadowaki, T., Yamauchi, T., Kubota, N., Hara, K., Ueki, K., and Tobe, K. (2006). Adiponectin and adiponectin receptors in insulin resistance, diabetes, and the metabolic syndrome. The Journal of clinical investigation *116*, 1784-1792.

Kahn, B.B., Alquier, T., Carling, D., and Hardie, D.G. (2005). AMP-activated protein kinase: ancient energy gauge provides clues to modern understanding of metabolism. Cell metabolism *1*, 15-25.

Kamada, Y., Tamura, S., Kiso, S., Matsumoto, H., Saji, Y., Yoshida, Y., Fukui, K., Maeda, N., Nishizawa, H., Nagaretani, H., et al. (2003). Enhanced carbon tetrachloride-induced liver fibrosis in mice lacking adiponectin. Gastroenterology *125*, 1796-1807.

Kamei, Y., Mizukami, J., Miura, S., Suzuki, M., Takahashi, N., Kawada, T., Taniguchi, T., and Ezaki, O. (2003). A forkhead transcription factor FKHR up-regulates lipoprotein lipase expression in skeletal muscle. FEBS letters *536*, 232-236.

Kanazawa, A., Tsukada, S., Sekine, A., Tsunoda, T., Takahashi, A., Kashiwagi, A., Tanaka, Y., Babazono, T., Matsuda, M., Kaku, K., et al. (2004). Association of the gene encoding wingless-type mammary tumor virus integration-site family member 5B (WNT5B) with type 2 diabetes. American journal of human genetics *75*, 832-843.

Kato, S., Ding, J., Pisck, E., Jhala, U.S., and Du, K. (2008). COP1 functions as a FoxO1 ubiquitin E3 ligase to regulate FoxO1-mediated gene expression. The Journal of biological chemistry *283*, 35464-35473.

Kawano, Y., and Cohen, D.E. (2013). Mechanisms of hepatic triglyceride accumulation in non-alcoholic fatty liver disease. Journal of gastroenterology *48*, 434-441.

Kelley, D.E., and Mandarino, L.J. (2000). Fuel selection in human skeletal muscle in insulin resistance: a reexamination. Diabetes *49*, 677-683.

Kelly, T., Yang, W., Chen, C.S., Reynolds, K., and He, J. (2008). Global burden of obesity in 2005 and projections to 2030. International journal of obesity (2005) *32*, 1431-1437.
Kiens, B. (2006). Skeletal muscle lipid metabolism in exercise and insulin resistance. Physiological reviews *86*, 205-243.

Kim, D., and Kim, W.R. (2017). Nonobese Fatty Liver Disease. Clinical gastroenterology and hepatology : the official clinical practice journal of the American Gastroenterological Association *15*, 474-485.

Kim, D.H., Burgess, A.P., Li, M., Tsenovoy, P.L., Addabbo, F., McClung, J.A., Puri, N., and Abraham, N.G. (2008a). Heme oxygenase-mediated increases in adiponectin decrease fat content and inflammatory cytokines tumor necrosis factor-alpha and interleukin-6 in Zucker rats and reduce adipogenesis in human mesenchymal stem cells. The Journal of pharmacology and experimental therapeutics *325*, 833-840.

Kim, J.A., Wei, Y., and Sowers, J.R. (2008b). Role of mitochondrial dysfunction in insulin resistance. Circulation research *102*, 401-414.

Kim, J.Y., van de Wall, E., Laplante, M., Azzara, A., Trujillo, M.E., Hofmann, S.M., Schraw, T., Durand, J.L., Li, H., Li, G., et al. (2007). Obesity-associated improvements in metabolic profile through expansion of adipose tissue. The Journal of clinical investigation *117*, 2621-2637.

Kim, J.K., Gavrilova, O., Chen, Y., Reitman, M.L., and Shulman, G.I. (2000). Mechanism of insulin resistance in A-ZIP/F-1 fatless mice. The Journal of biological chemistry *275*, 8456-8460.

Kim, K.S., Park, K.S., Kim, M.J., Kim, S.K., Cho, Y.W., and Park, S.W. (2014). Type 2 diabetes is associated with low muscle mass in older adults. Geriatrics & gerontology international *14 Suppl 1*, 115-121.

Kisselev, A.F., and Goldberg, A.L. (2001). Proteasome inhibitors: from research tools to drug candidates. Chemistry & biology *8*, 739-758.

Klee, S., Lehmann, M., Wagner, D.E., Baarsma, H.A., and Konigshoff, M. (2016). WISP1 mediates IL-6-dependent proliferation in primary human lung fibroblasts. Scientific reports *6*, 20547.

Kleiner, D.E., Brunt, E.M., Van Natta, M., Behling, C., Contos, M.J., Cummings, O.W., Ferrell, L.D., Liu, Y.C., Torbenson, M.S., Unalp-Arida, A., et al. (2005). Design and validation of a histological scoring system for nonalcoholic fatty liver disease. Hepatology (Baltimore, Md.) *41*, 1313-1321.

Kloting, N., Fasshauer, M., Dietrich, A., Kovacs, P., Schon, M.R., Kern, M., Stumvoll, M., and Bluher, M. (2010). Insulin-sensitive obesity. American journal of physiology. Endocrinology and metabolism *299*, E506-515.

Knebel, B., Haas, J., Hartwig, S., Jacob, S., Kollmer, C., Nitzgen, U., Muller-Wieland, D., and Kotzka, J. (2012). Liver-specific expression of transcriptionally active SREBP-1c is associated with fatty liver and increased visceral fat mass. PloS one *7*, e31812.

Knebel, B., Hartwig, S., Haas, J., Lehr, S., Goeddeke, S., Susanto, F., Bohne, L., Jacob, S., Koellmer, C., Nitzgen, U., et al. (2015). Peroxisomes compensate hepatic lipid overflow in mice with fatty liver. Biochimica et biophysica acta *1851*, 965-976.

Knebel, B., Hartwig, S., Jacob, S., Kettel, U., Schiller, M., Passlack, W., Koellmer, C., Lehr, S., Muller-Wieland, D., and Kotzka, J. (2018). Inactivation of SREBP-1a Phosphorylation Prevents Fatty Liver Disease in Mice: Identification of Related Signaling Pathways by Gene Expression Profiles in Liver and Proteomes of Peroxisomes. International journal of molecular sciences *19*.

Koh, A., Lee, M.N., Yang, Y.R., Jeong, H., Ghim, J., Noh, J., Kim, J., Ryu, D., Park, S., Song, P., et al. (2013). C1-Ten is a protein tyrosine phosphatase of insulin receptor substrate 1 (IRS-1), regulating IRS-1 stability and muscle atrophy. Molecular and cellular biology *33*, 1608-1620.

Komolka, K., Albrecht, E., Wimmers, K., Michal, J.J., and Maak, S. (2014). Molecular heterogeneities of adipose depots - potential effects on adipose-muscle cross-talk in humans, mice and farm animals. Journal of genomics *2*, 31-44.

Konigshoff, M., Kramer, M., Balsara, N., Wilhelm, J., Amarie, O.V., Jahn, A., Rose, F., Fink, L., Seeger, W., Schaefer, L., et al. (2009). WNT1-inducible signaling protein-1 mediates pulmonary fibrosis in mice and is upregulated in humans with idiopathic pulmonary fibrosis. The Journal of clinical investigation *119*, 772-787.

Koliaki, C., Szendroedi, J., Kaul, K., Jelenik, T., Nowotny, P., Jankowiak, F., Herder, C., Carstensen, M., Krausch, M., Knoefel, W.T., et al. (2015). Adaptation of hepatic mitochondrial function in humans with non-alcoholic fatty liver is lost in steatohepatitis. Cell metabolism *21*, 739-746.

Krook, A., Roth, R.A., Jiang, X.J., Zierath, J.R., and Wallberg-Henriksson, H. (1998). Insulin-stimulated Akt kinase activity is reduced in skeletal muscle from NIDDM subjects. Diabetes *47*, 1281-1286.

Korner, Z., Fontes-Oliveira, C.C., Holmberg, J., Carmignac, V., and Durbeej, M. (2014). Bortezomib partially improves laminin alpha2 chain-deficient muscular dystrophy. The American journal of pathology *184*, 1518-1528.

Kotzka, J., Knebel, B., Haas, J., Kremer, L., Jacob, S., Hartwig, S., Nitzgen, U., and Muller-Wieland, D. (2012). Preventing phosphorylation of sterol regulatory element-binding protein 1a by MAP-kinases protects mice from fatty liver and visceral obesity. PloS one *7*, e32609.

Kozakowska, M., Szade, K., Dulak, J., and Jozkowicz, A. (2014). Role of heme oxygenase-1 in postnatal differentiation of stem cells: a possible cross-talk with microRNAs. Antioxidants & redox signaling *20*, 1827-1850.

Krawiec, B.J., Nystrom, G.J., Frost, R.A., Jefferson, L.S., and Lang, C.H. (2007). AMP-activated protein kinase agonists increase mRNA content of the muscle-specific ubiquitin ligases MAFbx and MuRF1 in C2C12 cells. American journal of physiology. Endocrinology and metabolism *292*, E1555-1567.

Krssak, M., Brehm, A., Bernroider, E., Anderwald, C., Nowotny, P., Dalla Man, C., Cobelli, C., Cline, G.W., Shulman, G.I., Waldhausl, W., et al. (2004). Alterations in postprandial hepatic glycogen metabolism in type 2 diabetes. Diabetes *53*, 3048-3056.

Kumashiro, N., Erion, D.M., Zhang, D., Kahn, M., Beddow, S.A., Chu, X., Still, C.D., Gerhard, G.S., Han, X., Dziura, J., et al. (2011). Cellular mechanism of insulin resistance in nonalcoholic fatty liver disease. Proceedings of the National Academy of Sciences of the United States of America *108*, 16381-16385.

Lacher, M.D., Siegenthaler, A., Jager, R., Yan, X., Hett, S., Xuan, L., Saurer, S., Lareu, R.R., Dharmarajan, A.M., and Friis, R. (2003). Role of DDC-4/sFRP-4, a secreted frizzled-related protein, at the onset of apoptosis in mammary involution. Cell death and differentiation *10*, 528-538.

Lambernd, S., Taube, A., Schober, A., Platzbecker, B., Gorgens, S.W., Schlich, R., Jeruschke, K., Weiss, J., Eckardt, K., and Eckel, J. (2012). Contractile activity of human skeletal muscle cells prevents insulin resistance by inhibiting pro-inflammatory signalling pathways. Diabetologia *55*, 1128-1139.

Leask, A., and Abraham, D.J. (2006). All in the CCN family: essential matricellular signaling modulators emerge from the bunker. Journal of cell science *119*, 4803-4810.

Lecker, S.H., Goldberg, A.L., and Mitch, W.E. (2006). Protein degradation by the ubiquitin-proteasome pathway in normal and disease states. Journal of the American Society of Nephrology : JASN *17*, 1807-1819.

Lecker, S.H., Solomon, V., Mitch, W.E., and Goldberg, A.L. (1999). Muscle protein breakdown and the critical role of the ubiquitin-proteasome pathway in normal and disease states. The Journal of nutrition *129*, 227s-237s.

Leenders, M., Verdijk, L.B., van der Hoeven, L., Adam, J.J., van Kranenburg, J., Nilwik, R., and van Loon, L.J. (2013). Patients with type 2 diabetes show a greater decline in muscle mass, muscle strength, and functional capacity with aging. Journal of the American Medical Directors Association *14*, 585-592.

Lefort, N., Glancy, B., Bowen, B., Willis, W.T., Bailowitz, Z., De Filippis, E.A., Brophy, C., Meyer, C., Hojlund, K., Yi, Z., et al. (2010). Increased reactive oxygen species production and lower abundance of complex I subunits and carnitine palmitoyltransferase 1B protein despite normal mitochondrial respiration in insulin-resistant human skeletal muscle. Diabetes *59*, 2444-2452.

Lehr, S., Hartwig, S., Lamers, D., Famulla, S., Muller, S., Hanisch, F.G., Cuvelier, C., Ruige, J., Eckardt, K., Ouwens, D.M., et al. (2012a). Identification and validation of novel adipokines released from primary human adipocytes. Molecular & cellular proteomics : MCP *11*, M111.010504.

Lee, A.V., Gooch, J.L., Oesterreich, S., Guler, R.L., and Yee, D. (2000). Insulin-like growth factor I-induced degradation of insulin receptor substrate 1 is mediated by the 26S proteasome and blocked by phosphatidylinositol 3'-kinase inhibition. Molecular and cellular biology *20*, 1489-1496.

Lehr, S., Hartwig, S., and Sell, H. (2012b). Adipokines: a treasure trove for the discovery of biomarkers for metabolic disorders. Proteomics. Clinical applications *6*, 91-101.

Lehtinen, M.K., Yuan, Z., Boag, P.R., Yang, Y., Villen, J., Becker, E.B., DiBacco, S., de la Iglesia, N., Gygi, S., Blackwell, T.K., et al. (2006). A conserved MST-FOXO signaling pathway mediates oxidative-stress responses and extends life span. Cell *125*, 987-1001.

Leitner, D.R., Fruhbeck, G., Yumuk, V., Schindler, K., Micic, D., Woodward, E., and Toplak, H. (2017). Obesity and Type 2 Diabetes: Two Diseases with a Need for Combined Treatment Strategies - EASO Can Lead the Way. Obesity facts *10*, 483-492.

Levy, J.C., Matthews, D.R., and Hermans, M.P. (1998). Correct homeostasis model assessment (HOMA) evaluation uses the computer program. Diabetes care *21*, 2191-2192.

Lewis, M.C., Phillips, M.L., Slavotinek, J.P., Kow, L., Thompson, C.H., and Toouli, J. (2006). Change in liver size and fat content after treatment with Optifast very low calorie diet. Obesity surgery *16*, 697-701.

Leyns, L., Bouwmeester, T., Kim, S.H., Piccolo, S., and De Robertis, E.M. (1997). Frzb-1 is a secreted antagonist of Wnt signaling expressed in the Spemann organizer. Cell *88*, 747-756.

Li, M., Kim, D.H., Tsenovoy, P.L., Peterson, S.J., Rezzani, R., Rodella, L.F., Aronow, W.S., Ikehara, S., and Abraham, N.G. (2008). Treatment of obese diabetic mice with a heme oxygenase inducer reduces visceral and subcutaneous adiposity, increases adiponectin levels, and improves insulin sensitivity and glucose tolerance. Diabetes *57*, 1526-1535.

Li, M., Peterson, S., Husney, D., Inaba, M., Guo, K., Kappas, A., Ikehara, S., and Abraham, N.G. (2007). Long-lasting expression of HO-1 delays progression of type I diabetes in NOD mice. Cell cycle (Georgetown, Tex.) *6*, 567-571.

Li, S., Tan, H.Y., Wang, N., Zhang, Z.J., Lao, L., Wong, C.W., and Feng, Y. (2015). The Role of Oxidative Stress and Antioxidants in Liver Diseases. International journal of molecular sciences *16*, 26087-26124.

Lin, K., Wang, S., Julius, M.A., Kitajewski, J., Moos, M., Jr., and Luyten, F.P. (1997). The cysteine-rich frizzled domain of Frzb-1 is required and sufficient for modulation of Wnt signaling. Proceedings of the National Academy of Sciences of the United States of America *94*, 11196-11200.

Lin, Y., and Sun, Z. (2010). Current views on type 2 diabetes. The Journal of endocrinology *204*, 1-11.

Liu, H., Fergusson, M.M., Wu, J.J., Rovira, II, Liu, J., Gavrilova, O., Lu, T., Bao, J., Han, D., Sack, M.N., et al. (2011). Wnt signaling regulates hepatic metabolism. Science signaling *4*, ra6.

Logan, C.Y., and Nusse, R. (2004). The Wnt signaling pathway in development and disease. Annual review of cell and developmental biology *20*, 781-810.

Lopez-Bermejo, A., Khosravi, J., Fernandez-Real, J.M., Hwa, V., Pratt, K.L., Casamitjana, R., Garcia-Gil, M.M., Rosenfeld, R.G., and Ricart, W. (2006). Insulin resistance is associated with increased serum concentration of IGF-binding protein-related protein 1 (IGFBP-rP1/MAC25). Diabetes *55*, 2333-2339.

Lopez-Velazquez, J.A., Silva-Vidal, K.V., Ponciano-Rodriguez, G., Chavez-Tapia, N.C., Arrese, M., Uribe, M., and Mendez-Sanchez, N. (2014). The prevalence of nonalcoholic fatty liver disease in the Americas. Annals of hepatology *13*, 166-178.

Lorenzatti, G., Huang, W., Pal, A., Cabanillas, A.M., and Kleer, C.G. (2011). CCN6 (WISP3) decreases ZEB1-mediated EMT and invasion by attenuation of IGF-1 receptor signaling in breast cancer. Journal of cell science *124*, 1752-1758.

Lowell, B.B., and Shulman, G.I. (2005). Mitochondrial dysfunction and type 2 diabetes. Science (New York, N.Y.) *307*, 384-387.

Lu, M., Wan, M., Leavens, K.F., Chu, Q., Monks, B.R., Fernandez, S., Ahima, R.S., Ueki, K., Kahn, C.R., and Birnbaum, M.J. (2012). Insulin regulates liver metabolism in vivo in the absence of hepatic Akt and Foxo1. Nature medicine *18*, 388-395.

Ludwig, J., Viggiano, T.R., McGill, D.B., and Oh, B.J. (1980). Nonalcoholic steatohepatitis: Mayo Clinic experiences with a hitherto unnamed disease. Mayo Clinic proceedings *55*, 434-438.

MacDonald, B.T., Tamai, K., and He, X. (2009). Wnt/beta-catenin signaling: components, mechanisms, and diseases. Developmental cell *17*, 9-26.

Maeda, A., Ono, M., Holmbeck, K., Li, L., Kilts, T.M., Kram, V., Noonan, M.L., Yoshioka, Y., McNerny, E.M., Tantillo, M.A., et al. (2015). WNT1-induced Secreted Protein-1 (WISP1), a Novel Regulator of Bone Turnover and Wnt Signaling. The Journal of biological chemistry *290*, 14004-14018.

Magana, M.M., Lin, S.S., Dooley, K.A., and Osborne, T.F. (1997). Sterol regulation of acetyl coenzyme A carboxylase promoter requires two interdependent binding sites for sterol regulatory element binding proteins. Journal of lipid research *38*, 1630-1638.

Magana, M.M., and Osborne, T.F. (1996). Two tandem binding sites for sterol regulatory element binding proteins are required for sterol regulation of fatty-acid synthase promoter. The Journal of biological chemistry *271*, 32689-32694.

Maganga, R., Giles, N., Adcroft, K., Unni, A., Keeney, D., Wood, F., Fear, M., and Dharmarajan, A. (2008). Secreted Frizzled related protein-4 (sFRP4) promotes epidermal differentiation and apoptosis. Biochemical and biophysical research communications *377*, 606-611.

Magnusson, I., Rothman, D.L., Katz, L.D., Shulman, R.G., and Shulman, G.I. (1992). Increased rate of gluconeogenesis in type II diabetes mellitus. A 13C nuclear magnetic resonance study. The Journal of clinical investigation *90*, 1323-1327.

Mahdi, T., Hanzelmann, S., Salehi, A., Muhammed, S.J., Reinbothe, T.M., Tang, Y., Axelsson, A.S., Zhou, Y., Jing, X., Almgren, P., et al. (2012). Secreted frizzled-related protein 4 reduces insulin secretion and is overexpressed in type 2 diabetes. Cell metabolism *16*, 625-633.

Marchesini, G., Bugianesi, E., Forlani, G., Cerrelli, F., Lenzi, M., Manini, R., Natale, S., Vanni, E., Villanova, N., Melchionda, N., et al. (2003). Nonalcoholic fatty liver, steatohepatitis, and the metabolic syndrome. Hepatology (Baltimore, Md.) *37*, 917-923.

Margalit, O., Eisenbach, L., Amariglio, N., Kaminski, N., Harmelin, A., Pfeffer, R., Shohat, M., Rechavi, G., and Berger, R. (2003). Overexpression of a set of genes, including WISP-1, common to pulmonary metastases of both mouse D122 Lewis lung carcinoma and B16-F10.9 melanoma cell lines. British journal of cancer *89*, 314-319.

Mastaitis, J., Eckersdorff, M., Min, S., Xin, Y., Cavino, K., Aglione, J., Okamoto, H., Na, E., Stitt, T., Dominguez, M.G., et al. (2015). Loss of SFRP4 Alters Body Size, Food Intake, and Energy Expenditure in Diet-Induced Obese Male Mice. Endocrinology *156*, 4502-4510.

Matsumoto, M., Han, S., Kitamura, T., and Accili, D. (2006). Dual role of transcription factor FoxO1 in controlling hepatic insulin sensitivity and lipid metabolism. The Journal of clinical investigation *116*, 2464-2472.

Matsumoto, M., Pocai, A., Rossetti, L., Depinho, R.A., and Accili, D. (2007). Impaired regulation of hepatic glucose production in mice lacking the forkhead transcription factor Foxo1 in liver. Cell metabolism *6*, 208-216.

Masuoka, H.C., and Chalasani, N. (2013). Nonalcoholic fatty liver disease: an emerging threat to obese and diabetic individuals. Annals of the New York Academy of Sciences *1281*, 106-122.

Matsuzaki, H., Daitoku, H., Hatta, M., Aoyama, H., Yoshimochi, K., and Fukamizu, A. (2005). Acetylation of Foxo1 alters its DNA-binding ability and sensitivity to phosphorylation. Proceedings of the National Academy of Sciences of the United States of America *102*, 11278-11283.

Matthews, D.R., Hosker, J.P., Rudenski, A.S., Naylor, B.A., Treacher, D.F., and Turner, R.C. (1985). Homeostasis model assessment: insulin resistance and beta-cell function from fasting plasma glucose and insulin concentrations in man. Diabetologia *28*, 412-419.

Meyer, C., Dostou, J.M., Welle, S.L., and Gerich, J.E. (2002). Role of human liver, kidney, and skeletal muscle in postprandial glucose homeostasis. American journal of physiology. Endocrinology and metabolism *282*, E419-427.

Michelotti, G.A., Machado, M.V., and Diehl, A.M. (2013). NAFLD, NASH and liver cancer. Nature reviews. Gastroenterology & hepatology *10*, 656-665.

Misra, A., and Vikram, N.K. (2003). Clinical and pathophysiological consequences of abdominal adiposity and abdominal adipose tissue depots. Nutrition (Burbank, Los Angeles County, Calif.) *19*, 457-466.

Mohamed-Ali, V., Pinkney, J.H., and Coppack, S.W. (1998). Adipose tissue as an endocrine and paracrine organ. International journal of obesity and related metabolic disorders : journal of the International Association for the Study of Obesity *22*, 1145-1158.

Moore, M.C., Coate, K.C., Winnick, J.J., An, Z., and Cherrington, A.D. (2012). Regulation of hepatic glucose uptake and storage in vivo. Advances in nutrition (Bethesda, Md.) *3*, 286-294.

Mori, H., Prestwich, T.C., Reid, M.A., Longo, K.A., Gerin, I., Cawthorn, W.P., Susulic, V.S., Krishnan, V., Greenfield, A., and Macdougald, O.A. (2012). Secreted frizzled-related protein 5 suppresses adipocyte mitochondrial metabolism through WNT inhibition. The Journal of clinical investigation *122*, 2405-2416.

Morino, K., Petersen, K.F., Dufour, S., Befroy, D., Frattini, J., Shatzkes, N., Neschen, S., White, M.F., Bilz, S., Sono, S., et al. (2005). Reduced mitochondrial density and increased IRS-1 serine phosphorylation in muscle of insulin-resistant offspring of type 2 diabetic parents. The Journal of clinical investigation *115*, 3587-3593.

Muley, A., Majumder, S., Kolluru, G.K., Parkinson, S., Viola, H., Hool, L., Arfuso, F., Ganss, R., Dharmarajan, A., and Chatterjee, S. (2010). Secreted frizzled-related protein 4: an angiogenesis inhibitor. The American journal of pathology *176*, 1505-1516.

Munday, M.R., Campbell, D.G., Carling, D., and Hardie, D.G. (1988). Identification by amino acid sequencing of three major regulatory phosphorylation sites on rat acetyl-CoA carboxylase. European journal of biochemistry *175*, 331-338.

Mueller, K.M., Themanns, M., Friedbichler, K., Kornfeld, J.W., Esterbauer, H., Tuckermann, J.P., and Moriggl, R. (2012). Hepatic growth hormone and glucocorticoid receptor signaling in body

growth, steatosis and metabolic liver cancer development. Molecular and cellular endocrinology *361*, 1-11.

Muoio, D.M., Dohm, G.L., Fiedorek, F.T., Jr., Tapscott, E.B., and Coleman, R.A. (1997). Leptin directly alters lipid partitioning in skeletal muscle. Diabetes *46*, 1360-1363.

Murahovschi, V., Pivovarova, O., Ilkavets, I., Dmitrieva, R.M., Docke, S., Keyhani-Nejad, F., Gogebakan, O., Osterhoff, M., Kemper, M., Hornemann, S., et al. (2015). WISP1 is a novel adipokine linked to inflammation in obesity. Diabetes *64*, 856-866.

Nakae, J., Biggs, W.H., 3rd, Kitamura, T., Cavenee, W.K., Wright, C.V., Arden, K.C., and Accili, D. (2002). Regulation of insulin action and pancreatic beta-cell function by mutated alleles of the gene encoding forkhead transcription factor Foxo1. Nature genetics *32*, 245-253.

Nakae, J., Kitamura, T., Silver, D.L., and Accili, D. (2001). The forkhead transcription factor Foxo1 (Fkhr) confers insulin sensitivity onto glucose-6-phosphatase expression. The Journal of clinical investigation *108*, 1359-1367.

Nakao, R., Hirasaka, K., Goto, J., Ishidoh, K., Yamada, C., Ohno, A., Okumura, Y., Nonaka, I., Yasutomo, K., Baldwin, K.M., et al. (2009). Ubiquitin ligase Cbl-b is a negative regulator for insulin-like growth factor 1 signaling during muscle atrophy caused by unloading. Molecular and cellular biology *29*, 4798-4811.

Nakashima, K., and Yakabe, Y. (2007). AMPK activation stimulates myofibrillar protein degradation and expression of atrophy-related ubiquitin ligases by increasing FOXO transcription factors in C2C12 myotubes. Bioscience, biotechnology, and biochemistry *71*, 1650-1656.

Niehrs, C. (2012). The complex world of WNT receptor signalling. Nature reviews. Molecular cell biology *13*, 767-779.

Nikolic, N., Bakke, S.S., Kase, E.T., Rudberg, I., Flo Halle, I., Rustan, A.C., Thoresen, G.H., and Aas, V. (2012). Electrical pulse stimulation of cultured human skeletal muscle cells as an in vitro model of exercise. PloS one *7*, e33203.

Nikoulina, S.E., Ciaraldi, T.P., Mudaliar, S., Mohideen, P., Carter, L., and Henry, R.R. (2000). Potential role of glycogen synthase kinase-3 in skeletal muscle insulin resistance of type 2 diabetes. Diabetes *49*, 263-271.

Nordlie, R.C., Foster, J.D., and Lange, A.J. (1999). Regulation of glucose production by the liver. Annual review of nutrition *19*, 379-406.

Nusse, R., and Clevers, H. (2017). Wnt/beta-Catenin Signaling, Disease, and Emerging Therapeutic Modalities. Cell *169*, 985-999.

Ohashi, K., Shibata, R., Murohara, T., and Ouchi, N. (2014). Role of anti-inflammatory adipokines in obesity-related diseases. Trends in endocrinology and metabolism: TEM *25*, 348-355.

Ono, M., Inkson, C.A., Kilts, T.M., and Young, M.F. (2011). WISP-1/CCN4 regulates osteogenesis by enhancing BMP-2 activity. Journal of bone and mineral research : the official journal of the American Society for Bone and Mineral Research *26*, 193-208.

Ostler, J.E., Maurya, S.K., Dials, J., Roof, S.R., Devor, S.T., Ziolo, M.T., and Periasamy, M. (2014). Effects of insulin resistance on skeletal muscle growth and exercise capacity in type 2 diabetic mouse models. American journal of physiology. Endocrinology and metabolism *306*, E592-605.

Ouchi, N., Higuchi, A., Ohashi, K., Oshima, Y., Gokce, N., Shibata, R., Akasaki, Y., Shimono, A., and Walsh, K. (2010). Sfrp5 is an anti-inflammatory adipokine that modulates metabolic dysfunction in obesity. Science (New York, N.Y.) *329*, 454-457.

Ouchi, N., Parker, J.L., Lugus, J.J., and Walsh, K. (2011). Adipokines in inflammation and metabolic disease. Nature reviews. Immunology *11*, 85-97.

Palsgaard, J., Emanuelli, B., Winnay, J.N., Sumara, G., Karsenty, G., and Kahn, C.R. (2012). Cross-talk between insulin and Wnt signaling in preadipocytes: role of Wnt co-receptor low density lipoprotein receptor-related protein-5 (LRP5). The Journal of biological chemistry *287*, 12016-12026.

Parisi, M.S., Gazzerro, E., Rydziel, S., and Canalis, E. (2006). Expression and regulation of CCN genes in murine osteoblasts. Bone *38*, 671-677.

Park, S.W., Goodpaster, B.H., Lee, J.S., Kuller, L.H., Boudreau, R., de Rekeneire, N., Harris, T.B., Kritchevsky, S., Tylavsky, F.A., Nevitt, M., et al. (2009). Excessive loss of skeletal muscle mass in older adults with type 2 diabetes. Diabetes care *32*, 1993-1997.

Pedersen, B.K., and Febbraio, M.A. (2012). Muscles, exercise and obesity: skeletal muscle as a secretory organ. Nature reviews. Endocrinology *8*, 457-465.

Petersen, K.F., Oral, E.A., Dufour, S., Befroy, D., Ariyan, C., Yu, C., Cline, G.W., DePaoli, A.M., Taylor, S.I., Gorden, P., et al. (2002). Leptin reverses insulin resistance and hepatic steatosis in patients with severe lipodystrophy. The Journal of clinical investigation *109*, 1345-1350.

Petersen, M.C., Vatner, D.F., and Shulman, G.I. (2017). Regulation of hepatic glucose metabolism in health and disease. Nature reviews. Endocrinology *13*, 572-587.

Petersen, T.N., Brunak, S., von Heijne, G., and Nielsen, H. (2011). SignalP 4.0: discriminating signal peptides from transmembrane regions. Nature methods *8*, 785-786.

Pennica, D., Swanson, T.A., Welsh, J.W., Roy, M.A., Lawrence, D.A., Lee, J., Brush, J., Taneyhill, L.A., Deuel, B., Lew, M., et al. (1998). WISP genes are members of the connective tissue growth factor family that are up-regulated in wnt-1-transformed cells and aberrantly expressed in human colon tumors. Proceedings of the National Academy of Sciences of the United States of America *95*, 14717-14722.

Perry, R.J., Camporez, J.G., Kursawe, R., Titchenell, P.M., Zhang, D., Perry, C.J., Jurczak, M.J., Abudukadier, A., Han, M.S., Zhang, X.M., et al. (2015). Hepatic acetyl CoA links adipose tissue inflammation to hepatic insulin resistance and type 2 diabetes. Cell *160*, 745-758.

Perry, R.J., Samuel, V.T., Petersen, K.F., and Shulman, G.I. (2014). The role of hepatic lipids in hepatic insulin resistance and type 2 diabetes. Nature *510*, 84-91.

Pilkis, S.J., and Claus, T.H. (1991). Hepatic gluconeogenesis/glycolysis: regulation and structure/function relationships of substrate cycle enzymes. Annual review of nutrition *11*, 465-515.

Ponugoti, B., Kim, D.H., Xiao, Z., Smith, Z., Miao, J., Zang, M., Wu, S.Y., Chiang, C.M., Veenstra, T.D., and Kemper, J.K. (2010). SIRT1 deacetylates and inhibits SREBP-1C activity in regulation of hepatic lipid metabolism. The Journal of biological chemistry *285*, 33959-33970.

Puigserver, P., Rhee, J., Donovan, J., Walkey, C.J., Yoon, J.C., Oriente, F., Kitamura, Y., Altomonte, J., Dong, H., Accili, D., et al. (2003). Insulin-regulated hepatic gluconeogenesis through FOXO1-PGC-1alpha interaction. Nature *423*, 550-555.

Purushotham, A., Schug, T.T., Xu, Q., Surapureddi, S., Guo, X., and Li, X. (2009). Hepatocyte-specific deletion of SIRT1 alters fatty acid metabolism and results in hepatic steatosis and inflammation. Cell metabolism *9*, 327-338.

Racanelli, V., and Rehermann, B. (2006). The liver as an immunological organ. Hepatology (Baltimore, Md.) *43*, S54-62.

Raschke, S., Eckardt, K., Bjorklund Holven, K., Jensen, J., and Eckel, J. (2013). Identification and validation of novel contraction-regulated myokines released from primary human skeletal muscle cells. PloS one *8*, e62008.

Raso, A., and Biassoni, R. (2014). Twenty years of qPCR: a mature technology? Methods in molecular biology (Clifton, N.J.) *1160*, 1-3.

Rattner, A., Hsieh, J.C., Smallwood, P.M., Gilbert, D.J., Copeland, N.G., Jenkins, N.A., and Nathans, J. (1997). A family of secreted proteins contains homology to the cysteine-rich ligand-binding domain of frizzled receptors. Proceedings of the National Academy of Sciences of the United States of America *94*, 2859-2863.

Reaven, G.M. (2005). The insulin resistance syndrome: definition and dietary approaches to treatment. Annual review of nutrition *25*, 391-406.

Ritov, V.B., Menshikova, E.V., Azuma, K., Wood, R., Toledo, F.G., Goodpaster, B.H., Ruderman, N.B., and Kelley, D.E. (2010). Deficiency of electron transport chain in human skeletal muscle mitochondria in type 2 diabetes mellitus and obesity. American journal of physiology. Endocrinology and metabolism *298*, E49-58.

Roach, P.J. (2002). Glycogen and its metabolism. Current molecular medicine *2*, 101-120.

Romacho, T., Elsen, M., Rohrborn, D., and Eckel, J. (2014). Adipose tissue and its role in organ crosstalk. Acta physiologica (Oxford, England) *210*, 733-753.

Romeo, S., Kozlitina, J., Xing, C., Pertsemlidis, A., Cox, D., Pennacchio, L.A., Boerwinkle, E., Cohen, J.C., and Hobbs, H.H. (2008). Genetic variation in PNPLA3 confers susceptibility to nonalcoholic fatty liver disease. Nature genetics *40*, 1461-1465.

Ross, S.E., Hemati, N., Longo, K.A., Bennett, C.N., Lucas, P.C., Erickson, R.L., and MacDougald, O.A. (2000). Inhibition of adipogenesis by Wnt signaling. Science (New York, N.Y.) *289*, 950-953.

Roszmusz, E., Patthy, A., Trexler, M., and Patthy, L. (2001). Localization of disulfide bonds in the frizzled module of Ror1 receptor tyrosine kinase. The Journal of biological chemistry *276*, 18485-18490.

Rotter, V., Nagaev, I., and Smith, U. (2003). Interleukin-6 (IL-6) induces insulin resistance in 3T3-L1 adipocytes and is, like IL-8 and tumor necrosis factor-alpha, overexpressed in human fat cells from insulin-resistant subjects. The Journal of biological chemistry *278*, 45777-45784.

Rui, L. (2014). Energy metabolism in the liver. Comprehensive Physiology *4*, 177-197.

Rui, L., Yuan, M., Frantz, D., Shoelson, S., and White, M.F. (2002). SOCS-1 and SOCS-3 block insulin signaling by ubiquitin-mediated degradation of IRS1 and IRS2. The Journal of biological chemistry *277*, 42394-42398.

Ruige, J.B., Bekaert, M., Lapauw, B., Fiers, T., Lehr, S., Hartwig, S., Herzfeld de Wiza, D., Schiller, M., Passlack, W., Van Nieuwenhove, Y., et al. (2012). Sex steroid-induced changes in circulating monocyte chemoattractant protein-1 levels may contribute to metabolic dysfunction in obese men. The Journal of clinical endocrinology and metabolism *97*, E1187-1191.

Saad, M.J., Araki, E., Miralpeix, M., Rothenberg, P.L., White, M.F., and Kahn, C.R. (1992). Regulation of insulin receptor substrate-1 in liver and muscle of animal models of insulin resistance. The Journal of clinical investigation *90*, 1839-1849.

Sabio, G., Das, M., Mora, A., Zhang, Z., Jun, J.Y., Ko, H.J., Barrett, T., Kim, J.K., and Davis, R.J. (2008). A stress signaling pathway in adipose tissue regulates hepatic insulin resistance. Science (New York, N.Y.) *322*, 1539-1543.

Sahin Ersoy, G., Altun Ensari, T., Subas, S., Giray, B., Simsek, E.E., and Cevik, O. (2017). WISP1 is a novel adipokine linked to metabolic parameters in gestational diabetes mellitus. The journal of maternal-fetal & neonatal medicine : the official journal of the European Association of Perinatal Medicine, the Federation of Asia and Oceania Perinatal Societies, the International Society of Perinatal Obstet *30*, 942-946.

Sainz, N., Rodriguez, A., Catalan, V., Becerril, S., Ramirez, B., Gomez-Ambrosi, J., and Fruhbeck, G. (2009). Leptin administration favors muscle mass accretion by decreasing FoxO3a and increasing PGC-1alpha in ob/ob mice. PloS one *4*, e6808.

Sainz, N., Rodriguez, A., Catalan, V., Becerril, S., Ramirez, B., Gomez-Ambrosi, J., and Fruhbeck, G. (2010). Leptin administration downregulates the increased expression levels of genes related to oxidative stress and inflammation in the skeletal muscle of ob/ob mice. Mediators of inflammation *2010*, 784343.

Sajan, M.P., Ivey, R.A., 3rd, and Farese, R.V. (2015). BMI-related progression of atypical PKC-dependent aberrations in insulin signaling through IRS-1, Akt, FoxO1 and PGC-1alpha in livers of obese and type 2 diabetic humans. Metabolism: clinical and experimental *64*, 1454-1465.

Salih, D.A., and Brunet, A. (2008). FoxO transcription factors in the maintenance of cellular homeostasis during aging. Current opinion in cell biology *20*, 126-136.

Samuel, V.T., and Shulman, G.I. (2012). Mechanisms for insulin resistance: common threads and missing links. Cell *148*, 852-871.

Samuel, V.T., and Shulman, G.I. (2018). Nonalcoholic Fatty Liver Disease as a Nexus of Metabolic and Hepatic Diseases. Cell metabolism *27*, 22-41.

Sanchez, A.M., Candau, R.B., and Bernardi, H. (2014). FoxO transcription factors: their roles in the maintenance of skeletal muscle homeostasis. Cellular and molecular life sciences : CMLS *71*, 1657-1671.

Sanders, F.W., and Griffin, J.L. (2016). De novo lipogenesis in the liver in health and disease: more than just a shunting yard for glucose. Biological reviews of the Cambridge Philosophical Society *91*, 452-468.

Sandri, M., Sandri, C., Gilbert, A., Skurk, C., Calabria, E., Picard, A., Walsh, K., Schiaffino, S., Lecker, S.H., and Goldberg, A.L. (2004). Foxo transcription factors induce the atrophy-related ubiquitin ligase atrogin-1 and cause skeletal muscle atrophy. Cell *117*, 399-412.

Satapathy, S.K., and Sanyal, A.J. (2015). Epidemiology and Natural History of Nonalcoholic Fatty Liver Disease. Seminars in liver disease *35*, 221-235.

Schauer, P.R., Bhatt, D.L., Kirwan, J.P., Wolski, K., Brethauer, S.A., Navaneethan, S.D., Aminian, A., Pothier, C.E., Kim, E.S., Nissen, S.E., et al. (2014). Bariatric surgery versus intensive medical therapy for diabetes--3-year outcomes. The New England journal of medicine *370*, 2002-2013.

Schmid, A.I., Szendroedi, J., Chmelik, M., Krssak, M., Moser, E., and Roden, M. (2011). Liver ATP synthesis is lower and relates to insulin sensitivity in patients with type 2 diabetes. Diabetes care *34*, 448-453.

Schmittgen, T.D., and Zakrajsek, B.A. (2000). Effect of experimental treatment on housekeeping gene expression: validation by real-time, quantitative RT-PCR. Journal of biochemical and biophysical methods *46*, 69-81.

Sell, H., Dietze-Schroeder, D., Kaiser, U., and Eckel, J. (2006). Monocyte chemotactic protein-1 is a potential player in the negative cross-talk between adipose tissue and skeletal muscle. Endocrinology *147*, 2458-2467.

Sell, H., Laurencikiene, J., Taube, A., Eckardt, K., Cramer, A., Horrighs, A., Arner, P., and Eckel, J. (2009). Chemerin is a novel adipocyte-derived factor inducing insulin resistance in primary human skeletal muscle cells. Diabetes *58*, 2731-2740.

Semenov, M.V., Habas, R., Macdonald, B.T., and He, X. (2007). SnapShot: Noncanonical Wnt Signaling Pathways. Cell *131*, 1378.

Semple, R.K., Sleigh, A., Murgatroyd, P.R., Adams, C.A., Bluck, L., Jackson, S., Vottero, A., Kanabar, D., Charlton-Menys, V., Durrington, P., et al. (2009). Postreceptor insulin resistance contributes to human dyslipidemia and hepatic steatosis. The Journal of clinical investigation *119*, 315-322.

Senf, S.M., Sandesara, P.B., Reed, S.A., and Judge, A.R. (2011). p300 Acetyltransferase activity differentially regulates the localization and activity of the FOXO homologues in skeletal muscle. American journal of physiology. Cell physiology *300*, C1490-1501.

Senn, J.J., Klover, P.J., Nowak, I.A., Zimmers, T.A., Koniaris, L.G., Furlanetto, R.W., and Mooney, R.A. (2003). Suppressor of cytokine signaling-3 (SOCS-3), a potential mediator of interleukin-6-dependent insulin resistance in hepatocytes. The Journal of biological chemistry *278*, 13740-13746.

Shah, A.D., Langenberg, C., Rapsomaniki, E., Denaxas, S., Pujades-Rodriguez, M., Gale, C.P., Deanfield, J., Smeeth, L., Timmis, A., and Hemingway, H. (2015). Type 2 diabetes and incidence of cardiovascular diseases: a cohort study in 1.9 million people. The lancet. Diabetes & endocrinology *3*, 105-113.

Shah, O.J., Wang, Z., and Hunter, T. (2004). Inappropriate activation of the TSC/Rheb/mTOR/S6K cassette induces IRS1/2 depletion, insulin resistance, and cell survival deficiencies. Current biology : CB *14*, 1650-1656.

Shi, J., Luo, L., Eash, J., Ibebunjo, C., and Glass, D.J. (2011). The SCF-Fbxo40 complex induces IRS1 ubiquitination in skeletal muscle, limiting IGF1 signaling. Developmental cell *21*, 835-847.

Shao, W., and Espenshade, P.J. (2012). Expanding roles for SREBP in metabolism. Cell metabolism *16*, 414-419.

Shi, J., Luo, L., Eash, J., Ibebunjo, C., and Glass, D.J. (2011). The SCF-Fbxo40 complex induces IRS1 ubiquitination in skeletal muscle, limiting IGF1 signaling. Developmental cell *21*, 835-847.

Shimomura, I., Hammer, R.E., Ikemoto, S., Brown, M.S., and Goldstein, J.L. (1999). Leptin reverses insulin resistance and diabetes mellitus in mice with congenital lipodystrophy. Nature *401*, 73-76.

Shimomura, I., Hammer, R.E., Richardson, J.A., Ikemoto, S., Bashmakov, Y., Goldstein, J.L., and Brown, M.S. (1998). Insulin resistance and diabetes mellitus in transgenic mice expressing nuclear SREBP-1c in adipose tissue: model for congenital generalized lipodystrophy. Genes & development *12*, 3182-3194.

Singh, A., Ye, M., Bucur, O., Zhu, S., Tanya Santos, M., Rabinovitz, I., Wei, W., Gao, D., Hahn, W.C., and Khosravi-Far, R. (2010). Protein phosphatase 2A reactivates FOXO3a through a dynamic interplay with 14-3-3 and AKT. Molecular biology of the cell *21*, 1140-1152.

Smith, S., and Tsai, S.C. (2007). The type I fatty acid and polyketide synthases: a tale of two megasynthases. Natural product reports *24*, 1041-1072.

Solini, A., Di Virgilio, F., Chiozzi, P., Fioretto, P., Passaro, A., and Fellin, R. (2001). A defect in glycogen synthesis characterizes insulin resistance in hypertensive patients with type 2 diabetes. Hypertension (Dallas, Tex. : 1979) *37*, 1492-1496.

Sparks, J.D., Sparks, C.E., and Adeli, K. (2012). Selective hepatic insulin resistance, VLDL overproduction, and hypertriglyceridemia. Arterioscler Thromb Vasc Biol *32*, 2104-2112.

Steensberg, A., Fischer, C.P., Keller, C., Moller, K., and Pedersen, B.K. (2003). IL-6 enhances plasma IL-1ra, IL-10, and cortisol in humans. American journal of physiology. Endocrinology and metabolism *285*, E433-437.

Steensberg, A., van Hall, G., Osada, T., Sacchetti, M., Saltin, B., and Klarlund Pedersen, B. (2000). Production of interleukin-6 in contracting human skeletal muscles can account for the exercise-induced increase in plasma interleukin-6. The Journal of physiology *529 Pt 1*, 237-242.

Stitt, T.N., Drujan, D., Clarke, B.A., Panaro, F., Timofeyva, Y., Kline, W.O., Gonzalez, M., Yancopoulos, G.D., and Glass, D.J. (2004). The IGF-1/PI3K/Akt pathway prevents expression of muscle atrophy-induced ubiquitin ligases by inhibiting FOXO transcription factors. Molecular cell *14*, 395-403.

Storlien, L., Oakes, N.D., and Kelley, D.E. (2004). Metabolic flexibility. The Proceedings of the Nutrition Society *63*, 363-368.

Stumvoll, M., Goldstein, B.J., and van Haeften, T.W. (2005). Type 2 diabetes: principles of pathogenesis and therapy. Lancet (London, England) *365*, 1333-1346.

Su, F., Overholtzer, M., Besser, D., and Levine, A.J. (2002). WISP-1 attenuates p53-mediated apoptosis in response to DNA damage through activation of the Akt kinase. Genes & development *16*, 46-57.

Sunny, N.E., Parks, E.J., Browning, J.D., and Burgess, S.C. (2011). Excessive hepatic mitochondrial TCA cycle and gluconeogenesis in humans with nonalcoholic fatty liver disease. Cell metabolism *14*, 804-810.

Szendroedi, J., Chmelik, M., Schmid, A.I., Nowotny, P., Brehm, A., Krssak, M., Moser, E., and Roden, M. (2009). Abnormal hepatic energy homeostasis in type 2 diabetes. Hepatology (Baltimore, Md.) *50*, 1079-1086.

Tacke, C., Aleksandrova, K., Rehfeldt, M., Murahovschi, V., Markova, M., Kemper, M., Hornemann, S., Kaiser, U., Honig, C., Gerbracht, C., et al. (2017). Assessment of circulating Wnt1 inducible signalling pathway protein 1 (WISP-1)/CCN4 as a novel biomarker of obesity. Journal of cell communication and signaling.

Takano, A., Usui, I., Haruta, T., Kawahara, J., Uno, T., Iwata, M., and Kobayashi, M. (2001). Mammalian target of rapamycin pathway regulates insulin signaling via subcellular redistribution of insulin receptor substrate 1 and integrates nutritional signals and metabolic signals of insulin. Molecular and cellular biology *21*, 5050-5062.

Tan, B.K., Adya, R., and Randeva, H.S. (2010). Omentin: a novel link between inflammation, diabesity, and cardiovascular disease. Trends in cardiovascular medicine *20*, 143-148.

Taneera, J., Lang, S., Sharma, A., Fadista, J., Zhou, Y., Ahlqvist, E., Jonsson, A., Lyssenko, V., Vikman, P., Hansson, O., et al. (2012). A systems genetics approach identifies genes and pathways for type 2 diabetes in human islets. Cell metabolism *16*, 122-134.

Tao, G.Z., Looi, K.S., Toivola, D.M., Strnad, P., Zhou, Q., Liao, J., Wei, Y., Habtezion, A., and Omary, M.B. (2009). Keratins modulate the shape and function of hepatocyte mitochondria: a mechanism for protection from apoptosis. Journal of cell science *122*, 3851-3855.

Telting, D., van der Zon, G.C., Dorrestijn, J., and Maassen, J.A. (2001). IRS-1 tyrosine phosphorylation reflects insulin-induced metabolic and mitogenic responses in 3T3-L1 pre-adipocytes. Archives of physiology and biochemistry *109*, 52-62.

Thiebaud, D., Jacot, E., DeFronzo, R.A., Maeder, E., Jequier, E., and Felber, J.P. (1982). The effect of graded doses of insulin on total glucose uptake, glucose oxidation, and glucose storage in man. Diabetes *31*, 957-963.

Tian, Y., Wang, W., Lu, Q., Chen, P., Ma, K., Jia, Z., and Zhou, C. (2016). Cross-talk of SFRP4, integrin alpha1beta1, and Notch1 inhibits cardiac differentiation of P19CL6 cells. Cellular signalling *28*, 1806-1815.

Titchenell, P.M., Chu, Q., Monks, B.R., and Birnbaum, M.J. (2015). Hepatic insulin signalling is dispensable for suppression of glucose output by insulin in vivo. Nature communications *6*, 7078.

Tolman, K.G., and Dalpiaz, A.S. (2007). Treatment of non-alcoholic fatty liver disease. Therapeutics and clinical risk management *3*, 1153-1163.

Tong, J.F., Yan, X., Zhu, M.J., and Du, M. (2009). AMP-activated protein kinase enhances the expression of muscle-specific ubiquitin ligases despite its activation of IGF-1/Akt signaling in C2C12 myotubes. Journal of cellular biochemistry *108*, 458-468.

Trayhurn, P., Drevon, C.A., and Eckel, J. (2011). Secreted proteins from adipose tissue and skeletal muscle - adipokines, myokines and adipose/muscle cross-talk. Archives of physiology and biochemistry *117*, 47-56.

Trayhurn, P., and Wood, I.S. (2004). Adipokines: inflammation and the pleiotropic role of white adipose tissue. The British journal of nutrition *92*, 347-355.

Trujillo, M.E., Sullivan, S., Harten, I., Schneider, S.H., Greenberg, A.S., and Fried, S.K. (2004). Interleukin-6 regulates human adipose tissue lipid metabolism and leptin production in vitro. The Journal of clinical endocrinology and metabolism *89*, 5577-5582.

Turer, A.T., and Scherer, P.E. (2012). Adiponectin: mechanistic insights and clinical implications. Diabetologia *55*, 2319-2326.

Turner, N., and Heilbronn, L.K. (2008). Is mitochondrial dysfunction a cause of insulin resistance? Trends in endocrinology and metabolism: TEM *19*, 324-330.

Uren, A., Reichsman, F., Anest, V., Taylor, W.G., Muraiso, K., Bottaro, D.P., Cumberledge, S., and Rubin, J.S. (2000). Secreted frizzled-related protein-1 binds directly to Wingless and is a biphasic modulator of Wnt signaling. The Journal of biological chemistry *275*, 4374-4382.

van Hall, G., Steensberg, A., Sacchetti, M., Fischer, C., Keller, C., Schjerling, P., Hiscock, N., Moller, K., Saltin, B., Febbraio, M.A., et al. (2003). Interleukin-6 stimulates lipolysis and fat oxidation in humans. The Journal of clinical endocrinology and metabolism *88*, 3005-3010.

Vanella, L., Kim, D.H., Sodhi, K., Barbagallo, I., Burgess, A.P., Falck, J.R., Schwartzman, M.L., and Abraham, N.G. (2011). Crosstalk between EET and HO-1 downregulates Bach1 and adipogenic marker expression in mesenchymal stem cell derived adipocytes. Prostaglandins & other lipid mediators *96*, 54-62.

Vanella, L., Sodhi, K., Kim, D.H., Puri, N., Maheshwari, M., Hinds, T.D., Bellner, L., Goldstein, D., Peterson, S.J., Shapiro, J.I., et al. (2013). Increased heme-oxygenase 1 expression in mesenchymal stem cell-derived adipocytes decreases differentiation and lipid accumulation via upregulation of the canonical Wnt signaling cascade. Stem cell research & therapy *4*, 28.

Venkatachalam, K., Venkatesan, B., Valente, A.J., Melby, P.C., Nandish, S., Reusch, J.E., Clark, R.A., and Chandrasekar, B. (2009). WISP1, a pro-mitogenic, pro-survival factor, mediates tumor necrosis factor-alpha (TNF-alpha)-stimulated cardiac fibroblast proliferation but inhibits TNF-alpha-induced cardiomyocyte death. The Journal of biological chemistry *284*, 14414-14427.

Venkatesan, B., Prabhu, S.D., Venkatachalam, K., Mummidi, S., Valente, A.J., Clark, R.A., Delafontaine, P., and Chandrasekar, B. (2010). WNT1-inducible signaling pathway protein-1 activates diverse cell survival pathways and blocks doxorubicin-induced cardiomyocyte death. Cellular signalling *22*, 809-820.

Visweswaran, M., Schiefer, L., Arfuso, F., Dilley, R.J., Newsholme, P., and Dharmarajan, A. (2015). Wnt antagonist secreted frizzled-related protein 4 upregulates adipogenic differentiation in human adipose tissue-derived mesenchymal stem cells. PloS one *10*, e0118005.

Waddell, D.S., Baehr, L.M., van den Brandt, J., Johnsen, S.A., Reichardt, H.M., Furlow, J.D., and Bodine, S.C. (2008). The glucocorticoid receptor and FOXO1 synergistically activate the skeletal muscle atrophy-associated MuRF1 gene. American journal of physiology. Endocrinology and metabolism *295*, E785-797.

Wallace, T.M., Levy, J.C., and Matthews, D.R. (2004). Use and abuse of HOMA modeling. Diabetes care *27*, 1487-1495.

Wang, F., Nguyen, M., Qin, F.X., and Tong, Q. (2007). SIRT2 deacetylates FOXO3a in response to oxidative stress and caloric restriction. Aging cell *6*, 505-514.

Wan, M., Leavens, K.F., Hunter, R.W., Koren, S., von Wilamowitz-Moellendorff, A., Lu, M., Satapati, S., Chu, Q., Sakamoto, K., Burgess, S.C., et al. (2013). A noncanonical, GSK3-independent pathway controls postprandial hepatic glycogen deposition. Cell metabolism *18*, 99-105.

Wang, F., Chan, C.H., Chen, K., Guan, X., Lin, H.K., and Tong, Q. (2012). Deacetylation of FOXO3 by SIRT1 or SIRT2 leads to Skp2-mediated FOXO3 ubiquitination and degradation. Oncogene *31*, 1546-1557.

Wang, Y., Yan, C., Liu, L., Wang, W., Du, H., Fan, W., Lutfy, K., Jiang, M., Friedman, T.C., and Liu, Y. (2015). 11beta-Hydroxysteroid dehydrogenase type 1 shRNA ameliorates glucocorticoid-induced insulin resistance and lipolysis in mouse abdominal adipose tissue. American journal of physiology. Endocrinology and metabolism *308*, E84-95.

Wawrzak, D., Metioui, M., Willems, E., Hendrickx, M., de Genst, E., and Leyns, L. (2007). Wnt3a binds to several sFRPs in the nanomolar range. Biochemical and biophysical research communications *357*, 1119-1123.

Weisberg, S.P., McCann, D., Desai, M., Rosenbaum, M., Leibel, R.L., and Ferrante, A.W., Jr. (2003). Obesity is associated with macrophage accumulation in adipose tissue. The Journal of clinical investigation *112*, 1796-1808.

Wellen, K.E., and Hotamisligil, G.S. (2005). Inflammation, stress, and diabetes. The Journal of clinical investigation *115*, 1111-1119.

Williams, C.D., Stengel, J., Asike, M.I., Torres, D.M., Shaw, J., Contreras, M., Landt, C.L., and Harrison, S.A. (2011). Prevalence of nonalcoholic fatty liver disease and nonalcoholic steatohepatitis among a largely middle-aged population utilizing ultrasound and liver biopsy: a prospective study. Gastroenterology *140*, 124-131.

Winer, J., Jung, C.K., Shackel, I., and Williams, P.M. (1999). Development and validation of real-time quantitative reverse transcriptase-polymerase chain reaction for monitoring gene expression in cardiac myocytes in vitro. Analytical biochemistry *270*, 41-49.

Wiza, C., Herzfeld de Wiza, D., Nascimento, E.B., Lehr, S., Al-Hasani, H., and Ouwens, D.M. (2013). Knockdown of PRAS40 inhibits insulin action via proteasome-mediated degradation of IRS1 in primary human skeletal muscle cells. Diabetologia *56*, 1118-1128.

Wolfe, R.R. (2006). The underappreciated role of muscle in health and disease. The American journal of clinical nutrition *84*, 475-482.

Woodworth-Hobbs, M.E., Hudson, M.B., Rahnert, J.A., Zheng, B., Franch, H.A., and Price, S.R. (2014). Docosahexaenoic acid prevents palmitate-induced activation of proteolytic systems in C2C12 myotubes. The Journal of nutritional biochemistry *25*, 868-874.

World Health Organization (WHO) (2018). http://www.who.int/topics/obesity/en/.

Wronska, A., and Kmiec, Z. (2012). Structural and biochemical characteristics of various white adipose tissue depots. Acta physiologica (Oxford, England) *205*, 194-208.

Xie, D., Nakachi, K., Wang, H., Elashoff, R., and Koeffler, H.P. (2001). Elevated levels of connective tissue growth factor, WISP-1, and CYR61 in primary breast cancers associated with more advanced features. Cancer research *61*, 8917-8923.

Xu, H., Barnes, G.T., Yang, Q., Tan, G., Yang, D., Chou, C.J., Sole, J., Nichols, A., Ross, J.S., Tartaglia, L.A., et al. (2003). Chronic inflammation in fat plays a crucial role in the development of obesity-related insulin resistance. The Journal of clinical investigation *112*, 1821-1830.

Xu, L., Corcoran, R.B., Welsh, J.W., Pennica, D., and Levine, A.J. (2000). WISP-1 is a Wnt-1- and beta-catenin-responsive oncogene. Genes & development *14*, 585-595.

Yamanaka, Y., Wilson, E.M., Rosenfeld, R.G., and Oh, Y. (1997). Inhibition of insulin receptor activation by insulin-like growth factor binding proteins. The Journal of biological chemistry *272*, 30729-30734.

Yamauchi, T., and Kadowaki, T. (2008). Physiological and pathophysiological roles of adiponectin and adiponectin receptors in the integrated regulation of metabolic and cardiovascular diseases. International journal of obesity (2005) *32 Suppl 7*, S13-18.

Yamauchi, T., Kamon, J., Minokoshi, Y., Ito, Y., Waki, H., Uchida, S., Yamashita, S., Noda, M., Kita, S., Ueki, K., et al. (2002). Adiponectin stimulates glucose utilization and fatty-acid oxidation by activating AMP-activated protein kinase. Nature medicine *8*, 1288-1295.

Yamauchi, T., Kamon, J., Waki, H., Terauchi, Y., Kubota, N., Hara, K., Mori, Y., Ide, T., Murakami, K., Tsuboyama-Kasaoka, N., et al. (2001). The fat-derived hormone adiponectin reverses insulin resistance associated with both lipoatrophy and obesity. Nature medicine *7*, 941-946.

Yamawaki, H., Kuramoto, J., Kameshima, S., Usui, T., Okada, M., and Hara, Y. (2011). Omentin, a novel adipocytokine inhibits TNF-induced vascular inflammation in human endothelial cells. Biochemical and biophysical research communications *408*, 339-343.

Yang, R.Z., Lee, M.J., Hu, H., Pray, J., Wu, H.B., Hansen, B.C., Shuldiner, A.R., Fried, S.K., McLenithan, J.C., and Gong, D.W. (2006). Identification of omentin as a novel depot-specific adipokine in human adipose tissue: possible role in modulating insulin action. American journal of physiology. Endocrinology and metabolism *290*, E1253-1261.

Yi, J.S., Park, J.S., Ham, Y.M., Nguyen, N., Lee, N.R., Hong, J., Kim, B.W., Lee, H., Lee, C.S., Jeong, B.C., et al. (2013). MG53-induced IRS-1 ubiquitination negatively regulates skeletal myogenesis and insulin signalling. Nature communications *4*, 2354.

Yoon, J.C., Ng, A., Kim, B.H., Bianco, A., Xavier, R.J., and Elledge, S.J. (2010). Wnt signaling regulates mitochondrial physiology and insulin sensitivity. Genes & development *24*, 1507-1518.

Yoon, J.C., Puigserver, P., Chen, G., Donovan, J., Wu, Z., Rhee, J., Adelmant, G., Stafford, J., Kahn, C.R., Granner, D.K., et al. (2001). Control of hepatic gluconeogenesis through the transcriptional coactivator PGC-1. Nature *413*, 131-138.

Yoshikawa, T., Shimano, H., Amemiya-Kudo, M., Yahagi, N., Hasty, A.H., Matsuzaka, T., Okazaki, H., Tamura, Y., Iizuka, Y., Ohashi, K., et al. (2001). Identification of liver X receptor-retinoid X receptor as an activator of the sterol regulatory element-binding protein 1c gene promoter. Molecular and cellular biology *21*, 2991-3000.

Younossi, Z.M., Koenig, A.B., Abdelatif, D., Fazel, Y., Henry, L., and Wymer, M. (2016). Global epidemiology of nonalcoholic fatty liver disease-Meta-analytic assessment of prevalence, incidence, and outcomes. Hepatology (Baltimore, Md.) *64*, 73-84.

Zatloukal, K.S., C; Fuchsbichler, A; Denk, H (2006). Keratins As Targets in and Modulators of Liver Diseases.

Zhan, T., Rindtorff, N., and Boutros, M. (2017). Wnt signaling in cancer. Oncogene *36*, 1461-1473.

Zhang, Q., Zhang, C., Li, X., Yu, Y., Liang, K., Shan, X., Zhao, K., Niu, Q., and Tian, Z. (2016). WISP1 Is Increased in Intestinal Mucosa and Contributes to Inflammatory Cascades in Inflammatory Bowel Disease. Disease markers *2016*, 3547096.

Zhang, W., Patil, S., Chauhan, B., Guo, S., Powell, D.R., Le, J., Klotsas, A., Matika, R., Xiao, X., Franks, R., et al. (2006). FoxO1 regulates multiple metabolic pathways in the liver: effects on gluconeogenic, glycolytic, and lipogenic gene expression. The Journal of biological chemistry *281*, 10105-10117.

Zhang, X., Ji, X., Wang, Q., and Li, J.Z. (2018). New insight into inter-organ crosstalk contributing to the pathogenesis of non-alcoholic fatty liver disease (NAFLD). Protein & cell *9*, 164-177.

Zhang, Y., Proenca, R., Maffei, M., Barone, M., Leopold, L., and Friedman, J.M. (1994). Positional cloning of the mouse obese gene and its human homologue. Nature *372*, 425-432.

Zhong, X., Tu, Y.J., Li, Y., Zhang, P., Wang, W., Chen, S.S., Li, L., Chung, A.C., Lan, H.Y., Chen, H.Y., et al. (2017). Serum levels of WNT1-inducible signaling pathway protein-1 (WISP-1): a noninvasive biomarker of renal fibrosis in subjects with chronic kidney disease. American journal of translational research *9*, 2920-2932.

Zhou, D., Strakovsky, R.S., Zhang, X., and Pan, Y.X. (2012). The skeletal muscle Wnt pathway may modulate insulin resistance and muscle development in a diet-induced obese rat model. Obesity (Silver Spring, Md.) *20*, 1577-1584.

Zhou, H., Song, X., Briggs, M., Violand, B., Salsgiver, W., Gulve, E.A., and Luo, Y. (2005). Adiponectin represses gluconeogenesis independent of insulin in hepatocytes. Biochemical and biophysical research communications *338*, 793-799.

Zhu, J.Z., Dai, Y.N., Wang, Y.M., Zhou, Q.Y., Yu, C.H., and Li, Y.M. (2015). Prevalence of Nonalcoholic Fatty Liver Disease and Economy. Digestive diseases and sciences *60*, 3194-3202.

Zong, H., Ren, J.M., Young, L.H., Pypaert, M., Mu, J., Birnbaum, M.J., and Shulman, G.I. (2002). AMP kinase is required for mitochondrial biogenesis in skeletal muscle in response to chronic energy deprivation. Proceedings of the National Academy of Sciences of the United States of America *99*, 15983-15987.

Zurlo, F., Larson, K., Bogardus, C., and Ravussin, E. (1990). Skeletal muscle metabolism is a major determinant of resting energy expenditure. The Journal of clinical investigation *86*, 1423-1427.

Contribution statement

Hörbelt, T., Tacke, C., Markova, M., Herzfeld de Wiza, D., Van de Velde, F., Bekaert, M., Van Nieuwenhove, Y., Hornemann, S., Rodiger, M., Seebeck, Friedl E., Jonas W., Thoresen GH., Kuss O., Rosenthal A., Lange V., Pfeiffer AFH., Schürmann A., Lapauw B., Rudovich N., Pivovarova O., Ouwens DM. (2018). The novel adipokine WISP1 associates with insulin resistance and impairs insulin action in human myotubes and mouse hepatocytes. Diabetologia. [Epub ahead of print].

The cited manuscript was with large proportion drafted and written by myself together with Prof. Dr. Margriet Ouwens, PD Dr. Natalia Rudovich, PD Dr. Olga Pivovarova. All human samples were recruited from Department of Internal medicine at Ghent University (Belgium) and kindly provided for this work by Prof. Dr. Bruno Lapauw as stated in 2.2.1. Human data were measured at Ghent University and kindly provided for analyses of the manuscript except for measurements of WISP1 in serum and *WISP1*, *ADIPOQ, RARRES2, CCL2* and *ITLN1* in VAT that were performed by myself. Conducting of *in vitro* experiments and collecting of corresponding data have been done by myself except for experiments presented in Figure 10C of this thesis (Figure 1C in manuscript) that were performed by PD Dr. Olga Pivovarova at the DIfE in Potsdam. Besides Figure 9 (ESM Figure 1 in manuscript) which has been prepared by Prof. Dr. Margriet Ouwens, all Figures and Tables presented in the manuscript and this thesis have been generated by myself.

Table 30. Summary of differential secreted proteins.

Comparison (group1/ group2)	Group	UniProt ID (Mouse)	Protein Descriptions	Gene names	AVG Log2 Ratio	*p*-value	[DEPRECATED] AVG Log2 Ratio	% Change	fold-change	Condition Numerator	signaling peptide prediction SP+/SP-	no signaling peptide prediction NP
aP2-SREBP-1c+sFRP4 / aP2-SREBP-1c	B2RQC6;B2RQC6-2	PYR1	CAD protein;Isoform 2 of CAD protein	Cad	1,44	1,29E-01	1,64	17,15	2,72	aP2-SREBP-1c+SFRP4		NP
	E9Q557	DESP	Desmoplakin	Dsp	2,38	2,05E-01	0,88	42,22	5,22	aP2-SREBP-1c+SFRP4		NP
	O35744	CHIL3	Chitinase-like protein 3	Chil3	-1,06	1,20E-01	-3,25	-51,93	0,48	aP2-SREBP-1c+SFRP4	SP+	
	O54988	SLK	STE20-like serine/threonine-protein kinase	Slk	-2,34	1,30E-01	-2,49	-80,30	0,20	aP2-SREBP-1c+SFRP4		NP
	P01942	HBA	Hemoglobin subunit alpha	Hba	-1,16	2,42E-02	-0,76	-55,33	0,45	aP2-SREBP-1c+SFRP4		NP
	P02088	HBB1	Hemoglobin subunit beta-1	Hbb-b1	-1,07	6,85E-03	-0,82	-52,51	0,47	aP2-SREBP-1c+SFRP4		NP
	P02463	CO4A1	Collagen alpha-1(IV) chain	Col4a1	1,99	1,91E-01	0,32	29,85	3,98	aP2-SREBP-1c+SFRP4	SP+	
	P07356	ANXA2	Annexin A2	Anxa2	2,02	1,83E-01	1,04	30,65	4,07	aP2-SREBP-1c+SFRP4		NP
	P11031	TCP4	Activated RNA polymerase II transcriptional coactivator p15	Sub1	1,42	1,94E-01	0,92	16,68	2,67	aP2-SREBP-1c+SFRP4		NP
	P17897	LYZ1	Lysozyme C-1	Lyz1	1,06	3,36E-02	1,09	10,82	2,08	aP2-SREBP-1c+SFRP4	SP+	
	P21570	ANGI	Angiogenin	Ang	-1,15	1,78E-02	-1,08	-55,03	0,45	aP2-SREBP-1c+SFRP4	SP+	
	P31725	S10A9	Protein S100-A9	S100a9	-1,11	5,22E-04	-1,05	-53,54	0,46	aP2-SREBP-1c+SFRP4		NP
	P50446	K2C6A	Keratin, type II cytoskeletal 6A	Krt6a	2,07	3,08E-02	1,24	31,98	4,20	aP2-SREBP-1c+SFRP4		NP
	Q00898	A1AT5	Alpha-1-antitrypsin 1-5	Serpina1e	-1,31	1,28E-04	-0,83	-59,61	0,40	aP2-SREBP-1c+SFRP4	SP+	
	Q02257	PLAK	Junction plakoglobin	Jup	2,02	5,16E-02	2,11	30,50	4,05	aP2-SREBP-1c+SFRP4		NP
	Q07235	GDN	Glia-derived nexin	Serpine2	-1,57	5,08E-02	-1,04	-66,25	0,34	aP2-SREBP-1c+SFRP4	SP+	
	Q497I4	KRT35	Keratin, type I cuticular Ha5	Krt35	-2,04	1,63E-01	-4,33	-75,63	0,24	aP2-SREBP-1c+SFRP4		NP
	Q61781	K1C14	Keratin, type I cytoskeletal 14	Krt14	2,81	2,64E-02	1,02	60,01	7,00	aP2-SREBP-1c+SFRP4		NP
	Q62376	RU17	U1 small nuclear ribonucleoprotein 70 kDa	Snrnp70	-1,01	1,47E-01	-0,57	-50,33	0,50	aP2-SREBP-1c+SFRP4		NP

	Q6GQT1	A2MG	Alpha-2-macroglobulin-P	A2m	-1,11	1,49E-01	-0,89	-53,69	0,46	aP2-SREBP-1c+SFRP4	SP+	
	Q6GQT9	NOMO1	Nodal modulator 1	Nomo1	-1,93	7,68E-02	-2,61	-73,72	0,26	aP2-SREBP-1c+SFRP4	SP+	
	Q8K1R3	PNPT1	Polyribonucleotide nucleotidyltransferase 1,	Pnpt1	-1,39	1,70E-01	-1,35	-61,84	0,38	aP2-SREBP-1c+SFRP4	SP+	
	Q91WG8	GLCNE	Bifunctional UDP-N-acetylglucosamine 2-epimerase	Gne	-1,43	1,91E-01	-1,28	-62,78	0,37	aP2-SREBP-1c+SFRP4		NP
	Q922U2	K2C5	Keratin, type II cytoskeletal 5	Krt5	2,26	6,39E-02	0,86	37,77	4,78	aP2-SREBP-1c+SFRP4		NP
	Q99MN9	PCC	Propionyl-CoA carboxylase beta chain	Pccb	-1,14	9,39E-02	-0,24	-54,69	0,45	aP2-SREBP-1c+SFRP4	SP+	
	Q9ERR7	SEP15	Selenoprotein F	Selenof	2,13	1,27E-01	5,15	33,87	4,39	aP2-SREBP-1c+SFRP4	SP+	
	Q9JI90	RNF14	E3 ubiquitin-protein ligase RNF14	Rnf14	1,39	1,30E-01	1,30	1,62	0,26	aP2-SREBP-1c+SFRP4		NP
	Q9R0G6	COMP	Cartilage oligomeric matrix protein	Comp	-1,16	1,33E-01	-1,14	-55,27	0,45	aP2-SREBP-1c+SFRP4	SP+	
	Q9Z2K1	K1C16	Keratin, type I cytoskeletal 16	Krt16	5,03	1,76E-01	1,93	31,58	3,26	aP2-SREBP-1c+SFRP4		NP
C57Bl6 / aP2-SREBP-1c	P04918	SAA3	Serum amyloid A-3 protein	Saa3	-2,39	5,61E-02	-2,49	-80,86	0,19	C57Bl6	SP+	
	P05366	SAA1	Serum amyloid A-1 protein	Saa1	-2,12	1,30E-07	-2,11	-76,97	0,23	C57Bl6	SP+	
	P05367	SAA2	Serum amyloid A-2 protein	Saa2	-2,03	1,42E-07	-2,40	-75,48	0,25	C57Bl6	SP+	
	P06728	APOA4	Apolipoprotein A-IV	Apoa4	-1,85	5,52E-34	-1,67	-72,25	0,28	C57Bl6	SP+	
	P06801	MAOX	NADP-dependent malic enzyme	Me1	-1,16	8,12E-11	-0,98	-55,14	0,45	C57Bl6		NP
	P10493	NID1	Nidogen-1	Nid1	1,56	1,70E-04	-0,91	19,40	2,94	C57Bl6	SP+	
	P10810	CD14	Monocyte differentiation antigen CD14	Cd14	-1,10	1,15E-12	-1,21	-53,26	0,47	C57Bl6	SP+	
	P12246	SAMP	Serum amyloid P-component	Apcs	-2,85	7,67E-09	-2,81	-86,14	0,14	C57Bl6	SP+	
	P14148	RL7	60S ribosomal protein L7	Rpl7	-1,11	7,87E-02	-1,22	-53,76	0,46	C57Bl6		NP
	P16045	LEG1	Galectin-1	Lgals1	-1,59	2,75E-08	-1,66	-66,83	0,33	C57Bl6		NP
	P28666	MUG2	Murinoglobulin-2	Mug2	3,45	8,52E-02	1,03	99,07	1,09	C57Bl6	SP+	
	P29268	CTGF	Connective tissue growth factor	Ctgf	-1,39	2,05E-01	-0,98	-61,91	0,38	C57Bl6	SP+	
	P31725	S10A9	Protein S100-A9	S100a9	-1,98	5,16E-02	-1,27	-74,68	0,25	C57Bl6		NP

C57Bl6 / aP2-SREBP-1c	P35980	RL18	60S ribosomal protein L18	Rpl18	-1,48	5,92E-03	-1,55	-64,24	0,36	C57Bl6		NP
	P47877	IBP2	Insulin-like growth factor-binding protein 2	Igfbp2	1,39	3,52E-10	1,64	16,12	2,61	C57Bl6	SP+	
	P47911	RL6	60S ribosomal protein L6	Rpl6	-1,10	6,01E-13	-0,94	-53,37	0,47	C57Bl6		NP
	P47963	RL13	60S ribosomal protein L13	Rpl13	-1,58	4,05E-05	-1,67	-66,64	0,33	C57Bl6		NP
	P51125;P51125-2;P51125-3;P51125-6	ICAL	Calpastatin	Cast	-1,13	6,65E-02	-0,78	-5,44	0,46	C57Bl6		NP
	P55065	PLTP	Phospholipid transfer protein	Pltp	-1,52	7,40E-02	-1,09	-65,22	0,35	C57Bl6	SP+	
	P61939	THBG	Thyroxine-binding globulin	Serpina 7	-1,01	1,08E-02	-1,13	-50,41	0,50	C57Bl6	SP+	
	P62918	RL8	60S ribosomal protein L8	Rpl8	-1,09	7,26E-04	-1,15	-52,92	0,47	C57Bl6		NP
	P63037	DNJA1	DnaJ homolog subfamily A member 1	Dnaja1	-2,86	1,55E-01	-0,83	-86,21	0,14	C57Bl6		NP
	P97798;P97798-2;P97798-3;P97798-4;P97798-5	NEO1	Neogenin	Neo1	-2,58	4,80E-02	-2,48	-83,32	0,17	C57Bl6	SP+	
	Q3U0B3	DHR11	Dehydrogenase/reductase SDR family member 11	Dhrs11	-1,24	1,73E-01	-3,59	-57,60	0,42	C57Bl6		NP
	Q497I4	KRT35	Keratin, type I cuticular Ha5	Krt35	-2,21	1,45E-01	-3,34	-78,42	0,22	C57Bl6		NP
	Q61704	ITIH3	Inter-alpha-trypsin inhibitor heavy chain H3	Itih3	-1,04	1,13E-10	-1,24	-51,53	0,48	C57Bl6	SP+	
	Q61805	LBP	Lipopolysaccharide-binding protein	Lbp	-1,14	4,05E-07	-1,10	-54,52	0,45	C57Bl6	SP+	
	Q62093	SRSF2	Serine/arginine-rich splicing factor 2	Srsf2	-2,30	1,45E-01	-1,55	-7,97	0,20	C57Bl6		NP
	Q6IFX2	K1C42	Keratin, type I cytoskeletal 42	Krt42	-2,38	1,55E-01	-1,83	-8,08	0,19	C57Bl6		NP
	Q6P9P6	KIF11	Kinesin-like protein KIF11	Kif11	1,49	1,82E-01	1,41	18,15	2,81	C57Bl6		NP
	Q6ZWV7	RL35	60S ribosomal protein L35	Rpl35	-1,04	5,44E-02	-1,28	-51,32	0,49	C57Bl6		NP

C57Bl6 / aP2-SREBP-1c	Q71KU9	FGL1	Fibrinogen-like protein 1	Fgl1	-1,15	1,25E-07	-1,21	-55,02	0,45	C57Bl6	SP+	
	Q80VJ3	DNPH1	2'-deoxynucleoside 5'-phosphate N-hydrolase 1	Dnph1	-1,33	1,74E-01	-1,37	-60,17	0,40	C57Bl6		NP
	Q8BRF7;Q8BRF7-3	SCFD1	Sec1 family domain-containing protein 1	Scfd1	-1,01	5,67E-02	-0,75	-50,29	0,50	C57Bl6		NP
	Q8BWR2;Q8BWR2-2	PITH1	PITH domain-containing protein 1	Pithd1	-1,02	5,77E-02	-1,15	-50,78	0,49	C57Bl6		NP
	Q8R574	KPRB	Phosphoribosyl pyrophosphate synthase-associated protein 2	Prpsap2	-1,26	1,35E-01	-1,20	-58,32	0,42	C57Bl6		NP
	Q8VC97	BUP1	Beta-ureidopropionase	Upb1	1,13	2,68E-08	1,35	1,18	0,22	C57Bl6		NP
	Q8VCC1	PGDH	15-hydroxyprostaglandin dehydrogenase [NAD(+)]	Hpgd	1,60	3,58E-02	1,80	2,04	3,04	C57Bl6		NP
	Q99KP3	CRYL1	Lambda-crystallin homolog	Cryl1	-1,00	1,08E-01	-0,67	-50,04	0,50	C57Bl6	SP+	
	Q99LY9	NDUS5	NADH dehydrogenase [ubiquinone] iron-sulfur protein 5	Ndufs5	-2,18	1,75E-01	-1,63	-77,96	0,22	C57Bl6		NP
	Q9CQC7	NDUB4	NADH dehydrogenase [ubiquinone] 1 beta subcomplex subunit 4	Ndufb4	-1,94	6,02E-02	-2,31	-74,02	0,26	C57Bl6		NP
	Q9CYZ6	CS060	Uncharacterized protein C19orf60 homolog	NaN	-2,07	5,37E-02	-1,98	-76,24	0,24	C57Bl6		NP
	Q9D8E6	RL4	60S ribosomal protein L4	Rpl4	-1,03	8,13E-05	-1,16	-51,13	0,49	C57Bl6		NP
	Q9JI90	RNF14	E3 ubiquitin-protein ligase RNF14	Rnf14	1,20	3,11E-02	1,22	13,02	2,30	C57Bl6		NP
	Q9JM99;Q9JM99-2;Q9JM9-3;Q9JM9-4;Q9JM9-5	PRG4	Proteoglycan 4	Prg4	-1,04	8,84E-03	-0,93	-51,52	0,48	C57Bl6	SP+	
	Q9QXG4	ACSA	Acetyl-coenzyme A synthetase, cytoplasmic	Acss2	-1,07	1,24E-01	0,53	-52,34	0,48	C57Bl6		NP
	Q9R257	HEBP1	Heme-binding protein 1	Hebp1	-1,23	1,69E-07	-2,03	-57,44	0,43	C57Bl6		NP
	Q9Z0K8	VNN1	Pantetheinase	Vnn1	-1,31	1,74E-03	-1,47	-59,64	0,40	C57Bl6	SP+	
	E9Q557	DESP	Desmoplakin	Dsp	-1,42	1,04E-01	-0,98	-62,70	0,37	C57Bl6+SFRP4		NP

C57Bl6+sFRP4/ aP2-SREBP-1c+sFRP4	O35405	PLD3	Phospholipase D3	Pld3	1,08	5,32E-03	0,94	11,07	2,11	C57Bl6+SFRP4		NP
	O35887	CALU	Calumenin	Calu	1,03	2,48E-12	0,83	10,46	2,05	C57Bl6+SFRP4	SP+	
	O35955	PSB10	Proteasome subunit beta type-10	Psmb10	-1,59	1,30E-01	-1,12	-66,88	0,33	C57Bl6+SFRP4		NP
	O54988	SLK	STE20-like serine/threonine-protein kinase	Slk	1,88	1,55E-01	2,55	26,80	3,68	C57Bl6+SFRP4		NP
	P01942	HBA	Hemoglobin subunit alpha	Hba	1,14	1,12E-01	0,82	1,21	2,21	C57Bl6+SFRP4		NP
	P02088	HBB1	Hemoglobin subunit beta-1	Hbb-b1	1,09	5,87E-02	0,99	11,36	2,14	C57Bl6+SFRP4		NP
	P05367	SAA2	Serum amyloid A-2 protein	Saa2	-1,05	1,30E-01	-1,07	-51,64	0,48	C57Bl6+SFRP4	SP+	
	P06728	APOA4	Apolipoprotein A-IV	Apoa4	-1,28	9,79E-47	-1,64	-58,93	0,41	C57Bl6+SFRP4	SP+	
	P06801	MAOX	NADP-dependent malic enzyme	Me1	-1,00	2,14E-15	-1,19	-50,12	0,50	C57Bl6+SFRP4		NP
	P0C0S6;Q3TH W5	H2AZ;H2AV	Histone H2A.Z;Histone H2A.V	H2afz; H2afv	-1,00	6,39E-02	-1,40	-50,15	0,50	C57Bl6+SFRP4		NP
	P10810	CD14	Monocyte differentiation antigen CD14	Cd14	-1,26	1,36E-04	-1,12	-58,34	0,42	C57Bl6+SFRP4	SP+	
	P11588	MUP1	Major urinary protein 1	Mup1	1,35	7,93E-02	2,37	15,57	2,56	C57Bl6+SFRP4	SP+	
	P12246	SAMP	Serum amyloid P-component	Apcs	-1,96	2,53E-05	-2,10	-7,43	0,26	C57Bl6+SFRP4	SP+	
	P16045	LEG1	Galectin-1	Lgals1	-1,98	1,70E-06	-2,52	-7,47	0,25	C57Bl6+SFRP4		NP
	P17717	UDB17	UDP-glucuronosyltransferase 2B17	Ugt2b17	1,11	3,43E-03	0,81	11,57	2,16	C57Bl6+SFRP4	SP+	
	P22892	AP1G1	AP-1 complex subunit gamma-1	Ap1g1	-1,03	1,41E-02	-0,71	-51,02	0,49	C57Bl6+SFRP4		NP
	P29758	OAT	Ornithine aminotransferase, mitochondrial	Oat	1,57	1,07E-33	1,61	19,63	2,96	C57Bl6+SFRP4		NP
	P42703;P42703-2	LIFR	Leukemia inhibitory factor receptor	Lifr	1,61	2,82E-26	1,55	20,62	3,06	C57Bl6+SFRP4	SP+	
	P43275	H11	Histone H1.1	Hist1h1a	1,59	1,62E-01	3,83	20,14	3,01	C57Bl6+SFRP4		NP
	P43883	PLIN2	Perilipin-2	Plin2	-2,71	1,61E-01	-2,91	-84,70	0,15	C57Bl6+SFRP4		NP
	P47877	IBP2	Insulin-like growth factor-binding protein 2	Igfbp2	1,41	1,23E-07	1,19	16,58	2,66	C57Bl6+SFRP4	SP+	

C57Bl6+sFRP4/ aP2-SREBP-1c+sFRP4	P50446	K2C6A	Keratin, type II cytoskeletal 6A	Krt6a	-1,64	6,33E-02	-0,75	-67,93	0,32	C57Bl6+SFRP4		NP
	P52623	UCK1	Uridine-cytidine kinase 1	Uck1	-1,42	4,20E-02	-1,50	-62,69	0,37	C57Bl6+SFRP4		NP
	P55065	PLTP	Phospholipid transfer protein	Pltp	-1,32	5,34E-04	-2,34	-59,86	0,40	C57Bl6+SFRP4	SP+	
	P58771-2	TPM1	Isoform 2 of Tropomyosin alpha-1 chain	Tpm1	1,32	1,41E-01	1,35	1,50	2,50	C57Bl6+SFRP4		NP
	P62754	RS6	40S ribosomal protein S6	Rps6	-1,15	7,91E-02	-0,69	-54,91	0,45	C57Bl6+SFRP4		NP
	P97390	VPS45	Vacuolar protein sorting-associated protein 45	Vps45	-2,05	6,29E-02	-3,15	-75,93	0,24	C57Bl6+SFRP4		NP
	Q07235	GDN	Glia-derived nexin	Serpine2	1,23	1,04E-02	0,89	13,39	2,34	C57Bl6+SFRP4	SP+	
	Q3UNX5; Q3UNX5-2	ACSM3	Acyl-coenzyme A synthetase ACSM3	Acsm3	1,13	2,49E-02	0,75	11,93	2,19	C57Bl6+SFRP4		NP
	Q60932;Q60932-2	VDAC1	Voltage-dependent anion-selective channel protein 1	Vdac1	1,57	5,71E-02	1,49	19,75	2,97	C57Bl6+SFRP4	SP+	
	Q60972	RBBP4	Histone-binding protein RBBP4	Rbbp4	2,95	1,44E-01	0,52	67,41	7,74	C57Bl6+SFRP4		NP
	Q61335	BAP31	B-cell receptor-associated protein 31	Bcap31	1,06	1,56E-01	0,85	10,81	2,08	C57Bl6+SFRP4	SP-	
	Q61781	K1C14	Keratin, type I cytoskeletal 14	Krt14	-1,92	5,18E-02	-0,99	-73,54	0,26	C57Bl6+SFRP4		NP
	Q62264	THRSP	Thyroid hormone-inducible hepatic protein	Thrsp	-1,09	9,55E-04	-1,29	-52,97	0,47	C57Bl6+SFRP4		NP
	Q63836	SBP2	Selenium-binding protein 2	Selenbp2	1,06	7,19E-48	1,70	10,84	2,08	C57Bl6+SFRP4		NP
	Q63886	UD11	UDP-glucuronosyltransferase 1-1	Ugt1a1	1,20	1,10E-02	0,97	12,90	2,29	C57Bl6+SFRP4	SP+	
	Q8BTJ4;Q8BTJ4-2	ENPP4	Bis(5'-adenosyl)-triphosphatase enpp4	Enpp4	1,04	2,00E-01	0,98	10,53	2,05	C57Bl6+SFRP4	SP+	
	Q8BWQ1	UD2A3	UDP-glucuronosyltransferase 2A3	Ugt2a3	1,23	4,51E-02	0,91	13,39	2,34	C57Bl6+SFRP4	SP+	
	Q8JZS9	RM48	39S ribosomal protein L48, mitochondrial	Mrpl48	-1,75	1,50E-01	-2,43	-70,24	0,30	C57Bl6+SFRP4		NP
	Q8VCU1-2	EST3B	Isoform 2 of Carboxylesterase 3B	Ces3b	1,09	1,03E-01	0,89	1,13	2,13	C57Bl6+SFRP4	SP+	
	Q99KC8	VMA5A	von Willebrand factor A domain-containing protein 5A	Vwa5a	1,07	9,55E-02	-0,61	10,92	2,09	C57Bl6+SFRP4		NP

C57Bl6+sFRP4/ aP2-SREBP-1c+sFRP4	Q99KP3	CRYL1	Lambda-crystallin homolog	Cryl1	-1,26	2,70E-04	-1,15	-58,33	0,42	C57Bl6+SFRP4	SP+	
	Q99MN9	PCCB	Propionyl-CoA carboxylase beta chain, mitochondrial	Pccb	1,36	3,39E-02	-0,26	15,75	2,58	C57Bl6+SFRP4	SP+	
	Q9D154	ILEUA	Leukocyte elastase inhibitor A	Serpin b1a	-1,10	5,17E-03	-0,92	-53,37	0,47	C57Bl6+SFRP4		NP
	Q9DCM2	GSTK1	Glutathione S-transferase kappa 1	Gstk1	-1,29	1,09E-11	-1,21	-59,05	0,41	C57Bl6+SFRP4		NP
	Q9DCX1	MD2BP	MAD2L1-binding protein	Mad2l 1bp	1,39	1,71E-01	1,27	16,15	2,62	C57Bl6+SFRP4		NP
	Q9JLC3	MSRB1	Methionine-R-sulfoxide reductase B1	Msrb1	1,07	1,51E-01	1,14	11,00	2,10	C57Bl6+SFRP4		NP
	Q9QWR8	NAGAB	Alpha-N-acetylgalactosaminidase	Naga	1,01	5,81E-08	0,90	10,20	2,02	C57Bl6+SFRP4	SP+	
	Q9QYR7; Q9QYR7-2	ACOT3	Acyl-coenzyme A thioesterase 3, mitochondrial	Acot3	-1,10	1,04E-01	-3,03	-53,31	0,47	C57Bl6+SFRP4		NP
	Q9QYR9	ACOT2	Acyl-coenzyme A thioesterase 2, mitochondrial	Acot2	-1,39	7,33E-09	-1,68	-61,79	0,38	C57Bl6+SFRP4		NP
	Q9R062	GLYG	Glycogenin-1	Gyg1	-1,25	3,44E-02	-1,38	-58,06	0,42	C57Bl6+SFRP4		NP
	Q9R0G6	COMP	Cartilage oligomeric matrix protein	Comp	1,26	4,31E-02	1,18	13,93	2,39	C57Bl6+SFRP4	SP+	
	Q9R1J0	NSDHL	Sterol-4-alpha-carboxylate 3-dehydrogenase, decarboxylating	Nsdhl	1,18	1,24E-01	1,03	12,72	2,27	C57Bl6+SFRP4		NP
	Q9R257	HEBP1	Heme-binding protein 1	Hebp1	-1,14	2,61E-03	-1,26	-54,58	0,45	C57Bl6+SFRP4		NP
	Q9WVM8	AADAT	Kynurenine/alpha-aminoadipate aminotransferase, mitochondrial	Aadat	1,05	1,91E-16	1,08	10,73	2,07	C57Bl6+SFRP4		NP
	Q9Z0K8	VNN1	Pantetheinase	Vnn1	-1,10	1,77E-05	-1,63	-53,41	0,47	C57Bl6+SFRP4	SP+	
	Q9Z1X4;Q9Z1X4-2;Q9Z1X4-3	ILF3	Interleukin enhancer-binding factor 3	Ilf3	1,54	1,78E-01	0,37	19,00	2,90	C57Bl6+SFRP4		NP
	E9Q557	DESP	Desmoplakin	Dsp	-1,31	1,35E-01	0,76	-5,97	0,40	C57Bl6+SFRP4		NP
	O55229	CHKB	Choline/ethanolamine kinase	Chkb	-1,41	1,01E-01	-0,89	-62,35	0,38	C57Bl6+SFRP4		NP

C57Bl6+sFRP4/ C57Bl6	P02535;P02535-2;P02535-3	K1C10	Keratin, type I cytoskeletal 10	Krt10	1,11	2,25E-02	0,85	11,66	2,17	C57Bl6+SFRP4		NP
	P07356	ANXA2	Annexin A2	Anxa2	2,03	7,02E-02	1,21	30,96	4,10	C57Bl6+SFRP4		NP
	P08121	CO3A1	Collagen alpha-1(III) chain	Col3a1	-1,19	1,98E-01	-1,63	-56,18	0,44	C57Bl6+SFRP4	SP+	
	P08730	K1C13	Keratin, type I cytoskeletal 13	Krt13	1,17	1,90E-01	0,91	12,56	2,26	C57Bl6+SFRP4		NP
	P17897	LYZ1	Lysozyme C-1	Lyz1	2,39	1,11E-01	1,85	4,23	5,23	C57Bl6+SFRP4	SP+	
	P35279;P35279-2;P61294	RAB6A; RAB6B	Ras-related protein Rab-6A	Rab6a; Rab6a; Rab6b	-1,16	1,94E-01	-1,04	-55,26	0,45	C57Bl6+SFRP4		NP
	P61255	RL26	60S ribosomal protein L26	Rpl26	-1,09	2,00E-01	-1,85	-53,14	0,47	C57Bl6+SFRP4		NP
	P97798;P97798-2;P97798-3;P97798-4;P97798-5	NEO1	Neogenin	Neo1	2,79	9,40E-02	2,94	59,03	6,90	C57Bl6+SFRP4	SP+	
	Q06185	ATP5I	ATP synthase subunit e, mitochondrial	Atp5i	1,53	1,24E-01	1,15	18,79	2,88	C57Bl6+SFRP4		NP
	Q3TLP5;Q3TLP5-2	ECHD2	Enoyl-CoA hydratase domain-containing protein 2, mitochondrial	Echdc2	1,06	1,37E-01	1,28	10,87	2,09	C57Bl6+SFRP4	SP-	
	Q3UV17	K22O	Keratin, type II cytoskeletal 2 oral	Krt76	1,51	7,91E-02	1,50	18,42	2,84	C57Bl6+SFRP4		NP
	Q60902;Q60902-2;Q60902-3;Q60902-4	EP15R	Epidermal growth factor receptor substrate 15-like 1	Eps15l1	2,93	1,18E-01	3,21	66,12	7,61	C57Bl6+SFRP4		NP
	Q61081	CDC37	Hsp90 co-chaperone Cdc37	Cdc37	1,71	1,47E-01	0,58	22,71	3,27	C57Bl6+SFRP4		NP
	Q61473	SOX17	Transcription factor SOX-17	Sox17	1,85	1,72E-01	2,72	26,17	3,62	C57Bl6+SFRP4		NP
	Q61781	K1C14	Keratin, type I cytoskeletal 14	Krt14	1,01	7,86E-07	1,68	10,16	2,02	C57Bl6+SFRP4		NP
	Q6IFX2	K1C42	Keratin, type I cytoskeletal 42	Krt42	2,16	6,22E-02	2,14	34,77	4,48	C57Bl6+SFRP4		NP
	Q6NXH9	K2C73	Keratin, type II cytoskeletal 73	Krt73	1,12	3,05E-02	1,16	11,69	2,17	C57Bl6+SFRP4		NP

	Q6P9P6	KIF11	Kinesin-like protein KIF11	Kif11	-1,23	1,44E-01	-0,60	-57,46	0,43	C57Bl6+SFRP4		NP
	Q7TMV3	FAKD5	FAST kinase domain-containing protein 5, mitochondrial	Fastkd 5	1,20	1,72E-01	1,62	1,29	2,29	C57Bl6+SFRP4		NP
	Q8JZS9	RM48	39S ribosomal protein L48, mitochondrial	Mrpl48	-1,50	6,39E-02	-4,31	-64,73	0,35	C57Bl6+SFRP4		NP
	Q8VED5	K2C79	Keratin, type II cytoskeletal 79	Krt79	1,38	1,77E-01	1,12	15,96	2,60	C57Bl6+SFRP4		NP
	Q8VEK3;Q8VEK3-2	HNRPU	Heterogeneous nuclear ribonucleoprotein U	Hnrnpu	1,07	1,36E-01	0,65	11,04	2,10	C57Bl6+SFRP4		NP
	Q922U2	K2C5	Keratin, type II cytoskeletal 5	Krt5	1,47	1,04E-06	1,29	17,61	2,76	C57Bl6+SFRP4		NP
	Q9DD02	HIKES	Protein Hikeshi	Hikeshi	1,06	1,12E-01	1,26	10,90	2,09	C57Bl6+SFRP4		NP
	Q9ERR7	SEP15	Selenoprotein F	Selenof	1,37	1,95E-01	1,82	15,79	2,58	C57Bl6+SFRP4	SP+	
	Q9QWL7	K1C17	Keratin, type I cytoskeletal 17	Krt17	1,32	5,37E-04	1,10	14,90	2,49	C57Bl6+SFRP4		NP
	Q9Z2K1	K1C16	Keratin, type I cytoskeletal 16	Krt16	1,48	1,24E-01	1,19	1,78	2,78	C57Bl6+SFRP4		NP

Mass spectrometry data were analyzed with Spectronaut® v11 to identify differential secreted proteins from mass spectrometry peptide data. Post Analyses to determine differential secreted proteins (>1.5-fold, *p*-value <0.05, *t*-test) were performed on the same platform. The presence of a classical or non-classical signal peptide was determined using open source databases.

Table 31. Differential secretome and core analyses of the comparisons C57Bl6 vs aP2-SREBP-1c, C57Bl6 sFRP4 vs aP2-SREBP-1c sFRP4, C57Bl6 sFRP4 vs C57Bl6, aP2-SREBP-1c sFRP4 vs aP2-SREBP-1c.

C57Bl6 vs aP2-SREBP-1c							
Canonical Pathways	***p*-value**	**Upstream Activators**	***p*-value**	**Disease, Function**	***p*-value**	**Interaction Network**	***p*-value**
EIF2 Signaling	4.47E-7	MYCN	5.95E-9	LXR/RXR Activation	6.61E-6	RHEBL1	6.84E-12
LXR/RXR Activation	6.17E-6	IL6	1.86E-8	Positive Acute Phase Response	3.63E-5	INSIG1	1.05E-10
Acute Phase Response	3.16E-5	RICTOR	1.27E-6	Increases Liver Steatosis	1.32E-3	ADRM1	4.9E-10
FXR/RXR Activation	2.51E-3	PPARA	2.99E-6	Hepatic Fibrosis	1.41E-3	TRPC4AP	6.99E-10
iNOS Signaling	4.27E-3	TNFRSF1A	2.04E-5	FXR/RXR Activation	2.51E-3	DSP	1.15E-9
D-glucuronate Degradation I	6.46E-3	CEBPA	3.32E-5	Increases Liver Damage	3.09E-3	TGFB1	1.91E-9
Hepatic Fibrosis /Stellate Cell Activation	7.59E-3	JUN	3.57E-5	Oxidative Stress	6.76E-3	MYCN	2.28E-9
Acetate Conversion to Acetyl-CoA	8.51E-3	SLC13A1	4.27E-5	Increases Liver Hepatitis	1.02E-2	RARB	2.64E-9
Thymine Degradation	8.51E-3	AHR	8.48E-5	Liver Proliferation	1.48E-2	ITGA6	6.97E-9
Uracil Degradation II	8.51E-3	Alpha catenin	1.20E-4	LPS/IL-1 Mediated Inhibition of RXR	1.62E-2	SENP1	8.15E-9

C57Bl6 sFRP4 vs aP2-SREBP-1c sFRP4							
Canonical Pathways	***p*-value**	**Upstream Activators**	***p*-value**	**Disease, Function**	***p*-value**	**Interaction Network**	***p*-value**
Thyroid Hormone Metabolism II	1.51E-4	PPARA	4.23E-13	LXR/RXR Activation	3.55E-4	NR2F1	5.92E-15
LXR/RXR Activation	3.31E-4	ACOX1	5.24E-9	Positive Acute Phase Response	3.02E-3	UBE2H	8E-14
Nicotine Degradation III	3.80E-4	NFE2L2	1.59E-7	FXR/RXR Activation	4.90E-3	ACOX1	9.93E-14
Acyl-CoA Hydrolysis	4.68E-4	GPD1	2.14E-7	Acute Renal Failure Panel	1.12E-2	PPARA	3.64E-13
Melatonin Degradation I	5.89E-4	SLC25A13	2.42E-7	PXR/RXR Activation	1.35E-2	HOXA10	5.6E-13
Nicotine Degradation II	6.17E-4	FOS	1.71E-6	Xenobiotic Metabolism Signaling	1.48E-2	TXNIP	1.53E-12
Melatonin Degradation	7.41E-4	PPARGC1A	4.28E-6	VDR/RXR Activation	1.91E-2	CREBBP	1.53E-12
Serotonin Degradation	9.12E-4	RORA	1.42E-5	TR/RXR Activation	2.95E-2	SREBF1	2.82E-12
FXR/RXR Activation	4.90E-3	CEBPA	2.25E-5	Increases Liver Steatosis	3.02E-2	KRAS	3.88E-12
Stearate Biosynth. I	6.46E-3	RORC	6.48E-5	Increases Liver Damage	5.25E-2	FOSL1	1.02E-11

C57Bl6 SFPR4 vs C57Bl6							
Canonical Pathways	***p*-value**	**Upstream Activators**	***p*-value**	**Disease, Function**	***p*-value**	**Interaction Network**	***p*-value**
Glucocorticoid Receptor Signaling	8.91E-9	KRT14	1.67E-5	Renal Ischemia-Reperfusion Injury	7.59E-4	MNK1/2	3.34E-6
Phosphatidylcholine Biosynth. I	9.12E-3	KLF4	1.80E-5	Acute Renal Failure Panel	2.88E-3	RPL11	4.26E-6
Phosphatidylethanolamine Biosynth. II	1.05E-2	MYC	4.42E-5	Genes associated with Chronic Allograft Nephropathy	8.71E-3	BIRC5	4.40E-6
Atherosclerosis Signaling	1.17E-2	PKP2	4.66E-5	Nongenotoxic Hepatocarcinogenicity Biomarker Panel	1.20E-2	MYC	7.80E-6
Intrinsic Prothrombin Activation Pathway	5.25E-2	IgG	6.34E-5	Hepatic Fibrosis	1.91E-2	FBXO5	9.56E-6
Mitotic Roles of Polo-Like Kinase	8.32E-2	NEUROG1	8.46E-5	LXR/RXR Activation	2.82E-2	KLF4	1.02E-5
LXR/RXR Activation	1.47E-1	MDM2	1.01E-4	Renal Necrosis/Cell Death	2.95E-2	PKP2	4.66E-5
PI3K/AKT Signaling	1.52E-1	PLA2G2E	1.29E-4	Cardiac Fibrosis	3.98E-2	Vacuolar H+ ATPase	4.70E-5
GP6 Signaling Pathway	1.62E-1	PRL	4.27E-4	Cardiac Necrosis/Cell Death	7.41E-2	IgG	5.23E-5
Wnt/β-catenin Signaling	2.03E-1	CST5	4.51E-4	Persistent Renal Ischemia-Reperfusion Injury	1.07E-1	NT5E	5.77E-5

aP2-SREBP-1c SRFP4 vs aP2-SREBP-1c							
Canonical Pathways	***p*-value**	**Upstream Activators**	***p*-value**	**Disease, Function**	***p*-value**	**Interaction Network**	***p*-value**
Glucocorticoid Receptor Signaling	5.37E-6	PLA2G2E	1.98E-9	Positive Acute Phase Response Proteins	7.59E-4	MET	4.58E-11
Coagulation System	1.02E-3	IL6	3.46E-6	Acute Renal Failure Panel	2.88E-3	ERBB4	4.66E-11
Uridine-5'-phosphate Biosynth.	2.69E-3	ERBB4	5.49E-6	Hepatic Fibrosis	8.71E-3	BET	5.81E-9
Methylmalonyl Pathway	5.37E-3	HRAS	9.93E-6	LXR/RXR Activation	1.20E-2	EDN3	7.44E-9
2-oxobutanoate Degradation I	6.76E-3	KRT14	1.86E-5	Recovery from Ischemic Acute Renal Failure	1.91E-2	EFNA1	7.87E-9
CMP-N-acetylneuraminate Biosynth. I	6.76E-3	PRL	3.10E-5	Genes associated with Chronic Allograft Nephropathy	2.82E-2	DOPAMINE D2 LIKE receptor	9.45E-9
LXR/RXR Activation	1.17E-2	ZNF106	3.12E-5	Nongenotoxic Hepatocarcinogenicity Biomarker Panel	2.95E-2	CTGF	1.18E-8
Atherosclerosis Signaling	1.26E-2	Brd4	3.55E-5	Persistent Renal Ischemia-Reperfusion Injury	3.98E-2	FGFR2	2.21E-8
IL-12 Signaling and Production in Macrophages	1.66E-2	TGFB1	5.76E-5	Oxidative Stress	7.41E-2	PTK6	3.37E-8
Role of IL-17A in Psoriasis	1.74E-2	MYC	5.84E-5	Increases Glomerular Injury	1.07E-1	NFE2	3.76E-8

Significant differences for enrichment of pathway molecules in the data set were indicated by *p*-value and derived by IPA® Core analyses.

Danksagung

Eine lange, aufregende und interessante Zeit mit vielen Höhen, aber auch den ein oder anderen Tiefen, geht nun zu Ende. Das Resultat dieser Zeit ist die vorliegende Arbeit, die durch die Unterstützung und Hilfe anderer erst ermöglicht wurde. An dieser Stelle allen ein ganz herzlicher Dank!

Mein Dank gilt Prof. Dr. Hadi Al-Hasani für die Möglichkeit meine Promotion am Institut für Klinische Biochemie und Pathobiochemie absolvieren zu können und die Freiheit in der Gestaltung des Themas. Weiterhin möchte ich mich für die wissenschaftliche Förderung, die ich als Mitglied des Graduiertenkollegs „vivid“ erhalten habe, sowie die Ermöglichung der Teilnahme an nationalen und internationalen Kongressen herzlich bedanken.

Bei Frau Prof. Dr. Margriet Ouwens möchte ich mich für die Hilfsbereitschaft und die Mitbetreuung dieser Arbeit und des Manuskriptes sowie die Bereitstellung projektbezogener Materialien bedanken.

Prof. Dr. Michael Feldbrügge danke ich für das Interesse und die bereitwillige Übernahme des Korreferats dieser Arbeit.

Besonders hervorheben möchte ich die intensive und konstruktive Zusammenarbeit mit Dr. Birgit Knebel und Dr. Jörg Kotzka: Ein großes Dankeschön, dass ihr zur richtigen Zeit am richtigen Ort wart! Ihr besonderes Engagement, die wertvollen Diskussionen, Anregungen und motivierenden Worte, die ich immer sehr zu schätzen wusste, haben wesentlich zur Entstehung und zum Abschluss dieser Arbeit beigetragen. Mein besonderer Dank an euch!

Weiterhin danke ich allen Kooperationspartnern für die konstruktive Zusammenarbeit und die Unterstützung in der Entstehung des Manuskriptes und beim Erlernen neuer Methoden. Insbesondere vielen Dank an Dr. Natalia Rudovich, Dr. Olga Pivovarova und Dr. Deike Hesse-Wiltling.

Ich möchte mich auch bei allen Arbeitskollegen für die äußerst angenehme Arbeitsatmosphäre und die Unterstützung in den letzten Jahren bedanken! Ein großes Dankeschön an Daniella für den unermüdlichen Einsatz und die tatkräftige Unterstützung im Labor sowie ihre unschlagbare Herzlichkeit. Pia und David, es war mir immer eine sehr große Freude mit euch zu arbeiten, zu lachen und zu diskutieren.

Einen unermesslichen Dank gilt meiner Familie und meinen Freunden. Meinen Eltern und meiner Schwester, Danke für eure Ermutigungen während dieser Zeit und die Ermöglichung meines Studiums.
Lieber Jens, Danke, dass du einfach für mich da bist, für deine positive Art und dass du immer an mich geglaubt hast. Ohne eure Unterstützung, bedingungslose Geduld und den tiefen Glauben an mich, hätte ich diesen Weg nicht einfach gehen können!

Eidesstattliche Erklärung

Ich versichere an Eides Statt, dass die Dissertation von mir selbständig und ohne unzulässige fremde Hilfe unter Beachtung der „Grundsätze zur Sicherung guter wissenschaftlicher Praxis an der Heinrich-Heine-Universität Düsseldorf“ erstellt worden ist. Die Dissertation wurde in der vorgelegten oder in ähnlicher Form noch bei keiner anderen Institution eingereicht. Ich habe bisher keine erfolglosen Promotionsversuche unternommen.

26. Juli 2018

(Datum) (Tina Hörbelt)